Dissertation

Kinematic evolution of the western Tethyan realm derived from paleomagnetic and geologic data

Ausgeführt zum Zwecke der Erlangung des akademischen Grades eines Doktors der montanistischen Wissenschaften

Leoben, Jänner 2008 Mag. rer. nat. Wolfgang Thöny

I DECLARE IN LIEU OF OATH THAT I DID THIS PHILOSOPHICAL DOCTOR'S THESIS IN HAND BY MYSELF USING ONLY THE LITERATURE CITED AT THE END OF THIS VOLUME

Mag. rer. nat. Wolfgang Thöny

Leoben, Jänner 2008

Acknowledgements

I want to thank my academic supervisors ao. Univ. Prof. Dr. Robert Scholger, Chair of Geophysics, University of Leoben and ao. Univ. Prof. Dr. Hugo Ortner, Institute for Geology and Palaeontology, University of Innsbruck, for the opportunity to write this thesis. Due to excellent scientific and personal support, it was a pleasure to me being a kind of link between the two disciplines of Geophysics and Geology during these times of research.
Benefit to the study was also derived from a fantastic "working climate" due to my co-students Dipl. Ing. Dr. Sigrid Hemetsberger and Dipl. Ing. Anna Selge.
Numerous colleagues and friends enabled site selection and sampling in the field, we got gratefully acknowledged support:

at Schliersee area from Roland Pilser and Michael Zerlauth (Univ.Innsbruck) and Dr. Ulrich Haas (Univ. München), **at Allgäu/Vorarlberg area** from Silvia Aichholzer, Monika Fischer, Sebastian Jacobs (Univ. Innsbruck) and Dr. Klaus Schwerd, Dr. Herbert Scholz, Dipl.Geol. Dorothea Frieling (Univ. München), **at Muttekopf area from** Dr. Herbert Haubold (Univ. Leoben), **at Thiersee area** from Peter Umfahrer and Mag. Barbara Simmer (Innsbruck), **at Lower Inn valley area** from Mag. Werner Thöny (Univ. Innsbruck), **at Sulden/Ortler area** from Dr. Volkmar Mayr (Bozen), **at Dolomites/Ra Stua** from Mag. Alfred Gruber, Mag. Andrea Schaber (Univ.Innsbruck), **at Dolomites/Fischleintal** from Mag. Alfred Gruber (Univ.Innsbruck), **at Nonstal area** from Patrik Ausserer, Mag. Werner Thöny (Univ.Innsbruck), **at Lake Garda area** from Dr. Vincenzo Picotti (Univ.Bologna) **at Belluno area** from Dr. Paolo Grandesso, Dr. Cristina Stefani, (Univ. Padova) and from Dipl. Ing. Hannes Geidl (Univ.Leoben);

I want to thank my partner Dr. Wilma Haushofer, my mother, and my families in Innsbruck and Frohnleiten who supported me whenever motivation was needed. I want to dedicate this study to our daddies, to SR Dir. Ferdinand Thöny and to BM Ing. Josef Haushofer. Thank you for all that wonderful support during these years.

This study was financially supported by the Austrian research fund, FWF projects P-13566-TEC: TRANSALP, Rotation von Segmenten der Nördlichen Kalkalpen and P-17767: Struktureller Ausdruck von großen Rotationen in den Alpen.

Zusammenfassung

In dieser Studie werden neue paläomagnetische Resultate von 140 sites (=Beprobungshorizonte) aus den Ost- und Südalpen präsentiert. 24 sites wurden im Nordalpinen Vorlandbecken untersucht - 16 sites in den helvetischen Decken- 51 sites in den Nördlichen Kalkalpen (NKA) -6 sites in den Zentralalpen -16 sites in den Südalpen (SA) und 27 sites im Südalpinen Vorlandbecken. Ermöglicht wurde diese paläomagnetische Studie durch zwei Forschungsprojekte des Österreichischen Forschungsfonds FWF (P-13566-TEC: TRANSALP, Rotation von Segmenten der Nördlichen Kalkalpen; P-17767: Struktureller Ausdruck von großen Rotationen in den Alpen).

Die auf paläomagnetischen und geologischen Daten basierende Beschreibung der geodynamischen Entwicklung, wird in einen Känozoischen und einen Mesozoischen Abschnitt unterteilt.

Im Zeitraum Frühes bis Spätes Rupel (32-29Ma) konnte für die Nördlichen Kalkalpen (NKA), die ostalpinen Zentralalpen, die Südalpen und das Südalpine Vorlandbecken eine erste Phase einer Rotation im Uhrzeigersinn erkannt werden. Diese Rotation wird mit den Deckenstapelungen innerhalb der Penninischen, Helvetischen und Kalkalpinen Einheiten in Zusammenhang gebracht, und wurde möglicherweise durch ein nordwärts gerichtetes Rückschreiten der in den Erdmantel abtauchenden europäischen Unterkruste bedingt. Die, der rückschreitenden Unterplatte folgende Oberplatte, wurde dadurch zu einer Rotation im Uhrzeigersinn um den Böhmischen Sporn gezwungen. Im weiteren erfährt diese Rotation im Uhrzeigersinn im Zeitraum Mittleres bis Spätes Chatt (25-23Ma) einen zweiten Schub, wobei die Subalpine Molasse sowie die Einheiten des Penninischen Tauern Fensters ebenfalls von der Rotation erfasst wurden. Die Rotation im Uhrzeigersinn wurde möglicherweise durch einen „slab break off“ der europäischen Unterkruste gestoppt, der einen „rebound“ der Unterplatte und eine Aufwölbung der Oberplatte bewirkte. Diese Aufwölbung initiierte möglicherweise den Beginn der „lateralen extrusion“. Die jüngste Rotation, die im Gegenuhrzeigersinn erfolgte, konnte mit Hilfe von Daten aus den nördlichen Venezianischen Alpen in einen Zeitraum jünger als 5Ma datiert werden. Nach N hin konnte die frontale Alpine Überschiebung als Begrenzung der rotierenden Großeinheit definiert werden, da altersgleiche Magnetisierungen nördlich der Alpinen Front keinen Rotationsbetrag aufweisen. Diese junge Rotation im Gegenuhrzeigersinn wird im Zusammenhang mit der Öffnung des Tyrrhenischen Meeres und der Spät Miozänen Rotation von Adria gesehen.

Die Mesozoische Kinematik die im Rahmen dieser paläomagnetischen Studie erkannt werden konnte, bezieht sich hauptsächlich auf die Prozesse während der Spät Kretazischen bis Eozänen Schließung des Piemont - Valais Ozeans.

Studien an Penninischen Einheiten (Pueyo et al., 2002; Hauck, 1998) belegen eine vor-Oligozäne Rotation von 30° im Gegenuhrzeigersinn. Höchstwahrscheinlich steht diese Rotation mit der Subduktion des Penninischen Ozeans im Zusammenhang. In Oberkretazischen Sedimenten aus den westlichen Nördlichen Kalkalpen konnten Magnetisierungen identifiziert werden, die vor der Verfaltung aufgeprägt wurden. Zusammen mit primären Magnetisierungen aus Tirolischen Einheiten südlich der SEMP Salzach/Ennstal/Mariazell/Puchberg Linie und primären Magnetisierungen die in Untereozänen Sedimenten aus den Südalpen isoliert werden konnten, kann für diesen bearbeiteten Raum eine zusätzlich Rotation im Gegenuhrzeigersinn vermutet werden. Bezugnehmend auf die vorhandene Fachliteratur und auf die tektonischen Einheiten, konnte diese Rotation in den Bajuvarischen Deckeneinheiten E des Inn Tales nicht nachgewiesen werden, konnte jedoch im Zuge dieser Studie in der Lechtal Decke der westlichen Nördlichen Kalkalpen sowie in den Tirolischen Einheiten sowie in den Südalpen erkannt werden. Die Bohrung Vordersee1, SE von Salzburg, durchteufte Tirolische Einheiten und konnte an der Deckengrenze zur liegenden Bajuvarischen Deckeneinheit Paleogene Sedimente belegen (Geutebrück et al., 1984). Somit konnte die Überschiebung (i.e. Brixlegg Störung) von Tirolikum auf Bajuvarikum auf ein Paleogenes Alter datiert werden (Ortner at al., 2006). Es wird vermutet, daß die Bajuvarischen Anteile W des Inntales (i.e. die Lechtal Decke) während dieser Überschiebung in die Hangendscholle miteinbezogen wurden. Dies könnte den relativen Unterschied der Rotationsbeträge innerhalb der oben beschriebenen Deckeneinheiten erklären.

Paläomagnetische Aussagen zur jurassischen Geodynamik die in Zusammenhang mit der Öffnung des Piemont Ozean zu sehen wären, können aufgrund eines geringen Datensatzes primärer Magnetisierungen nur bedingt getätigt werden. Nachdem die Miozäne bis Eozäne Rotationsgeschichte rückgeführt wurde, zeichnen sich NKA und SA durch Primärmagnetisierungen Kretazischer und Jurassischer Lithologien aus, die N gerichtete Deklinationen aufweisen. Offensichtlich waren die NKA bzw. die EA und SA von der großräumigen Rotation im Gegenuhrzeigersinn der Afrikanischen Platte, die im Zusammenhang mit der Öffnung des Zentralatlantiks steht, nicht betroffen.

EA und SA waren möglicherweise nach S hin an einer sinistral aktiven Scherzone von der rotierenden Großeinheit getrennt. Marton (2006) konnte für die Adriatische Platte eine Rotation von 20° im Gegenuhrzeigersinn relativ zu Afrika für das Späte Miozän bis Pliozän belegen. Nachdem diese Komponente rückrotiert wurde, konnte gezeigt werden, daß die Jurassische Primärmagnetisierungen der Adriatischen Platte einen eindeutigen Afrikanischen Trend aufweisen. Die beobachteten im Gegenuhrzeigersinn rotierten Remanenzen, werden ebenfalls mit der Öffnung des Zentralatlantiks in Zusammenhang gebracht.

Zusammenfassend läßt sich eine getrennte Rotationsgeschichte für Adria/Afrika einerseits und die EA/SA andererseits ab der Jurassischen Öffnung des Zentralatlantiks feststellen.
Während der alpinen Kontinent/Kontinent Kollision läßt sich in den EA/SA eine zweiphasige Uhrzeigersinn Rotation nachweisen. Diese kann innerhalb der Adriatischen Platte nicht erkannt werden. Erst im Späten Miozän, jünger als 5Ma, ist eine gemeinsame Rotation im Gegenuhrzeigersinn belegt, die EA/SA gleichermaßen wie Adria und wie Teile der Westalpen erfasst hat.

Abstract

New paleomagnetic results from 140 sites in the Eastern and Southern Alps are presented.
- 24 sites were investigated in the North Alpine foreland basin, (NAFB), - 16 sites in the Helvetic nappes,- 51 sites in the Northern Calcareous Alps (NCA)- 6 sites in the Central Alps (CA),- 16 sites in the Southern Alps (SA), and- 27 sites in the Southern Alpine foreland basin (SAFB). Paleomagnetic work was carried out in the frame of two FWF projects (P-13566-TEC: TRANSALP, Rotation von Segmenten der Nördlichen Kalkalpen; P-17767: Struktureller Ausdruck von großen Rotationen in den Alpen).

The description of the geodynamic evolution as interpreted from paleomagnetic and geologic data is divided into a Cenozoic and a Mesozoic part. Cenozoic remance directions of the Eastern and Southern Alps are similar. Declinations change synchronously. Three phases of joined vertical axis rotations in the study area are observed.

A first phase of clockwise rotation is active between Early Rupelian to Late Rupelian times (32-29Ma) affecting the NCA, eastern CA, SA and SAFB. This rotation can be related to the thrusting of NCA, Flysch and Helvetic units and was possibly driven by a retreat of the European lower lithosphere, forcing the Eastern/Southern Alps in upper plate position to follow while rotating around the Bohemian spur. A second phase of clockwise rotation, still related to slab retreat of the European lower lithosphere, is dated to Middle to Latest Chattian (25-23Ma) and incorporates the Subalpine Molasse and the units of the Penninic Tauern window. Dynamics responsible for clockwise rotation were stopped by the slab break-off of the European lower lithosphere, which caused successive rebound of the lower plate that possibly triggered the initiation of lateral extrusion in the upper plate (i.e. the Austro-Alpine nappe stack). The youngest, counterclockwise vertical axis rotation is postdating the folding of Messinian Montello conglomerates of the northern Venetian Alps and consequently must be younger than 5Ma. This rotation is observed in the Subalpine Molasse, EA, SA, SAFB and the northern parts of Adria (Marton et al., 2003). To the north the rotating units are limited by the frontal Alpine thrusts as sites with synchronous magnetization ages north of the Alpine front (tilted Molasse, autochthonous Molasse) do not indicate any vertical axis rotation. The young counterclockwise rotation is probably related to the opening (5-3Ma) of the Tyrrhenian Sea/ Vavilov basin and the resulting young rotation of Adria (Marton et al., 2003).

The Mesozoic kinematics that could be identified during this paleomagnetic study are mainly connected to the Late Cretaceous to Eocene closure of the Piemontais/Valais Ocean.
Data from Penninic nappes from previous studies (Pueyo et al., 2002; Hauck, 1998) indicate 30° of counterclockwise rotation relative to the Late Cretaceous/ Eocene reference direction, before Oligocene kinematics, which were described above. Most probably this rotation is caused by the subduction of the Penninic Ocean. Prefolding magnetizations from Late Cretaceous sediments from the western part of the NCA, primary magnetizations from Late Cretaceous sediments from the NCA south of Salzach/Ennstal/Mariazell/Puchberg (SEMP) line and primary magnetizations from Lower Eocene sediments of the Southern Alps are characterized by an additional counterclockwise rotation of 30° compared with the data from the Penninic units. According to the available literature this additional post Early Eocene rotation is not known in the Bajuvaric units of the central NCA east of the Inn valley, but was identified during this study in the Lechtal nappe of the western NCA, the Tirolic units and the Southern Alps. The well Vordersee 1, located SE of the city of Salzburg was penetrating the Tirolic unit and reached Paleogene sediments on top of the underlying Bajuvaric unit (Geutebrück et al., 1984). Consequently the thrust of the Tirolic unit onto the Bajuvaric unit (Brixlegg thrust) has a Paleogene age (Ortner et al., 2006). Possibly W of the Inn valley also the Bajuvaric Lechtal nappe was incorporated into the hangingwall of the Brixlegg thrust that possibly was accomodating 30° of relative counterclockwise rotation between the nappe units mentioned above.

Only few interpretations are possible about Jurassic vertical axis rotations related to the opening of the Piemontais Ocean due to scarce primary magnetizations. After restoring the Miocene to Eocene vertical axis rotations that affected NCA and Southern Alps Jurassic to Cretaceous paleomagnetic data are showing approximately N-directed declinations. Obviously during opening of the Central Atlantic and the counterclockwise rotation of Africa the Eastern/Southern Alps did not rotate and were probably separated from the rotating units by an approximately E-W striking shear zone. Marton (2006) was identifying a 20° counterclockwise rotation of stable (autochthonous) Adria in Late Miocene to Pliocene times relative to Africa. After restoring this component, declinations of Jurassic primary magnetizations indicate 30° of counterclockwise rotation (Muttoni et al., 2001), which is very similar to the African reference directions and is also related to the opening of the Central Atlantic.

Summarizing, from the Jurassic onwards, when the Central Atlantic Ocean opened, Adria/Africa and the EA/SA did not rotate uniformly. During Alpine continental collision in the Oligocene the EA/SA performed clockwise rotations between 32-29Ma and between 25-23Ma, which cannot be found in stable Adria. Concerning the counterclockwise rotation at 5-3Ma, EA/SA and stable Adria joined, including parts of the Swiss and Western Alps.

Content

1. Introduction

The architecture of orogens is mostly discussed in cross sections perpendicular to the strike of the main thrusts, as the main tectonic units usually have an extremely elongate geometry parallel to the strike of the orogen. Rotational components during convergence are usually neglected because changing directions of shortening through time hinder interpretation and balancing of sections. Nevertheless, rotations are extremely important in orogeny, both on the local and on the orogen scale (Allerton, 1998). This study aims to document the Mesozoic to Cenozoic rotational history of parts of the NW Tethyan realm, i.e. the Alpine part of the Adriatic microplate, which is identical to the Austroalpine units of the Eastern Alps together with the Southern Alps (Froitzheim et al., 1996). Focused on the NW-Tethyan realm data acquisition during this PhD-thesis was concentrating on Mesozoic carbonates of Northern Calcareous Alps, the Southern Alps, the autochthonous cover of the distal European continental rim and on Cenozoic sediments which were sampled in the synorogenic north- and south-Alpine foreland basins. Results from the Central Alps enabled a kinematic link between Northern Calcareous Alps (NCA) and Southern Alps. These data are interpreted in a larger frame and are therefore compared to data from the autochthonous Adriatic plate, the Western Alps and stable Europe.

2. Geological setting

2.1. Apulian plate north of the Periadriatic line: Austroalpine nappe system

The term “Apulian plate” denotes the continental paleogeograhic realm situated south of the Alpine Tethys (Piedmont-Liguria Ocean) and north of Neotethys. Hence this term also includes the Southern foreland of the Alps. North of the Periadriatic line remnants of the Apulian Plate are only preserved in the form of basement and cover slices (Austroalpine nappes). Moreover Apulia was bordered to the east by a westwards closing oceanic embayment that formed in Triassic times, referred to as Meliata Ocean. Only after closure of the Meliata Ocean during the Cretaceous orogeny, did Apulia behave as a coherent block (Schmid et al., 2004).

The Alpine orogenic belt in its present shape is a result of Eocene to Oligocene collision of the Apulian plate with the Lower European plate. As a consequence of that collision the load of the thickened crust caused flexural bending of the lower plate and thus formation of the Alpine peripheral foreland basin (e.g. Lemcke, 1984). Prior to continental collision the Penninic Ocean, which separated the two plates between the Early Jurassic and the Eocene, was subducted below the Apulian plate.

Along the northern margin of the Apulian plate, the Northern Calcareous Alps form a thin-skinned foreland fold-and-thrust belt built mainly of Mesozoic rocks (e.g. Linzer et al., 1995). The thin-skinned units are partly still in contact with their basement units along their southern margin, which are Paleozoic low-grade metamorphic rocks (Greywacke zone). The Northern Calcareous Alps and their basement are tectonically underlain by Paleozoic and older polymetamorphic rocks, which are part of a thick-skinned nappe stack (Innsbruck Quartzphyllite unit; Ötztal, Silvretta and Campo basement units), which formed during an older, Cretaceous orogeny, (Eoalpine event). Thin and thick skinned nappes together form the so called Austroalpine nappes. The geometry of the Cretaceous nappe stack did not significantly change during Eocene/Oligocene continental collision, when it moved as a rigid block over tectonically deeper units ("orogenic lid"; Laubscher, 1988).

These Austroalpine nappes may be subdivided into the Lower Austroalpine (former NW passive margin of the Austroalpine-Apulian continent), the Northern Calcareous Alps, and the Central Austroalpine (= all nappes above the Lower Austroalpine, south of the NCA, and N of the Periadriatic Fault). The Central Austroalpine is subdivided into an upper part with only anchizonal to greenschist-facies Cretaceous metamorphism (UCA=Upper Central Austroalpine, including Northern Greywacke Zone, Gurktal nappes, Graz Paleozoic etc.), and a lower part (LCA=Lower Central Austroalpine) with stronger Cretaceous metamorphism, including eclogite-bearing nappes in Koralpe, Saualpe, Pohorje, etc. The Bajuvaric nappes of the Northern Calcareous Alps are locally connected by transgressive contacts with the LCA (Phyllitgneis Zone /Silvretta nappe), and the Tirolic nappes with the UCA (Greywacke Zone) (Froitzheim, 2007; Janák et al., 2004). In the western part of the Northern Calcareous Alps the Bajuvaric unit is further subdivided into the Allgäu and the tectonically higher Lechtal nappes, whereas the Inntal nappe is thought to be part of the Tirolic nappe complex (Tollmann, 1976) (Ortner et al., 2006).

During Cretaceous orogeny, the UCA represented the upper plate, and the LCA the lower plate of a southeast-dipping intra-continental subduction zone. It does not coincide with the suture of the Meliata Ocean, neither in space (the Cretaceous subduction boundary is below the UCA, whereas the Meliata suture was originally above the Tirolic nappes and therefore above the UCA) (Frisch and Gawlick, 2003; Gawlick et al., 2007); nor in time (high-P metamorphism took place in the Meliata rocks at c. 150 Ma, in the LCA at c. 95-90 Ma). Moreover, no relics of Meliata oceanic crust are found between LCA and UCA. Permian gabbros in the LCA, e.g. in Koralpe, are not related to Meliata (which opened in the Middle Triassic) but to the widespread Permian rifting event affecting all paleogeographic units of the Alps (Froitzheim, 2007).

Post-collisional deformation, however, changed the geometry of the nappe stack strongly: The metamorphic core complex of the Tauern window formed by stacking of crustal flakes of the subducting European plate during the Oligocene and Miocene (Lammerer and Weger, 1998). These tectonically deepest units of the Eastern Alps exposed e.g. in the Tauern window are referred to as Penninic units. Stacking of crustal flakes during the Miocene was combined with major orogen-parallel extension (e.g. Ratschbacher et al., 1991, Lammerer and Weger, 1998). Eastward moving crustal blocks were delimited by a system of steep faults diverging to the east, which obliquely cut through the Alpine nappe stack (Ratschbacher et al., 1991).

2.2. Apulian plate south of the Periadriatic line: Southern Alps and Adriatic indenter

Together with the external Dinarides, the Southern Alps represent that part of the Apulian Plate which is located south of the Periadriatic lineament, and that is often referred to as “Adriatic micro-plate” or “Adriatic indenter” (part of the greater Apulian Plate) (Schmid et al., 2004).

The Alpine geological history of the Southern Alps is directly connected to the evolution of the Alpine Jurassic Tethys. In fact, the Southern Alps are considered to be a significant preserved portion of the S continental margin of the oceanic Tethys. In the Southern Alps the synsedimentary extensional tectonics of the Norian-Liassic continental rifting up to the emplacement of the initial oceanic crust has been recognized in the whole Southern Alpine area (Bosellini, 1973; Bernoulli et al., 1979; Winterer and Bosellini, 1981; Bertotti et al., 1993).

At the end of the Early Cretaceous a basic change occurred in the kinematics of the plates, which inverted their motion. It corresponds to the beginning of the continental margin convergence, which controlled the subsequent pre-collisional, collisional and post-collisional evolution of the Alps up to their present setting (see Coward and Dietrich, 1989; Roure et al., 1990a; Dal Piaz, 1995) (Castellarin and Cantelli, 2000).

The Eastern Alps include the following main compression events: the Upper Cretaceous pre-collision with oceanic lithosphere subduction; the Eocene continental margin collision and the Paleogene–Neogene post-collision (Neo-Alpine phase) (Dal Piaz, 1999). The Cretaceous compressive events do not have any structural indication in the Venetian and eastern Southern Alps. They are revealed only by the Upper Cretaceous local change in the marine sedimentation with siliciclastic inputs in the basinal areas. Intense Eocene tectonic deformation, related to the ongoing collision, affected the Carnic Alps and the eastern sector of the Dolomites (Doglioni, 1987) (Castellarin et al., 2006). The Lower Eocene siliciclastic Flysch filling the Friuli and the Belluno zones (Bigi et al., 1990) is the sedimentary marker of these processes. This oldest structural system corresponds to the Mesoalpine (Eocene) and early Neoalpine (Oligomiocene) compressional events, which originated the Dinaric system (NW-SE trending). The subsequent tectonic belt is the Valsugana structural system, ENE-WSW trending, Serravallian- Tortonian in age. The intense activity of this compressional event is documented both by stratigraphic and structural data and by Fission track studies, which indicate uplifting of some 4 km in the hangingwall of the Valsugana overthrust between 12 and 8 Ma B.P. The more external structures NE-SW trending, are located in the Montell- Friuli zone, which were generated by the Messinian- Pliocene compressions (whose principal stress axis is SE / NW oriented) (Castellarin and Cantelli, 2000).

3. Fundamentals

This glossary, taken from the paper "Glossary of basic paleomagnetic and rock magnetic terms" by Morris (2003), attempts to cover most of the terms used in this study. For full and detailed treatments of palaeomagnetic methodology and practice, see Collinson (1983), Tarling (1983), O'Reilly (1984), Piper (1987), Butler (1992), Van der Voo (1993), Dunlop and Özdemir (1997) and Tauxe (1998).

α_{95} : The semi-angle of the cone of 95% confidence surrounding a mean direction of magnetization or pole positions.

Alternating field (AF) demagnetization: This is carried out by subjecting a specimen to an alternating magnetic field of gradually decreasing magnitude in the presence of a zero direct magnetic field. The alternating field is produced by passing an alternating current through a coil. All magnetic grains with coercivities less than the peak applied field will have their magnetizations pulled into alignment with the alternating magnetic field. As the magnitude of the applied field decreases during each alternating cycle, a fraction of the magnetic grains present in the specimen will cease to be affected by the field. Approximately half of these grains will be left with their magnetizations aligned along their preferred axes (see Domains) with a component along the axis of the demagnetizer coil, with the other half having a component in the opposite direction. The total magnetic moments of these grains will approximately cancel out. Subsequent cycles result in cancelling out of the magnetizations of successively lower and lower coercivity fractions. AF demagnetization is most effective for rocks in which magnetite or titanomagnetite is the dominant ferromagnetic mineral present. An advantage of the technique is that it does not produce chemical alteration in a specimen, which is a common problem with thermal demagnetization. AF treatment, however, is ineffective in demagnetizing rocks where the remanence is carried by haematite or goethite, which have coercivities that exceed those of most AF demagnetization systems.

Anisotropy of magnetic susceptibility (AMS): A property of a material whereby identical magnetic fields applied in different directions produce different intensities of induced magnetization. AMS reflects the statistical alignment of platy or elongate magnetic (usually ferromagnetic) grains. AMS is defined in terms of the magnetic susceptibility ellipsoid, which has principal axes along the directions of maximum (k1), intermediate (k2) and minimum (k3) susceptibility.

If k1 = k2 = k3, the ellipsoid is spherical and the specimen has an isotropic magnetic susceptibility. If k1 ~ k2 > k3 , the ellipsoid is oblate (disc-shaped). If k1 > k2 ~ k3, the ellipsoid is prolate (cigar-shaped). Oblate susceptibility ellipsoids are commonly observed in sedimentary rocks and in rocks with a significant foliation, with k3 oriented perpendicular to the bedding and foliation, respectively. Prolate ellipsoids can be observed in volcanic lava flows and current-deposited sediments, where k1 is aligned parallel to the palaeoflow direction. Significant AMS can also be produced during straining of rocks, and has been used to infer the orientation of the strain ellipsoid (e.g., Kligfield et al., 1983). Anisotropy of remanent magnetization is also of interest in palaeomagnetic studies. A full treatment of anisotropies of susceptibility and remanent magnetization is given in Tarling and Hrouda (1993).

Apparent polar wander path (APWP): A plot of sequential positions of palaeomagnetic poles from a particular lithospheric plate or tectonostratigraphic terrane, usually presented on the present-day geographic grid. APWPs allow presentation of palaeomagnetic data covering significant periods of geological time. Comparison of APWPs from different continents and terranes allows documentation of the timing of continental and terrane separation and collision (docking). APWPs also form the basis for one method of magnetic dating, whereby poles obtained from a unit of uncertain age are compared with well-dated poles from an appropriate reference APWP (e.g., Najman et al., 1994).

Blocking temperature: Magnetic relaxation time is exponentially inversely proportional to temperature. For any given volume of an SD grain of a certain composition, there is a temperature above which relaxation times are so short that the grain cannot hold a fixed magnetization direction on a laboratory timescale and displays superparamagnetism.
As the grain cools below this temperature, it exhibits stable SD behaviour. This transition temperature is called the blocking temperature. At temperatures between the Curie temperature and the blocking temperature, the grain is ferromagnetic but the remanent magnetization of an assemblage of such grains will quickly decay to zero. Below the blocking temperature, the remanent magnetization rapidly becomes increasingly stable as relaxation times increase dramatically with decreasing temperature. Relaxation time and blocking temperature are fundamental to theories of thermoremanent magnetization.

Blocking volume: Magnetic relaxation time is directly proportional to grain volume. Above the blocking volume, a grain exhibits SD (Single-domain) behaviour and the remanent magnetization of an assemblage of such grains can be stable. Relaxation time and blocking volume are fundamental to theories of chemical remanent magnetization.

Characteristic Remanent Magnetization (ChRM): The highest-stability component of NRM isolated during demagnetization. Unlike the term primary remanence, ChRM does not imply a time of acquisition of the magnetic component.

Chemical Remanent Magnetization (CRM): A magnetic remanence acquired as a ferromagnetic grain nucleates and grows below the Curie temperature in the presence of a magnetic field. For a palaeomagnetically useful stable remanence to be acquired, grains must only grow to stable SD(Single-domain) or PSD(Pseudosingle-domain) size and no greater. Reactions which produce a CRM include: (i) alteration of an existing mineral to a ferromagnetic mineral; and (ii) direct precipitation of a ferromagnetic mineral from solution (Butler,1992).

Coercivity: Magnetic grains are magnetized along 'easy' axes. The coercivity of an SD grain is the magnetic field, which must be applied to force its magnetization to flip direction by 180° (i.e., to result in a 'permanent' change in direction of magnetization upon removal of the field).

Coercivity of remanence: If successively increasing fields are first applied and then removed in the direction opposite to the saturation IRM until the IRM is reduced to zero, then the "backfield" required to reduce this to zero is called the coercivity of remanence (H_{cr}) (McElhinny and McFadden, 2000).

Curie temperature: The temperature above which ferro- and ferrimagnetic substances behave paramagnetically. Since interatomic distances increase upon heating, the strength of exchange coupling between atomic magnetic moments decreases with increasing temperature, thereby reducing the resultant magnetization. At the Curie temperature, interatomic distances become so great that exchange coupling breaks down, the atomic magnetic moments become independent, and the material exhibits paramagnetism. Upon cooling below the Curie temperature exchange coupling and ferro- or ferrimagnetism reappear.

Curie temperatures of the two most common palaeomagnetic carriers are 580 °C for magnetite and680 °C for haematite.

Declination: The horizontal angle between either amagnetization vector or the Earth's magnetic field and geographic north.

Detrital Remanent Magnetization (DRM): A remanent magnetization acquired during deposition and lithification of sedimentary rocks. The most common ferromagnetic carrier of DRM is detrital magnetite. DRM acquisition is a complex process affected by depositional environment and post-depositional disturbances such as bioturbation. Detrital remanences can be subdivided into those produced by physical alignment of ferromagnetic particles with the ambient geomagnetic field during deposition (referred to as depositional detrital remanent magnetizations), and those arising from post-depositional alignment (referred to as post-depositional detrital remanent magnetizations or PDRMs). The total DRM observed in a sedimentary rock usually results from a combination of depositional and post depositional alignments. Finegrained sediments are more accurate recorders of the geomagnetic field direction during (or soon after) deposition since they contain a high proportion of stable single-domain and pseudo-single-domain grains, and these finer grains are likely to have strong magnetizations and are hence more effectively aligned by the geomagnetic field. Larger multi-domain grains are less stable. They are also less likely to move freely within pore spaces in a water-saturated sediment, and are therefore less effectively aligned by either depositional or post-depositional processes. For these reasons, fine-grained sediments such as siltstones are widely sampled for palaeomagnetic study.

Diamagnetism: In diamagnetic substances, the application of an external magnetic field produces a small induced magnetization in the opposite direction to the applied field. The magnetization is proportional to the applied field, and decays to zero when the field is removed. Magnetic susceptibility for a diamagnetic substance is negative. Examples of diamagnetic minerals are quartz, calcite and dolomite.

Domains: The magnetization within a small region within a ferromagnetic grain is uniform in direction and has a preferred orientation, aligned either along specific crystallographic axes, known as magnetocrystalline 'easy' axes or along the length of the grain (for small, elongate grains).

These axes are referred to as 'preferred axes'. In larger grains (e.g., >10 μm), however, a number of volume elements are present, each of which has its magnetization aligned along a preferred axis. These volume elements are called magnetic domains. The domains form an arrangement, which minimises the total magnetic energy of the grain.

Ferromagnetism: Ferromagnetism (sensu lato) refers to all solids with exchange coupling of atomic magnetic moments, including materials displaying antiferromagnetism and ferrimagnetism. Ferromagnetism (sensu stricto) describes the behaviour of solids with parallel coupling between adjacent layers of atomic magnetic moments, producing a strong magnetization (even in the absence of an external magnetic field).

Geocentric axial dipole (GAD): A fundamental assumption of the palaeomagnetic method is that the time-averaged geomagnetic field can be modelled by a single magnetic dipole at the centre of the Earth which is aligned along the rotation axis, the geocentric axial dipole (GAD) model. The magnetic field inclination in this model is related to geographic latitude by the dipole equation: $\tan I = 2 \tan \lambda$. The declination of the field is zero everywhere. This model does not describe the present geomagnetic field, which is more closely modelled by a geocentric dipole inclined at 11.5° to the rotation axis. This best fitting inclined dipole accounts for approximately 90% of the present geomagnetic field at the surface. The remaining c. 5% is called the non-dipole field. However, palaeomagnetic records spanning the last 5 million years show that the average position of the geomagnetic pole is indistinguishable from the rotation axis. Thus, over periods sufficient to average out secular variation (c.10^5years) the geomagnetic field appears to be adequately described by the GAD model. The GAD assumption is equally valid for periods of normal and reversed polarity of the geomagnetic field, but does not apply to periods when the field is transitional between the two polarity states. The GAD model cannot be used to interpret components of remanence acquired during such transitions.

Goethite: An oxyhydroxide of iron with the composition αFeOOH, which displays imperfect antiferromagnetism or weak ferromagnetism. It has a very high coercivity of >5 T with a low maximum unblocking temperature of 80–120 °C. Natural dehydration of goethite produces haematite which acquires a chemical remanent magnetization (CRM) by grain growth, and is an important process in the magnetization of red beds.

Goethite is common in limestones, and forms by either direct precipitation from seawater or by diagenetic alteration or subaerial weathering of pyrite. The dehydration of goethite to haematite at 300–400 °C produces complications during laboratory thermal demagnetization. The presence of goethite is easy to establish using IRM acquisition experiments (see Isothermal remanent magnetization) in high applied fields, since it has a higher coercivity than haematite. It can also be distinguished by a rapid intensity decrease by 120 °C during thermal demagnetization of NRM or IRM.

Haematite: A mineral with the composition αFe_2O_3 with hexagonal structure. Atomic magnetic moments of Fe^{3+}cations are parallel coupled within basal planes, but adjacent layers of cations are approximately anti-parallel coupled. A net magnetization in the basal plane arises from this imperfect anti-parallel coupling. The resulting imperfect antiferromagnetism is referred to as canted antiferromagnetism. In addition, some naturally occurring haematite has a defect ferromagnetism caused by lattice defects or impurities. The overall effect is one of weak but very stable ferromagnetism. Haematite has a maximum unblocking temperature of 675 °C and a maximum coercivity of 1.5–5.0 T (O'Reilly, 1984; Lowrie,1990). Haematite can be the dominant ferromagnetic material in highly silicic and/or highly oxidised igneous rocks, and is nearly always the dominant ferromagnetic material in red beds (Butler, 1992).

Inclination: The angle between either a magnetization vector or the Earth's magnetic field and the horizontal plane.

Isothermal Remanent Magnetization (IRM): An artificial magnetization imparted by subjecting a specimen to a direct magnetic field in the laboratory. IRMs are also produced naturally by lightning strikes. Laboratory IRMs are used extensively to determine the nature of the magnetic minerals which are capable of carrying a natural remanence in a specimen. The standard procedure is to apply progressively increasing magnetic fields to a specimen, measuring the IRM produced after each field application. The shape of the resulting graph of IRM against applied field is characteristic for different ferromagnetic minerals. For example, rapid increases in IRM and subsequent flattening off of the curve (saturation) by applied fields of 100–300 mT indicate the presence of magnetite, titanomagnetite or maghemite. In contrast, haematite does not reach saturation until 1.5 –5.0 T, whereas goethite only saturates in applied fields greater than 5.0 T.

The interpretation of these curves can be improved by stepwise thermal demagnetization of the acquired IRM, particularly if three different fields are applied along the three orthogonal axes of a specimen (Lowrie, 1990), thereby allowing unblocking temperature spectra to be deduced for different coercivity fractions of IRM.

Maghemite: A ferromagnetic mineral (γFe_2O_3) with the composition of haematite but the cubic(spinel) structure of magnetite. It forms by low-temperature (< 200 °C) oxidation of magnetite during subaerial or subaqueous weathering. It has a maximum coercivity of 300 mT (O'Reilly, 1984), equivalent to that of magnetite. It is destroyed by heating to350 °C when it inverts to haematite.

Cryogenic magnetometer: These are the most sensitive magnetometers available. They employ a magnetic field sensor called a SQUID (acronym for Superconducting QUantum Interference Device), which operates at liquid helium temperatures. They are capable of measuring magnetic moments of the order of 10^{-10} Am^2. Full details of principles of cryogenic magnetometers are given by Collinson (1983).

Natural Remanent Magnetization (NRM): The summation of all components of magnetic remanence acquired by natural processes. The NRM of a specimen can consist of several components (a multi-component remanence) acquired at different times during its history.
For example, the NRM of a lava may comprise a primary thermoremanent magnetization, a secondary magnetization acquired during low-grade metamorphism, and a viscous remanent magnetization acquired in the present-day field. Components of magnetization are separated in laboratory studies using stepwise (progressive) demagnetization.

Orthogonal demagnetization diagram: The most common method of displaying the variations in intensity and direction of magnetization of a sample resulting from progressive demagnetization. The data from each demagnetization step are plotted as points on two sets of superimposed axes. The N and E Cartesian components of magnetization are plotted on N–S/E–W axes. The projection of the vertical Cartesian component of magnetization Z is plotted on to either N–S/Up–Down or E–W/Up–Down axes. Successive points are usually joined by straight lines. The angle subtended by each point with the N axis is the declination. The angle between each point and the horizontal in the vertical plane gives the apparent inclination.

The distance of each point from the origin is proportional to the intensity of the component of magnetization plotted on to that plane. A linear segment in the demagnetization path defined by a number of successive points on these plots indicates demagnetization of a single component of magnetization with a constant direction (or conceivably two components of magnetization with identical unblocking temperature or coercivity spectra). The declination and inclination of successively removed components can be easily calculated. Partial overlap of unblocking temperature or coercivity spectra of two components produces curved demagnetization paths, and may require the use of great circle analysis to determine the magnetization direction(s).

Paramagnetism: Describes the behaviour of solids containing atoms with atomic magnetic moments but where no interaction occurs between adjacent atomic moments. The atomic magnetic moments oscillate rapidly and randomly in orientation at any temperature above absolute zero, producing no net magnetization in the absence of an applied magnetic field. Application of a magnetic field exerts an aligning torque on the atomic magnetic moments, but this is effectively overcome by thermal energy (even at room temperature) and only a small net magnetization is produced. The magnetization disappears when the field is removed. Paramagnetic minerals have a positive susceptibility. Examples are pyroxenes and olivine.

Primary magnetization: That component of magnetisation acquired at the time of formation of a rock unit. For igneous rocks the primary magnetization is the TRM acquired during initial cooling, whereas for sedimentary rocks it is the DRM acquired during deposition. In general, it is difficult to prove whether a characteristic magnetization (ChRM) isolated by demagnetization is the true primary remanence in a sampled rock unit. Fold tests can only be used to identify the timing of remanence acquisition relative to deformation (pre- or post-folding), and cases of pre-folding remagnetization have been reported. Most interpretations of ChRM directions as primary magnetizations are therefore based on assumption.

Pyrrhotite: A ferrimagnetic iron sulphide with monoclinic crystal structure and composition in the range Fe_7S_8 to Fe_9S_{10}. It has a maximum unblocking temperature of 325 °C and a maximum coercivity of 0.5 –1.0 T. Pyrrhotite forms during diagenesis of marine sediments and in contact metamorphic aureoles.

Reference direction: The expected magnetization direction at a site or locality, usually derived from a coeval reference pole obtained outside the area of interest (normally from a stable region outside the deformed zone under study).

Secondary magnetization (or overprint): Any component of magnetization which was acquired subsequent to initial formation of a rock unit. Secondary magnetizations can be produced by a wide variety of mechanisms, including: reheating events (e.g., burial and subsequent exhumation) giving rise to thermoviscous remanent magnetizations; chemical alteration (e.g., by orogenic fluids or during weathering) producing CRMs; lightning strikes, which impart an IRM; and acquisition of viscous magnetization (VRM) by exposure to the geomagnetic field. Secondary magnetizations may be distinguished using a variety of field tests (e.g., Morris and Robertson, 1993). Demagnetization (magnetic cleaning) of the natural remanence (NRM) can be used to remove such secondary components, as they will normally have a different stability to thermal or AF demagnetization than the primary magnetization component.

Susceptibility: A measure of the ease with which a material can be magnetized. In magnetic fields as weak as the Earth's, the magnetization J_i induced in a material is directly proportional to the field strength H. The constant of proportionality is called the magnetic Susceptibility κ (i.e., $\kappa = J_i /H$), and is dimensionless in SI units. The determination of susceptibility is useful for an estimate of the total magnetic content of a specimen (see Thompson and Oldfield, 1986), and as an important monitor of thermochemical changes during thermal demagnetization. See also Anisotropy of magnetic susceptibility.

Thermal demagnetization: Involves heating a specimen to an elevated temperature and then cooling to room temperature in zero magnetic field. The magnetizations of all ferromagnetic grains within the specimen with unblocking temperatures less than or equal to the demagnetization temperature are randomised upon heating. In the absence of a magnetic field, the magnetizations retain this random distribution upon subsequent cooling. A stepwise demagnetization procedure is usually followed, with successively increasing temperatures demagnetizing successively higher unblocking temperature fractions. In addition to being able to demagnetize magnetite and titanomagnetite, thermal demagnetization is effective in removing magnetization components carried by haematite and goethite, which usually have coercivities exceeding the maximum field produced by AF demagnetization apparatus.

Problems can arise from thermochemical alteration of specimens at high temperatures, with resulting production of new magnetic phases (e.g., pyrite altering to magnetite at 350–500 °C). To monitor such changes, the magnetic susceptibility of specimens is routinely measured after each heating step, as any change in susceptibility indicates the destruction or creation of magnetic minerals.

Thermoremanent magnetization (TRM): A remanent magnetization acquired upon cooling from temperatures above the Curie temperature in the presence of a magnetic field. Most igneous rocks acquire a TRM during initial cooling. A range of blocking temperatures, distributed downward from the Curie temperature, will be present in the rock due to a distribution of ferromagnetic grain sizes and compositions.

Titanomagnetites: Ferrimagnetic minerals of the composition $Fe_{3-x}Ti_xO_4$ (where $0 < x < 1$), ranging from magnetite (Fe_3O_4) to ulvöspinel (Fe_2TiO_4). They have a cubic (spinel) structure at room temperature and form a solid–solution series at temperatures above 800°C. Under slow cooling conditions, the high-temperature solid solution unmixes or exsolves into fairly pure magnetite and either ilmenite or ulvöspinel, of which only magnetite is magnetic at room temperature (Tarling, 1983). Rapid cooling can, however, preserve intermediate titanomagnetite compositions. The end-member magnetite has a maximum unblocking temperature of 575 °C and a maximum coercivity of 300mT. Maximum unblocking temperatures and coercivities of titanomagnetites both decrease with increasing Ti content, being 350 °C and 200 mT, respectively, for x = 0.3, and 150 °C and 100 mT, respectively, for x = 0.6 (O'Reilly, 1984; Lowrie, 1990).

Unblocking temperature: The temperature at which a component of magnetization in a specimen becomes thermally demagnetized in a laboratory experiment. Unblocking occurs during laboratory heating when the relaxation times of the grains carrying the magnetization become equivalent to the length of time at which the specimen is held at elevated temperature.

4. Sampling sites

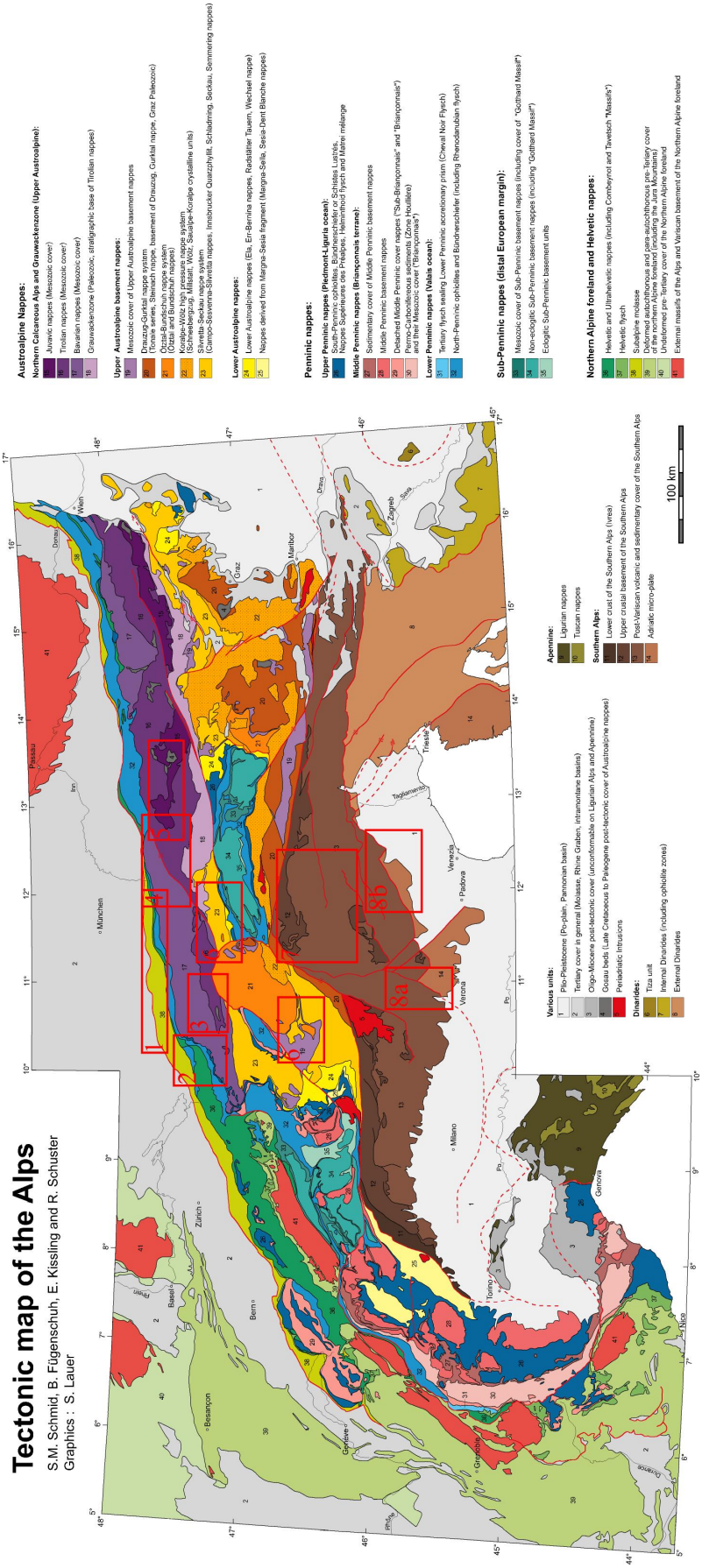

Fig. 1. Geological sketch of the Western, Eastern and Southern Alps (Schmid et al., 2004) with structural units sampled during this study. Red frames indicate sampling areas. Numbering of the frames refers to Tab.1. Frames 8a and 8b mark the sampling areas of Lake Garda and Belluno/Follina, respectively.

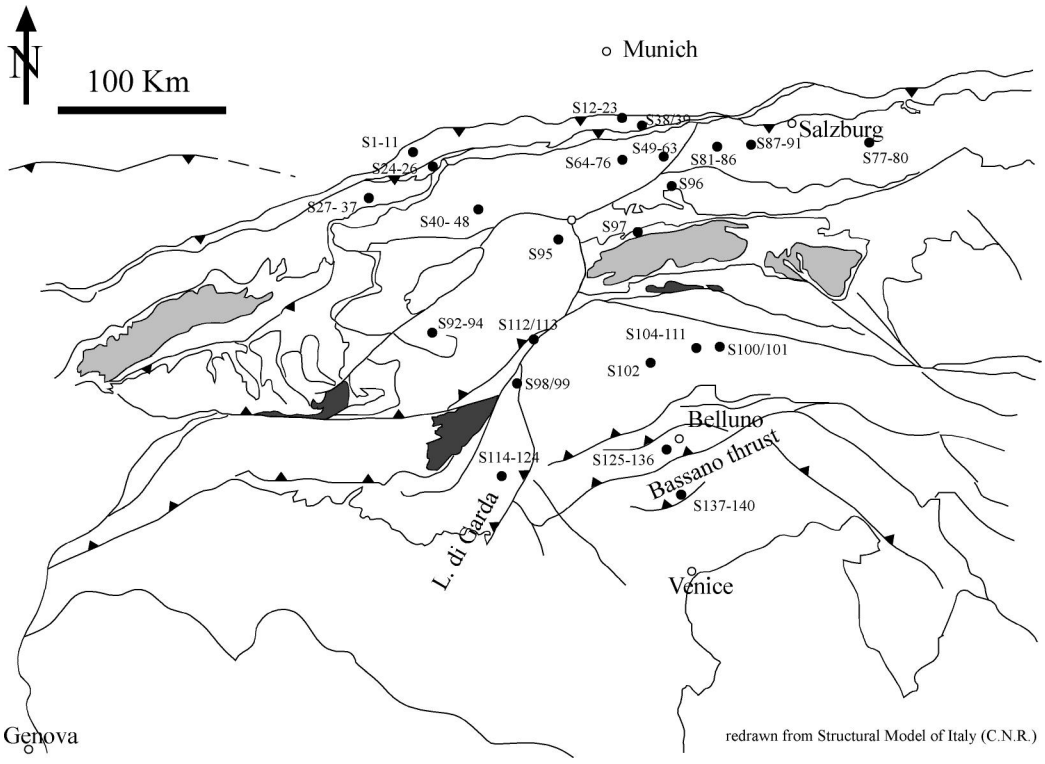

Fig. 2. **A**: Geological sketch of the Eastern and Southern Alps with structural units sampled during this study. S(ite) numbers refer to Tab.1.

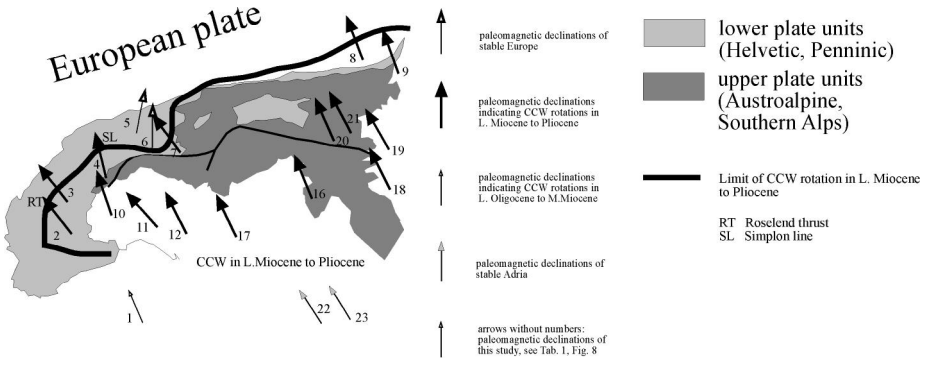

Fig. 2B: Geological sketch of the Western, Eastern and Southern Alps with paleomagnetic results from previous studies. Locality numbers refer to Tab.2.

4.1. Northern Alpine foreland basin

4.1.1. Western part- Allgäu area

The Northern Alpine foreland basin (NAFB) can be divided into an autochthonous part north of the Alpine front and an allochthonous part south of it (Vollmayr, 1958; Grottenthaler, 1966; Stephan & Hesse, 1966; Pflaumann & Stephan, 1968; Vollmayr & Ziegler, 1976; Schwerd et al., 1983). Sampling focused on both parts to identify possible different kinematics. Two sites from the northern, autochthonous part of the Molasse basin at locality Enschenstein yielded results (Tab.1, sites 1,2; Fig.1,2). These silt/sandstones of Late Aquitanian to Burdigalian age represent the transition from the Kojen beds of the Lower Freshwater Molasse (LFM) to the Upper Marine Molasse (UMM) (Kuhlemann and Kempf, 2001; Richter, 1978; Jürges, 1970).

From the southern, the allochthonous part, results were derived from 9 sites. The stratigraphy of the sampled sites ranges from Rupelian Lower Marine Molasse (LMM) to Upper Aquitanian Lower Freshwater Molasse (LFM) (Mulheim, 1934; Scholz, 1993, 1999, 2000). In the northernmost allochthonous Molasse slice at the northern limb of the Salmaser synform, marls from the Upper Aquitanian Lower Freshwater Molasse (LFM) were sampled at locality Sulzberg (Tab.1, site 3; Fig.1,2). The southerly juxtaposed Horn synform, yielded results from 3 sites that were sampled at its northern limb. 2 sites from Horn synform at locality Littenbach (Tab.1, site 4,5; Fig.1,2) comprise silt/sandstones from Chattian Lower Freshwater Molasse (LFM). At locality Krumbach also from Horn synform 1 site (Tab.1, site 6; Fig.1,2) in Rupelian to Chattian Baustein beds of the Lower Marine Molasse (LMM) was sampled. Steineberg syncform is the southernmost allochthonous Molasse slice. At the northern limb 4 sites from locality Eibele Alm yielded results. Silt/sandstones of the Rupelian/ Chattian Baustein beds and Rupelian marls, both belonging to the Lower Marine Molasse were sampled as well as silt/sandstones from the Lower Freshwater Molasse of Early Chattian Weißach beds and of Early Late Chattian Steigbach beds (Tab.1, sites 7-10; Fig.1,2).

At the southern, overturned limb of the Steineberg syncline 1 site, located in the Rupelian marls of the Lower Marine Molasse (Tab.1, site 11; Fig.1,2) yielded results.

4.1.2. Eastern part- Schliersee area

Similar to the western part of the Northern Alpine foreland basin (NAFB) also in the vicinity of Schliersee sampling focused on a N/S striking cross section, including the transition from the northern, undeformed, autochthonous to the southern, deformed, allochthonous Molasse units.

North of the Alpine front, at locality Karlingergraben/Mangfall 2 sites from Serravallian marls of the Upper Freshwater Molasse (UFM) yielded results (Tab.1, sites 12,13; Fig.1,2). South of the frontal Alpine thrust sampling focused on both limbs of the Miesbach syncline (Stephan and Hesse, 1966). From the northern limb results were derived from 2 sites of Latest Chattian Cyrena beds, belonging to the Lower Freshwater Molasse (Tab.1, sites 14,15; Fig.1,2). At the southern limb 1 site of Early Late Chattian silt/sandstones of the ”Sattelflözgruppe” could be demagnetized successfully (Tab.1, site 16; Fig.1,2). These units belong to the Lower Freshwater Molasse. Further to the south sampling focused on both limbs of the Hausham syncline (Pflaumann and Stephan, 1968). 4 sites yielded results at the northern limb (Tab.1, sites 17-20; Fig.1,2). 2 sites were sampled in Rupelian marls, silt/sandstones of Late Rupelian Baustein beds and Early Chattian Flöz group were sampled each in 1 site. The Rupelian lithologies belong to the Lower Marine Molasse, the Chattian Flöz group to the Lower Freshwater Molasse.

The overturned southern limb was sampled in 3 sites (Tab.1, sites 21-23; Fig.1,2) comprising a similar stratigraphy. One site in Rupelian marls of the Lower Marine Molasse yielded results as well as 2 sites in silt/sandstones from the Early Chattian Flöz group that belong to the Lower Freshwater Molasse (LFM).

4.2. Helvetic units

4.2.1. Western Helvetic units

Sampling in the western Helvetic units focused on the northern Allgäu area with one locality and the Bregenzer Wald area to the south with 3 localities.

In the Allgäu area 3 sites from a stratigraphic section at locality Starzlachklamm (Tab.1, sites 24-26; Fig.1,2) yielded results. Carbonates and marls of the Campanian to Maastrichtian Wang Fm. were sampled in 2 sites. The Late Maastrichtian Dreiangelserie was sampled in 1 site (Schwerd et al., 1983; Freudenberger and Schwerd, 1996).

In the northernmost Bregenzer Wald area, results were derived from an anticlinal deformed stratigraphic section south of Schwarzenberg. 4 sites from individual stratigraphic units, located at the northern limb yielded results (Tab.1, sites 27-30; Fig.1,2). From the southern limb no results could be derived. The stratigraphy at the northern limb ranges from Late Berrisianian Örfla Fm., Barremian Drusberg Fm., Barremian/Aptian Schrattenkalk to Coniancian/ Campanian Amdener marls (Wyssling, 1986). 3 sites from 3 different localities yielded results at southerly juxtaposed Kanisfluh/ Mittagsfluh anticline (Felber and Wyssling, 1979; Freudenberger and Schwerd, 1996). Malmian Quinten Fm. from the southern limb was sampled at locality Au. Tithonian/Berriasian Zementstein Fm. and Barremian Drusberg Fm. were sampled in the northern limb at localities Ortberg/Vorsäß and Schnepfegg (Tab.1, sites 31-33; Fig.1,2).

In the southernmost Bregenzer Wald area an anticline-syncline structure was sampled at locality Sünserspitze (Felber and Wyssling, 1979). 4 sites from 3 limbs of the tectonic structure yielded results (Tab.1, sites 34-37; Fig.1,2). Results from 1 site in Aptian Mittagsspitz beds were derived from the southern anticlinal limb. 1 site in the northern anticlinal/southern synclinal limb was sampled in Maastrichtian Leimern Fm. The northern synclinal limb was sampled in 2 sites in Maastrichtian Leimern Fm. and Early Eocene Schelpen group.

4.2.2. Eastern Helvetic units

West of Hausham sampling of Helvetic units focused on a stratigraphic section near Ostin (U. Haas, pers. comm.; Stephan and Hesse, 1966). Only 2 sites from Barremian/Aptian Schrattenkalk Fm. and Late Cenomanian/Coniancian Seewerkalk Fm. yielded results (Tab.1, sites 38,39; Fig.1,2).

4.3. Penninic units

Penninic units were sampled in a stratigraphic section south of Schliersee. Due to extreme weak magnetizations no results could be derived.

4.4. Northern Calcareous Alps

4.4.1. Western Northern Calcareous Alps

4.4.1.1. Western Northern Calcareous Alps (western part)

Santonian marls from the westernmost part of the Northern Calcareous Alps yielded results at locality Muttekopf (Tab.1, site 40; Fig.1,2). This locality placed in the Inntal nappe, is characterized by a northward overturned syncline with a fold axis trending WSW-ENE (fold axis 71/25). The final stage of folding is not reached before the Paleocene (Ortner, 2001). From both limbs of this syncline, 6 sites were chosen in Coniacian neritic to Santonian deep marine marls.

Results from Jurassic to Early Cretaceous sediments were derived from stratigraphic sections Lähnbach (Tab.1, sites 41-45; Fig.1,2) and Kotbach (Tab.1, sites 46-48; Fig.1,2), both belonging to the Lechtal nappe, located west and south of Zugspitz massive, close to Puitental zone (Eisbacher and Brander, 1995; Eisbacher and Brander, 1996). Bedding in section Lähnbach is tilted towards N about an E/W trending fold axis. Minor deformation is also contributed by a NNW/SSE striking fold axis. Results were derived from carbonates of the Middle Liassic Lower Allgäu Fm., radiolarites of the Oxfordian Ruhpolding Fm. and carbonates of the Malmian Lower and Upper Ammergau Fm. Each stratigraphic unit was sampled in 1 site, the Lower Ammergau Fm. in 2 sites.

Section Kotbach is tilted 90° about a horizontal, E/W trending fold axis. This section exhibits the contact aureole of a radiometrically-dated (Trommsdorf et al., 1990) Albian (100Ma) sill and the adjacent country rocks of Oxfordian Ruhpolding Fm. and Tithonian Ammergau Fm. All 3 sites yielded results.

4.4.1.2. Western Northern Calcareous Alps (central part)

Inside and south of the Inn valley fault system Oligocene sediments were sampled at 4 localities (Tab. 1). Chattian fluvial sandstones were sampled at locality Oberangerberg (Tab.1, site 49; Fig.1,2), lithostratigraphically just above the Upper Rupelian turbiditic silt/sandstones that were sampled in Unterangerberg (Tab.1, sites 50,51; Fig.1,2). Locality Häring comprises two sites (Tab.1, site 52; Fig.1,2) with Lower to Upper Rupelian marls belonging to the Paisslberg Formation (Ortner and Stingl, 2001). Carbonates of the Lower Rupelian Werlberg Member (Ortner and Stingl, 2001) were sampled at locality Bruckhäusl (Tab.1, site 53; Fig.1,2).

Upper Cretaceous carbonates and marls as well as Eocene turbidites were sampled in Lechtal and Tirolic nappes north and south of Inn valley. The stratigraphic age of these sites ranges from Early Santonian to Upper Eocene.

Arenites at locality Gfallermühle belong to the Upper Eocene Oberaudorf Formation (Tab.1, site 54; Fig.1,2), which exhibits a prominent erosive unconformity from the Gosau Group (Ortner and Stingl, 2001). At locality Sebi Middle Eocene turbidites (Tab.1, site 55; Fig.1,2) (Hagn et al., 1982) and nearby Maastrichtian carbonates (Tab.1, site 56; Fig.1,2) (Jung et al., 1978) are exposed. At locality Mühlbergerbach (Tab.1, site 57; Fig.1,2) placed inside the Inn valley shear zone Maastrichtian to Campanian marls were sampled. Campanian silt/sandstones (Risch, 1985) could be sampled at locality Hechtsee (Tab.1, site 58), and Upper Campanian marls (Gruber, 1997) at locality Schwoich (Tab.1, site 59; Fig.1,2). Upper Santonian marls (Sanders, 1998) were sampled in 4 sites at locality Mühlbach (Tab.1, site 60; Fig.1,2) and Lower Santonian marls in two sites at locality Mösl (Tab.1, site 61; Fig.1,2).

Also in the Inn valley sites were sampled in Early Cretaceous sediments. Cenomanian/ Turonian Branderfleck Fm. was sampled at locality Niederndorf (Tab.1, site 62; Fig.1,2). Sampling in the Aptian/Albian Tannheim Fm at locality Kurz yielded results as well (Tab.1, site 63; Fig.1,2). Locality Kurz is placed at the southern overturned limb of the Thiersee-syncline, west of Kiefersfelden.

Concerning the central part of the western Northern Calcareous Alps Jurassic to Early Cretaceous sediments were sampled in 2 stratigraphic sections on the northern and southern limb of the Thiersee syncline.
At section Guffert (Nagel et al., 1976; Sausgruber, 1995) placed at the upright, northern limb of the Thiersee syncline, Late Triassic to Early Cretaceous carbonates were sampled. Results could be derived from 6 sites (Tab.1, sites 64-69; Fig.1,2). The carbonate facies is different compared to the basin facies at Ampelsbach section (Channel et al., 1992). At Guffert section, Liassic to Doggerian carbonates are condensed, Oxfordian radiolarites of Ruhpolding Fm. do not exist. These facies conditions are indicating a swell position for the Guffert section (Sausgruber, 1995). Paleomagnetic results were derived from the Late Triassic Hochalm Mb./Kössen Fm., the condensed carbonates of Liassic Adnet Fm. and Doggerian Klauskalk Fm., from cherty carbonates of Oxfordian Ruhpolding Fm. and from Malmian Lower and Upper Ammergau Fm.

At section Ampelsbach (Channel et al., 1992), placed at the steeply overturned, southern limb 7 sites yielded results (Tab.1, site 70-76; Fig.1,2). Late Triassic rocks of the Kössen Fm. did not yield any results, but these were derived from Liassic carbonates of Lower Allgäu Fm. and Scheibelberg Fm. Late Toarcian Middle Allgäu Fm. and Oxfordian Chiemgau Fm. also yielded results. Sites in Malmian carbonates were sampled in Lower and Upper Ammergau Fm. Neocomian Schrambach Fm. was the stratigraphic highest unit that was sampled at the southern limb of the Thiersee syncline. Each stratigraphic unit was sampled in 1 site.

4.4.2. Central Northern Calcareous Alps

In the area south of Strobl/Wolfgangsee 4 sites from Upper Cretaceous sediments yielded results. These sites were selected to identify different kinematics West and East of Königsee-Lammertal-Traunsee fault. Coniacian carbonates of Schmalnau Fm. were sampled on both limbs of an overturned, south verging syncline at locality Gall (Tab.1, sites 79,80). Further results were derived from 2 sites in Early Santonian carbonates of Grabenbach Fm at localities Weißenbach and Wirling (Tab.1, sites 77,78; Fig.1,2). Results from Jurassic to Early Cretaceous sediments were derived from stratigraphic sections at localities Kohlstatt (Tab.1, sites 81-86; Fig.1,2) and Unken (Tab.1, sites 87-91; Fig.1,2).

Locality Kohlstatt (Mohtat-Aghai, 1999; Jaksch, 1996) is placed in the Staufen-Höllengebirgs nappe of the Tirolic nappe unit of the central Northern Calcareous Alps.

The sampled stratigraphic section includes marls of the Late Triassic Eiberg Mb./Kössen Fm, carbonates of the Middle to Upper Liassic Scheibelberg Fm., carbonates of Doggerian Klauskalk and the Tithonian Upper Ammergau Fm. The Neocomian Schrambach Fm. is the stratigraphically highest unit that was sampled at Kohlstatt section. Each stratigraphic unit was sampled in 1 site, except the Upper Ammergau Fm. where a fold test was performed in the limbs of a meter-scale syncline.

In the Tirolic Unken syncline the stratigraphic section Karnergraben (Krainer and Mostler, 1997) was sampled. 5 sites yielded results (Tab.1, sites 87-91; Fig.1,2). Results were derived from carbonates of Late Triassic Eiberg Mb./Kössen Fm., from Liassic Hierlatzkalk Fm. and Scheibelberg Fm., from radiolarites of Oxfordian Ruhpolding Fm. and, stratigraphically highest, from Tithonian carbonates of the Ammergau Fm in the Unkenbach valley.

4.5. Central Alps (Eastern Alps)

Oligocene dykes were sampled in 2 sites in the Campo nappe of the Central Alps (Tab. 1; Fig.1,2). The dykes outcropping at sites 92 and 93 (Hintergrat and Gran Zebru) are related to the Oligocene (Late Rupelian) Gran Zebru pluton (Dal Piaz et al., 1988). Permoskythian conglomerates of the "Alpine Verrucano" were sampled at locality Schaubach Hütte (site 94; Fig.1,2) on the eastern flank of Sulden valley, opposite sites 92 and 93. For comparison Permoskythian sediments were also sampled at Serles/Margarethenbach (site 95; Fig.1,2) in the parautochtonous sedimentary cover of the Oetztal/Stubai basement complex (Stingl and Krois, 1990; Krois et al., 1990) (Tab. 1; Fig.1,2).
At locality Kopfraderjoch (site 96) sampling focused on the Paleozoic, diabasic rocks of the western Greywacke zone. Marbles of the Sub-Penninic Hochstegen-zone (site 97; Fig.1,2) of the Venediger nappe complex were sampled at the northern rim of the Tauern Window (Lammerer, 1986; Thiele, 1976).

4.6. Southern Alps

Sampling in the Southern Alps focused on carbonates west of Etsch valley at locality Nonsberg and carbonates and magmatic rocks in the Dolomites east of Etsch valley. Also Permian magmatic rocks in the paleozoic basement of the Southern Alps were sampled.
At locality Revo/ Nonsberg syncline, only 2 sites in carbonates of Upper Cretaceous Scalia rossa and Lower to Middle Eocene Fm. di Ponte Pia yielded results due to intense brittle tectonics and related weathering induced remagentizations (Tab.1, sites 98,99; Fig.1,2).
In the Dolomites 2 dykes, together with their country rocks could be sampled. 1 sill was sampled in the eastern Dolomites at locality Fischleintal. Radiometrically dated to Early Rupelian (Lucchini, 1983) the sill yielded results as well as the Ladinian carbonates of the Schlern Fm. that represent the country rocks of the sill (Tab.1, sites 100,101; Fig.1,2). Also, at locality Braida Freida, south of Corvara results were derived from a radiometrically dated (Lucchini, 1983) sill of Latest Cretaceous age and from the country rocks of the Upper Ladinian carbonates of the Kassian Fm. (Tab.1, sites 102,103; Fig.1,2).
North of Cortina d`Ampezzo a stratigraphic section was sampled in 7 sites at locality Alpe di Ra Stua (Tab.1, sites 105-111; Fig.1,2) (Horrelt, 1987; Siorpaes, 1994). 1 site in carbonates of Albian/Turonian Ruoibes Fm. (Stock, 1994) was sampled southwest of the section (Tab.1, site 104; Fig.1,2), separated by an E/W striking thrust fault (Siorpaes, 1994).

At the Ra Stua section results were derived from Doggerian to Malmian carbonates of Rosso Ammonitico Fm. (Channell and Doglioni, 1994). Another site was sampled in micrites of Berriasian/Valanginian Maiolica Fm. Hauterivian/Barremian red silty limestones were sampled in 2 sites. From the same stratigraphic range results could be derived from 1 site in marls of Puez Fm. Red, cherty, Aptian/Albian limestones yielded results as well as Albian turbiditic sandstones of Ra Stua Flysch Fm..
At locality Ultental, close to the Insubric line results were derived from a radiometrically dated Permian mafic dyke (pers. comm. L. Keim) and the Permian granitic country rocks (Kreuzberg granite; Tab.1, sites 112, 113; Fig.1,2).

4.7. Southern Alpine foreland basin

The Southern Alpine foreland basin was sampled at localities Lake Garda, Belluno syncline and Follina south of Bassano thrust fault. At localities Lake Garda and Belluno syncline also the Mesozoic basement of the foreland basin was sampled. At locality Lake Garda the Mesozoic basement was sampled in 2 sites in the area around Passo San Giovanni, west of Rovereto and in 2 sites close to the villages of Nago and Torbole at the eastern shore of Lake Garda (Luciani, 1989). At Passo San Giovanni results were derived from Liassic carbonates of Ronzo Fm. and Malmian micrites of Maiolica Fm. (Tab.1, sites 123,124; Fig.1,2). Carbonates of Campanian Scaglia rossa were sampled at the eastern shore of Lake Garda (Tab.1, sites 121,122; Fig.1,2).
At Lake Garda area, close to villages of Nago and Torbole, results (Tab.1, sites 117,118,120; Fig.1,2) were derived from Early Middle Eocene carbonates of the Torbole Fm. and Late Middle Eocene to Early Late Eocene Nago Fm. (Luciani, 1989; Geyer, 1993). Below the Nago carbonates volcanoclastic sediments are outcropping. Both lithologies were sampled. Late Middle Eocene tuffs were also sampled east of lake Garda, near San Vigilio at the eastern flank of Mt. Baldo (Tab.1, site 119; Fig.1,2).
At the northern shore of Lake Garda 1 site was sampled in Late Early Rupelian carbonates of the Linfano Fm. (Tab.1, site 116; Fig.1,2), 2 sites were sampled in Chattian to Aquitanian sandstones of the lower and higher parts of the Mt. Brione Fm. (Tab.1, sites 114,115; Fig.1,2).
At locality Belluno Mesozoic carbonates representing the basement of the foreland basin were sampled on both limbs of the NE/SW striking syncline (Di Napoli Alliata et al., 1970).

North of Mis in the village of Pescoli the steeply SE dipping northern limb was sampled in 1 site in Malmian Rosso Ammonitico Fm. (Tab.1, site 136; Fig.1,2) and 1 site in Malmian to Early Cretaceous micrites of Maiolica Fm. (Channell and Grandesso, 1987; Tab.1, site 135; Fig.1,2).

Stratigraphically higher Scaglia rossa Fm. was sampled in 5 sites comprising Coniac/Santonian to Late Maastrichtian times along the Torrente Mis (Casati and Tomei, 1969; Tab.1, sites 130-134; Fig.1,2). North of Passo San Boldo at the gently north dipping southern limb of the Belluno syncline the youngest, Late Maastrichtian parts of the Scaglia rossa Fm. were sampled in 1 site near the Cretaceous/Tertiary boundary at Ponte Brent (Di Napoli Alliata et al., 1970). Directly at the K/T boundary stratigraphically following Scaglia cinerea did not yield results but these could be derived from a site in the same formation but of Early Eocene age, some tens of meters north (Tab.1, site 129; Fig.1,2).

Results from Lower Eocene sandstones of the Belluno Flysch could only be derived from 1 site at Ponte di Mas, structurally located in the northern limb of the syncline (l.c.; Tab.1, site 128; Fig.1,2). Results from the southern limb were derived from Early Rupelian Curzoi sandstones that were sampled at Sedico (Tab.1, site 127; Fig.1,2) and from the Lower Burdigalian Bolago marls (Massari et al. 1986; Tab.1, site 126; Fig.1,2). Langhian Monfumo marls sampled in the northern limb of the syncline represent the stratigraphically youngest units that yielded results (Grandesso and Stefani, 1990; Tab.1, site 125; Fig.1,2).

Locality Follina south of Miocene Bassano thrust fault represents the most southern part of the Venetian Alps. 4 sites sampled at the southern limb of Monte Grappa anticline, south of Follina yielded results (Massari et al., 1993; Tab.1, sites 137-140; Fig.1,2). 1 site was sampled in Serravallian Tarzo marls. Sandy intercalations of Mt. Piai conglomerates were sampled in 3 sites. Results from 1 site in Messinian sandstones of the Mt. Piai conglomerate represent the paleomagnetic data of the stratigraphically youngest unit of the study area at all.

5. Methods

5.1. Paleomagnetic procedures

The paleomagnetic samples were collected with a water cooled coring apparatus and oriented with a magnetic compass. Natural remanent magnetization was measured on a three-axis cryogenic magnetometer with an in -line degausser (2G Enterprises). Specimens were subjected to detailed stepwise demagnetization procedure (alternating field and/or thermal treatment). During thermal demagnetization, the bulk susceptibility of the specimens was routinely measured to observe possible mineral transformations (Collinson, 1983).

Isothermal remanent magnetization (IRM) acquisition and backfield experiments aimed at the identification of the magnetic mineral content of a representative number of pilot specimens (Lowrie, 1990). A three component IRM was induced at 2.5T, 0.5T and 0.1T and demagnetised thermally afterwards (Lowrie, 1990). Additionally IRM acquisition curves were analysed using the programm IRM-CLG 1.0 by Kruiver et al. (2001). The method discriminates on the basis of different mineral coercivities. The field at which half of the SIRM is reached ($B_{1/2}$) can characterize a single magnetic mineral. Using this method in the frame of this study, the coercivity spectra were separated into magnetic minerals showing $B_{1/2}$ < 50mT (e.g. magnetite), 50mT< $B_{1/2}$ < 150mT (sulfides) and 150mT< $B_{1/2}$ < 500mT (hematite), $B_{1/2}$ > 500mT (goethite).

A Geofyzika KLY-2 susceptibilimeter was used for measuring magnetic susceptibility and anisotropy of the magnetic susceptibility (AMS). The latter (Tarling and Hrouda, 1993) aimed at determining the origin of the magnetic fabric with respect to the sedimentary bedding planes. The magnetic fabric was described by the degree of anisotropy P=L*F (Tarling and Hrouda, 1993) and using the Flinn-diagramm ratio K=L/F (Flinn, 1962; Soffel, 1991) for distinction between prolate and oblate fabrics. The significance of the mean susceptibility values was determined at $8*10^{-6}$ SI units.

Paleomagnetic data analysis included principal component analysis (Kirschvink, 1980) based on visual inspection of orthogonal projections (Zijderveld, 1967). Mean directions were calculated using TectonicsFP (Ortner et al., 2002).

Fold tests after McElhinny (1964) were carried out with the help of SuperIAPD by T. H. Torsvik, J. C. Briden and M. A. Smethurst (1996). All measurements were carried out in the Paleomagnetic Laboratory of the University of Leoben.

5.2. Combining geological and paleomagnetic data

In structural geology, there is generally a gap between paleomagnetic studies, which define vertical axis rotations of crustal blocks or continents (e.g. Márton et al., 2003b for the Adriatic microplate), and structural studies, in which the kinematics of large allochthons within orogens are traditionally studied in cross sections oriented parallel to the direction of transport (e.g. Eisbacher et al., 1990; Auer and Eisbacher, 2003 in the Northern Calcareous Alps). Some models have been formulated to explain small scale rotations in the range of 10° in areas of transcurrent tectonics (e.g. Peacock et al., 1998), but up to now no model exists to explain large rotations of more than 30°.

In this study, it was tried to fill the gap between paleomagnetic and structural studies.
The main problem of paleomagnetic work in orogens is to identify primary magnetizations. Sampling of continuous stratigraphic sections proved to be helpful, as a "section test" can be applied: the trend of the declinations should change through time, if sections covering long time spans are analysed.

Additionally the standard method to distinguish between primary and secondary magnetizations, the fold test (Mc Elhinny, 1964), is used. When applying this fold test it is generally assumed that the rocks have undergone rigid-body rotation.
Restoring rocks to their original untilted position by rotation of the bedding around the strike line back to the horizontal should strictly apply only in case of parallel folds with a horizontal axis without any strain (i.e. sampling at the fold limbs far from the fold hinge) (McElhinny and McFadden, 2000).

During this study most of the observed remanence directions were calculated in tilted position due to not interpretable results after bedding correction (e.g. after bedding correction a supposed primary Tertiary remanence derived from a site located in the Eastern Alps is indicating a paleogeographic position at the southern hemisphere).

5.2.1. Rotations around vertical axes

Concerning rotations around vertical axes, site means characterized by Fisherian distributions of remanence directions are calculated relatively easy. Declinations, which deviate from the geographic N direction, can be directly related to vertical axes rotations of the value of deviation from N. Distributions of the remanence directions along small circles are related to effects of tilting around a horizontal axis. In this case the observed deviation of the declination from geographic N is a combination of tilting and vertical axes rotation. The discrimination and separation of the two rotations can be handled with the small circle method (see chapters 3.2.2., 3.2.3).

5.2.1.1. Handling primary magnetizations

Declinations of primary magnetizations in tectonically undisturbed stratigraphic sections should be aligned N/S, according to the dipole field. If the declinations systematically deviate from N, the whole stratigraphic section should be affected by vertical axis rotation. If declinations deviate from N only in an older part of a stratigraphic section, tectonism (translation, vertical and horizontal axis rotation) took place during lithification (blocking of the remanence directions) at the time of the change in declination orientation.

With this approach it is possible to date rotations and consequently construct a succession of rotations in time. Starting with primary magnetizations of the stratigraphically youngest sediments the finite value of vertical axes rotations is restored back in time always restoring the deviations from the geographic N direction.

5.2.1.2. Handling secondary magnetizations

If secondary magnetizations postdated folding, the magnetic vectors should show a Fisherian distribution. If magnetic vectors were distributed along small circles, the magnetization should be contemporaneous to folding. Growth strata geometries (progressive unconformities) allow dating of folding and consequently also dating of synfolding remagnetization. Post folding remagnetizations cannot be dated directly. Remagnetization can affect a folded/tilted site at any time after deformation.

If two remagnetizations, indicating different vertical axes rotations, occurred successively in a stratigraphic section only scarce interpretations about a kinematic evolution are possible due to lack of constraints on the age of remagnetizations. It cannot be decided whether successively appearance of different declination values is caused by changing kinematics or by petrological aspects. A second time of remagnetization may pervasively overprint the older remagnetization extincting all older magnetic information. Only comparing the characteristic declinations/inclinations to primary magnetization directions possibly enables dating.

5.2.2. Rotations around horizontal axes (tilting)

A few localities/sites were characterised by distributions of remanence directions that were distributed along small circles. Synfolding magnetizations are acquired dynamically as the fold grows. Thus, one would expect a synfolding magnetization to be a composite of several magnetizations whose directions would lie on a small circle parallel to the π-circle of bedding. The basic idea is as follows: during tilting, the insitu remanence directions rotate on a small circle (remanence small circle). The axis of the small circle cone is identical with the tilt axis. For different tilt angles within a folded sequence or for synorogenic remanence acquisition, the remanence directions will be distributed about a mean small-circle. The position of such a small circle depends on the field direction during remanence acquisition and the trend of the tilt axis. This would imply that the only way to identify a synfolding magnetization with certainty would be to identify components with these characteristics during demagnetization (Shipunov, 1997; McFadden, 1998; Waldhör, 1999; Waldhör and Appel, 2006).

5.2.3. Combining Rotations around vertical and horizontal axes

The maximum of data concentration along the small circle distributions was calculated with contouring grids using the programm TectonicsFP (Ortner et al., 2002). This data cluster represents the final phase of tilting and related remagnetization. Assuming constant remagnetization during tilting, remagnetizations acquired during early stages of tilting are constantly overprinted and reoriented. Only a few “older” remagnetizations survive this process that depends on permeability and porosity of the affected sites. The maximum concentration of remanence directions, representing the final stage of tilting, is compared with the reference direction, known from literature (e.g. Besse and Courtillot, 2002). Consequently the time of remagnetization has to be known (e.g. by progressive unconformities).

Resulting deviations of the declinations from that reference direction are explained by vertical axes rotations. On the other hand also paleo orientation of the tilt axes can be calculated by restoring the maximum remanence direction to the reference value. The tilt axis has to be identical with the axis of the small circle cone. The minimum Eigenvalue of Eigenvector-analysis (Bingham, 1964) represents azimuth and plunge of the tilt axis.

6. Results

Due to the complex kinematics including folding and vertical axis rotations, each chapter starts with a short summary, restoring the geodynamic evolution of each larger study area, always starting with the youngest dynamics. The area and site descriptions are organized following the sedimentary process, i.e. from old to young. Exceptions to this organization are descriptions of the North Alpine Foreland basin and of the Late Cretaceous to Oligocene sites of the western Northern Calcareous Alps. Rotations mentioned in the following descriptions and interpretations are understood as vertical axis rotations, unless stated otherwise.

6.1. Northern Alpine Foreland basin

6.1.1. Restoration of vertical/horizontal axes rotations

Primary magnetizations derived from the Miesbach and Hausham synclines indicate two phases of vertical axis rotation. Latest Chattian marls (sites14, 15) show NW directed declinations dating a supposed counterclockwise rotation to younger than 23Ma. Primary magnetizations from sediments of Rupelian to Early Chattian age are characterized by S directed declinations and negative inclinations indicating a remanence acquisition during a reversed polarity period. After restoring the younger counterclockwise rotation these values indicate 30° of clockwise rotation. Early Late Chattian silts (site 16) represent the youngest sediments where 30° clockwise rotation could be interpreted. Consequently the 30° clockwise rotation can be dated to younger than Early Late Chattian and older than latest Chattian (25-23Ma). North of the frontal Alpine thrust no vertical axis rotations could be detected (Fig.5).

6.1.2. Western part- Allgäu area

At locality Enschenstein magnetic carrier minerals of Late Aquitanian to Burdigalien carbonates were determined by acquisition of isothermal remanent magnetization and thermal demagnetization of three component IRM (Lowrie, 1990). IRM acquisition curves were interpreted with the method by Kruiver et al. (2001).

At both Enschenstein sites (1,2; Tab.1; Fig.1,2,3) the remanent magnetization was carried by magnetite and goethite, site 2 also showed a contribution from hematite. Alternating field demagnetization in the range of 3-100mT could isolate this magnetization component.

Relatively high alternating field values necessary for full demagnetizations were explained by variations in magnetite grain size. This interpretation was also supported by thermal demagnetization of three component IRM that was identifying a medium coercive component that is thermally stable below 600°C. Magnetic fabrics could be derived from site1, showing a degree of anisotropy of 2,3%. K_{max} is horizontally, K_{min} vertically oriented, indicating an undisturbed sedimentary fabric. The characteristic remanent magnetization carried by magnetite showed N directed declinations before and after bedding correction, indicating no vertical axis rotation at no time north of the Alpine front..

Late Aquitanian marls at locality Sulzberg (site 3, Tab.1, Fig.1,2) showed a remanent magnetization that is carried by magnetite, hematite and goethite. Like thermal demagnetization of three component IRM (Lowrie, 1990) also the interpretation of IRM acquisition curves with the method by Kruiver et al. (2001) was identifying a system of three magnetization components. The characteristic remanent magnetization was carried by hematite and could be determined with thermal demagnetization between 620-680°C. Magnetic fabrics were showing a slightly inclined K_{min} axis, possibly indicating weak disturbance of the sedimentary fabrics, degree of anisotropy was low (2,7%).
After bedding correction the declinations were NE directed, possibly indicating a transition area between non rotated parts of the Molasse basin north of the Alpine front and counterclockwise rotated parts further to the south. A dextral wrench corridor may explain these diverging, clockwise rotated declinations.

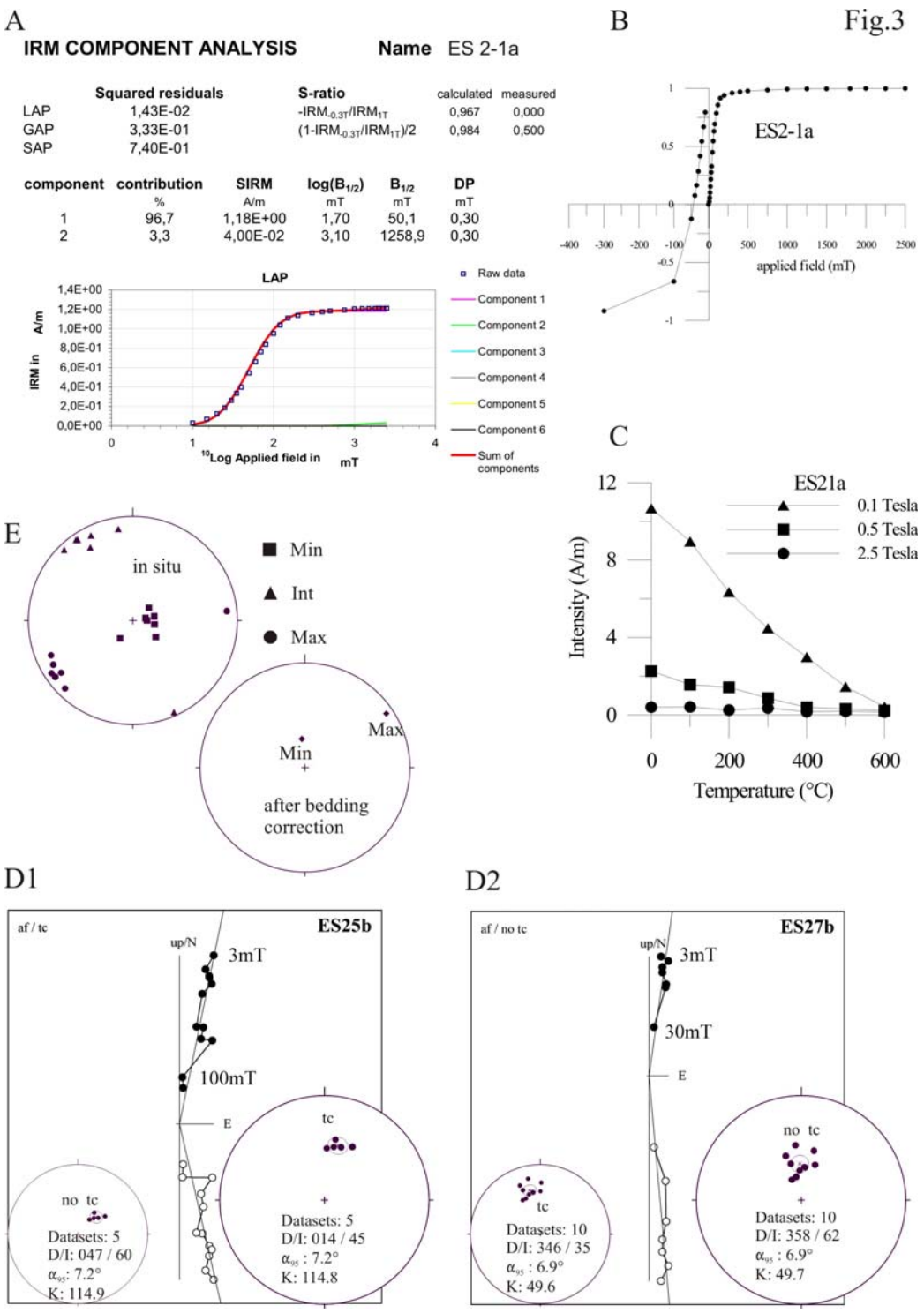

Fig. 3. Rock magnetic properties, demagnetization behavior and statistical parameters from site 2 (ES2), (Tab.1).

A= IRM component analysis according to Kruiver et al. (2001); **B**= Typical IRM acquisition curves; **C**= Thermal demagnetization of three component IRM (Lowrie, 1990); **D**= Zijderveld demagnetograms of representative samples in stratigraphic (tc, **D1**) and geographic (no tc, **D2**) coordinates, in the Zijderveld diagrams, full/hollow circles: projection of the NRM in the horizontal/vertical plane. Stereogeographic projection of the characteristic remanence magnetization direction, bedding corrected (tc), in situ (no tc) coordinates; **E**= AMS results, after bedding correction/ in situ coordinates.

Chattian silt/sandstones at locality Littenbach (sites 4, 5; Tab.1, Fig.1,2) were demagnetized with the alternating field in the range of 3-15mT. The corresponding unblocking temperatures were observed between 200-450°C. Most probably the characteristic remanent magnetization that was showing NW directed declinations before bedding correction was carried by magnetite. Acquisition of isothermal remanent magnetization, thermal demagnetization of three component IRM (Lowrie, 1990) and interpretation of IRM acquisition curves with the method by Kruiver et al. (2001) were indicating a system of magnetite/goethite to carry the remanent magnetization. At site 5 also a contribution by hematite could be stated.

Samples from Rupelian/ Chattian silt/sandstones of site 6 (Tab.1, Fig.1,2) at locality Krumbach were successfully demagnetized using the alternating field method in the range between 3-15mT.
Thermal demagnetization of three component IRM (Lowrie, 1990) was indicating a low and a medium coercive component that were thermally stable below 600°C.
Interpreting IRM acquisition curves with the method by Kruiver et al.(2001) identified one carrier mineral that showed a $B_{1/2}$ (the field at which half of the saturation magnetizaton is reached) of 39,8mT. Most probably magnetite with differing grain sizes carried the characteristic remanent magnetization that showed NW directed declinations before bedding correction.

Steineberg syncline was sampled at localities Eibele Alm and Wilhelmine Alpe. At locality Eibele Alm results were derived from Rupelian/Chattian silt/sandstones (site 9, Tab.1, Fig.1,2) that are characterized by a remanent magnetization with NW directed declinations before bedding correction. Demagnetization with the alternating field method was successful between 3-21mT. Acquisition of isothermal remanent magnetization, thermal demagnetization of three component IRM (Lowrie, 1990) and interpretation of IRM acquisition curves with the method by Kruiver et al. (2001) indicated a low coercive mineral (most probably magnetite) and a small contribution by a high coercive mineral such as goethite. At sites 7 and 8 (Tab.1, Fig.1,2) similar rock magnetic properties could be detected from sandstones of Early Chattian to Early Late Chattian age. The remanent magnetization is carried by two components of magnetite and goethite. Demagnetization of the characteristic remanent magnetization was achieved by using the alternating field method in the range between 3-30mT. The declinations again were directed northwesterly before bedding correction.

At both localities Rupelian marls (sites10/11, Tab.1, Fig.1,2,4) showed primary magnetizations with S directed declinations and negative inclinations after bedding correction. The fold test (Fig.4) is positive and yielded the maximum *k*-value (according to McElhinny (1964)) at 100% unfolding; Cr=2,05. The characteristic remanent magnetization most probably carried by magnetite was isolated using the alternating field method in the range between 25-80mT. At site 10 a contribution to the remanent magnetization by pyrrhotite is suspected. Interpreting IRM acquisition curves with the method by Kruiver et al. (2001) is indicating two components carrying the remanent magnetization. These components were identified by $B_{1/2}$ of 39,8mT and 141,3mT. The latter $B_{1/2}$ of 141,3mT is interpreted to indicate pyrrhotite. Bedding corrected magnetic fabrics show horizontally oriented K_{max} and vertically oriented K_{min} axis, indicating no disturbances to the primary sedimentary fabrics. The magnetic fabric is typically foliated, the degree of anisotropy is between 5,8% to 6,5%.

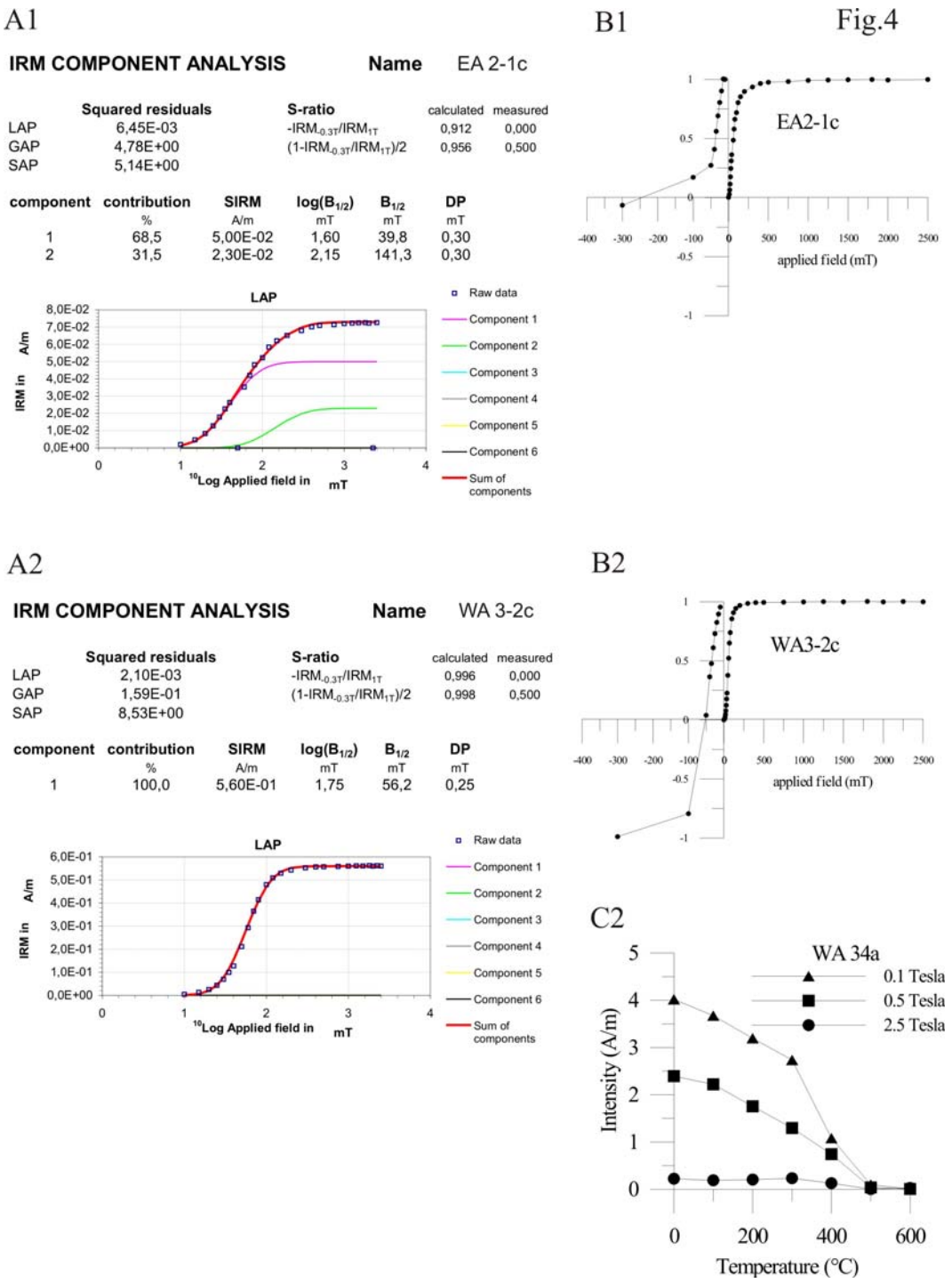

Fig.4

Fig. 4. Rock magnetic properties, demagnetization behavior and statistical parameters from site 10 (EA2, **A1-F1**) and site 11 (WA3, **A2-F2**), (Tab.1).

A= IRM component analysis according to Kruiver et al. (2001); **B**= Typical IRM acquisition curves; **C**= Thermal demagnetization of three component IRM (Lowrie, 1990);

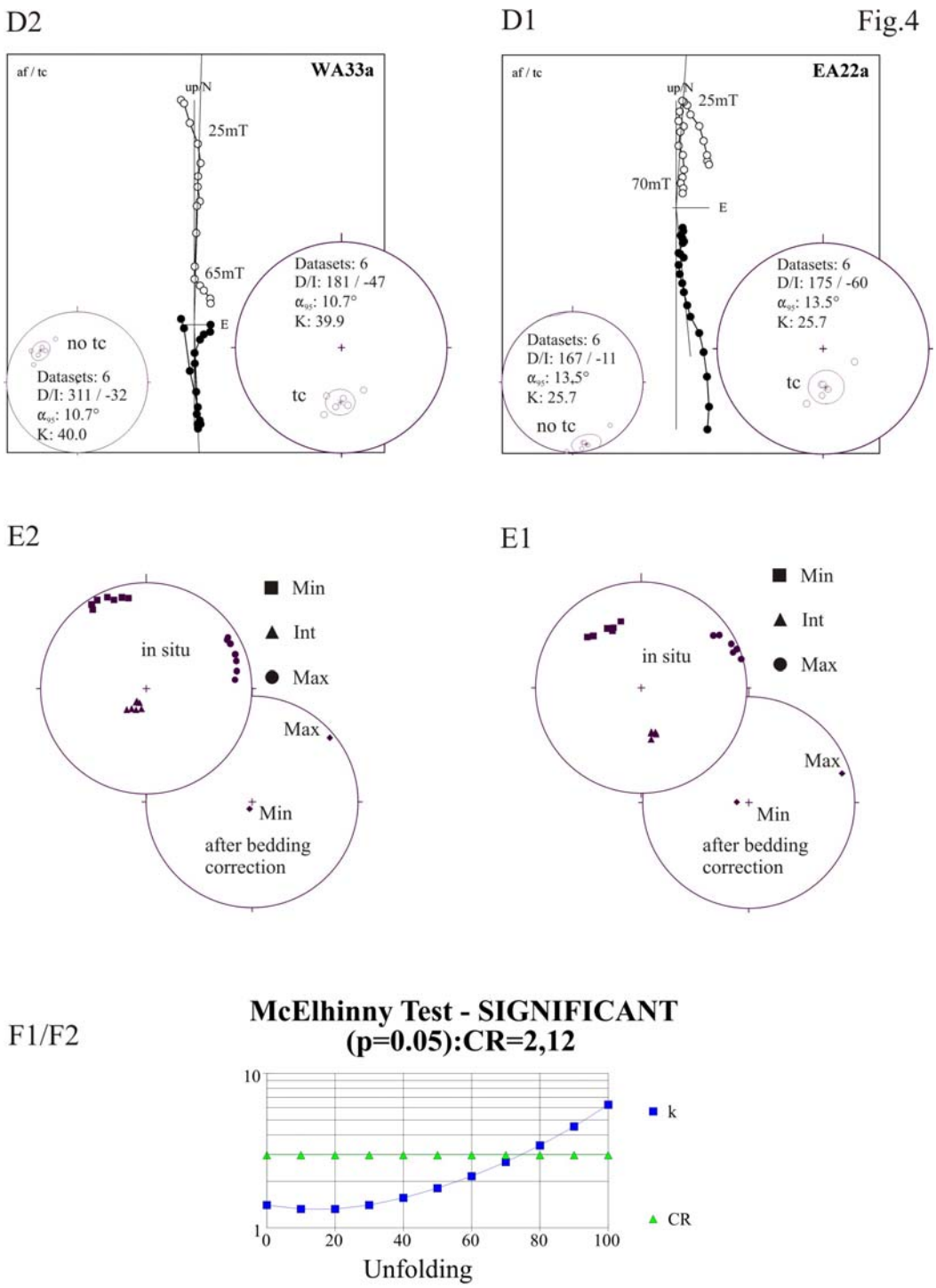

Fig. 4. Rock magnetic properties, demagnetization behavior and statistical parameters from site 10 (EA2, **A1-F1**) and site 11 (WA3, **A2-F2**), (Tab.1).

D= Zijderveld demagnetograms of representative samples in stratigraphic (tc) and geographic (no tc) coordinates, in the Zijderveld diagrams, full/hollow circles: projection of the NRM in the horizontal/vertical plane. Stereogeographic projection of the characteristic remanence magnetization direction, bedding corrected (tc), in situ (no tc) coordinates; **E**= AMS results, after bedding correction/ in situ coordinates; **F**= fold test according to McElhinny (1964).

6.1.3. Eastern part- Schliersee area

In the vicinity of Schliersee three localities with 12 sites yielded results. Results from 2 sites were derived from the autochthonous Molasse at locality Mangfall. The Subalpine, allochthonous Molasse yielded results from 3 sites from both limbs of the northern Miesbach syncline and from 7 sites from both limbs of the southerly juxtaposed Hausham syncline.

At locality Mangfall two sites (12,13; Tab.1, Fig.1,2) were sampled in marls of Serravallian UFM. The characteristic remanent magnetization, carried by magnetite, showed N directed declinations before bedding correction. The remagnetization is most probably related to folding that started around Aquitanian/ Burdigalian age, according to the first observable progressive unconformities (see cross sections in Ganns and Schmidt-Thomé, 1953). Interpreting these remanence directions by a weathering component caused by the (sub) recent earth magnetic field is not very plausible due to the relatively shallow inclination values (51°-56°) that are observed. A component derived from the (sub) recent earth magnetic field is supposed to present inclination values of 65° at 47°-48° geographic latitude. Moreover the sites (12,13; Fig.1,2) are overturned, dipping towards south. A post-folding north and down oriented component should show an even steeper inclination, when folding possibly proceeds. Together with the results from locality Enschenstein/ Allgäu no vertical axis rotation can be detected from sites north of the Alpine front. Demagnetization with the alternating field method could isolate this component in the range between 5-50mT. Interpretation of the IRM acquisition by the method of Kruiver et al. (2001) identified a small contribution to the remanent magnetization by goethite, at both sites.

From the northern limb of the Miesbach syncline two sites (14,15; Tab.1, Fig.1,2,6) in Latest Chattian sandstones and marls of the Cyrena beds yielded results. The characteristic remanent magnetization showed NW directed declinations after bedding correction. No polarity change could be observed. A prefolding magnetization is supposed. Progressive unconformities date the initiation of folding to Aquitanian/ Burdigalian.
Demagnetization with the alternating field in the range between 20-70mT as well as thermal demagnetization of 3 component IRM (Lowrie, 1990) was identifying magnetite as the main carrier mineral of the remanent magnetization. Using the method by Kruiver et al. (2001) also a small contribution to the remanent magnetization by goethite was supposed.

An undisturbed sedimentary fabric is indicated at site 15, which showed a horizontally oriented K_{max} axis and a vertically oriented K_{min} axis. The magnetic fabric is slightly oblate (L/F=0,995) the degree of anisotropy is low (3,3%).

Similar magnetic properties could be derived from site 16 (Tab.1, Fig.1,2,6) from the southern limb of the Miesbach syncline in sandstones of Early Late Chattian Sattelflözgruppe.
Contrarily to sites 14 and 15 the characteristic remanent magnetization carried by magnetite showed N directed declinations after bedding correction at site 16. This magnetic component is most probably of primary origin according to positive fold and reversal tests (comparing with sites 17- 22). This implies 30°-40° of relative, clockwise vertical axis rotation between post Early Late Chattian (site 16) and pre- Aquitan/ Burdigalian times (sites 14,15) as the prefolding, Aquitan/ Burdigalian remagnetizations at sites 14, 15 showed no clockwise rotated declinations.

Consequently in Chattian times the whole not yet existing "Miesbach syncline" was affected by clockwise rotation that was active post Early Late Chattian and stopped before Latest Chattian. At locality "Miesbach syncline" folding must be younger than clockwise rotation but also must be younger than the Aquitan/ Burdigalian prefolding remagnetization that affected the Latest Chattian siltstones/marls at sites (14, 15).

All these arguments are implying a clockwise vertical axis rotation on a flat before thin skinned thrusting that caused evolving of the"Miesbach syncline". As it is usually assumed that rotation has to be related to deformation this kinematic interpretation based on prefolding/primary paleomagnetic data is contradicting any model by means of structural geology. At the moment, no solution is known, how to combine paleomagnetic and geologic data concerning this specific situation.

Results from 7 sites could be derived from both limbs of locality Hausham syncline.
At the northern limb Rupelian marls of LMM were sampled in 2 sites (19, 20; Tab.1, Fig.1,2). Demagnetization with the alternating field method was successful in the range between 20-60mT, indicating magnetite as main carrier mineral of the remanent magnetization. At site 19, using the method by Kruiver et al. (2001), a small contribution to the remanent magnetization by goethite was detected. After bedding correction both sites were characterized by a horizontally oriented K_{max} axis and a vertically oriented K_{min} axis.

An isotropic magnetic fabric (L/F=0,99) and very low degrees of anisotropy (P=3,1%) also indicated an undisturbed sedimentary fabric.

Two more sites from the northern limb were sampled in Late Rupelian (site18; Tab.1, Fig.1,2) to Early Chattian (site 17; Tab.1, Fig.1,2,7) silt/sandstones. Again magnetite and magnetite/goethite (site 17, Tab.1, Fig.6) were identified as main carrier minerals of the remanent magnetization. At site 18 also the magnetic fabric could be measured. After bedding correction K_{max} and K_{min} axes were oriented horizontally and vertically, again indicating an undisturbed sedimentary fabric. The orientation of the characteristic remanent magnetization is similar concerning all 4 sites (17-20; Tab.1, Fig.1,2) at the northern limb of the Hausham syncline. After bedding correction the declinations were directed towards south, the inclinations were negative.

At the southern overturned limb of the Hausham syncline also Rupelian marls of LMM were sampled (site 21; Tab.1, Fig.1,2). Based on the interpretation of the IRM acquisition by the method of Kruiver et al. (2001) and thermal demagnetization of 3 component IRM (Lowrie, 1990) magnetite and goethite were identified to carry the remanent magnetization. The characteristic component of the remanent magnetization was isolated with the alternating field method in the range between 20-50mT and showed NW directed declinations before bedding correction. Two sites from silt/sandstones of the Early Chattian "Flözgruppe" also sampled in the southern overturned limb yielded results. Rock magnetic investigations again identified magnetite (site 22; Tab1; Fig.7) and magnetite/goethite (site 21; Tab 1) as main carrier of the remanent magnetization. Demagnetization with the alternating field succeeded in the range between 15-50mT, concerning both sites. The characteristic remanent magnetization, most probably carried by magnetite, again showed south directed declinations and negative inclinations. At site 22 (Fig.6) also AMS measurements were successful, indicating an undisturbed sedimentary fabric. The fold test concerning sites 17 and 22 (Tab.1, Fig.7) is positive and yielded the maximum *k*-value (according to McElhinny (1964)) at 100% unfolding; Cr=1,89.

Values of clockwise vertical axis rotation as well as the strike of the bedding planes are constant concerning Rupelian to Early Late Chattian sites from Miesbach and Hausham syncline. Consequently also folding and evolving of Hausham syncline should have acted after clockwise rotation. This kinematics might be only possible with a paleoposition on a flat during rotation. Again, at the moment no solution is known, how to combine contradicting paleomagnetic and geologic data. As like mentioned before, structural geology requires deformation i.e. folding contemporaneous to vertical axis rotations.

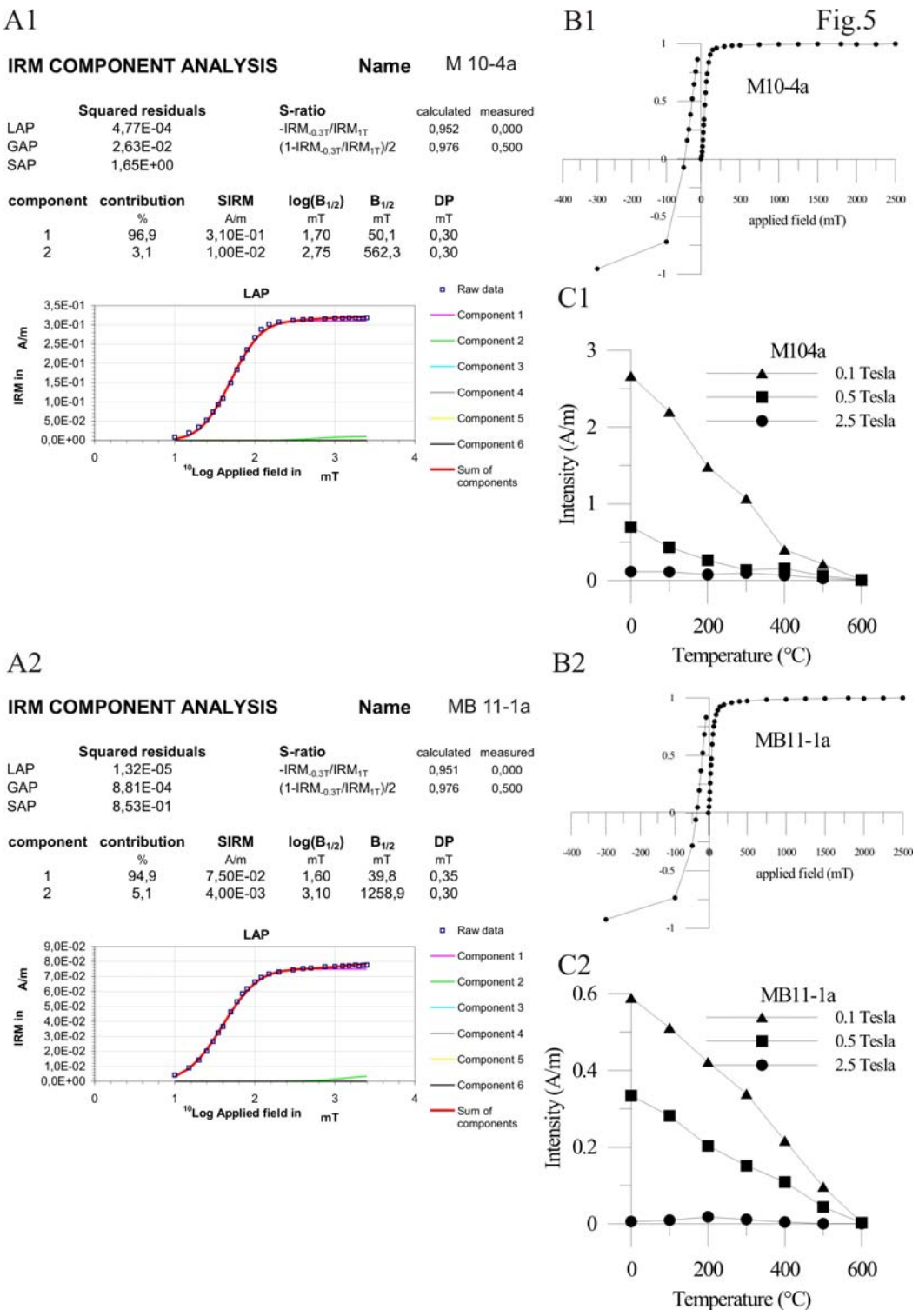

Fig. 5. Rock magnetic properties, demagnetization behavior and statistical parameters from site 16 (M10, **A1-E1**) and site 14 (MB11, **A2-E2**), (Tab.1).

A= IRM component analysis according to Kruiver et al. (2001); **B**= Typical IRM acquisition curves; **C**= Thermal demagnetization of three component IRM (Lowrie, 1990);

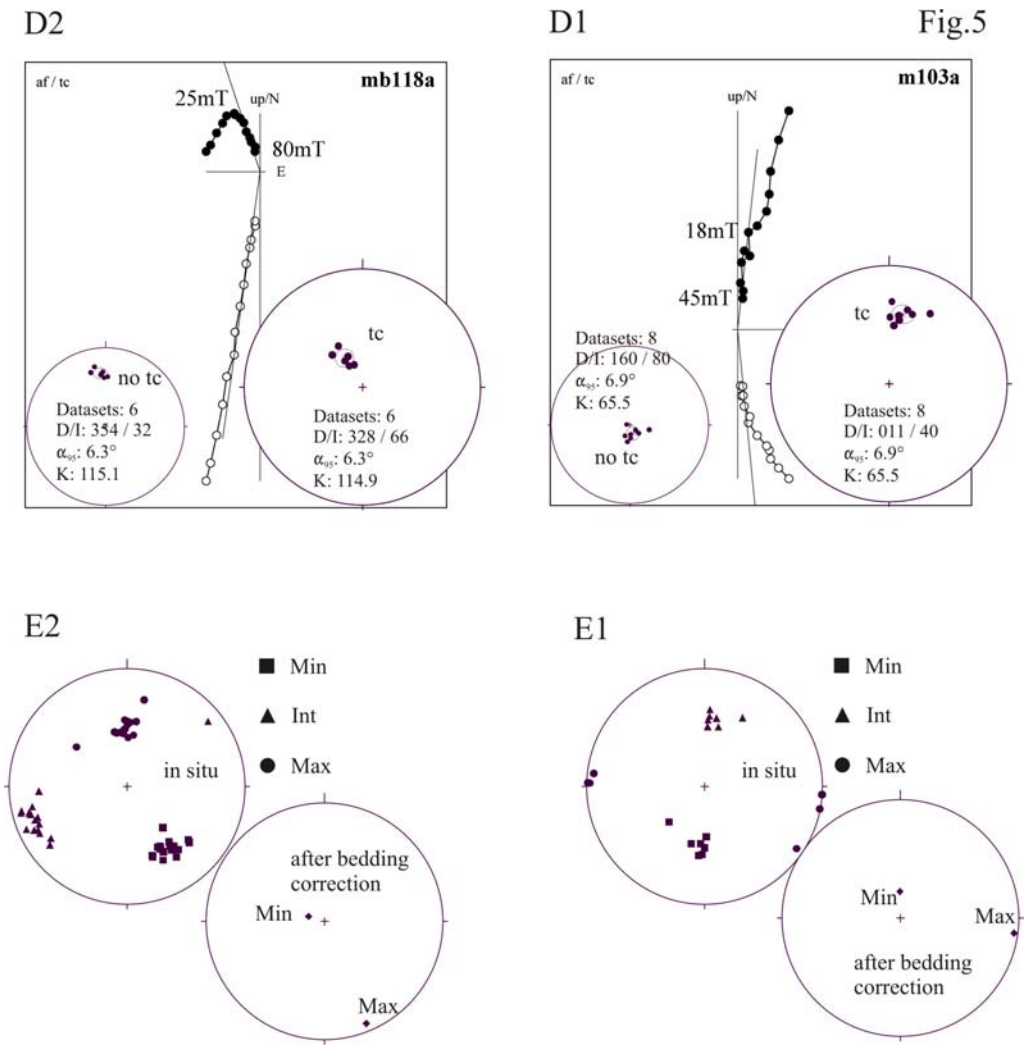

Fig. 5. Rock magnetic properties, demagnetization behavior and statistical parameters from site 16 (M10, **A1-E1**) and site 14 (MB11, **A2-E2**), (Tab.1).

D= Zijderveld demagnetograms of representative samples in stratigraphic (tc) and geographic (no tc) coordinates, in the Zijderveld diagrams, full/hollow circles: projection of the NRM in the horizontal/vertical plane. Stereogeographic projection of the characteristic remanence magnetization direction, bedding corrected (tc), in situ (no tc) coordinates; **E**= AMS results, after bedding correction/ in situ coordinates.

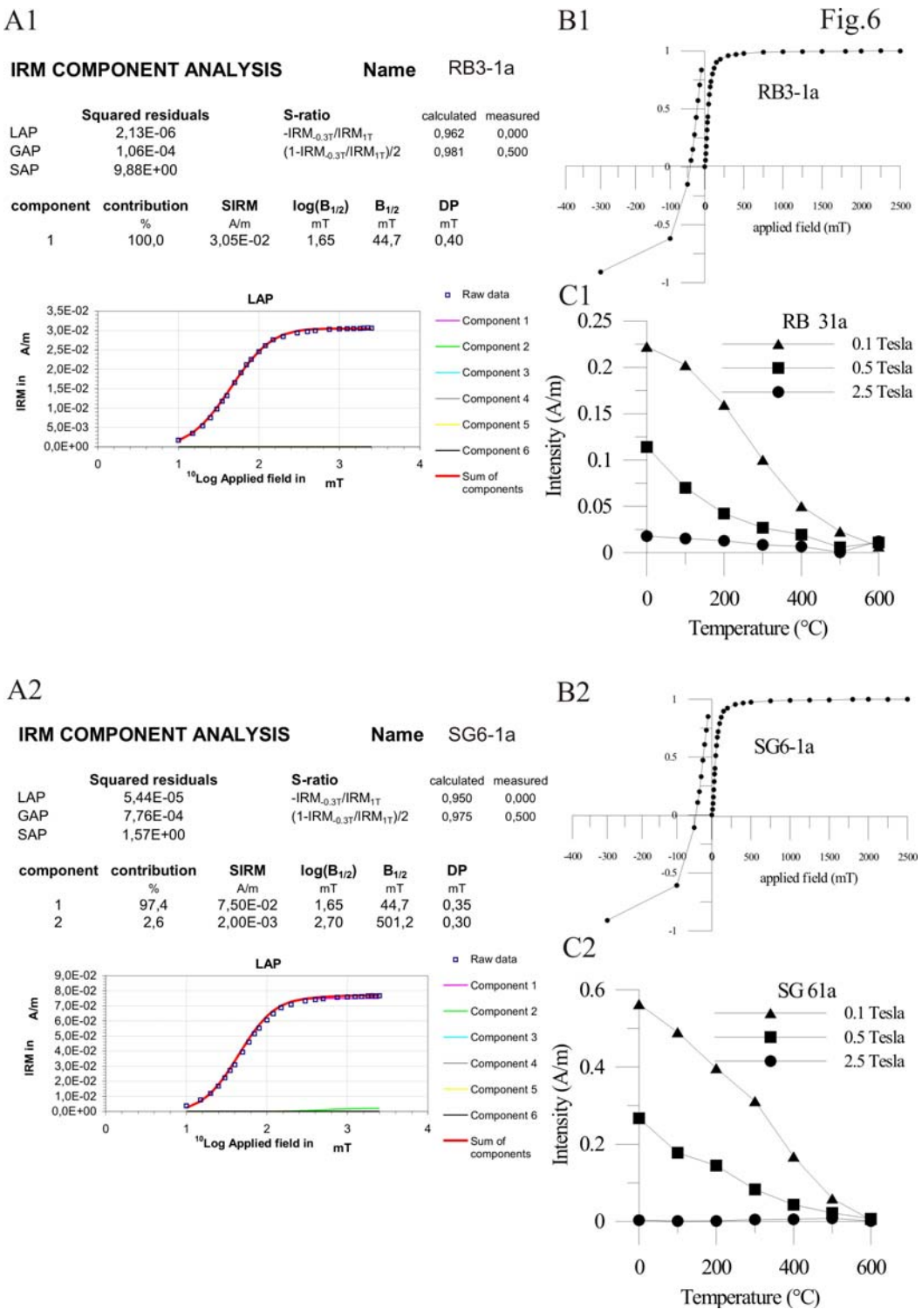

Fig. 6. Rock magnetic properties, demagnetization behavior and statistical parameters from site 22 (RB3, **A1-F1**) and site 17 (SG6, **A2-F2**), (Tab.1).

A= IRM component analysis according to Kruiver et al. (2001); **B**= Typical IRM acquisition curves; **C**= Thermal demagnetization of three component IRM (Lowrie, 1990);

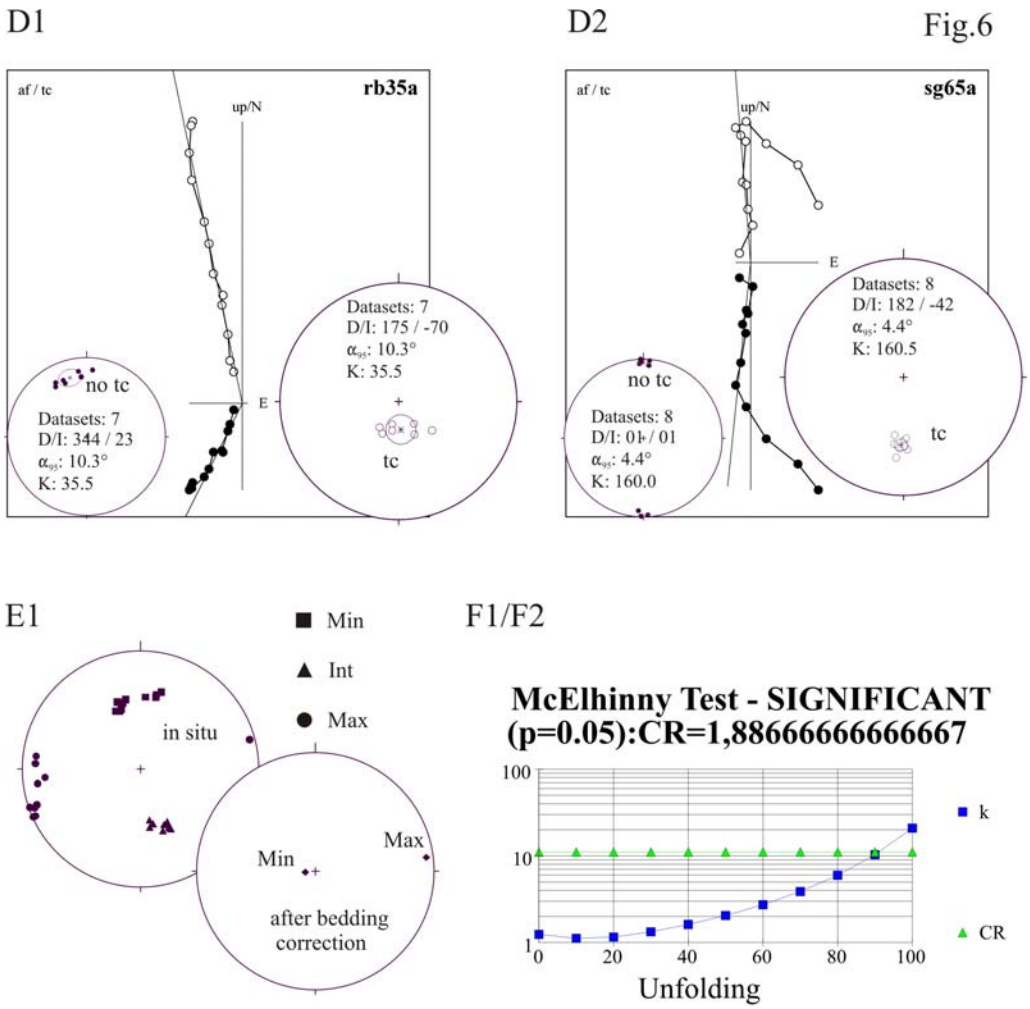

Fig. 6. Rock magnetic properties, demagnetization behavior and statistical parameters from site 22 (RB3, **A1-F1**) and site 17 (SG6, **A2-F2**), (Tab.1).

D= Zijderveld demagnetograms of representative samples in stratigraphic (tc) and geographic (no tc) coordinates, in the Zijderveld diagrams, full/hollow circles: projection of the NRM in the horizontal/vertical plane. Stereogeographic projection of the characteristic remanence magnetization direction, bedding corrected (tc), in situ (no tc) coordinates; **E**= AMS results, after bedding correction/ in situ coordinates; **F**= fold test according to McElhinny (1964).

Summary of paleomagnetic data from Allgäu area and western Helvetic units

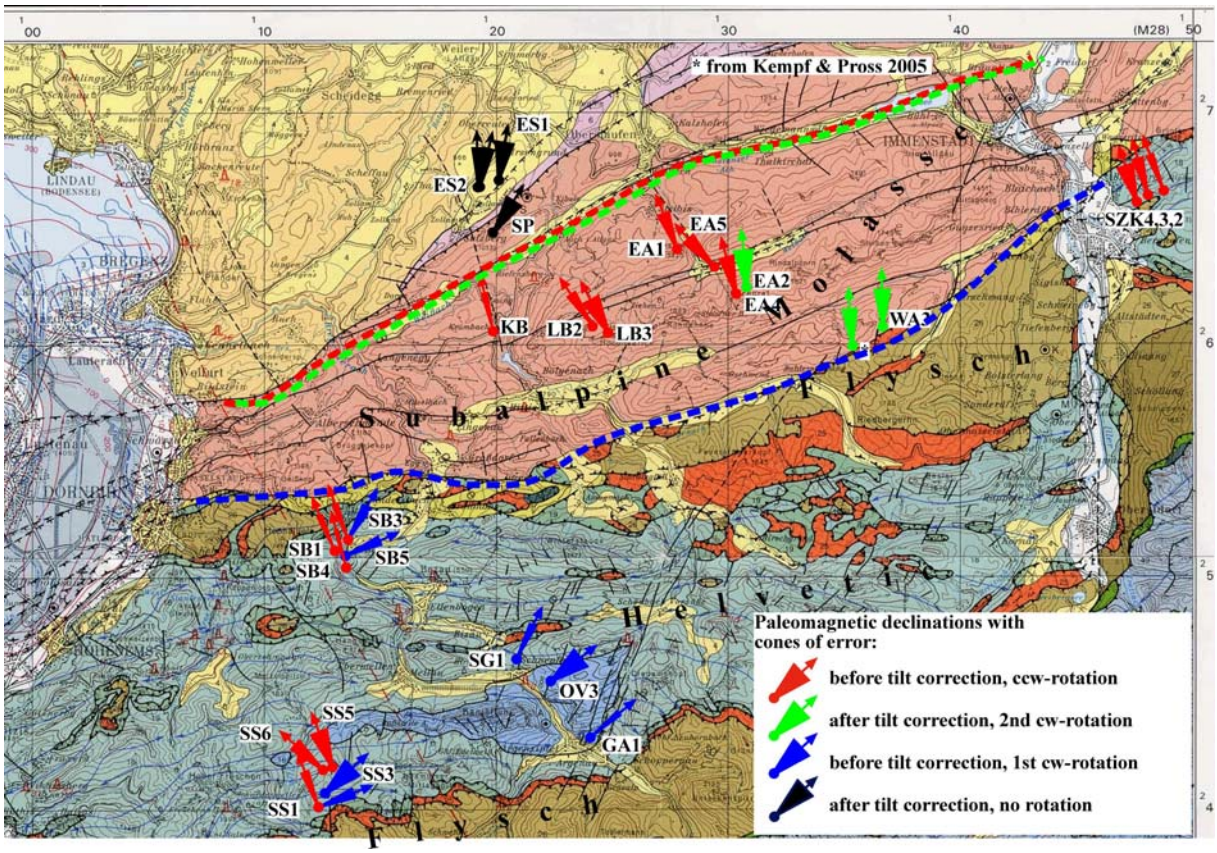

Fig. 7. Results from Allgäu and Bregenzer Wald area, sites were sampled in Autochthonous to Allochthonous Molasse units and Helvetic nappes. Site abbreviations refer to Tab.1. Colors of red, green and blue indicate counterclockwise, moderate clockwise and strong clockwise rotation, respectively. (Tectonic map of Voralrberg, 1: 200.000, Oberhauser and Rataj, 1998).

6.2. Helvetic units

6.2.1. Restoration of vertical/horizontal axes rotations

No primary magnetization could be derived from sites sampled in Helvetic units. Remagnetizations showing normal and reverse polarity were acquired in pre- to post folding positions. Two mean groups of characteristic components can be distinguished, characterized by NW and NE directed declinations (Fig.8). Compared with the results from the Northern Foreland basin, the NW directed declinations were interpreted to result from the same counterclockwise rotation. Concerning the clockwise rotation the observed declinations are similar only in very few cases.

From the Northern Foreland basin 30° of clockwise rotations are derived after restoring the younger counterclockwise rotation values. Similar rotation values characterize 2 sites in carbonates of northernmost Helvetic units at locality Ostin. If a similar restoration is done with data from the Helvetic units further to the south, a finite 60° clockwise rotation results. Consequently the clockwise rotation is separated into two phases of 30° rotation each. As the thrust activity is moving from internal parts of the orogen to the external parts, clockwise rotation is affecting internal units earlier than external units, causing less clockwise rotated declination values towards the external units of the orogen. Especially at locality Kanisfluh a relationship between folding and vertical axis rotation can be stated: Characteristic components indicating clockwise rotation are identical concerning declinations and inclinations before and after bedding correction (sites 32, 33). These data imply syn-to post-folding remagnetization prior to clockwise rotation.

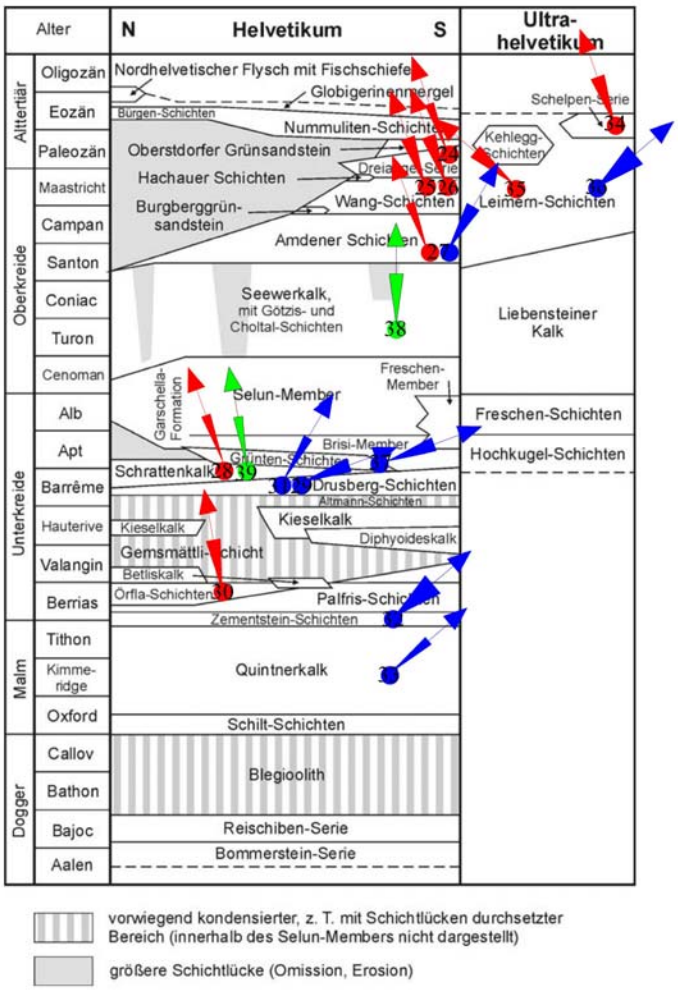

Fig. 8. Lithostratigraphy of Helvetic units (Freudenberger and Schwerd, 1996). Declination orientations and α95 cones indicate results. Colors of red, green and blue indicate counterclockwise, moderate clockwise and strong clockwise rotation, respectively. Sites 34-37, at locality Sünserspitze belong to South-Helvetic units, characterized by Ultra-Helvetic facies.

6.2.2. Western Helvetic units

Results from the western Helvetic units in the Allgäu area were derived from 3 sites at locality Starzlachklamm.
The Campanian/-Maastrichtian Wang Fm. is characterized by alternating limestone and marls. The characteristic remanent magnetization is carried by magnetite concerning both lithologies (sites 25,26; Tab.1). Demagnetization with the alternating field method in the range between 3-30mT could isolate a component with NW directed declinations before bedding correction. Interpretation of the IRM acquisition by the method of Kruiver et al. (2001) indicated small contributions to the remanent magnetization of goethite concerning the marls, and of hematite concerning the limestones.
The Late Maastrichtian Dreiangel Fm. showed a characteristic remanent magnetization carried by magnetite with NW directed declinations before bedding correction (site 24; Tab.1). Again a small contribution of hematite to the remanent magnetization was interpreted, using the method by Kruiver et al. (2001).
Further to the south in the Bregenzer Wald area 11 sites, derived from three larger localities yielded results.

Most northern located Schwarzenberg section yielded results from 4 sites (27-30; Tab.1). Carbonates from Late Berriasian Örfla Fm. (site 30; Tab.1) were demagnetized with the alternating field method in the range between 3-20mT. Magnetite as main carrier of the remanent magnetization was also identified through acquisition of isothermal remanent magnetization and thermal demagnetization of 3 component IRM (Lowrie, 1990). A small contribution by goethite to the remanent magnetization was identified with the method by Kruiver et al. (2001).
The characteristic remanent magnetization, calculated with the analysis of remagnetization circles (McFadden and McElhinny, 1988) showed NW directed declinations before bedding correction.
Marls from Barremian Drusberg Fm. (site 29; Tab.1) were demagnetized with the alternating field method in the range between 35-70mT. Thermal demagnetization of 3 component IRM (Lowrie, 1990) identified a low to medium coercive component, thermally stable till 500°C and a medium coercive component that was thermally stable between 200-400°C.
Also the interpretation of the IRM acquisition using the method by Kruiver et al. (2001) was indicating a system of magnetite/pyrrhotite as main carriers of the remanent magnetization.

The characteristic remanent magnetization interpreted as prefolding overprint showed SE directed declinations and negative inclinations after bedding correction.
Very similar rock magnetic properties could be stated at site 28, belonging to Barreme/Aptian carbonates of the Schrattenkalk Fm. Also a system of magnetite/ pyrrhotite carried the characteristic remanent magnetization, which showed SE directed declinations and negative inclinations before bedding correction.
Coniacian to Late Campanian marls from Amden Fm. (site 27; Tab.1), representing the stratigraphic highest units, yielded results at locality Schwarzenberg. Thermal demagnetization of 3 component IRM (Lowrie, 1990) and interpreting the IRM acquisition according to Kruiver et al. (2001) identified magnetite and goethite as carrier minerals of the remanent magnetization. Demagnetization was successful with the alternating field method in the range between 3-30mT and isolated 2 components of the remanent magnetization that showed positive inclinations and NW and NE directed declinations before bedding correction. These data imply 2 phases of vertical axis rotation after folding.

Also in Bregenzer Wald area, results could be derived from 3 sites (31-33; Tab.1) at both limbs of Kanisfluh/Mittagsfluh anticline. Oxfordian/Tithonian carbonates of Quintenkalk Fm. were sampled at the southern limb of the anticline near Au (site 33; Tab.1). Demagnetization with the alternating field succeeded in the range between 35-80mT isolating the component of characteristic remanent magnetization. Before bedding correction declinations are SW directed, the inclinations are negative. Thermal demagnetization of 3 component IRM (Lowrie, 1990) and interpreting the IRM acquisition according to Kruiver et al. (2001) identified magnetite, hematite and goethite as carrier minerals of the remanent magnetization.
At the northern limb of the anticline, 2 sites (31,32; Tab.1) yielded results.

Marls from Tithonian/Berriasian Zementstein Fm. (site 32) were demagnetized with the alternating field in the range between 50-110mT. Although these fields are relatively high, thermal demagnetization of 3 component IRM (Lowrie, 1990) and interpreting the IRM acquisition according to Kruiver et al.(2001) could only identify magnetite as carrier of the remanent magnetization. An increased magnetite grain size is suspected. AMS measurements showed a horizontally oriented K_{max} axis and a vertically oriented K_{min} axis. The magnetic fabric was slightly foliated; the degree of anisotropy was low (P=8,4%).

All these data were indicating an undisturbed sedimentary fabric. The characteristic remanent magnetization again showed SW directed declination and negative inclinations but contrarily to site 33 after bedding correction. The amount of vertical axis rotation is identical to the values calculated for site 33, indicating that magnetizations acquired before and after folding were rotated uniform and contemporaneous. Therefore folding has to be older than clockwise rotation.

At Barremian marls from the Drusberg Fm. (site 31) a system of titanomagnetite, pyrrhotite and goethite was identified by thermal demagnetization of 3 component IRM (Lowrie, 1990) and interpreting the IRM acquisition according to Kruiver et al. (2001) to carry the remanent magnetization. The characteristic remanent magnetization was isolated by demagnetization with the alternating field method in the range between 40-80mT. After bedding correction the declinations were SSW directed, the inclinations were negative.

In the southernmost Bregenzer Wald area, sampling focused on an anticline/syncline structure at locality Sünserspitze. 4 sites from 3 limbs of the structure yielded results. Sites 37 and 36 were sampled in a supposed ramp anticline of the hanging wall, sites 34 and 35 in a supposed folded flat of the footwall.

Aptian carbonates (site37) sampled in the southern limb of the anticline were demagnetized with the alternating field in the range between 20-70mT. A small contribution to the remanent magnetization by goethite could be identified through interpretation of the IRM acquisition according to Kruiver et al. (2001). The characteristic remanent magnetization, most probably carried by magnetite showed SW directed declinations and negative inclinations before bedding correction.

At the northern limb of the anticline Maastrichtian marls of Leimern Fm. (site 36) yielded results. Thermal demagnetization of 3 component IRM (Lowrie, 1990) and interpreting the IRM acquisition according to Kruiver et al. (2001) identified a complex mineralogy of magnetite, pyrrhotite and hematite to carry the remanent magnetization.

The characteristic component of remanent magnetization, possibly carried by magnetite/pyrrhotite was isolated with the alternating field in the range between 40-70mT. Again declinations and inclinations were oriented SW and negative before bedding correction. Similar remagnetizations at both limbs of the anticline were explained as postfolding overprint that was followed by clockwise vertical axis rotation.

Concerning the south dipping northern limb of the successive syncline 2 sites (34,35; Tab.1) yielded results. Marls of Maastrichtian Leimern Fm. (site 35; Tab.1) and Early Eocene Schelpen Fm. (site 34; Tab.1) showed similar rock magnetic properties and comparable characteristic remanent magnetizations, but the mineralogy as well as the components of magnetization are different from the southerly juxtaposed anticline (sites 36,37; Tab.1).
Thermal demagnetization of 3 component IRM (Lowrie, 1990) and interpreting the IRM acquisition according to Kruiver et al. (2001) was identifying a 3 component system of magnetite, hematite and goethite to carry the remanent magnetization. At site 35 AMS measurements resulted in horizontally oriented K_{max} axis and vertically oriented K_{min} axis after bedding correction, indicating an undisturbed sedimentary fabric. Samples from both sites were demagnetized with the alternating field in the range between 10-50mT.
The characteristic remanent magnetizations carried by magnetite, showed both polarities and declinations that were oriented NW/SE after bedding correction. This component of magnetization is interpreted as a prefolding overprint, which only affected the footwall of the supposed ramp-flat structure overprinting all other magnetic information. Most probably the remagnetization and the successive tilting of the footwall is much younger than folding and clockwise rotation that can be observed at the ramp anticline. Following this interpretation the NW directed declinations and the prefolding magnetizations are related to the youngest, counterclockwise vertical axis rotation. As shortening mostly is active at the frontal thrusts of the orogen it is speculated that tilting of Helvetic units most probably was active before counterclockwise rotation. On the other hand this young folding is also possible by out of sequence thrusting during frontal thrusting and contemporaneous internal shortening.

6.2.3. Eastern Helvetic units

In the vicinity of Schliersee sampling focused on a stratigraphic section near locality Ostin. Only 2 sites (38, 39; Tab.1, Fig.8) yielded results.

Compared with sites 10, 11 and sites 16-22 from the northern Alpine Foreland Basin similar components of the characteristic remanent magnetization could be calculated. Declinations were oriented N to NNW, the inclinations showed positive polarity after bedding correction. Again a prefolding overprint is supposed, indicating 30° of clockwise rotation after restoration of the younger counterclockwise rotation. Tilting of the sites should be older than counterclockwise rotation.

At site 39 (Tab.1), sampled in carbonates of Barremian/-Aptian Schrattenkalk Fm. rock magnetic properties could be defined by thermal demagnetization of 3 component IRM (Lowrie, 1990) and interpreting the IRM acquisition according to Kruiver et al. (2001). A system of magnetite, hematite and goethite was identified to carry the remanent magnetization. Demagnetization with the alternating field isolated the characteristic component of magnetization carried by magnetite, in the range between 20-100mT.
Carbonates from Late Cenomanian-/Coniacian Seewerkalk Fm. (site 38; Tab.1) were demagnetized with the alternating field in the range between 20-50mT. The characteristic component of magnetization was carried by magnetite. A small contribution of goethite to the remanent magnetization was identified through interpretation of IRM acquisition according to Kruiver et al. (2001).

6.3. Penninic units

6.3.1. Restoration of vertical/horizontal axes rotations

Results from Penninic units only concern AMS measurements. The magnetic fabric was showing vertical K_{min} axis after bedding correction. K_{max} was oriented horizontally, parallel to the strike of the bedding.
Paleomagnetic data by Hauck (1998) from Barremian-/Aptian rocks of the Rhenodanubian Flysch in the vicinity of Schliersee area and Pueyo et al. (2002) from Rhenodanubian Flysch rocks in the Mariazell meridian show N directed declinations after bedding correction. Primary magnetizations are indicated by positive fold and reversal tests. Although both sampling areas are separated by several 100km along the strike of the Alpine orogen, no relative vertical axis rotations could be found.

6.4. Northern Calcareous Alps

6.4.1. Restoration of vertical/horizontal axes rotations

A remagnetization acquired in folded position was found in sandstones of Chattian age (site 49; Tab.1, Fig. 12), indicating counterclockwise rotation after folding of the Chattian sediments. Primary magnetization were derived from Late Rupelian siltstones (sites 50, 51; Tab.1, Fig. 10,12) showing SSE directed declinations and negative inclinations.
Consequently, after restoring the younger counterclockwise rotation, the declination values from the late Rupelian siltstones indicate 30°-50° of clockwise rotation. These kinematics are identical to geodynamics observed in the Northern Molasse basin and joined vertical axis rotations from the Rupelian onward are supposed.
Site 53 (Tab.1, Fig. 11,12) from Early Rupelian carbonates yielded results in folded position. Similar to the data from the Helvetic units, this site also indicated 60°-80° of clockwise rotation after restoring 30° of younger, counterclockwise rotation.
Therefore magnetizations in Early Rupelian and Mid/Late Rupelian rocks show a 30° difference in clockwise rotation. Consequently a first clockwise rotation (Fig.12) that also affected the Helvetic units postdates folding of Early Rupelian carbonates (site 53; Tab.1) and predates sedimentation of Late Rupelian siltstones (sites 50, 51; Tab.1).

Similar to the Helvetic units, these clockwise- rotated components were acquired before and after folding, indicating syn-to post folding remagnetization (e.g. sites 46-48; sites 64-76; Tab.1). Primary magnetizations from Early Cretaceous to Late Cretaceous sediments (sites 46, 57, 60, 63; Tab.1) and pervasive pre- to synfolding overprints (sites 42-45; sites 81-86; Tab.1) are characterized by NW directed declinations, indicating counterclockwise rotation in post Late Cretaceous times, prior to the first clockwise rotation in Early to Late Rupelian times (Fig. 12, 23).

6.4.2. Western Northern Calcareous Alps (western part)

At locality Muttekopf (site 40; Tab.1, Fig.1,2,9) two components of magnetization with different directions were observed, which resided in the same magnetic mineral with unblocking temperatures up to 500 °C. Alternating field demagnetization was successful in the range between 3 and 30 mT. IRM acquisition curves indicated magnetite as main magnetic carrier mineral.

The declinations of the two components were NW and NE-directed (Tab. 1). Both components yielded negative fold tests with the maximum *k*-value (according to Mc Elhinny, 1964) at 0 % unfolding: Cr= 1.89 for the NE-component; Cr= 2.69 for the NW-component (Fig. 9). Measurements of anisotropy of magnetic susceptibility typically yielded sedimentary, foliated fabrics with a varying degree of anisotropy that is mostly below 5 %. The differences were interpreted to result from the deposition by turbidity currents, due to variable current velocities at different times. There was no evidence for a correlation between the distribution of the paleomagnetic vector components and the magnetic fabric (Thöny et al., 2006).

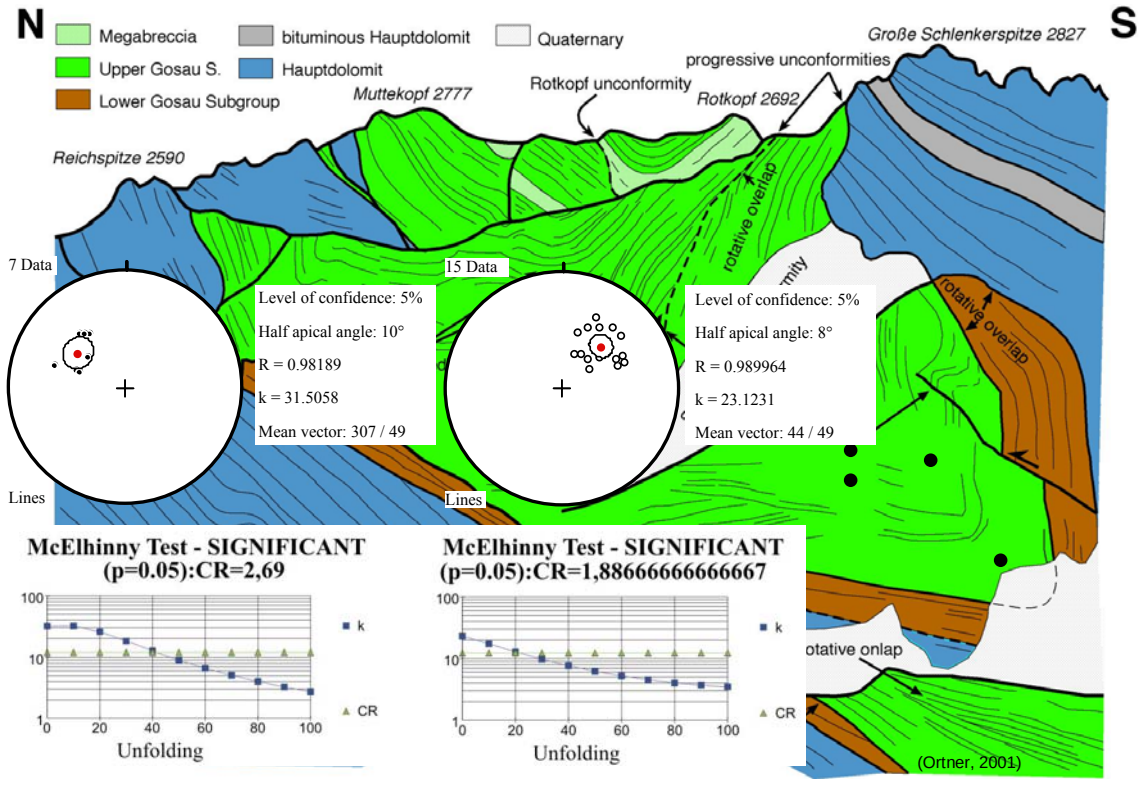

Fig. 9. Results from Muttekopf area indicating two times of remagnetization and two times of successive vertical axis rotations in post-folding times (personal comment H.Ortner).

A stratigraphic section was sampled at locality Lähnbach, 5 sites (41-45; Tab.1) yielded results. Early Liassic carbonates from the Lower Allgäu Fm. (site 45; Tab.1) were demagnetized with the alternating field in the range between 10-70mT. Corresponding unblocking temperatures during thermal demagnetization were observed between 200-400°C. Thermal demagnetization of 3 component IRM (Lowrie, 1990) was identifying a system of magnetite and goethite to carry the remanent magnetitzation.

During demagnetization 2 components, both carried by magnetite could be isolated. The declinations of the 2 components were NW and NE directed. NW directed declinations could be calculated after bedding correction, indicating magnetization and counterclockwise rotation before folding. In contrast the second component with NE directed declinations was acquired in folded position.
Similar rock magnetic properties, a system of magnetite and goethite, were also detected in radiolarites from Oxfordian Ruhpolding Fm.. The characteristic component of magnetization could be isolated during thermal demagnetization and was unblocking between 530-560°C. Carried by magnetite, this component showed again NW directed declinations after bedding correction. AMS measurements were indicating some disturbance to the sedimentary fabric, as K_{min} is tilted 50° to the north. The orientation of K_{min} =29/36.
Malmian, red carbonates of Lower Ammergau Fm were sampled in 2 sites (42,43; Tab.1). At site 43 thermal demagnetization of 3 component IRM (Lowrie, 1990) was identifying a system of magnetite and hematite to carry the remanent magnetization. Isolation of the characteristic component of the magnetization was achieved by thermal demagnetization between 300-580°C. AMS measurements were indicated an undisturbed, typically foliated sedimentary fabric (L/F=0,989; P=1,7%). Also this site showed NW directed declinations after bedding correction. The inclinations were positive throughout the section.

Site 42 also from red carbonates of the Lower Ammergau Fm. showed minor change in mineralogy as magnetite and goethite could be identified as carrier of the remanent magnetization. The characteristic component of magnetization carried by magnetite was identical to sites 43 and 44 and showed NW directed declinations after bedding correction.
Micrites of Tithonian Upper Ammergau Fm. were characterized by a magnetite/pyrrhotite system, which carried the remanent magnetization. Thermal demagnetization of 3 component IRM (Lowrie, 1990) identified a low coercive component, unblocking below 600°C and a medium coercive component that was unblocking at 200°C.

Demagnetization with the alternating field was successful in the range between 3-15mT. With the thermal demagnetization method unblocking temperatures between 100-330°C were observed. Most probably both minerals carry the characteristic component of magnetization, that showed N directed declinations.

At sites 42-45 a significant fold test is indicating maximum *k*- values (according to Mc Elhinny, 1964) at 40% unfolding: Cr= 1,72. Due to the fact that no polarity change could be detected, these remanences are interpreted as a synfolding overprint magnetization that possibly was acquired in Late Cretaceous times during the long normal chron. Before bedding correction, at site 45 a characteristic component with NE directed declinations could be obtained. This insitu component most probably is related to the first clockwise vertical axis rotation in Early Rupelian to Late Rupelian times. Consequently synfolding magnetizations have to be acquired earlier, possibly in Late Cretaceous.

A second stratigraphic section was sampled in Oxfordian to Albian rocks of Puitental zone (sites 46-48; Tab.1). The Albian rocks represent a magmatic sill that intruded into Oxfordian (site 48) to Tithonian (site 47) carbonates. Samples from the sill and the country rock yielded results. At site 48 interpretation of IRM acquisition according to Kruiver et al. (2001) was identifying magnetite and hematite to carry the remanent magnetization. Also thermal demagnetization of 3 component IRM (Lowrie, 1990) at site 47 was indicating a low coercive component, thermally stable below 600°C and a medium/high coercive component that was thermally stable above 600°C. Concerning both sites isolation of the characteristic component of magnetization was challenged by thermal demagnetization. Unblocking temperatures were observed in the range between 300-550°C indicating magnetite as carrier mineral. Before bedding correction the declinations were NE directed, the inclinations were positive.

The Albian sill (site 46) was demagnetized with the alternating field method in the range between 20-50mT. The corresponding unblocking temperatures were observed between 200-550°C. Two components of the remanent magnetization, both carried by magnetite could be isolated. A first component again showed NE directed declinations and positive inclinations but was acquired in a folded position. Values of clockwise rotation are identical concerning components in bedding corrected (site 46) and in tilted position (sites 47, 48), indicating clockwise rotation after folding. The second component presented SE directed declinations and negative inclinations after bedding correction, indicating counterclockwise rotation.

Interpreted as primary magnetization, this component was dating the observed counterclockwise rotation to later than the intrusion of the sill into the stratigraphic section and to earlier than the time of folding of the section.

6.4.3. Western Northern Calcareous Alps (eastern part)

6.4.3.1. Oligocene sediments

At locality Oberangerberg (site 49; Tab.1) Chattian sandstones showed a remanent magnetization that is carried by magnetite and hematite. The carrier minerals of remanent magnetization could be identified through acquisition of isothermal remanent magnetization and thermal demagnetization of 3 component IRM (Lowrie, 1990). The characteristic remanent magnetization carried by magnetite was acquired after tilting and was characterized by NW directed declinations. Alternating field demagnetization was successful in the range between 6-12mT, corresponding unblocking temperatures between 300-450°C were observed during thermal demagnetization. Chattian Oberangerberg Fm. represented the youngest stratigraphic unit that yielded results in the study area of Northern Calcareous Alps. NW directed declinations that were acquired in tilted position indicated remagnetization and counterclockwise rotation around a vertical axis younger than the folding of the Chattian Oberangerberg Fm.

The remanent magnetization of the Rupelian siltstones and marls at localities Unterangerberg (sites50, 51; Tab.1, Fig.1,2,10) and Häring (site 52) was dominated by a magnetite-like phase, which could be identified through acquisition of isothermal remanent magnetization and demagnetization paths towards the origin during alternating field demagnetization in the range between 5 and 15 mT. The corresponding unblocking temperatures were observed during thermal demagnetization around 350 °C. Both sites (50, 52) yielded well grouped magnetization components with NW directed declinations before bedding correction (Tab. 1), indicating counter-clockwise rotation after remagnetization. A statistically significant negative fold test (Cr= 1.98 according to Mc Elhinny (1964)) indicated that the overprint took place after folding. The time of remagnetization and rotation is therefore younger than the age of folding of the Rupelian sediments (Thöny et al., 2006).

Concerning the Late Rupelian Unterangerberg Fm. a second, most probably primary component of the remanent magnetization could be isolated (sites 50,51, Tab.1, Fig.1,2,10, 12). Also carried by magnetite, this component was characterized by S directed declinations and negative inclinations after bedding correction. A positive McElhinny (1964) test indicated maximum k-values at 100% unfolding: Cr=1,84. Due to weak susceptibilities only the Kmin axis was significantly defined. Steep orientations at both sites (253/82; 324/77; Tab.1) were indicating undisturbed sedimentary fabrics.

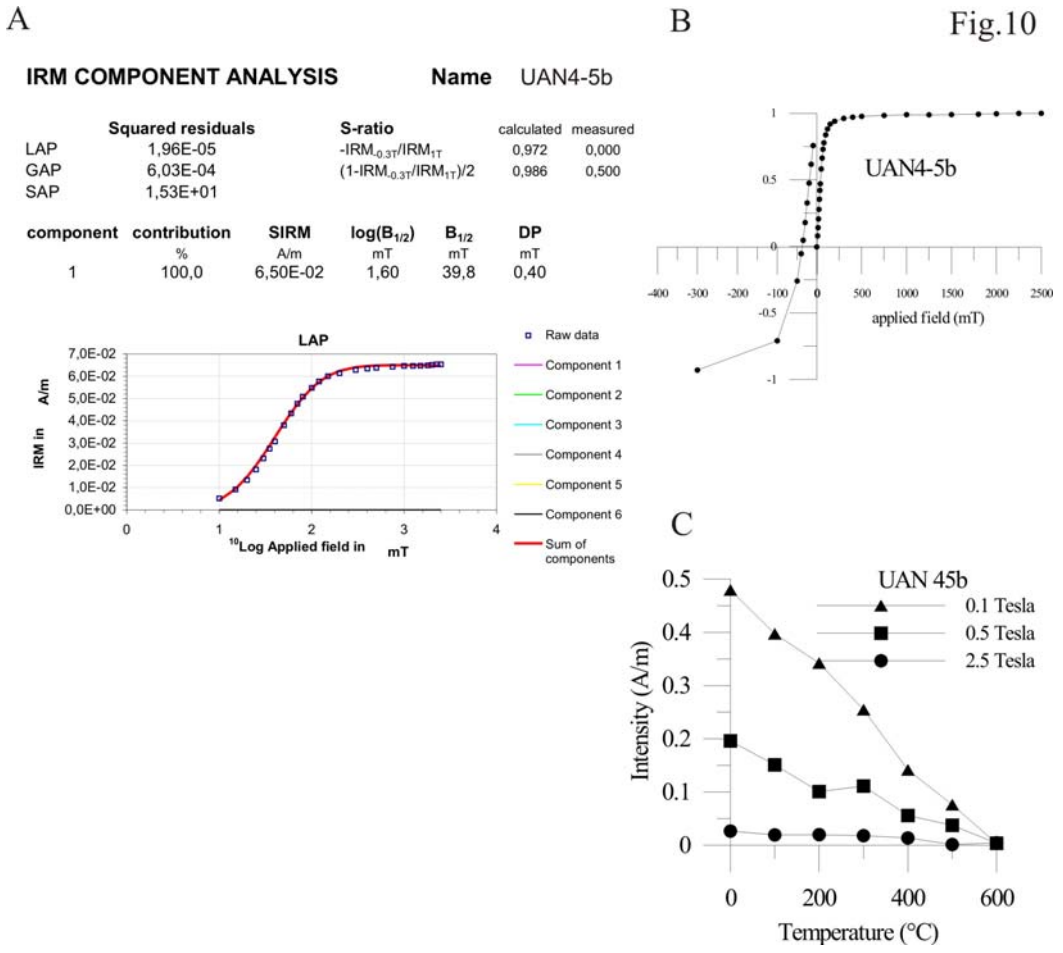

Fig. 10. Rock magnetic properties, demagnetization behavior and statistical parameters from site 50 (UAN2/3/4, **A-C, D1, F1, D3, F3, G3**) and site 51 (OA2, **A-C, D2, F2**), (Tab.1).

A= IRM component analysis according to Kruiver et al. (2001); **B**= Typical IRM acquisition curves; **C**= Thermal demagnetization of three component IRM (Lowrie, 1990).

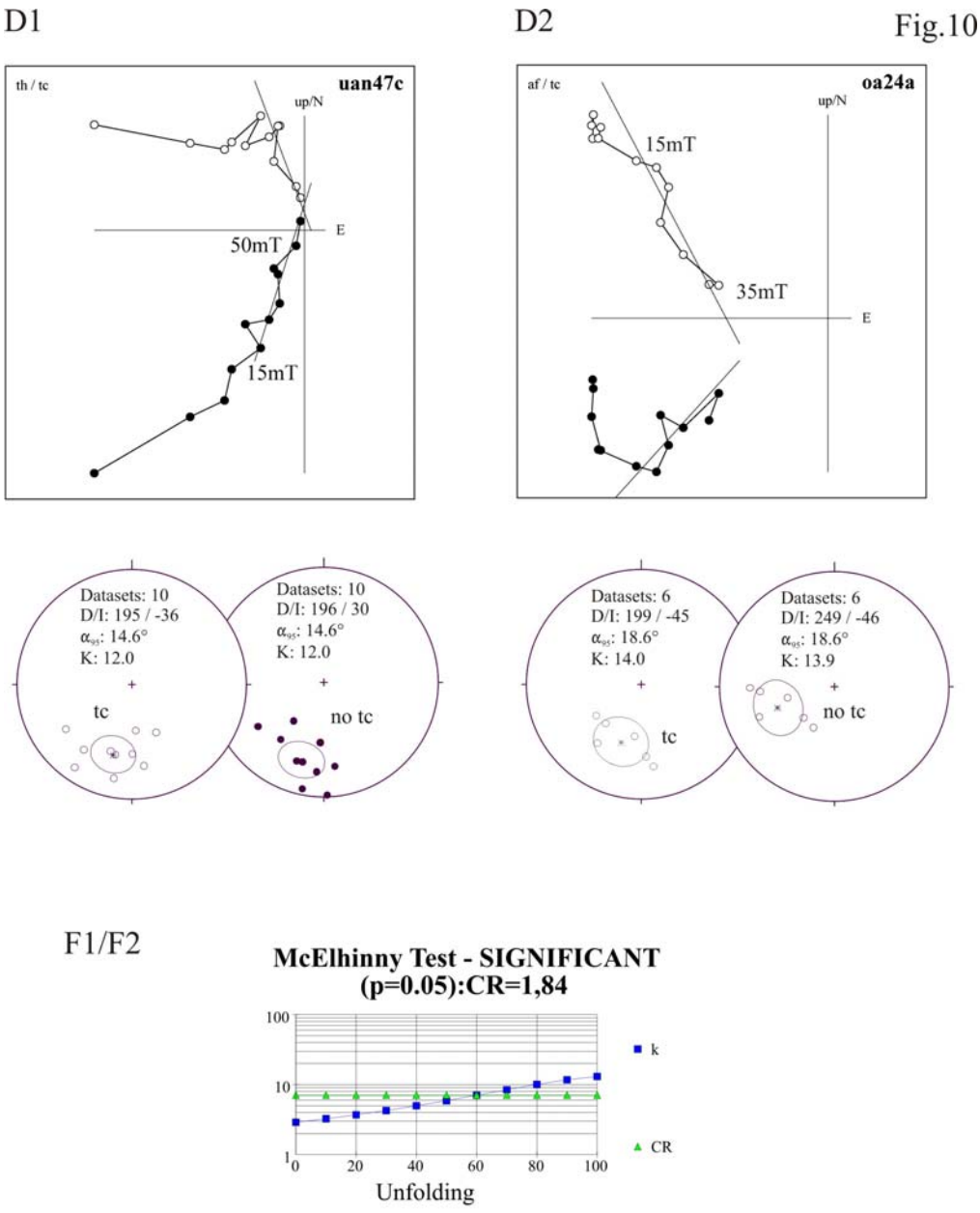

Fig. 10. Rock magnetic properties, demagnetization behavior and statistical parameters from site 50 (UAN2/3/4, **A-C, D1, F1, D3, F3, G3**) and site 51 (OA2, **A-C, D2, F2**), (Tab.1).

D= Zijderveld demagnetograms of representative samples in stratigraphic (tc) and geographic (no tc) coordinates, in the Zijderveld diagrams, full/hollow circles: projection of the NRM in the horizontal/vertical plane. Stereogeographic projection of the characteristic remanence magnetization direction, bedding corrected (tc), in situ (no tc) coordinates; **F**= fold test according to McElhinny (1964).

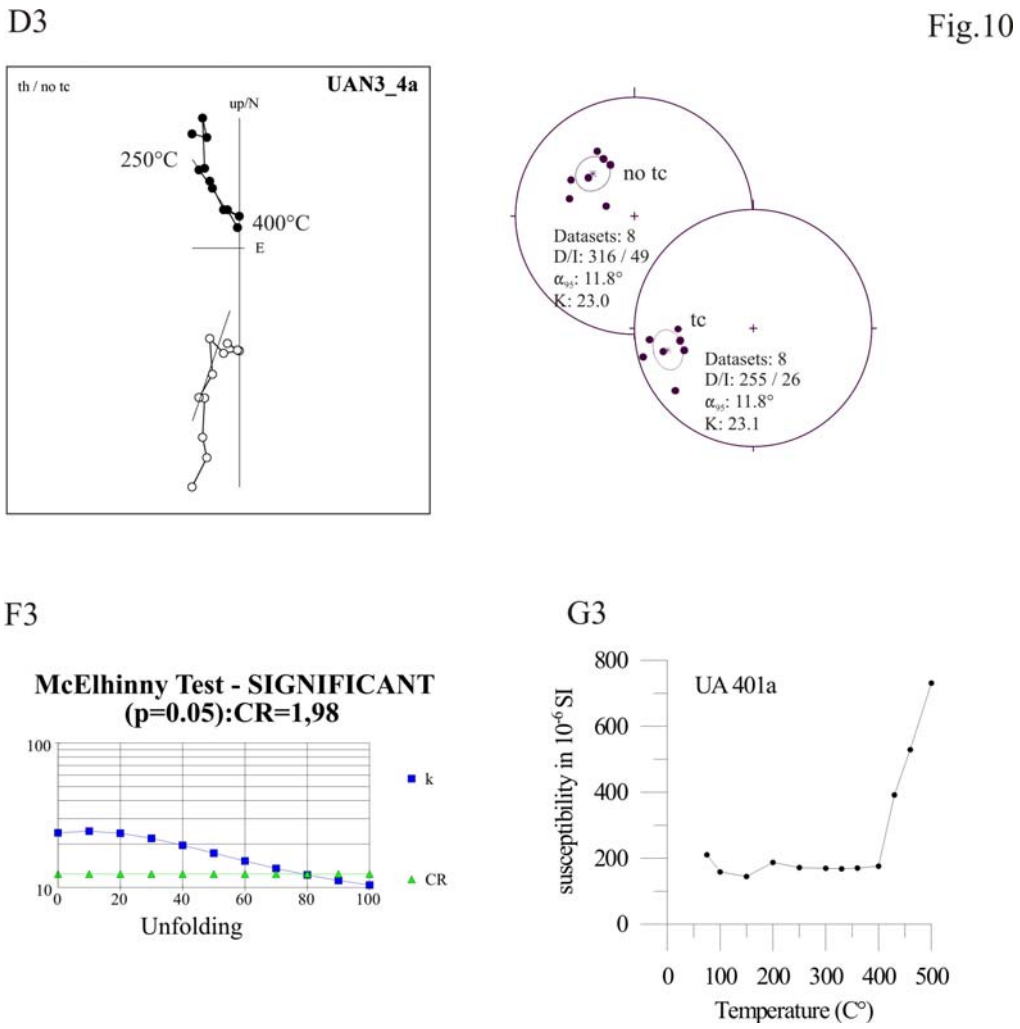

Fig. 10. Rock magnetic properties, demagnetization behavior and statistical parameters from site 50 (UAN2/3/4, **A-C, D1, F1, D3, F3, G3**) and site 51 (OA2, **A-C, D2, F2**), (Tab.1).

D= Zijderveld demagnetograms of representative samples in stratigraphic (tc) and geographic (no tc) coordinates, in the Zijderveld diagrams, full/hollow circles: projection of the NRM in the horizontal/vertical plane. Stereogeographic projection of the characteristic remanence magnetization direction, bedding corrected (tc), in situ (no tc) coordinates; **F**= fold test according to McElhinny (1964), **G**= Susceptibility versus temperature curves.

Lower Rupelian carbonates (site 53, Tab.1, Fig.1,2,11) from locality Bruckhäusl were characterized by demagnetization paths towards the origin in the range from 300 to 500°C, or between 15 and 80 mT. Magnetite was the main carrier of the remanent magnetization, but minor contributions from pyrrhotite were observed in some samples. The mean paleomagnetic direction for this group showed southwesterly declinations and negative inclinations before bedding correction (Tab. 1) (Thöny et al., 2006).

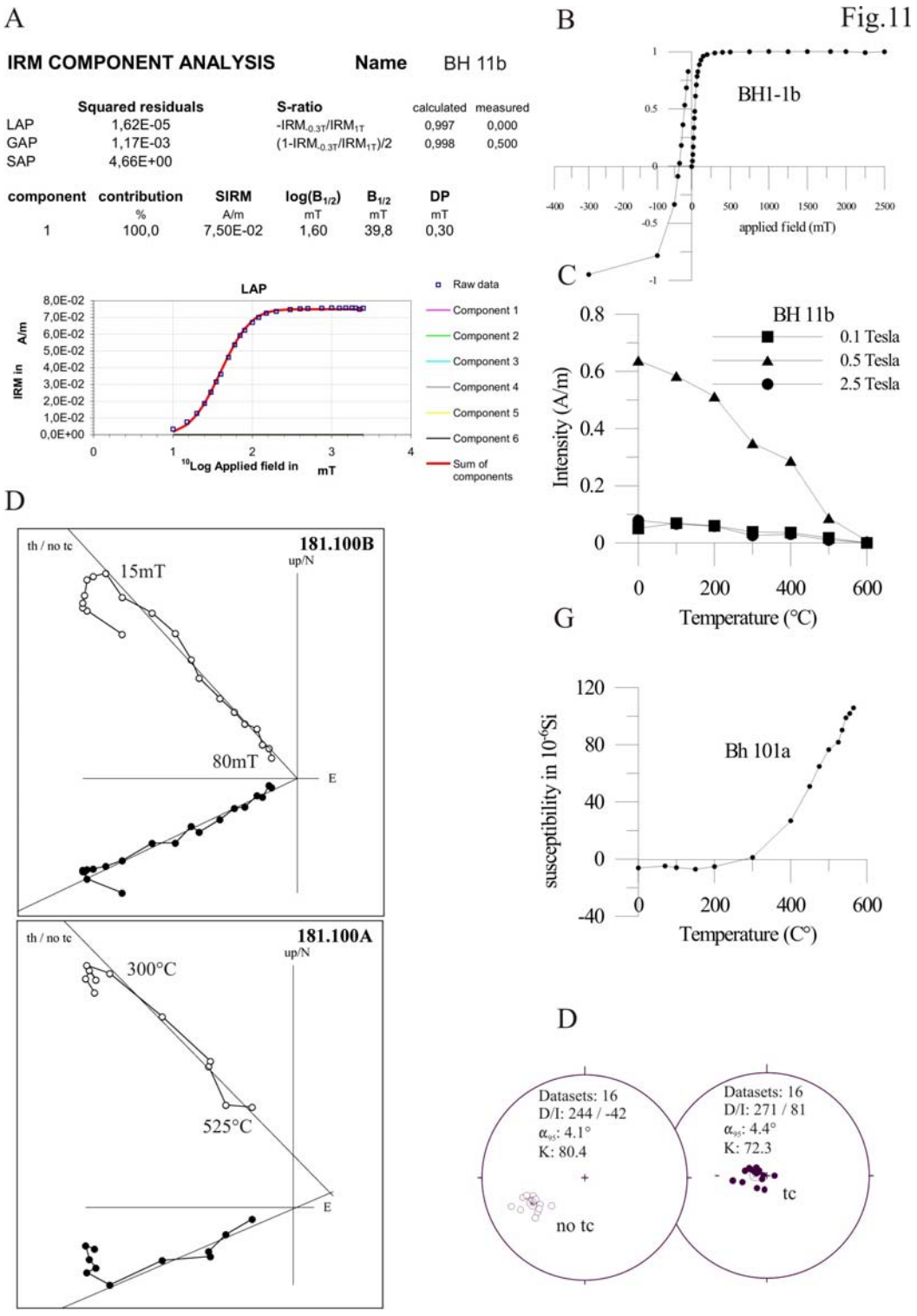

Fig. 11

Fig. 11. Rock magnetic properties, demagnetization behavior and statistical parameters from site 53 (BH), (Tab.1). **A**= IRM component analysis according to Kruiver et al. (2001); **B**= Typical IRM acquisition curves; **C**= Thermal demagnetization of three component IRM (Lowrie, 1990); **D**= Zijderveld demagnetograms of representative samples in stratigraphic (tc) and geographic (no tc) coordinates, in the Zijderveld diagrams, full/hollow circles: projection of the NRM in the horizontal/vertical plane. Stereogeographic projection of the characteristic remanence magnetization direction, bedding corrected (tc), in situ (no tc) coordinates; **G**= Susceptibility versus temperature curves.

6.4.3.2. Cretaceous to Eocene sedimentary rocks

Samples from Eocene and Upper Cretaceous sedimentary rocks at sites 54 to 58 showed successful demagnetization with the alternating field method. Well grouped demagnetization vectors, which typically deflected from the origin, were observed in the range between 5 and 30 mT (Tab.1). Thermal demagnetization in the temperature range up to 500 °C was successful as well. IRM acquisition curves clearly identified magnetite to be the main carrier mineral (Thöny et al., 2006).

The two sites in Eocene carbonates and marls (54, 55; Tab.1) yielded statistically significant negative fold tests (Tab. 1). McElhinny tests indicated best k-values at 20 % unfolding (Cr = 2.22 and 2.33 for 54 and 55, respectively). At site 55 the observed clockwise rotation occurred subsequent to the remanence acquisition, which took place in a late stage of folding (Thöny et al., 2006). Also, at site 55 a second component of magnetization, showing northwesterly declinations before bedding correction was calculated. This component indicated counterclockwise rotation after folding. Consequently a temporal succession can be defined, starting with the synfolding, clockwise rotated magnetization that is followed by a postfolding magnetization, rotated counterclockwise afterwards. Site 54 is characterized by synfolding magnetization. The remanences are distributed along a small circle, after restoring the characteristic component to the reference direction (N/50), the tilt axis is trending SSW/NNE (202/35).

Undisturbed magnetic fabrics were observed in the Campanian silt-/sandstones at site 58 (Hechtsee) with K_{min}- axis oriented vertically and K_{max}-axis aligned WSW within the bedding plane. The characteristic component of magnetization was calculated before bedding correction. Comparable with results from Maastrichtian carbonates at site 56, the declinations were NE directed, the inclinations were positive.

At site 57, locality Mühlbergerbach (Tab.1) Maastrichtian to Campanian marls yielded results. Thermal demagnetization yielded unblocking temperatures around 600°C. After bedding correction the AMS measurements yielded horizontally oriented K_{max} -axis and vertically oriented K_{min} -axis. An undisturbed sedimentary fabric was supposed. The magnetic fabric was typically foliated (F=11,8%; P=14,3%) a possible inclination flattening could not be excluded. The characteristic component, interpreted as primary magnetization was calculated after bedding correction and showed northwesterly declinations and positive inclinations.

Two sub-parallel components of magnetization could be isolated in marls of Late Campanian age from locality 8, Schwoich. Thermal demagnetization yielded unblocking temperature spectra of 100°- 300°C and 400°-500°C (Tab. 1). Accordingly, the same components could be discriminated by applying alternating fields in the ranges between 2–20 and 30–50 mT. Also IRM acquisition curves indicated two different magnetic minerals, a low-coercive mineral (most probably magnetite) and a high coercive mineral such as pyrrhotite.

Each of these minerals was carrying about 50 % of the observed natural remanent magnetization, but no significant differences in the directions could be observed.

The mean paleomagnetic direction before bedding correction (Tab. 1) derived from well grouped vectors representing both polarities gave evidence for counter-clockwise rotation (Dec=326; Inc=51) (Thöny et al., 2006).

Due to very similar bedding planes there was no significant proof for the timing of the remanence acquisition with respect to the tectonic tilting from a fold-test. However, the observed larger scatter of the vectors after bedding correction gave evidence for post-tilting remagnetization and subsequent counter-clockwise rotation.

At locality Mühlbach/ Brandenberg marls of Santonian age (sites 60,61; Tab.1) yielded well defined demagnetization paths towards the origin during thermal demagnetization. Three different components of magnetization were observed (Tab. 1).

The lower temperature component unblocked at temperatures below 400° - 450°C and was characterized by NW-directed declinations with positive inclinations before bedding correction. The second component was isolated up to 560 – 580°C and showed NNE-directed declinations before bedding correction. Similar to results from site 57 (Tab.1) the third component, most probably of primary origin, again carried by magnetite was acquired before folding and showed NW directed declinations as well.

AMS measurement indicated an undisturbed sedimentary fabric. K_{max} and K_{min} axis were oriented horizontally and vertically, respectively. Samples from one site in red marly mudstone at site 60 showed a significant contribution from hematite in the IRM-curves, although the main carrier of the natural remanent magnetization was magnetite.

Sites sampled in Early Cretaceous sediments yielded results at localities Niederndorf (site 62) and Kurz (site 63). One site in carbonates of Cenomanian Branderfleck Fm. (site 62) was demagnetized thermally, yielding unblocking temperatures around 670°C. IRM acquisition curves identified a contribution of magnetite to the remanent magnetization. The characteristic component of magnetization most probably carried by hematite showed NE directed declinations and positive inclinations before bedding correction. At Albian to Aptian carbonates of Tannheim Fm. (site 63) thermal demagnetization in the range between 300-550°C identified magnetite to carry the remanent magnetization. The characteristic component of magnetization, carried by magnetite, showed SE directed declinations and negative inclinations after bedding correction. Results from Lower Inn valley area are summarized in Fig. 12.

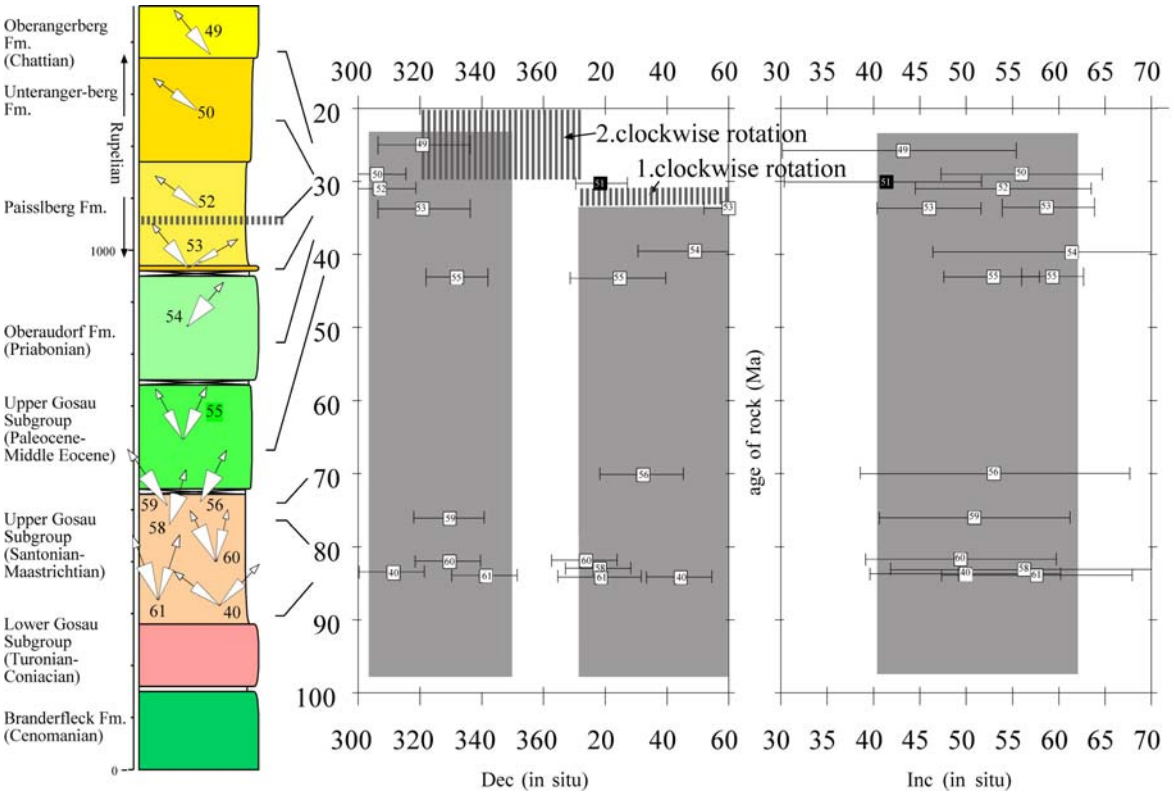

Fig. 12. Stratigraphic summary section of Late Cretaceous to Oligocene rocks in the Unterinntal area and associated cross plots of age of rock and declination/inclination of secondary/primary magnetizations. Note that declinations do not change systematically with age of rock. Shaded squares illustrate mean direction of inclinations and declinations of clockwise and counter-clockwise rotated remagnetizations in the Unterinntal area in Cenozoic times. Numbers at arrows refer to Tab. 1. The black square marks the only primary magnetization that could be derived in the Lower Inn valley area (sites 50, 51; Tab.1).

6.4.3.3. Stratigraphic sections

At section Guffert, placed at the northern limb of the Thiersee syncline, 5 sites sampled in Late Triassic to Early Cretaceous carbonates (Nagel et al., 1976; Sausgruber, 1995) yielded results (Fig.13a, 13b). Alternating field demagnetization was successful at sites 69, 66 and 64 isolating the characteristic component between 5-60mT.
At sites 66 from Oxfordian radiolarites of Ruhpolding Fm. and 64 from Malmian carbonates from Upper Ammergau Fm. this component showed NNE directed declinations and positive inclinations before bedding correction, indicating clockwise rotation after folding. Partly the inclinations showed flattening and the characteristic components of magnetization were distributed on a N/S aligned small circle (Waldhör, 1999).
From sites 68, 67 and 65 nearly identical characteristic components could be derived, also indicating clockwise rotation after folding. At sites 67, 68 magnetite as carrier minerals of remanent magnetization was identified by thermal demagnetization, yielding unblocking temperatures around 550°C. Contributions by hematite and goethite were interpreted from the IRM acquisition according to Kruiver et al. (2001). A similar system of magnetite, hematite and goethite was also identified to carry the remanent magnetization at site 65 but unblocking temperatures of 645°C during thermal demagnetization indicated a contribution to the characteristic component of magnetization by hematite as well.
Only site 69, sampled in Late Triassic Kössen Fm. presented a characteristic component, carried by magnetite that differed from the rest of the site means. Declinations were NE directed, inclinations positive, but in contrast to the rest of the section after bedding correction. Consequently this component was interpreted as prefolding overprint and the remanent magnetizations of the remaining sites as post folding overprint. Therefore the stratigraphic section experienced prefolding to syn/post folding remagnetization, before clockwise rotation.

At section Ampelsbach (Fig. 13A-C), placed at the southern, overturned limb of the Thiersee syncline, 7 sites sampled in Late Triassic to Early Cretaceous carbonates, including red and grey nodular limestones, yielded results (Channel et al., 1992; Sausgruber, 1995). In contrary to the Guffert section at Ampelsbach locality only carbonates from basin to slope facies were sampled. Demagnetization with the alternating field in the range between 5-40mT and unblocking temperatures of 450-550°C during thermal demagnetization identified magnetite as carrier of the characteristic component of magnetization.

Site 74, sampled in red carbonates of Lower Toarcian Middle Allgäu Fm. showed contributions to the remanent magnetization resulting from hematite. The characteristic component unblocked in the range of 600°C, while alternating field demagnetization yielded no results. The intensity of the remanent magnetization in the range higher than 600°C was too weak to deduce a significant magnetisation vector. The interpretation of the IRM acquisition according to Kruiver et al. (2001) and unblocking temperatures of 300°C observed during thermal demagnetization were indicating titanomagnetite and goethite as carrier minerals or the remanent magnetization at site 76 that was sampled in Liassic carbonates of Lower Allgäu Fm.

Concerning all sites the characteristic component showed NE to ESE directed declinations and positive inclinations before bedding correction, indicating clockwise rotation after folding. Especially the declinations showed a distribution along a small circle (Waldhör, 1999). The great circle of the Thiersee syncline, which is defined by the bedding planes, was oriented parallel to it. Consequently a syn- to post-folding remagnetization is supposed. The observed pervasive remagnetization that was acquired on the southern limb of the syncline in steep to overturned position, had to be corrected from NE/SW to E/W striking site-bedding planes as dextral strike slip faults (Sausgruber, 1995) that were active after remagnetization and after tilting, disintegrated the overturned sites.

At locality Thiersee the two sections, described above, presented characteristic components of magnetization that were placed on a small circle (Waldhör, 1999) that was nearly identical to the great circle of the local fold structure (Thiersee-syncline). The McElhinny Test (Mc Elhinny, 1964) is showing best concentration (Cr= 1.98) of directions of characteristic components at 30% unfolding (Fig. 13A-C). This situation was interpreted as synfolding overprint that was acquired diachronously depending on permeability/porosity properties of the sampled lithologies. Several phases of remagnetization during folding could be distinguished. The first remagnetization event was active in a position with 30% of unfolding in comparison with today's syncline geometries.

The characteristic components of single sites were rotated together with the sites along the subhorizontal trending fold axis of the Thiersee-syncline. Characteristic components of magnetization that showed no flattening of inclination marked the end of folding and rotation along the horizontal axis. After folding and rotation along the subhorizontal fold axis the Thiersee syncline was affected by clockwise rotation along a vertical axis causing a NE directed declination of the characteristic component of magnetization (Dec=39; Inc=54). After restoring this characteristic component to the reference direction (N/50) the tilt axis is trending SW/NE (227/26).

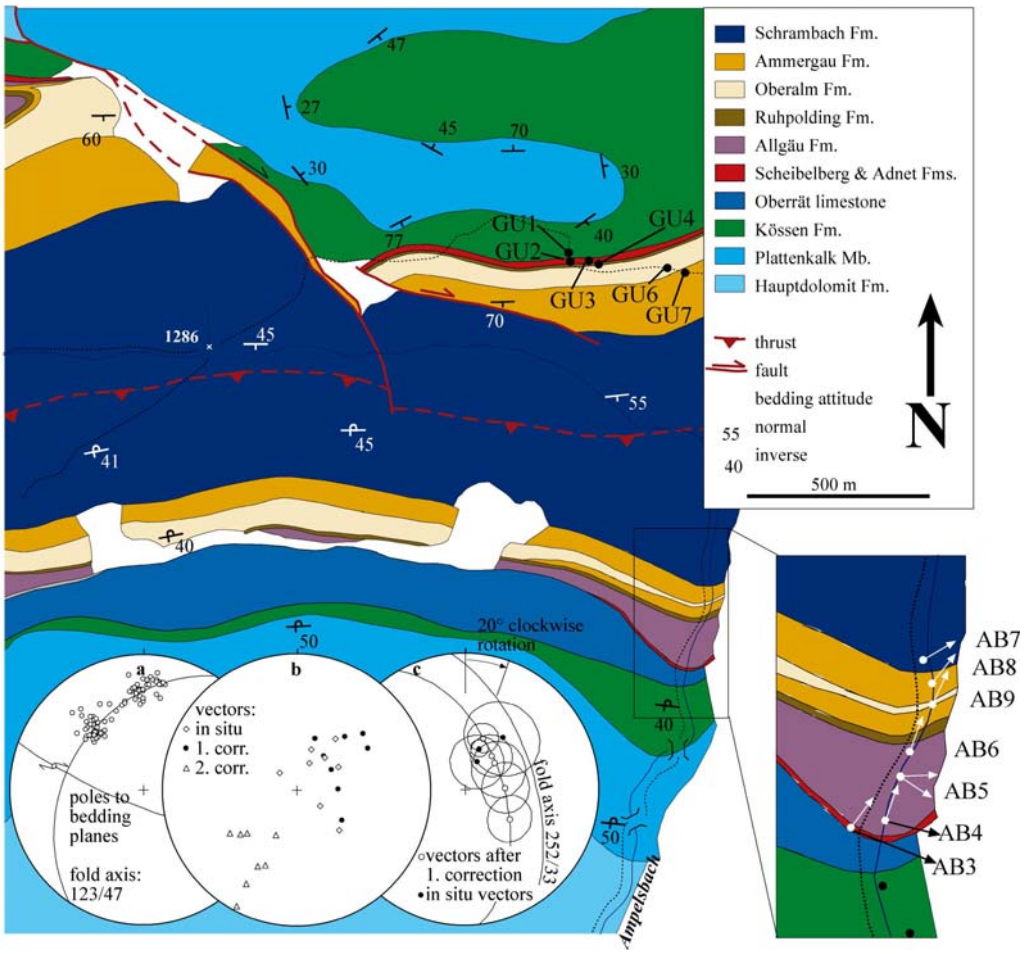

Fig. 13. **A:** Geologic sketch of the Ampelsbach area (Ortner, personal communication). Geology redrawn from Sausgruber (1994). Declinations of magnetizations are indicated by arrows. Inset a) local fold axes related to fault activity calculated from bedding planes, Inset b) orientation of paleomagnetic vectors insitu and after first and second correction, Inset c) orientations of paleomagnetic vectors after first correction with cones of confidence arranged along a small circle. This is interpreted to be the result of remagnetizing during folding. Site abbreviations AB3-AB9 (=Sites 70-76) and GU1-GU7 (=Sites 64-69) refer to Table 1.

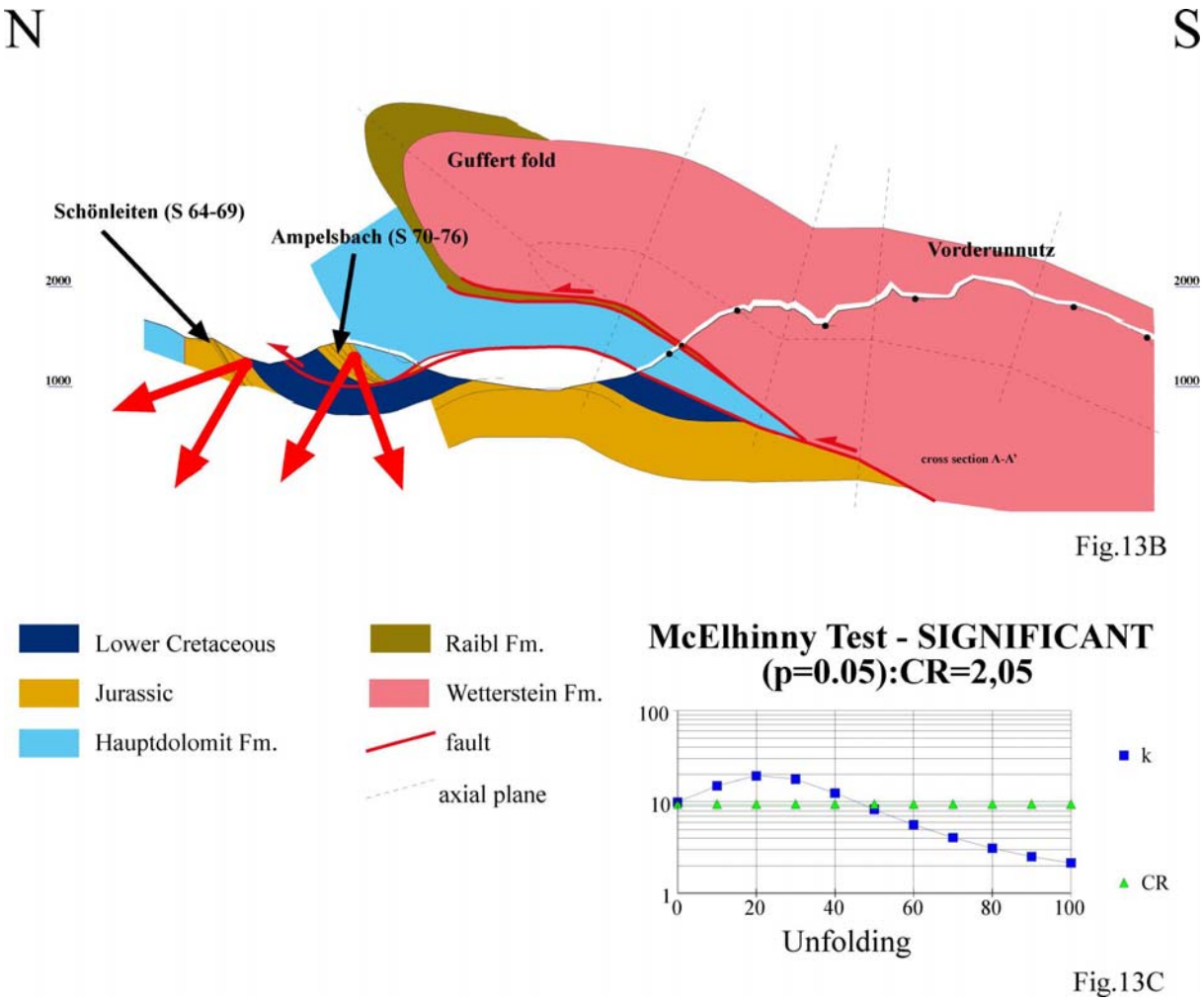

Fig. 13B: N/S oriented cross section illustrating tilting of remagnetization vectors during folding (Ortner, personal communication). Fig.13C: Fold test according to McElhinny (1964).

6.4.4. Central Northern Calcareous Alps

6.4.4.1. Restoration of vertical/horizontal axes rotations

Paleomagnetic data derived from sediments younger than Late Cretaceous indicate identical kinematics compared with the results from contemporaneous lithologies from the western Northern Calcareous Alps. Significant differences are possibly indicated by preliminary data by Pueyo et al. (2002). Magnetizations from sites, sampled in Mesozoic carbonates of the Bajuvaric Frankenfels, Lunz and Reisalpen nappe units along the Mariazell meridian, characterized by positive fold and reversal tests were showing N/S directed declinations and positive/negative inclinations, respectively.

In contrast primary magnetizations from synchronous sediments sampled in the Lechtal nappe (sites 42-45; Mauritsch and Becke, 1987) of the western Northern Calcareous Alps and in the Tirolic (sites 81-86) and Juvavic nappes (Haubold et al., 1999) of the Central/Eastern Northern Calcareous Alps are indicating a counterclockwise rotation of 30°.

Primary magnetizations from Penninic units do not show any differences, although they were derived from sampling localities in the west (Schliersee; Hauk, 1998) and east (Mariazell, Pueyo et al., 2002). The well Vordersee 1 penetrated the Tirolic unit SE of Salzburg and reached the underlying Bajuvaric unit with Paleogene sediments on top (Geutebrück et al., 1984). Consequently the relative rotation in a counterclockwise sense that is observed between Lechtal/Tirolic/Juvavic nappes relative to Bajuvaric units E of the Inn valley might be related to thin-skinned nappe thrusting, postdating the sedimentation of the Paleogene lithologies, mentioned above. During Mid Eocene closure of the Penninic Ocean (Frisch, 1981), joined kinematics of Lechtal/Tirolic/Juvavic and Bajuvaric nappes resulted in identical paleomagnetic data.

6.4.4.2. Late Cretaceous sediments

At locality Gall 2 sites (79, 80; Tab.1) sampled in Coniacian Carbonates of Schmalnau Fm. were demagnetized with the alternating field in the range between 3-30mT. The characteristic remanent magnetization was showing NE directed declinations before bedding correction, concerning both sites. The significant negative fold test (according to McEllhinny (1964)) yielded maximum k-values at 0% unfolding.

Early Santonian carbonates of Grabenbach Fm. were sampled at localities Weißenbach and Wirling. At two sites (77,78; Tab.1) demagnetization with the alternating field method could isolate the characteristic component of magnetization in the range between 30-90mT. Corresponding unblocking temperatures were observed around 525°C. This component, carried by magnetite, showed NW and NE directed declinations before and after bedding correction, respectively. After bedding correction the orientation of this characteristic component is D/I= 25/45. Sites 79 and 80 are characterized by a similar component that is oriented D/I= 55/58 but is contrarily presenting a significant negative fold test, indicating remagnetization after folding. Consequently these differing declinations directions can be interpreted in two ways.

Interpretation 1: All four sites (77-80) were affected by a single event of remagnetization, starting as prefolding overprint (sites 77,78) and finishing as postfolding overprint at sites 79,80. Differences concerning declinations (30°) are explained by the site locations close to the KLT-fault (Decker et al., 1994). Additional rotations of single blocks around vertical axes cannot be excluded.

Interpretation 2: This model is based on two times of remagnetization. An earlier postfolding overprint was affecting sites 79,80 (neg. foldtest). After clockwise rotation, sites 77,78 faced a second remagnetization. The characteristic component was indicating counterclockwise rotation afterwards. This second interpretation is not favored, because absolutely no overlapping of the two events of remagnetization can be detected from these four sites (Tab.1).

6.4.4.3 Stratigraphic sections:

At locality Kohlstatt (Fig.14) 6 sites in Rhaetian to Neocomian carbonates yielded results. The characteristic remanent magnetization of all sites was isolated during thermal demagnetization and showed NW directed declinations after bedding correction. No polarity changes could be observed. Except site 84, sampled in red carbonates of Klauskalk Fm., magnetite carried the characteristic component of magnetization. At Sites 82 and 83 a positive fold test (according to McEllhinny, 1964) yielded maximum k-values at 90% unfolding (Cr=1,98). At site 84, unblocking temperatures around 660°C, observed during thermal demagnetization, suggest a contribution to the characteristic remanent magnetization by hematite as well.

Due to the absence of polarity changes the observed characteristic remanent magnetization of all sites was interpreted as a prefolding overprint, probably acquired in the Late Cretaceous during the long normal chron.

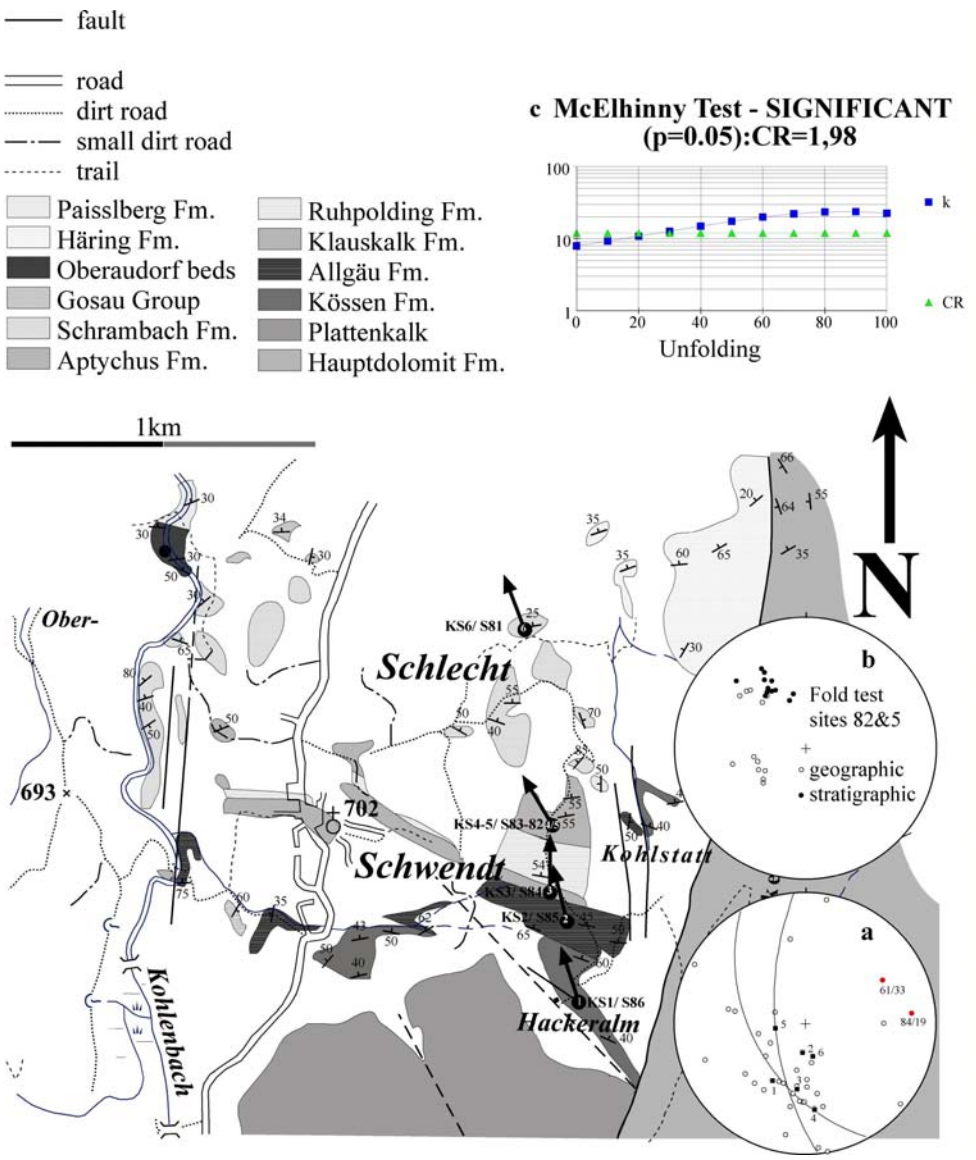

Fig. 14. Geologic sketch of the Schwendt area. Declinations of magnetization are indicated by arrows (Ortner, personal communication). Sites were sampled in Late Triassic to Early Cretaceous rocks. Inset **a**) circles: poles to bedding planes of Jurassic rocks, black squares: mean orientation of bedding in paleomagnetic sampling sites, numbers correspond to numbers in arrows. Inset **b**) a positive foldtest indicates prefolding magnetization (sites 82/83, Ks4/5, Tab.1). Inset **c**) positive Fold test according to McElhinny (1964).

In the Unken syncline (Fig.15) the sampled stratigraphic column ranges from the Early to Late Jurassic and includes mostly red and grey nodular limestones (Vecsei et al., 1989; Krainer and Mostler, 1997).

Sites 89-91 and 87 were characterised by low coercive minerals with unblocking temperatures between 400° and 450°C. Using alternating field demagnetization the characteristic component of magnetization could be isolated between 10 and 15mT. IRM measurements also yielded a low coercive mineral, most probably magnetite to be the main magnetic carrier mineral for sites 89-91and 87.

Only at site 88, sampled in radiolarites of Oxfordian Ruhpolding Fm. IRM measurements were indicating a 50% contribution of a high coercive mineral, possibly hematite. During thermal demagnetisation the characteristic component of magnetization was unblocking at 525°C indicating magnetite. No polarity changes could be observed in the whole section. Due to similar bedding data concerning all 5 sites no fold tests could be performed.

At locality Unken syncline the insitu locality mean (Dec=18; Inc=54) derived from 5 sites was interpreted to be a result of a post folding, most probably Tertiary remagnetisation and successive clockwise rotation.

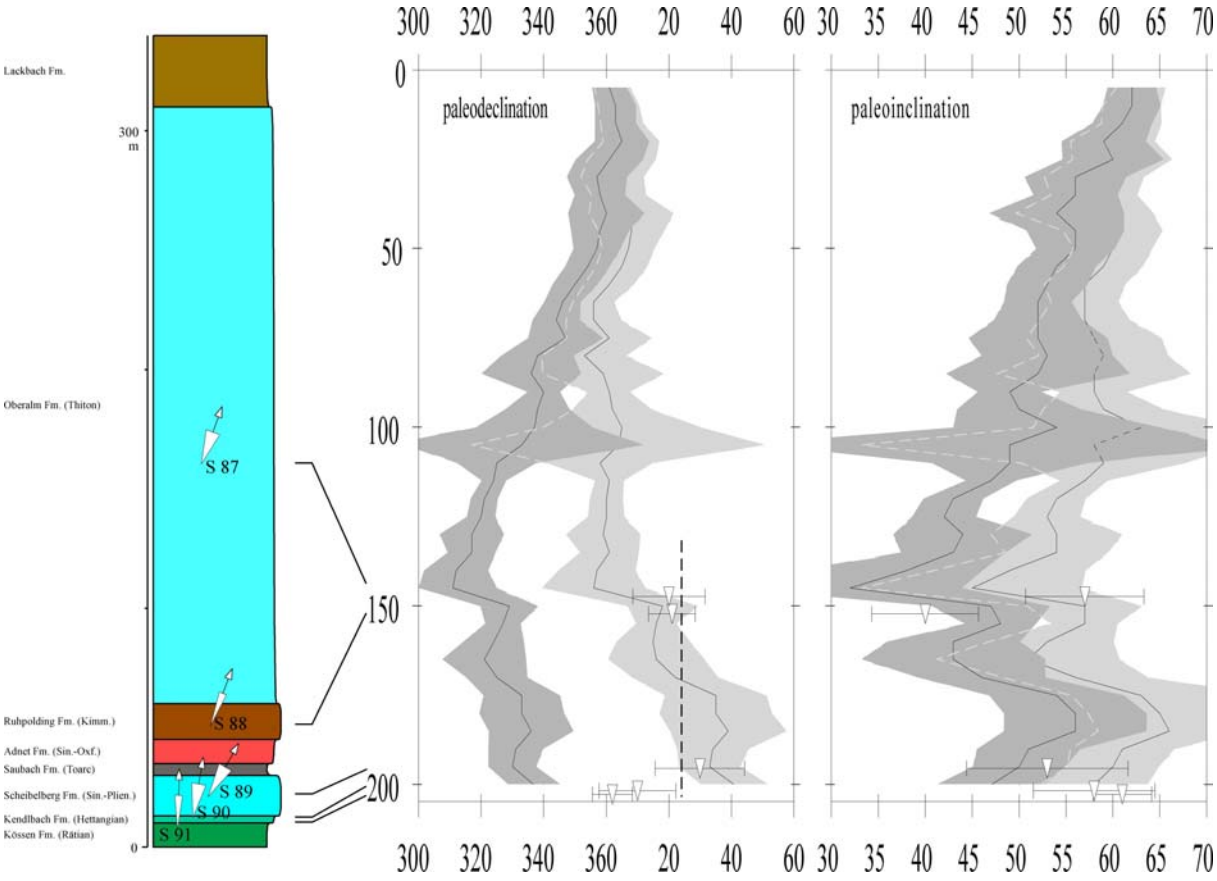

Fig. 15. Stratigraphic section of Late Triassic to Early Cretaceous rocks in the Unken syncline area and associated cross plots of age of rock and declination/inclination of secondary magnetizations. For comparison: African and European "APWP (apparent polar wander path)" are marked by dark- and light gray curves, respectively (Ortner, personal communication). Numbers (S87-S91) refer to Tab.1.

6.5. Central Alps

6.5.1. Restoration of vertical/horizontal axes rotations

Characteristic components of magnetization are indicating clockwise and counterclockwise rotations. All magnetizations were interpreted as CRM (chemical remanent magnetization), possibly resulting from fluid derived alteration. As dykes at sites 92 and 93 are radiometrically dated to 32Ma, remagnetization and successive counterclockwise rotation must be younger. Nevertheless a kinematical evolution of the Central Alps based on paleomagnetic data only can be defined by comparing these results to primary, synchronous magnetizations from Northern Calcareous and Southern Alps.

6.5.2. Oligocene dykes

After removal of a viscous magnetization component at the beginning, all samples from sites 92 and 93 (Tab.1, Fig.16) yielded one-component demagnetization paths towards the origin. The component could be thermally demagnetized in the temperature range between 460 and 550 °C, and with alternating fields between 3–50 mT. Three-component IRM experiments were identifying a system of low to medium coercive minerals. Due to the relatively high alternating fields that were needed to demagnetize the ChRM and varying unblocking temperatures, titanomagnetite with different titanium content was supposed to be the main magnetic carrier mineral. However, the susceptibility decrease between 250 and 500° C on heating gives evidence for maghemite in the samples (Thöny et al., 2006).

Well grouped vector components gave mean paleomagnetic directions before bedding correction (Dec=335; Inc=56 and Dec= 316; Inc=60) for sites 92 and 93 (Tab.1, Fig.16), with evidence for counter-clockwise rotation after cooling below Curie temperatures or subsequent remagnetization (Thöny et al., 2006).

All samples showed similar magnetic fabrics, with subhorizontal K_{max}- and nearly vertical K_{int}-axes in alignment with the orientation of the dyke, except for a single site where the magnetization vectors were aligned with the K_{min}-axes.

All other sites showed no dependence from the magnetic fabric. The degree of anisotropy is low (0.9–4.7 %), the fabrics are foliated (Thöny et al., 2006).

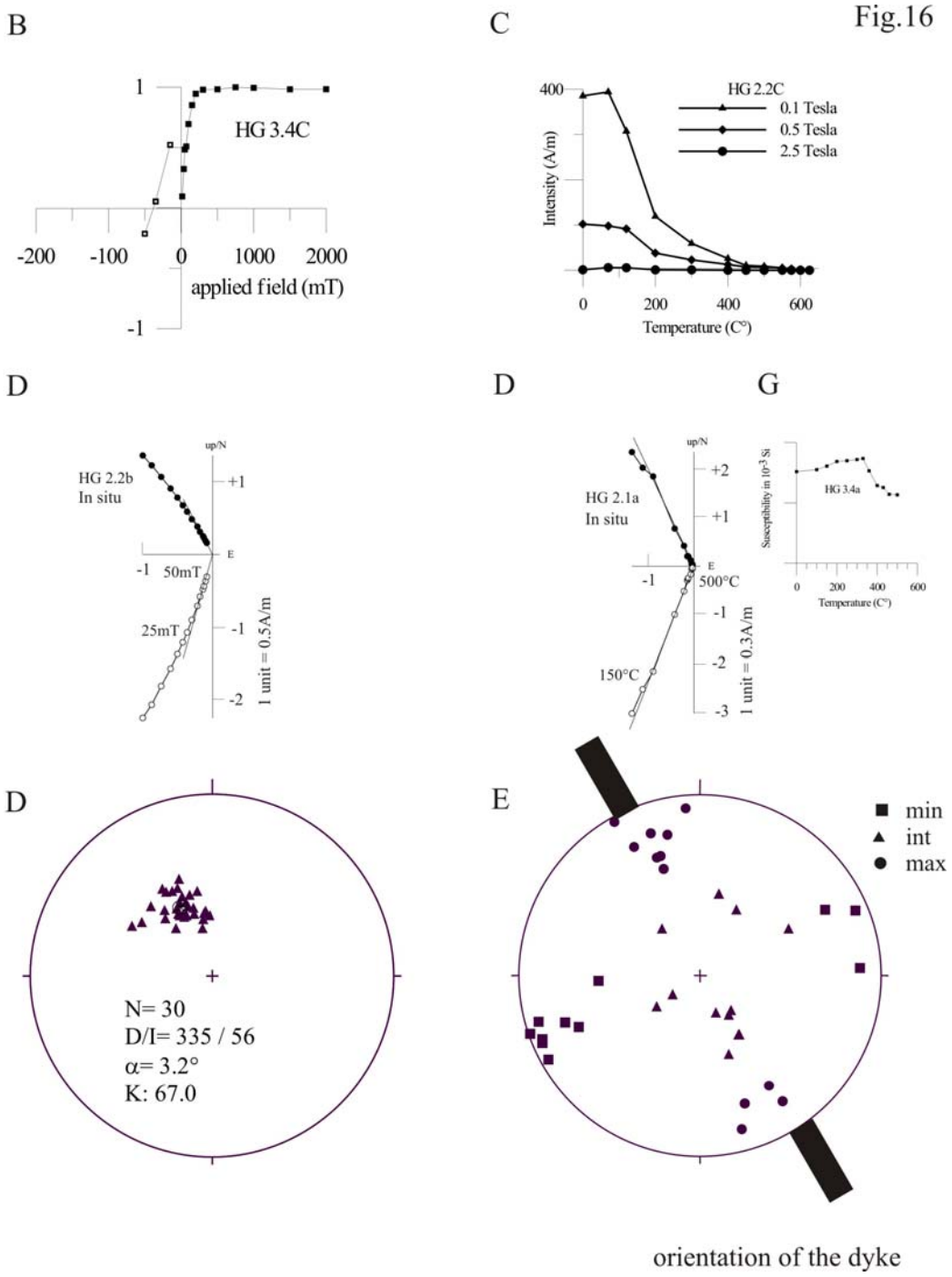

Fig. 16. Rock magnetic properties, demagnetization behavior and statistical parameters from site 92 (HG), (Tab.1).

C= Thermal demagnetization of three component IRM (Lowrie, 1990); **D**= Zijderveld demagnetograms of representative samples in stratigraphic (tc) and geographic (no tc) coordinates, in the Zijderveld diagrams, full/hollow circles: projection of the NRM in the horizontal/vertical plane. Stereogeographic projection of the characteristic remanence magnetization direction, bedding corrected (tc), in situ (no tc) coordinates; **E**= AMS results, after bedding correction/ in situ coordinates; **G**= Susceptibility versus temperature curves.

6.5.3. Metamorphic rocks

Alternating field demagnetization was successful concerning samples from locality Schaubachhütte (site 94; Tab.1; Tab.1, Fig.1,2,17). The characteristic component carried by magnetite could be isolated in the range between 5-50mT. The Permoskythian conglomerates showed magnetizations with NNE directed declinations and inclinations of more than 60° before bedding correction. AMS measurements indicated a strong degree of anisotropy (P= 16,2%) and a magnetic fabric that was dominated by lineation. However, no dependence on the magnetic vectors from the magnetic fabric could be observed. Due to the very steep inclinations these magnetizations were interpreted as post tilting, most probably Tertiary overprints.

Samples of Permoskythian sandstones from site 95 (Serles/Margarethenbach) could be successfully demagnetized with temperatures ranging up to 500 °C and with alternating field strengths between 3 and 30 mT. Susceptibility did not change during heating up to 600 °C. Well grouped vectors gave a mean direction with a declination of 320° and an inclination of 14° before bedding correction (Tab. 1, Fig.1,2). The shallow inclination of this overprint magnetization may be explained by southward tilting of the Ötztal-Stubai basement nappe during northward directed thrust movement upon the Northern Calcareous Alps during a very young process.
All samples showed similar magnetic fabrics, with a subvertical orientation of K_{min} and subhorizontal, SW and SE directed orientation of K_{int} and K_{max}. The degree of anisotropy is between 26 to 38.8 %. The degree of lineation and foliation is between 10.9 to 20.9 %. The magnetic vectors showed no dependence from the magnetic fabric (Thöny et al., 2006).

Paleozoic diabasic rocks from western Greywacke zone yielded results at locality Kopfraderjoch (site 96; Tab.1, Fig.1,2,18). Thermal demagnetization isolated 2 components of remanent magnetization, both unblocking at 575°C. Both carried by magnetite, these components showed NW and NE directed declinations. The inclinations were steep and positive. Concerning the component with NE directed declinations a synfolding remagnetization was interpreted, as the declinations were distributed on a small circle.
After restoring the vertical axis rotation back to the reference direction (N/50) the tilt axis is oriented sub- horizontally, trending SW/NE (228/26).

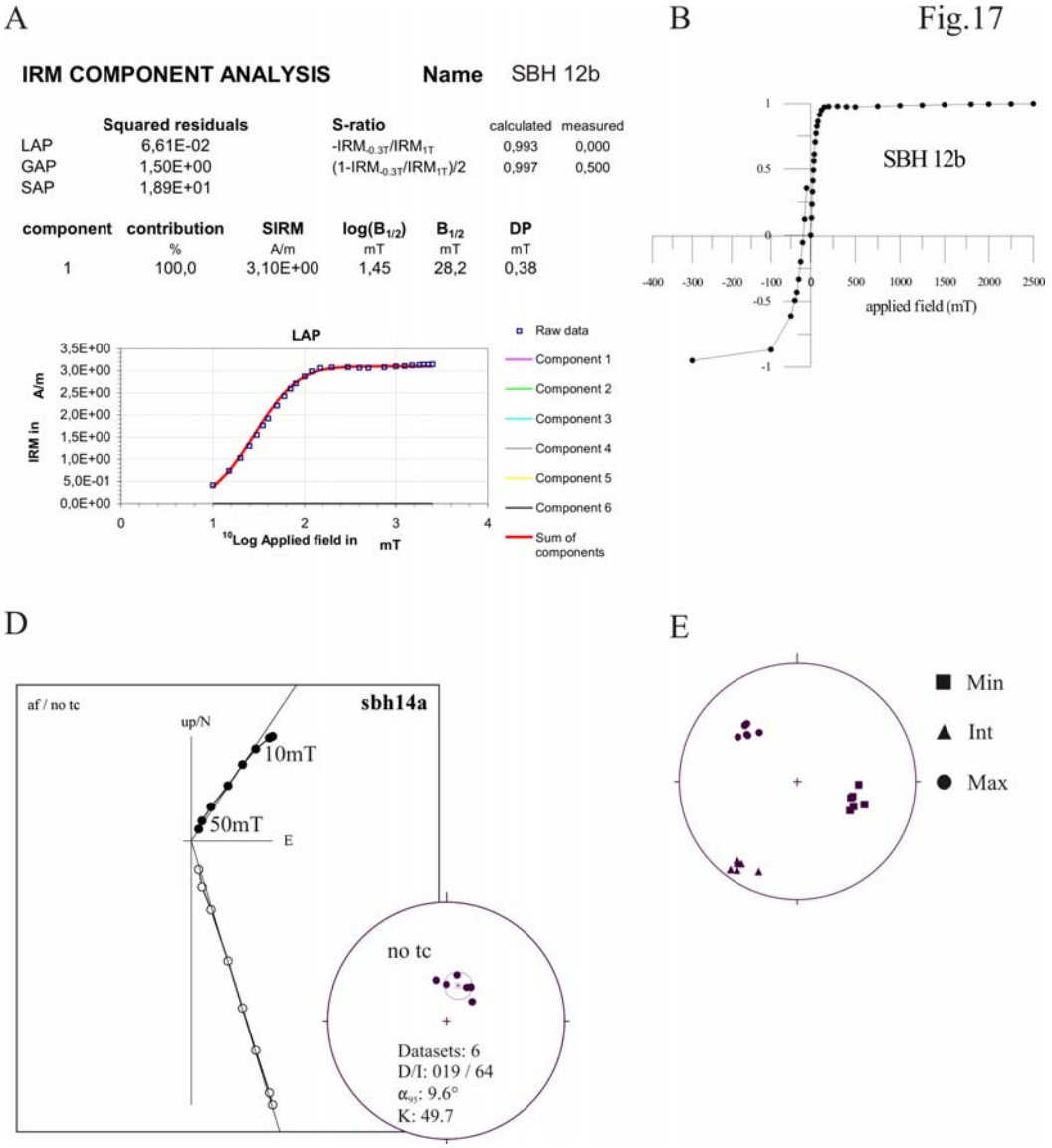

Fig. 17. Rock magnetic properties, demagnetization behavior and statistical parameters from site 94 (SBH), (Tab.1). **A**= IRM component analysis according to Kruiver et al. (2001); **B**= Typical IRM acquisition curves; **D**= Zijderveld demagnetograms of representative samples in stratigraphic (tc) and geographic (no tc) coordinates, in the Zijderveld diagrams, full/hollow circles: projection of the NRM in the horizontal/vertical plane. Stereogeographic projection of the characteristic remanence magnetization direction, bedding corrected (tc), in situ (no tc) coordinates; **E**= AMS results, after bedding correction/ in situ coordinates.

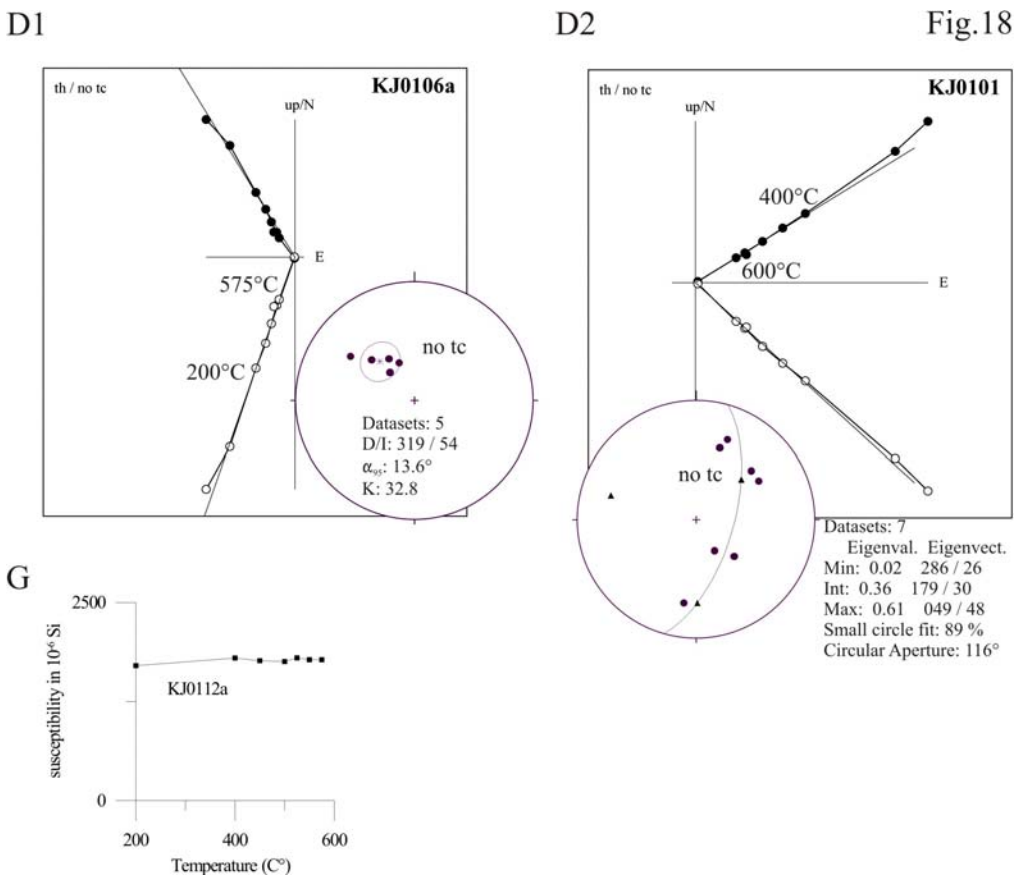

Fig. 18. Rock magnetic properties, demagnetization behavior and statistical parameters from site 96 (KJ), (Tab.1). **D**= Zijderveld demagnetograms of representative samples in stratigraphic (tc) and geographic (no tc) coordinates, in the Zijderveld diagrams, full/hollow circles: projection of the NRM in the horizontal/vertical plane. **D1**= counterclockwise rotated magnetization component, **D2=** clockwise rotated magnetization component. Stereogeographic projection of the characteristic remanence magnetization direction, bedding corrected (tc), in situ (no tc) coordinates; **G**= Susceptibility versus temperature curves.

Thermal demagnetization of marbles from locality Hochstegen (site 97; Tab.1, Fig.19) yielded very low unblocking temperatures in the range between 250–360 °C. During isothermal remanent magnetization experiments, the samples rapidly acquired saturation at field strengths below 100 mT, but the backfield curves showed a relatively high remanence coercivity. According to Maher et al. (1999) IRM(1T)/χ ratio was indicating MD (multi-domain) titanomagnetite, maghemite or magnetite as carrier minerals. From these observations, especially due to the very low unblocking temperatures, titanomagnetite was supposed as carrier mineral of magnetization. The decrease of the susceptibility during heating cannot be explained by now. Analyses of the demagnetization paths yielded two groups of magnetization components, which differed in the orientation but are carried by the same mineral. The components were directed NW and N, both with positive inclination values before bedding correction (Tab. 1).

Most of the samples showed negative susceptibilities. Therefore a magnetic fabric could not be measured (Thöny et al., 2006).

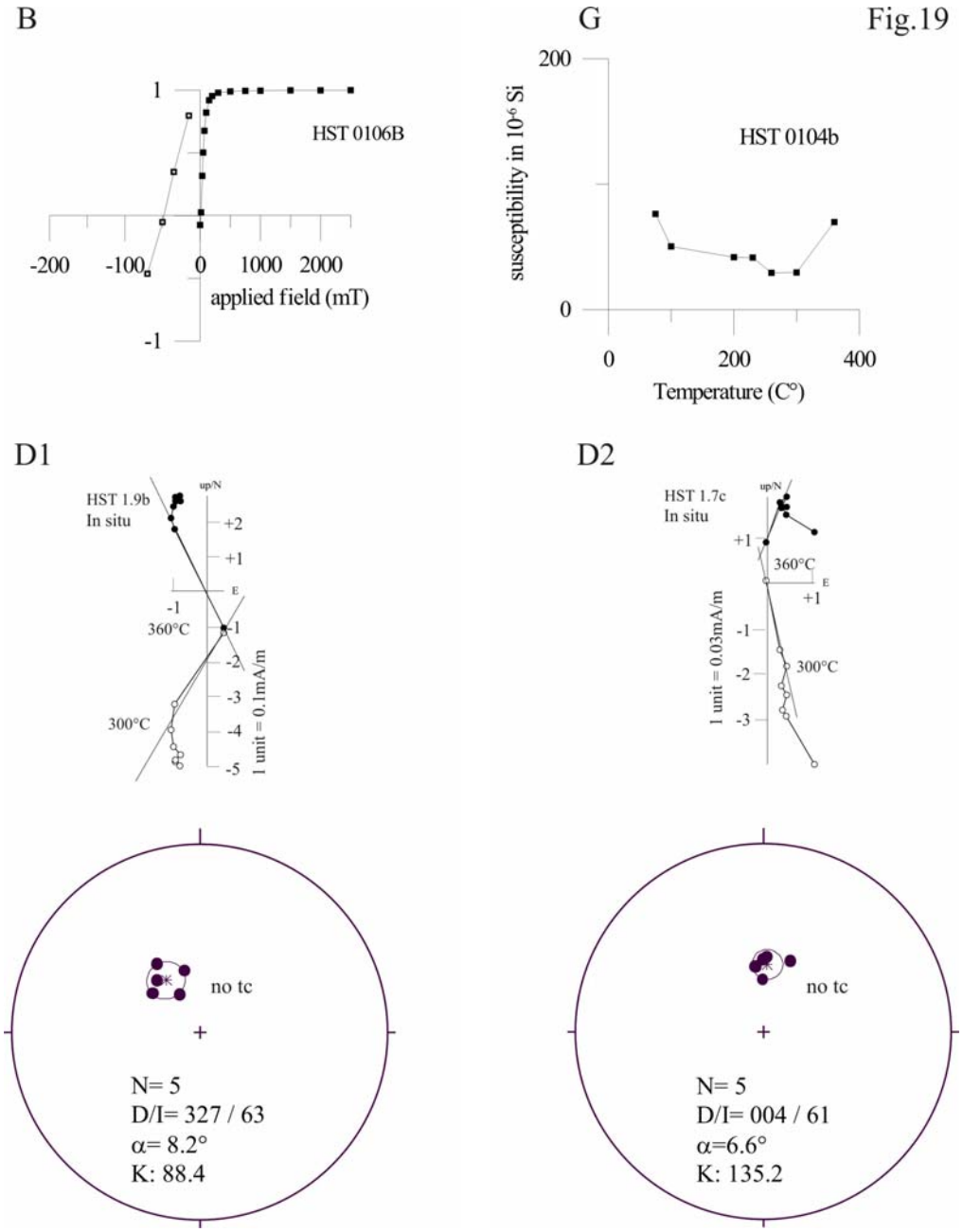

Fig. 19. Rock magnetic properties, demagnetization behavior and statistical parameters from site 97 (HST), (Tab.1). **B**= Typical IRM acquisition curves; **D**= Zijderveld demagnetograms of representative samples in stratigraphic (tc) and geographic (no tc) coordinates, in the Zijderveld diagrams, full/hollow circles: projection of the NRM in the horizontal/vertical plane. **D1**= counterclockwise rotated magnetization component, **D2=** clockwise rotated magnetization component. Stereogeographic projection of the characteristic remanence magnetization direction, bedding corrected (tc), in situ (no tc) coordinates; **G**= Susceptibility versus temperature curves.

6.6. Southern Alps

6.6.1. Restoration of vertical/horizontal axes rotations

The Southern Alps are traditionally interpreted as most northern part of the African plate, forming the so-called African promontory (Channell and Horvath, 1976). Main arguments for distinction between European and African affinities were based on declinations measured in Mesozoic rocks, which are rotated clockwise on stable Europe and rotated counterclockwise on the African plate. Surprisingly, samples from the Southern Alps have, similar to the Northern Calcareous Alps and Central Alps two characteristic components of magnetization indicating clockwise and counterclockwise rotation, e.g. at Alpe di Ra Stua (sites 104-111; Tab.1, Fig.20, 22a-c). Acquired after folding, showing no polarity changes, these components support the interpretation of two remagnetization events and successive rotation postdating folding like in the Eastern Alps (Fig.23). Concerning paleomagnetic data from the Southern Alps only, the succession of vertical axis rotations cannot be decided definitely. A primary magnetization was derived from a basaltic dyke (Site 100; Tab.1, Fig.21), which is dated to Early Rupelian 34Ma. Southwest directed declinations and negative inclinations argued for clockwise rotation younger than 34Ma.

One site from Eocene carbonates (site 98; Tab.1; see section 4.6.2 below) was characterized by a prefolding/primary magnetization, indicating counterclockwise rotation before folding, and before clockwise rotation, observably at site 100 (Tab.1, Fig.21).

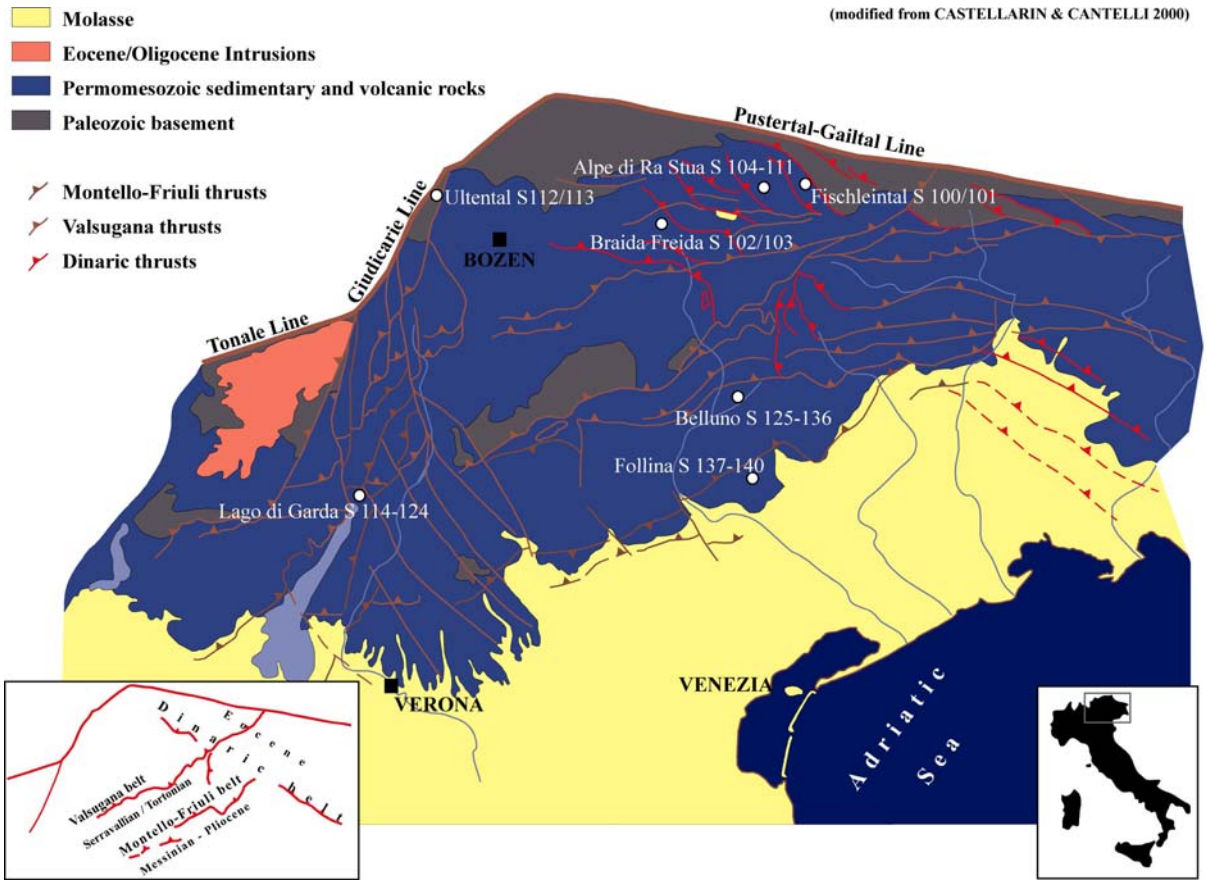

Fig. 20. Geological sketch of the Southern Alps with structural units sampled during this study. S(ite) numbers refer to Tab.1.

6.6.2. Nonsberg syncline

Near locality Revo the eastern limb of Nonsberg syncline was sampled, 2 sites yielded results. Carbonates from Late Cretaceous Scaglia rossa Fm. (site 99; Tab.1) showed N directed declinations and steep inclinations before bedding correction. This component of remanent magnetization, interpreted as (sub) recent overprint of the earth magnetic field, was isolated during thermal demagnetization. Unblocking temperatures of 500°C identified magnetite as carrier mineral of the characteristic remanent magnetization. Based on the interpretation of IRM acquisition according to Kruiver et al. (2001) a contribution of hematite to the remanent magnetization was suscpected. AMS measurements indicated a typically foliated magnetic fabric. The degree of anisotropy was relatively high (P=11,2%).

Eocene carbonates of Fm. di Ponte Pia (site 98; Tab.1) were demagnetized with the alternating field in the range between 3-40mT. The characteristic component of magnetization carried by magnetite, showed NW directed declinations after bedding correction. This component was interpreted as prefolding/ primary magnetization, indicating counterclockwise rotation in post Eocene times.

6.6.3. Dolomites/magmatic dykes

At locality Fischleintal a contact zone between a magmatic dyke (site 100; Tab.1 Tab.1, Fig.1,2,21) radiometrically dated to 34Ma (Lucchini et al., 1983) and the country rocks (site 101; Tab.1) that belong to the carbonates of the Ladinian Schlerndolomit Fm. is exposed. Concerning the dyke, unblocking temperatures during thermal demagnetization were observed around 560°C. Thermal demagnetization of 3 component IRM (Lowrie, 1990) and interpreting the IRM acquisition according to Kruiver et al. (2001) was identifying magnetite as carrier of the remanent magnetization.

At the country rocks, the same measurements indicated a system of titanomagnetite, pyrrhotite and goethite as carrier minerals. At both sites the characteristic component of magnetization showed SW directed declinations and steep, negative inclinations. The magnetization of the dyke is interpreted as TRM (Thermo-remanent magnetization) that remagnetized the country rocks. Both sites were rotated clockwise afterwards.

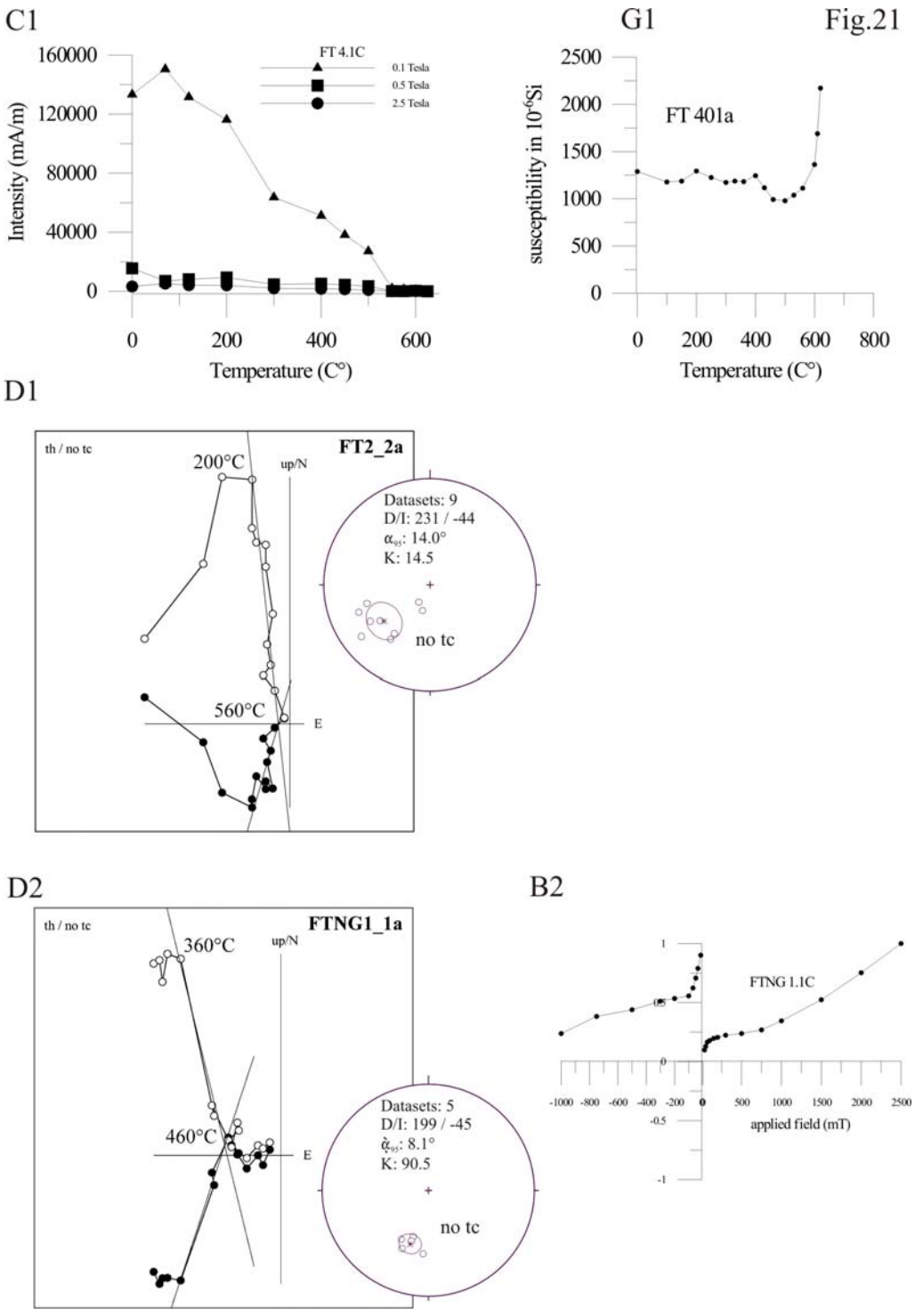

Fig. 21. Rock magnetic properties, demagnetization behavior and statistical parameters from site 100 (FT, **C1, D1, G1**) and site 101 (FTNG, **B2, D2**), (Tab.1).

B= Typical IRM acquisition curves; **C**= Thermal demagnetization of three component IRM (Lowrie, 1990); **D**= Zijderveld demagnetograms of representative samples in stratigraphic (tc) and geographic (no tc) coordinates, in the Zijderveld diagrams, full/hollow circles: projection of the NRM in the horizontal/vertical plane. Stereogeographic projection of the characteristic remanence magnetization direction, bedding corrected (tc), in situ (no tc) coordinates; **G**= Susceptibility versus temperature curves.

At locality Braida Freida near Corvara a basaltic sill (site 102; Tab.1) radiometrically dated to 68Ma (Lucchini et al., 1983) was sampled. Also a site sampled in the country rocks of Late Ladinian vulcanoclastic sediments of the Kassian Fm. (site 103; Tab.1) yielded results. Thermal demagnetization of 3 component IRM (Lowrie, 1990) and interpreting the IRM acquisition according to Kruiver et al. (2001) as well as thermal demagnetization and demagnetization with the alternating field method were used to identify the carrier minerals of remanent magnetization at both sites. Thermal demagnetization of the magmatic dyke (site 102; Tab.1) isolated 2 components. These components both showed unblocking temperatures around 575°C and SE directed declinations and negative inclinations concerning both components. Distinction was possible due to acquisition of these two components in unfolded and folded position, indicating that counterclockwise rotation occurred post folding.

6.6.4. Dolomites/ Alpe di Ra Stua

A previous study by Channell and Doglioni (1994) derived results, indicating a counterclockwise rotation when sampling Rosso Ammonitico limestones and Puez marls at locality Ra Stua. The site mean directions were interpreted to indicate 20° of clockwise rotation relative to primary magnetizations of Upper Jurassic to Lower Cretaceous sites from the Venetian prealps.

The results of this sudy were derived from eight sites that were sampled in a Malmian to Turonian stratigraphic section (Sauro & Meneghel, 1995; Horrelt, 1987) at locality Alpe di Ra Stua (sites 104-111; Tab.1, Fig.22a-c). Sites 107 to 111 were characterized by a component of magnetization with SE directed declinations and negative inclinations before bedding correction, observably in all 5 sites. No polarity changes could be observed.

Thermal demagnetization of 3 component IRM (Lowrie, 1990) identified a low to medium coercive component, thermally stable below 600°, as main carrier mineral of the remanent magnetization. During thermal demagnetization the characteristic component, most probably carried by magnetite, yielded unblocking temperatures below 590°C. Additionally, a second component showing NE directed declination and positive inclinations, also acquired in folded position could be isolated at sites 109 and 110. Again no polarity changes could be observed. Demagnetization with the alternating field in the range between 3-10mT and corresponding unblocking temperatures around 360°C observed during thermal demagnetization identified titanomagnetite as carrier mineral of the second component.

Thermal demagnetization of 3 component IRM (Lowrie, 1990) and interpreting the IRM acquisition according to Kruiver et al. (2001) support a contribution to the second component by pyrrhotite as well. All sampled lithologies enabled AMS measurements except micrites from Maiolica Fm.. In most cases the magnetic fabric is foliated (P=6-12%), K_{max} is horizontally oriented and K_{min} vertically, all indicating an undisturbed sedimentary fabric. Although no influence from the magnetic fabric on the magnetic vectors could be observed, the calculated components of magnetization, concerning sites 107-111 were not of primary origin, but were interpreted as result of 2 phases of remagnetization, acquired in folded position each time.

Sites 105 and 106 yielded results from Aptian to Albian carbonates and sandstones. During thermal demagnetization unblocking temperatures between 560-590°C were observed. Additional to magnetite that carried the characteristic component of magnetization also contributions by hematite and goethite were identified (Lowrie, 1990; Kruiver et al., 2001). Independently from the tectonic correction, the declinations were north directed, the inclinations were positive (site 105/106; Tab.1). Consequently deciding between pre- or post-folding age of the magnetization was not possible.

Turonian carbonates of Ruoibes Fm. (site 104) present the stratigraphically youngest sediments that yielded results in the Alpe Rastua area. Thermal demagnetization of 3 component IRM (Lowrie, 1990) and interpreting the IRM acquisition according to Kruiver et al. (2001) were identifying magnetite, hematite and goethite to carry the remanent magnetization. The characteristic component, carried by magnetite was showing NE directed declinations before bedding correction. Together with sites 109 and 110 these components indicate clockwise rotation after folding.

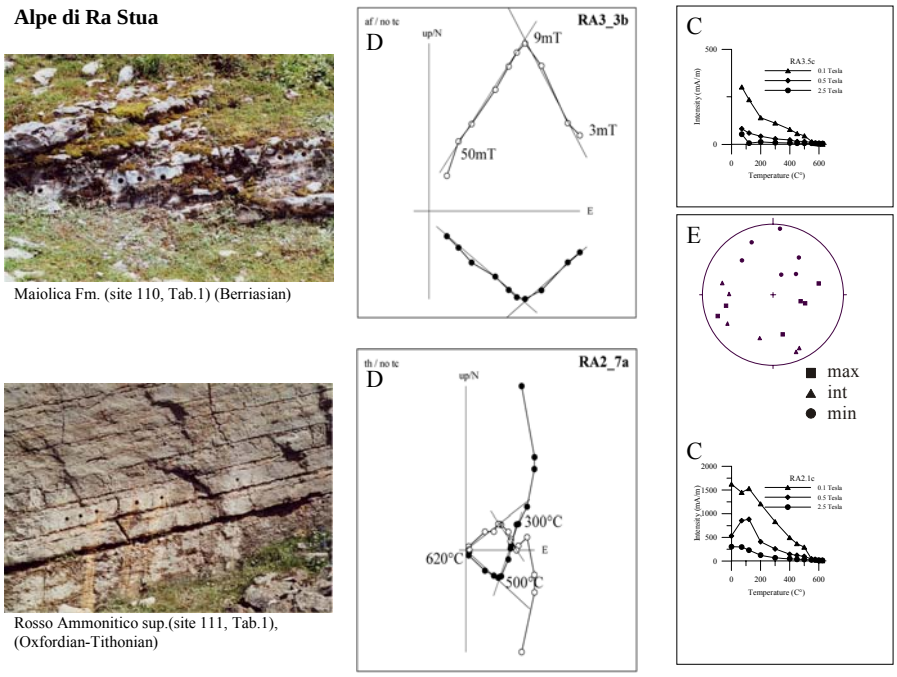

Fig. 22a. Rock magnetic properties, demagnetization behavior and statistical parameters from sites 111 (RA2, **C, D, E**) and site 110 (RA3, **C**, **D**), (Tab.1).

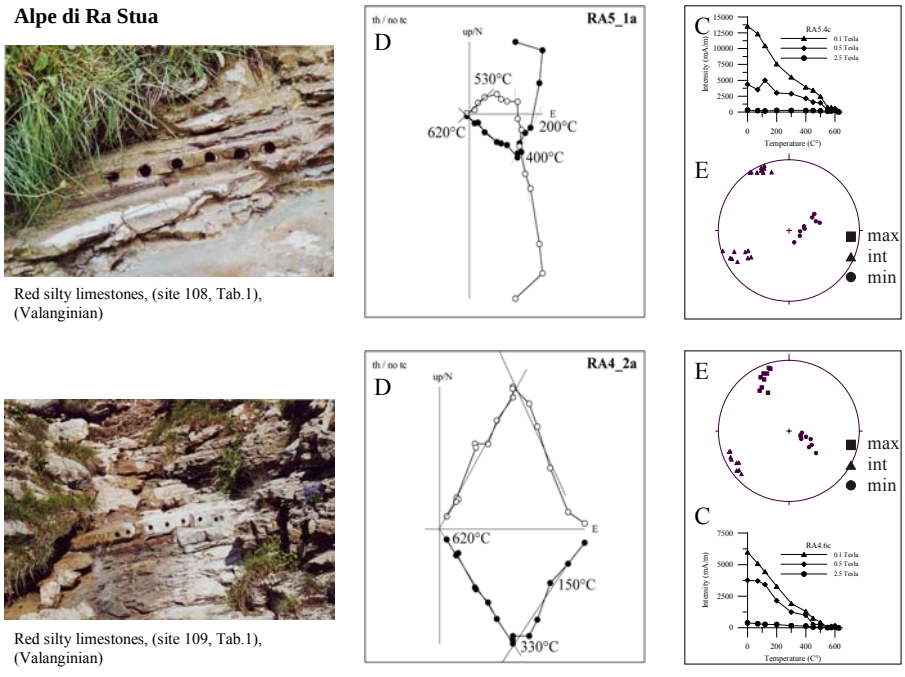

Fig. 22b. Rock magnetic properties, demagnetization behavior and statistical parameters from sites 109 (RA4, **C, D, E**) and site 108 (RA5, **C**, **D, E**), (Tab.1). **C**= Thermal demagnetization of three component IRM (Lowrie, 1990); **D**= Zijderveld demagnetograms of representative samples in stratigraphic (tc) and geographic (no tc) coordinates, in the Zijderveld diagrams, full/hollow circles: projection of the NRM in the horizontal/vertical plane; **E**= AMS results, after bedding correction/ in situ coordinates.

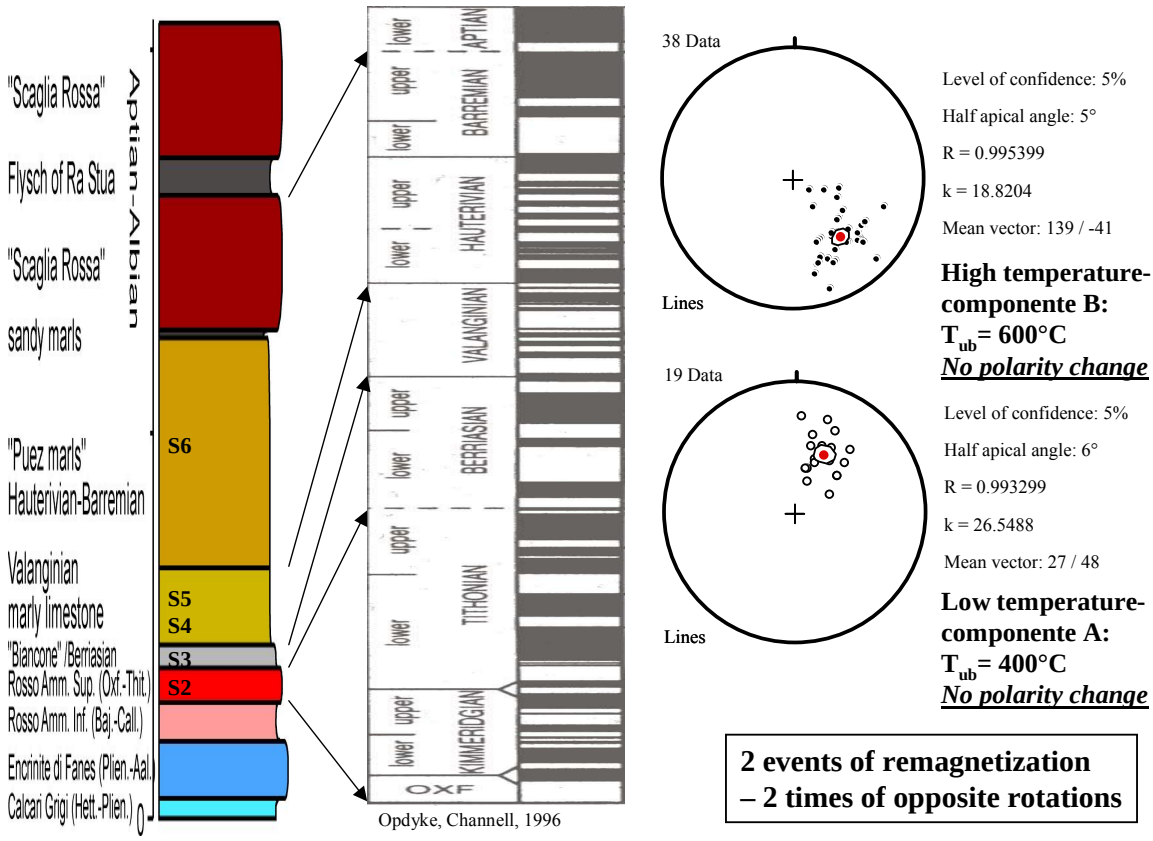

Fig. 22c. Lithostratigraphy and summary of paleomagnetic results at locality Alpe di Ra Stua (Sites 107-111, Tab.1). For comparison: Magnetic polarity time scale with polarity zones indicated by black (normal polarity) and white (reverse polarity) fields.

6.6.5. Paleozoic basement

At locality Ultental two different Permian rocks were sampled. A Late Early Permian basaltic dyke (site 112; Tab.1) geochronologically dated to 275 Ma (pers. comm. L. Keim) was indicating a primary magnetization characterised by WNW-directed declination and very shallow inclination (287/11). AMS measurements yielded a mean degree of anisotropy of 2,8%, K_{max} was sub-horizontally oriented (322/20). A possible influence of the magnetic fabric on the magnetic vectors could not be excluded.

Thermal demagnetization was successful in the range between 200-580°C, identifying together with the thermal demagnetization of 3 component IRM (Lowrie, 1990) magnetite as carrier mineral of the characteristic component of magnetization. This dyke is steeply cutting the surrounding granitic country rock that is also of Permian age (site 113; Tab.1).

The characteristic component showed NW directed declinations and steep inclinations (58°) and was interpreted as Tertiary overprint. Thermal demagnetization could isolate this component in the range between 200-360°C, indicating titanomagnetite as carrier mineral.

Summary of paleomagnetic data from Northern Calcareous Alps, Central Alps and Southern Alps

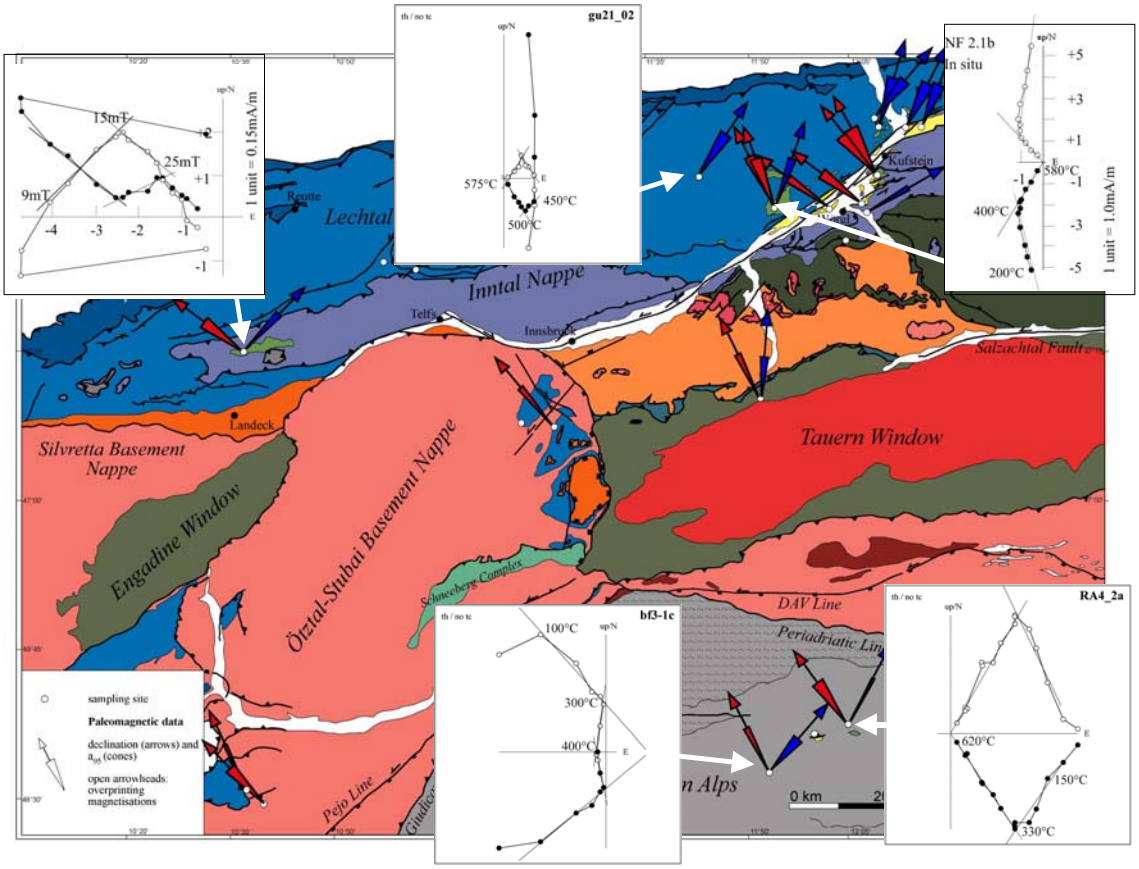

Fig. 23. Geological sketch of the study area comprising the western part of the Eastern Alps and the northern part of the Southern Alps (Thöny et al., 2006). Arrows indicate trend of declinations, and cones depict α_{95}. Characteristic zijderveld demagnetograms that are indicating 2 component magnetization systems are pasted. Numbers at arrows refer to Tab. 1. In the Northern Calcareous Alps and the Southern Alps two magnetic components occur during demagnetization in single samples. Small scale vertical axis rotations can be excluded therefore.

6.7. Southern Alpine Foreland Basin and Mesozoic basement units

6.7.1. Restoration of vertical/horizontal axes rotations

Primary magnetizations from Serravallian to Tortonian marls (sites 138-140; Tab.1, Fig. 20) sampled in the southern limb of Monte-Grappa anticline, indicated counterclockwise rotation after Tortonian. An identical value of counterclockwise vertical axis rotation, calculated in folded position was derived from Messinian (7-5Ma) sandstones, also sampled in the southern limb of Monte-Grappa anticline. Consequently counterclockwise rotation has to be younger than the folding of the Messinian site i.e. younger than 5Ma. When comparing these data from the Monte Grappa area to data from the Lake Garda area, the Dolomites and the Belluno syncline area, identical counterclockwise-rotated magnetic components can be found, although these areas are separated by prominent fault systems (e.g. Bassano-, Belluno-, Val Sugana and Guidicarie thrust systems). Similar to the distribution of the counterclockwise component, also the clockwise rotated component could be observed in all sampled areas of the Southern Alps, despite crossing prominent thrust belts, like Belluno and Val Sugana thrust.

At Lake Garda (Fig.20) a stratigraphic section of carbonates of Late Early Rupelian Linfano Fm. (site 116; Tab.1, Fig.24), sandstones of Chattian/Miocene Lower Mt. Brione Fm. (site 115; Tab.1, Fig.24) and sandstones of Aquitanian Upper Mt. Brione Fm. (site 114; Tab.1, Fig.24) was sampled in one site each. The stratigraphic section is overthrusted by Mesozoic carbonates. As Aquitanian Upper Mt. Brione Fm. represent the youngest lithology below the thrust plain, tectonics and tilting of the sampled sites is dated to post Aquitanian (23-20Ma) i.e. younger than 20Ma (Castellarin et al., 2006).

Sandstones of Aquitanian Upper Mt. Brione Fm. (site 114; Tab.1, Fig.24) are interpreted in folded position. The declinations are oriented NW/SE, indicating counterclockwise rotation sometime younger than the folding of the Aquitanian sandstone. A site in Chattian/Miocene sandstones (site 115; Tab.1, Fig.24) shows N directed declinations and positive inclinations. The two mean remanence directions, calculated before and after tectonic correction, are nearly identical. After bedding correction statistics present slightly improved values. Interpreting the remanence in bedding-corrected position was decided after comparing the characteristic components to the results from the surrounding working areas.

As indicated by primary magnetizations (e.g. Northern Alpine Foreland Basin), after 23Ma only counterclockwise rotated declinations could be isolated. Concerning the stratigraphic section of sites (114-116) tilting was active in post Aquitanian. Consequently post-folding remanences should show counterclockwise-rotated declinations.

Therefore at site 115 the characteristic component is interpreted as primary magnetization, because the uncorrected component does not show counterclockwise- rotated but N-directed declinations. After restoring the youngest counterclockwise rotation these results indicate 30° clockwise rotation after sedimentation in Chattian/Miocene (26-20Ma) and before 23Ma (see data from Northern Alpine Foreland Basin). Carbonates of Late Early Rupelian age (site 116) were the stratigraphically youngest units that yielded clockwise-rotated declination values, presenting a maximum value of 70° after restoration of the younger counterclockwise rotation. Whether to interpret the characteristic component before or after bedding correction again was decided by comparing the declination values to the surrounding areas. Both corrections yielded declinations that indicated prominent clockwise rotation. If this remanence (site 116) was interpreted as postfolding remagnetization, clockwise rotation should have been active in post Aquitanian times. This is not known from any site in the working area. Consequently the characteristic remanence at site 116 was interpreted in bedding corrected position, indicating a primary/prefolding magnetization that was rotated clockwise. Additionally this site (116) is characterized by a second, prefolding magnetization component that is identical compared to the component at site 115, which was showing N directed declinations and was interpreted as primary magnetization.

Therefore, most probably the primary magnetization derived from the Chattian/Miocene (26-20Ma) Lower Mt. Brione sandstone (site 115) is used to date a first clockwise rotation of 30°-50° to post Late Early Rupelian (32Ma) and before Chattian times (26Ma) and to date the second clockwise rotation of 30° to synsedimentary times i.e. between 26Ma to 23Ma (Fig. 24). Similar to the distribution of the counterclockwise component, also the clockwise rotated component could be observed in all sampled areas of the Southern Alps, despite crossing prominent thrust belts, like Belluno and Val Sugana thrust.

6.7.2. Lake Garda

Primary magnetizations were derived from 4 sites in Liassic to Campanian carbonates. In all cases the characteristic component of magnetization indicated counterclockwise rotation after bedding correction. At sites 124 and 123 (Tab.1), sampled from carbonates of Liassic Ronzo Fm. and Malmian Maiolica Fm., demagnetization with the alternating field in the range between 3-60mT identified magnetite as carrier of the remanent magnetization. A contribution to the remanent magnetization by goethite was indicated by the interpretation of the IRM acquisition according to Kruiver et al. (2001). Compared to each other the characteristic remanent magnetizations showed a polarity change. The inclinations, differing in 30° (sites 124/123; Tab.1) were interpreted to represent a prominent S directed drift during Liassic to Malmian times (see also: Muttoni et al., 2005).
Campanian carbonates of Scaglia Rossa Fm. (sites 121, 122; Tab.1) yielded results from two sites, both again indicating counterclockwise rotation after bedding correction. During thermal demagnetization unblocking temperatures of 300°C and 575°C were observed. The high temperature component showed identical NW directed declination and positive inclinations at both sites. The low temperature component was similar but showed reverse polarity at site 122 (Tab.1) and normal polarity at site 121. This component most possibly carried by titanomagnetite is interpreted to be a primary magnetization showing the polarity change at the Santonian/Campanian boundary. The high temperature components, carried by magnetite were interpreted as prefolding overprints. Using the method by Kruiver et al. (2001) a small contribution to the remanent magnetization by hematite and goethite could also be identified.
Eocene sediments mark the transition to the synorogenic sedimentation on the South Alpine Foreland basin (Castellarin and Cantelli, 1999).

Four sites (117-120; Tab.1) sampled in a stratigraphic section of carbonates of Nago Fm. and Torbole Fm. and in intercalated vulcanoclastic/tuffitic rocks yielded results. Demagnetization with the alternating field in the range between 3-100mT was successful at all sites, indicating magnetite as main carrier of the remanent magnetization. Interpreting the IRM acquisition according to Kruiver et al. (2001) was identifying a contribution to the remanent magnetization by goethite at all sites, except site 118. There, only magnetite carried the remanent magnetization. Higher susceptibilities concerning the vulcanoclastic rocks (sites 118, 119; Tab.1) enabled AMS measurements.

No dependence of the magnetic vectors from the magnetic fabric could be observed. The characteristic component of magnetization showed S directed declinations and negative inclinations after bedding correction, concerning sites 118, 119 and 120. Site 117 showed normal polarity and N directed declinations of the characteristic component of magnetization after bedding correction. The bedding orientation is identical to sites 114-116 (see Tab.1), implying a joined tilting/folding in post Aquitanian times. Consequently in situ remanences that were acquired after folding should be characterized by counterclockwise rotated declinations as outlined above (6.7.1. Restoration of vertical/horizontal axes rotations). Contrarily, at sites 117-120 declinations are NE directed before any correction. Therefore these results were interpreted as primary magnetizations, calculated after bedding correction.

Different characteristic components of remanent magnetization, carried by magnetite, could be derived from carbonates of Late Early Rupelian Linfano Fm. (site 116, Tab.1, Fig.1,2,24). After bedding correction the declinations are directed NE, the inclinations are positive. Demagnetization with the alternating field method in the range between 3-50mT, thermal demagnetization of 3 component IRM (Lowrie, 1990) and interpreting the IRM acquisition according to Kruiver et al. (2001) was identifying a system of magnetite, hematite and goethite to carry the remanent magnetization.

In the range between 3-30mT the Chattian Lower Mt. Brione sandstone (site 115, Tab.1, Fig.1,2,24) was demagnetized with the alternating field method, indicating, like thermal demagnetization of 3 component IRM (Lowrie, 1990) magnetite as main carrier of the remanent magnetization. Interpreting of the IRM acquisition according to Kruiver et al. (2001) as well supported this interpretation. A small contribution to the remanent magnetization by goethite could also be identified. The characteristic component of magnetization was calculated after bedding correction, showing N directed declinations and normal polarities.

In contrary the characteristic component calculated from Aquitanian Upper Mt. Brione sandstone (site 114; Tab.1, Fig.1,2,24) showed SE directed declinations and negative inclinations before bedding correction, indicating counterclockwise rotation in folded position. Magnetite as main carrier of the remanent magnetization and a contribution by goethite were identified, using the same method as described at site 115.

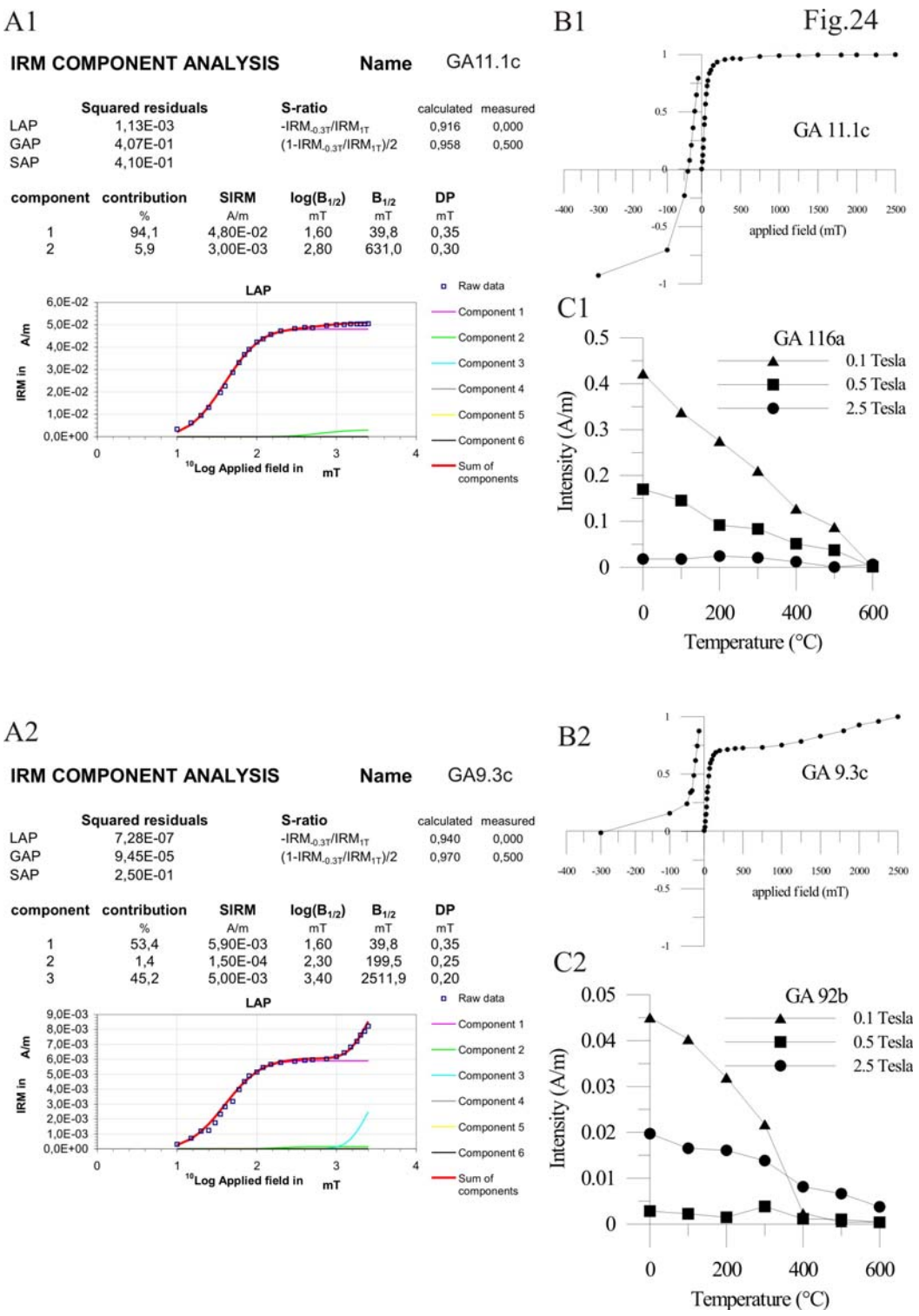

Fig. 24. Rock magnetic properties, demagnetization behavior and statistical parameters from site 115 (GA11, **A1-D1**), site 116 (GA9, **A2-D2**) and site 114 (GA10, **D3**), (Tab.1).

A= IRM component analysis according to Kruiver et al. (2001); **B**= Typical IRM acquisition curves; **C**= Thermal demagnetization of three component IRM (Lowrie, 1990).

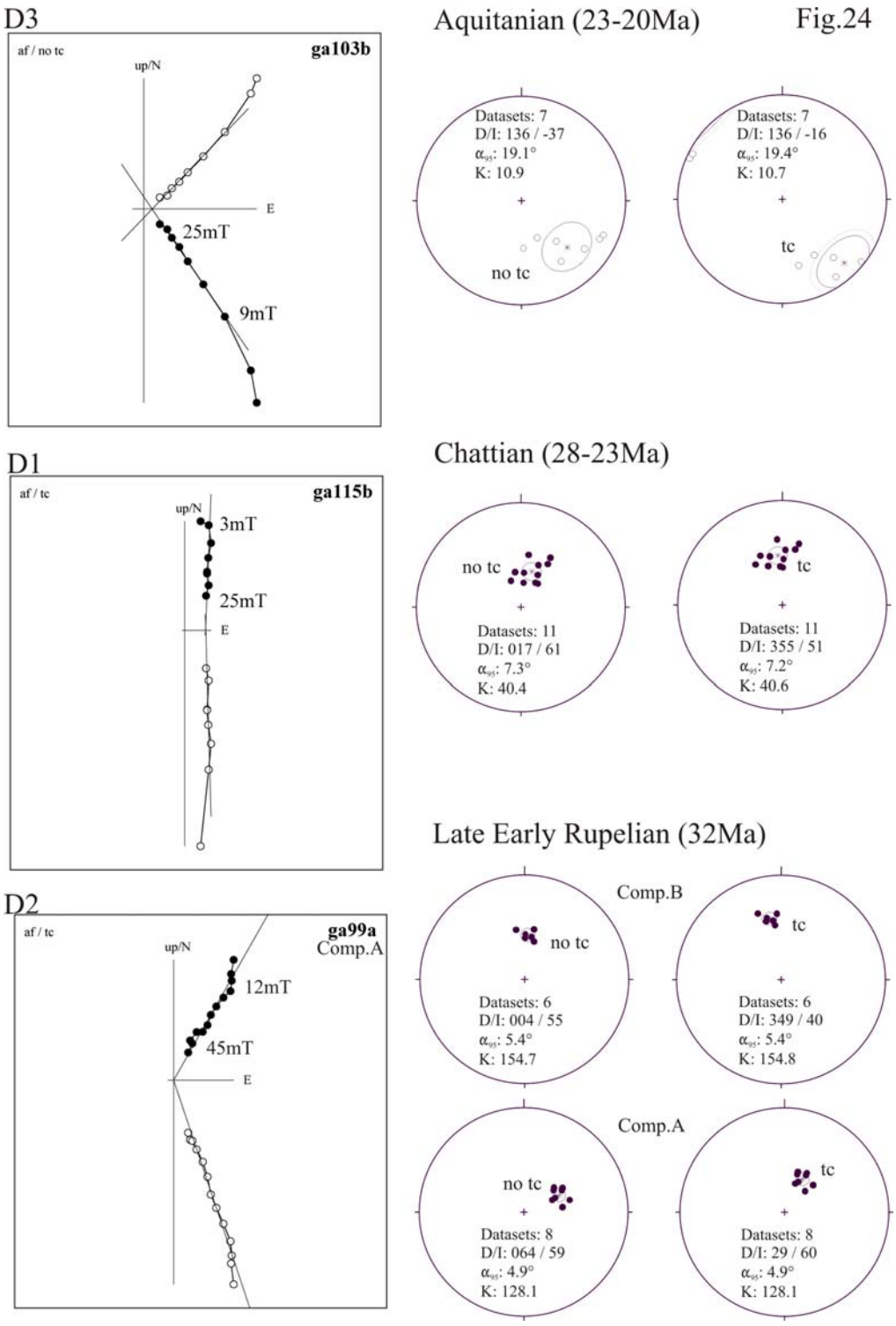

Fig. 24. Rock magnetic properties, demagnetization behavior and statistical parameters from site 115 (GA11, **A1-D1**), site 116 (GA9, **A2-D2**) and site 114 (GA10, **D3**), (Tab.1).

D= Zijderveld demagnetograms of representative samples in stratigraphic (tc) and geographic (no tc) coordinates, in the Zijderveld diagrams, full/hollow circles: projection of the NRM in the horizontal/vertical plane. Stereogeographic projection of the characteristic remanence magnetization direction, bedding corrected (tc), in situ (no tc) coordinates.

6.7.3. Belluno area

Primary magnetizations were derived from 5 sites sampled in the northern limb of Belluno syncline. Two sites sampled in carbonates of Malmian Rosso Ammonitico Fm. (site 136; Tab.1) and Lower Cretaceous Maiolica Fm. (site 135; Tab.1), indicated similar kinematics like sites from contemporaneous sediments at Lake Garda area. The characteristic component of magnetization showed SE directed declinations and negative inclinations, concerning both sites. The inclination values of 30°, similar to the results from sites 123 and 124 at Lake Garda, also supported the interpretation of a significant south-directed drift during Liassic to Malmian times (see also: Muttoni et al., 2005).

Red carbonates of Rosso Ammonitico Fm. (site 136; Tab.1) were demagnetized thermally, yielding unblocking temperatures around 500°C. Additional interpretation of the IRM acquisition according to Kruiver et al. (2001) identified magnetite as main carrier mineral of the remanent magnetization and a contribution to it by goethite.

Site 135 was demagnetized thermally, observing unblocking temperatures around 550°C and with the alternating field method in the range between 20-80mT, both indicating magnetite as main carrier mineral of the remanent magnetization. Relatively high alternating fields during demagnetization and the interpretation of the IRM acquisition according to Kruiver et al. (2001) indicated a possible contribution to the characteristic component of magnetization by pyrrhotite.

Another three sites (132-134; Tab.1) with primary magnetizations were derived from carbonates sampled in Coniacian to Campanian Scaglia rossa Fm.. Concerning all 3 sites, one component of remanent magnetization, carried by magnetite, showed NW directed declinations and normal inclinations. The identification of the carrier mineral was achieved during thermal demagnetization, observing unblocking temperatures of 500 to 575°C.

At site 133 a second component of magnetization that was acquired before folding indicated clockwise rotation (Tab.1). This component was isolated during thermal demagnetization and showed stable decay of magnetization between 300°C to 500°C.

Using the method by Kruiver et al. (2001), contributions to the remanent magnetization by hematite and goethite were identified at sites 133 and 134. At site 132 only a system of magnetite/goethite carried the remanent magnetization. Relatively high susceptibilities enabled AMS measurements at sites 132 and 133. The magnetic fabric was typically foliated; the degree of anisotropy was low (7,1%-8,8%). After bedding correction horizontally oriented K_{max} axis and vertically oriented K_{min} axis indicated an undisturbed sedimentary fabric.

Two sites (131, 130) in Maastrichtian to Late Maastrichtian Scaglia Rossa Fm. yielded results before bedding correction and were interpreted as post folding overprints. The declinations of the characteristic component were N to NW directed, the inclinations were positive. Demagnetization with the alternating field in the range between 3-20mT at site 130, and observed unblocking temperatures of 500°C during thermal demagnetization at site 131 identified magnetite as main carrier mineral of the remanent magnetization. Contributions to the remanent magnetization of hematite at both sites and additionally goethite at site 131 were indicated through the interpretation of the IRM acquisition according to Kruiver et al. (2001).

Similar to the study area Lake Garda, also in the Belluno syncline Eocene sediments mark the transition to the foreland basin evolution (Castellarin and Cantelli, 1999). Two sites sampled in Early Eocene carbonates of Scaglia cinerea and stratigraphically successive sandstones of Belluno Flysch yielded results.

At Site 129 from Scaglia cinerea the characteristic component of magnetization could be isolated during thermal demagnetization yielding unblocking temperatures of 500°C. This component, carried by magnetite showed SW directed declinations and negative inclinations before bedding correction. Interpretation of the IRM acquisition according to Kruiver et al. (2001) identified an additional contribution to the remanent magnetization by hematite and goethite.

Early Eocene sandstones from Belluno Flysch were demagnetized with the alternating field method, isolating three components of remanent magnetization. Although interpreting of the IRM acquisition according to Kruiver et al. (2001) identified a system of magnetite and hematite as carrier of the remanent magnetization, the three calculated components were all carried by magnetite.
A lower coercive component, isolated between 3-30mT during demagnetization, was characterized by N directed declinations and positive inclinations. Alternating field demagnetization at both remaining components was successful in the range between 3-80mT. Both components also showed similar NW directed declinations and positive inclinations. Distinction was only possible due to defining the time of acquisition of the 2 components, which was before and after folding.

Concerning Rupelian sediments only one site (127; Tab.1) sampled in Curzoi sandstones yielded results. Alternating field demagnetization in the range between 3-20mT isolated the characteristic component. Carried by magnetite this component showed NW directed declination and positive inclinations. A contribution to the remanent magnetization by goethite was identified by the method of Kruiver et al., (2001).

Results from Miocene sediments could be derived from 2 sites sampled in Early Burdigalian marls of Bolago Fm. and Langhian marls of Monfumo Fm.. Concerning all sites the characteristic component of magnetization could be identified through alternating field demagnetization in the range between 3-20mT. The declinations were directed N to NW, the inclinations were positive. Beside magnetite as main carrier of the remanent magnetization, again a contribution of goethite was identified by thermal demagnetization of 3 component IRM (Lowrie, 1990) and interpreting the IRM acquisition according to Kruiver et al. (2001).

6.7.4. Follina

South of Messinian Bassano thrust 4 sites that were sampled in Serravallian to Messinian sediments yielded results. Concerning all 4 sites demagnetization was successful with the alternating field method.
At Site 140 (Tab.1, Fig.1,2,) sampled in marls of Serravallian Tarzo Fm. the characteristic component of magnetization could be isolated in the range between 15-40mT, showing SE directed declinations and negative inclinations after bedding correction.
Thermal demagnetization of 3 component IRM (Lowrie, 1990) and interpreting the IRM acquisition according to Kruiver et al. (2001) were identifying, beside a contribution of goethite, magnetite as main carrier of the magnetization.

Intercalated sandstone layers of the Tortonian Mt. Piai conglomerate yielded results in two sites. At site 138 (Tab.1, Fig.1,2,25) the characteristic component was isolated during demagnetization with the alternating field in the range between 20-60mT.

Showing SE directed declinations and negative inclinations after bedding correction this component was exclusively carried by magnetite. Site 139 also sampled in sandstones intercalated with the Mt. Piai conglomerate was characterized by a system of magnetite/pyrrhotite that carried the remanent magnetization.

Identification of the carrier minerals was achieved by thermal demagnetization of 3 component IRM (Lowrie, 1990) and interpreting the IRM acquisition according to Kruiver et al. (2001). Demagnetization with the alternating field in the range between 3-12mT and 20-40mT isolated two components, both indicating counterclockwise rotation. Before bedding correction the low coercive component showed NW directed declinations and positive inclinations. The higher coercive component, possibly carried by pyrrhotite showed SE directed declinations and negative inclinations, but after bedding correction.

Results from site 137 (Tab.1, Fig.1,2,25) sampled in sandy intercalations of Messinian Montello conglomerates represented the youngest paleomagnetic data, derived from the whole study area. The characteristic component, carried by magnetite, showed NW directed declinations and positive inclinations before bedding correction, indicating counterclockwise rotation younger than the folding of Messinian sediments. Thermal demagnetization of 3 component IRM (Lowrie, 1990) and interpreting the IRM acquisition according to Kruiver et al. (2001) were indicating a system of magnetite/pyrrhotite as carrier minerals of the remanent magnetization.

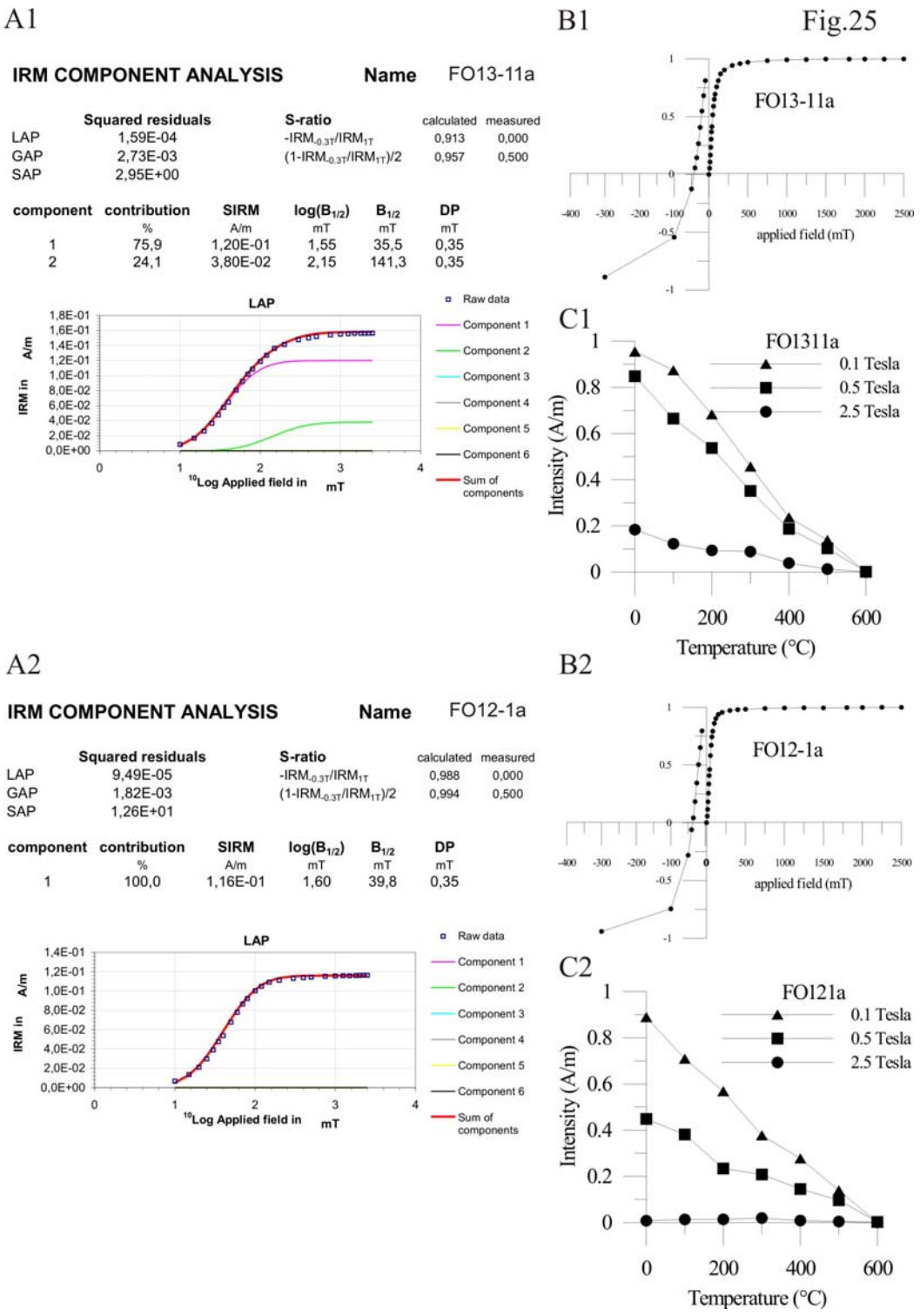

Fig. 25. Rock magnetic properties, demagnetization behavior and statistical parameters from site 137 (FO13, **A1-D1**) and site 138 (FO12, **A2-D2**), (Tab.1).

A= IRM component analysis according to Kruiver et al. (2001); **B**= Typical IRM acquisition curves; **C**= Thermal demagnetization of three component IRM (Lowrie, 1990).

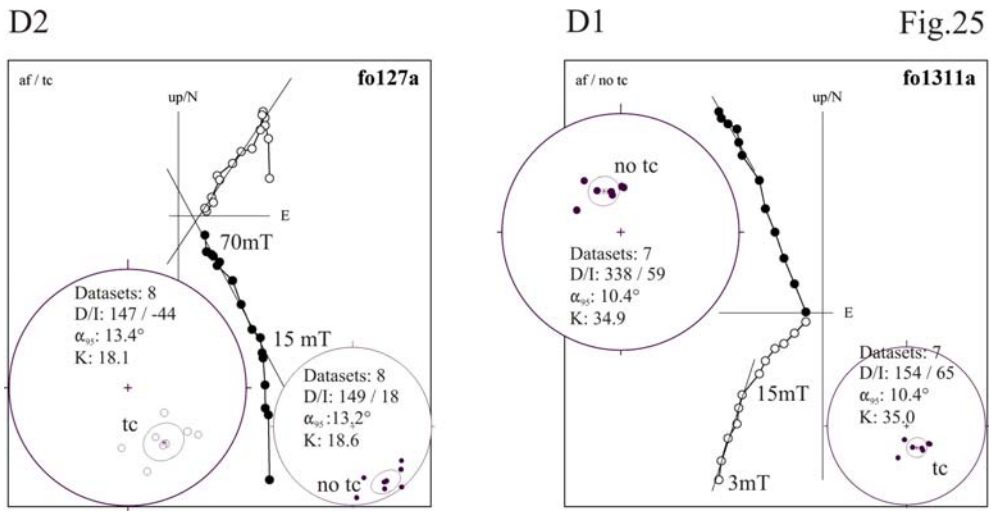

Fig. 25. Rock magnetic properties, demagnetization behavior and statistical parameters from site 137 (FO13, **A1-D1**) and site 138 (FO12, **A2-D2**), (Tab.1).

D= Zijderveld demagnetograms of representative samples in stratigraphic (tc) and geographic (no tc) coordinates, in the Zijderveld diagrams, full/hollow circles: projection of the NRM in the horizontal/vertical plane. Stereogeographic projection of the characteristic remanence magnetization direction, bedding corrected (tc), in situ (no tc) coordinates.

7. Discussion and conclusions

7.1 Mechanism and age of remagnetization

The hypotheses presented in this paper rely on primary magnetizations and magnetic overprints acquired after tectonic deformation. The interpretation as primary/secondary magnetizations is based on positive/negative fold tests (McElhinny, 1964), respectively. As the Northern Calcareous Alps were not affected by metamorphism, except in their southernmost part, increased fluid flow causing diagenetic alteration of carbonates is most probably the reason for chemical remagnetization, even if this alteration is not easy to see in thin section. Magnetic particles are extremely small and can be mobilized or grow also when the amount of fluid passing the rocks is small (Suk et al., 1993). In regional studies of carbonate cements from the Eastern Alps, Zeeh et al. (1997) and Kappler and Zeeh (2000) concluded that five of six generations of cements occurring in carbonates are of Cenozoic age, most of them even of post-Oligocene age. Ortner (2003) described intense local cementation of Oligocene age. This gives evidence for intense fluid flow during continental collision and post-collisional deformation in the Eastern Alps, which most probably caused chemical remanent remagnetization. Two events of remagnetization at 45-32 Ma and younger than 23Ma can be distinguished in the working area.

The first remagnetization, in Oligocene times can possibly be related to magma, ascending from the upper mantle due to slab break off of European oceanic lithosphere at 45Ma (von Blanckenburg und Davies, 1995). The intense fluid flow might be explained by heat advection by magma, which produced an increased geothermal gradient (Stuewe, 2007). The distribution of heat and fluid flow may follow the Alpine basal thrust plane. Possibly deep seating shear zones like Inn valley fault, SEMP (Salzach-Ennstal-Mariazell-Puchberg) line and Periadriatic line transferred the remagnetizing fluids to higher structural units. This remagnetization must have been finished at 32Ma as paleomagnetic results from younger lithologies are characterized by strongly clockwise rotated declinations. If the remagnetization would have been still active, these declinations would have been reset, according to the actual earth magnetic field, that was characterized by an approximately N/S oriented dipole (Besse and Courtillot, 2002).

A second time of intense remagnetization nearly unanimously was acquired in folded position. This remagnetization, characterized by counterclockwise rotated declinations is dated to sometime younger than Late Chattian (23Ma) as primary magnetizations from Early Late Chattian sites do not show the characteristic declination values but N directed declinations (e.g. site 16). Late Oligocene to Miocene remagnetization and fluid flow might be explained in two ways.

First, again remagnetization might be possible due to intense magmatic activity that is thought to be related to a possible slab break off of the lower European continental lithoshere. The upper mantle is thought to ascent, again raising the local heat flow, which possible caused increased fluid flow that was possibly active till Late Miocene times, according to sites from Messinian marls that are remagnetized in tilted position.

Secondly, also metamorphic fluids from the Central Alps/ Tauern window may cause widespread remagnetization (Zeeh et al., 1997; Kappler and Zeeh, 2000). Northward- and southward- directed gravity driven fluid flows from the Central Eastern Alps could have started immediately after the climax of metamorphism and due to high uplift rates at 20Ma (Blanckenburg et al., 1989). These fluids may explain similar developments of cementation sequences on both sides of the Central Alps, as well as steep thermal gradients observed at the western border of the unroofing Tauern footwall (Fügenschuh et al., 1997). Additionally, indications of fluids circulating in steep faults deeper than 20km were found by Selverstone et al. (1995).

Both events of remagnetization could be detected in a large area, including the NAFB/NCA/CA/SA/SAFB together. Most probably, only processes in the scale of lithosphere geodynamics might explain these pervasive overprints.

Some of the magnetization directions found in the Northern Calcareous Alps with NE-trending declinations are close to the magnetization values for stable Europe at 10-5 Ma (Besse and Courtillot, 2002). Consequently, an unrotated overprint magnetization of Late Miocene age might also cause these directions. Thus, no components carried by goethite were included into mean value calculations as goethite is the main carrier mineral of the (sub) recent earth magnetic field.

7.2. Clockwise rotation

Reliable data indicating Cenozoic clockwise rotation of the Northern Calcareous Alps and their basement were presented previously (Pueyo et al., 2002; Schätz et al., 2002; Thöny et al., 2006; Pueyo et al., 2007), additional data from Northern Alpine foreland basin, Northern Calcareous Alps, Central Alps, Southern Alps and Southern Alpine foreland basin are presented in this study. Haubold et al. (1999) and Schätz et al. (2002) already suggested that many of the "primary" paleomagnetic data from the Northern Calcareous Alps with clockwise rotated declinations (e.g. Hargraves and Fisher, 1959; Mauritsch and Becke, 1987; Channell et al., 1990, 1992) are in fact secondary magnetizations.

A previous working hypothesis for the Cenozoic clockwise rotation of the Northern Calcareous Alps independently of the Central Alps proposes clockwise rotation of segments of the Northern Calcareous Alps between ENE- to NE-trending sinistral faults in a domino style (Thöny et al., 2006). The young anticlockwise rotation of Adria and the Central Alps in respect to Europe (e.g., Besse and Courtillot, 2002) was interpreted to be possibly responsible for this process, which was leading to the formation of a mega-shear zone ("dextral wrench corridor") in the area of the Northern Calcareous Alps between the Central Alps and the European Foreland.

Two problems regarding this interpretation have to be kept in mind: The amount of clockwise rotation is 60°, which is the difference between the mean of the clockwise rotated magnetizations and the mean of the counter-clockwise rotated magnetizations. Such large rotations within the dextral wrench corridor would only be possible if using a "soft domino model" instead of a "rigid domino model" (Peacock et al., 1998) due to major space problems: 60° rigid block rotation of blocks with a height to width ratio of 1:1.5 would cause elongation of 100 percent parallel to the wrench corridor. Large gaps would open at the edges of the rotating blocks. Therefore the blocks must be allowed to deform internally, and we should expect inhomogeneous clockwise rotation. Neither the gaps, i.e. sedimentary basins, are observed nor is the space available for 100 % elongation, and clockwise rotation is rather homogeneous (Thöny et al., 2006).

Secondly, finite counter-clockwise rotation of the units south of the Northern Calcareous Alps should be larger than counter-clockwise rotation within the Northern Calcareous Alps, because, according to the model presented above, these units should rotate counter-clockwise, while the latter rotated clockwise. According to the data presented in this study, all units were subject to a uniform counter-clockwise rotation.

Therefore it was speculated (Thöny et al., 2006) that the Northern Calcareous Alps and the units to the south rotated clockwise uniformly, in spite of scarce direct evidence of clockwise rotation in the latter units. This speculation could be confirmed with magnetization data derived from the whole working area (Fig.26). Clockwise rotation could be separated into two phases (Fig.27).

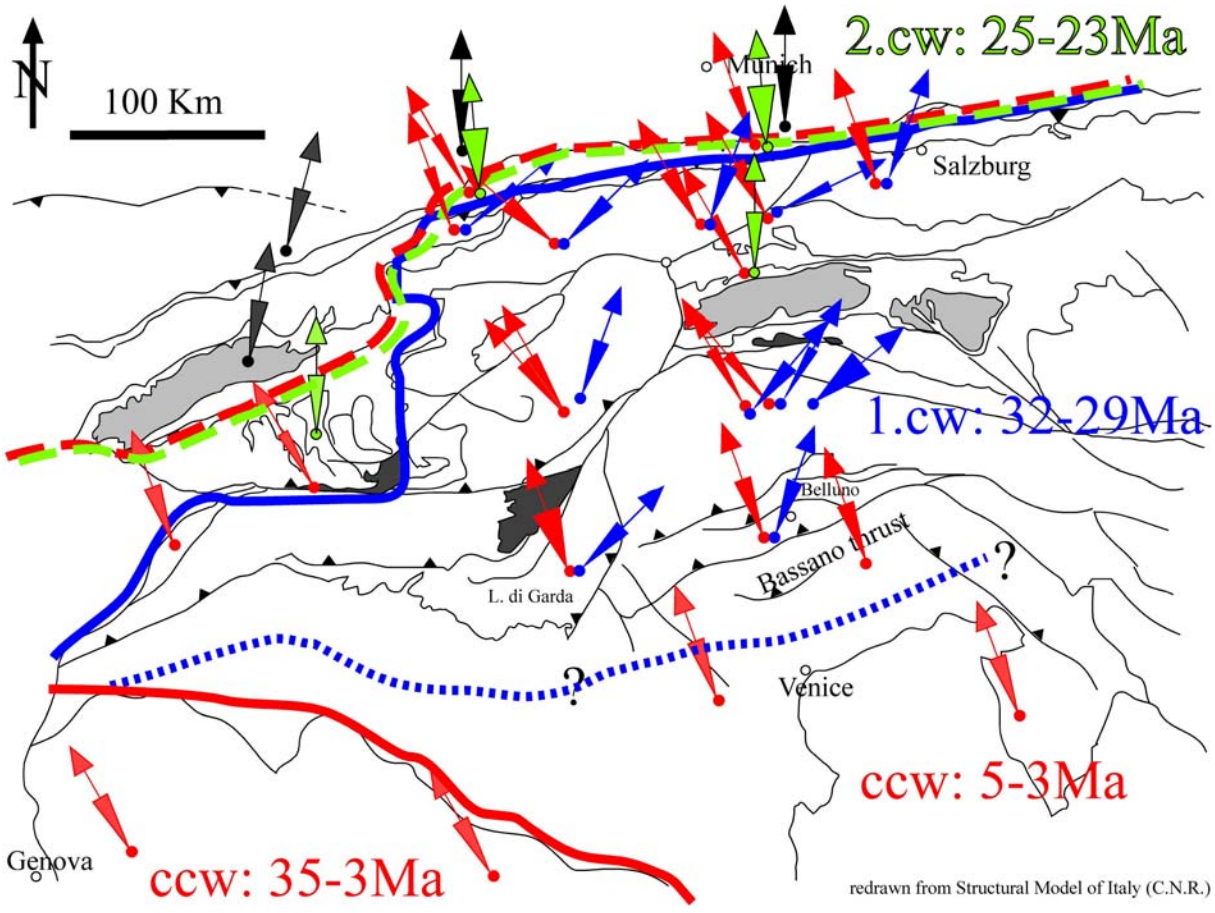

Fig. 26. Paleomagnetic results from the study area. Results are indicated by declination orientations and α_{95} cones. Colors of red, green and blue indicate counterclockwise, moderate clockwise and strong clockwise rotation, respectively.

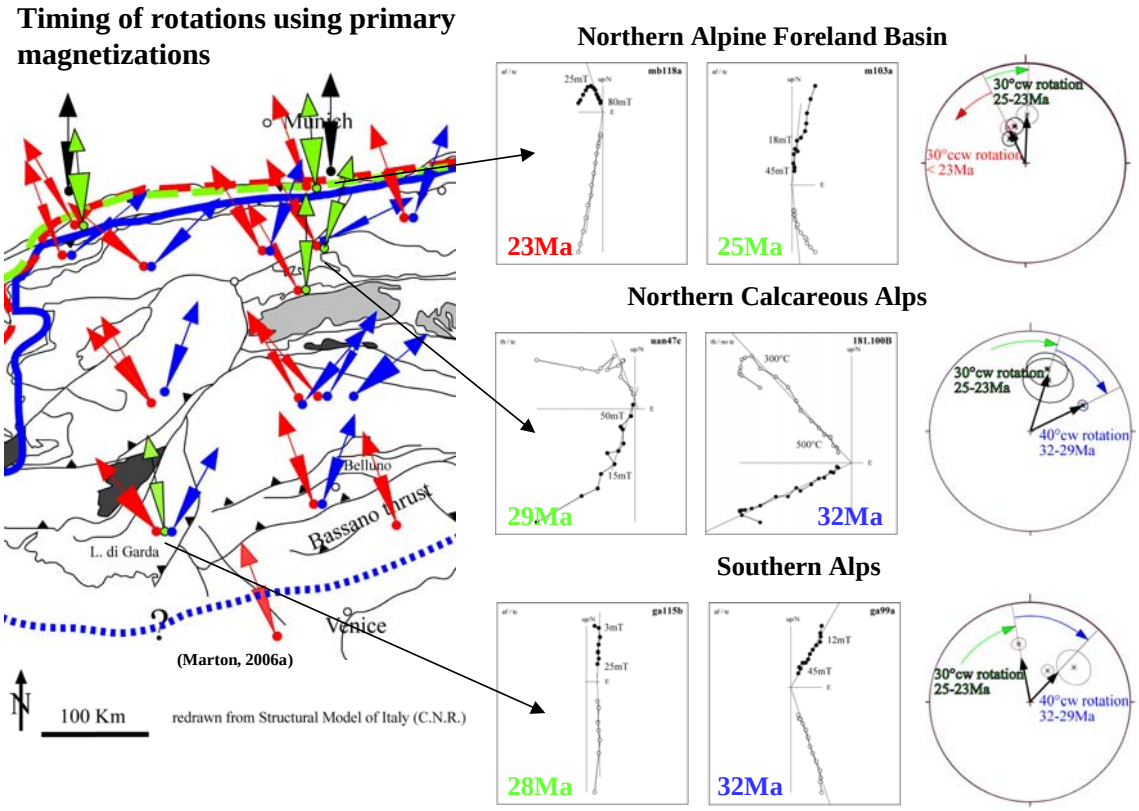

Fig. 27. Paleomagnetic results from the study area. Primary magnetizations from the Northern Alpine Foreland basin, the Northern Calcareous Alps and the Southern Alpine Foreland basin are indicating contemporaneous, identical vertical axis rotations.

Characteristic remanence vectors of postfolding magnetizations of Early Rupelian (34Ma) carbonates in the NCA and Mesozoic carbonates from the Helvetic nappes show declination values of 40°. Primary magnetizations from Late Rupelian (29Ma) marls from the NCA show N- directed declinations. N-directed declinations also characterize the primary magnetizations of Late Rupelian to Middle Chattian (29-25Ma) marls from the Northern Alpine Foreland basin, whereas prefolding magnetizations with declination values of 330° are observed in marls younger than Latest Chattian (23Ma). Progressive unconformities date the initiation of folding at these sites to Aquitanian/ Burdigalian times (23-16Ma).

In metamorphic marbles of the Penninic zone (site 97, HST, Tab.1, Fig. 1,2,19) at the northern margin of the Tauern window, we isolated two components of remagnetization, with N-directed and counter-clockwise rotated declinations, respectively. Both overprints were blocked below temperatures between 300–360 °C, as the carrier mineral of magnetization is titanomagnetite.
^{40}Ar-^{39}Ar data from white mica from samples in the same structural position east of our site HST (locality 14) gave formation ages of 28 – 35Ma (Urbanek et al., 2001). This gives a maximum age estimate for both remagnetizations observed (i.e.younger than 28Ma), as the ^{40}Ar-^{39}Ar system for white mica closes between 325–375 °C.

In the SA and SAFB all results from rocks older than Late Early Rupelian times (32Ma) are rotated 40° clockwise. N-directed declination values from primary magnetizations characterize lithologies of Chattian age (25Ma).

Concluding, the Eastern and Southern Alps are characterized by very similar characteristic remanence directions. The declination values are changing synchronously, indicating two phases of joined, clockwise vertical axis rotations in the study area (Fig.26, 27).

A first clockwise rotation is active between Early Rupelian to Late Rupelian times (32-29Ma) affecting the Helvetic units, the NCA, eastern CA, SA and SAFB. This rotation can be related with the thrusting of NCA, Flysch and Helvetic units. Contemporaneous with this first phase of rotation the climax of crystallization of Periadriatic intrusions can be observed (Rosenberg, 2004). The initiation of intrusion of calcalkaline, magmatic rocks along the Periadriatic line, is interpreted to result from the slab break off of the oceanic part of the Piemontais ocean lithosphere (von Blanckenburg and Davies, 1995; Kissling, 2007).
The first clockwise rotation acted later than the initiation of intrusions. Paleomagnetic data (Kipfer and Heller, 1988) from syn-magmatically metamorphosed Permian red beds from the contact aureole of the southern/older part of Adamello pluton (40Ma, Rosenberg, 2004) possibly indicate a bimodale distribution of remanence directions with concentrations of data at D/I= 333/69 and D/I= 21/57. Possibly this distribution is caused by vertical axis rotations.
Concerning the first clockwise rotation (32-29Ma) the internal massifs (Zentralgneis of Tauern window, Lepontine nappes) do not seem to be incorporated into the rotating units, as both of them were not exhumed yet (Fügenschuh et al., 1997; Rosenberg and Heller 1997).

Assuming structural continuity of the Helvetic nappes from western Austria, where they were sampled, to Switzerland, the first clockwise rotation is linked to the Oligocene out of sequence precursor of the Miocene Glarus thrust (Badertscher and Burkhard, 2000). After intensive folding during the Calanda phase (Pfiffner, 1977) and metamorphism, the western (Eastern Swiss Alps) nappe stack was overthrusted by Helvetic nappes along the Glarus thrust that was active postmetamorphically, between 25-20Ma (Hunziker et al., 1986).
This is exactly the time of the second clockwise rotation (25-23Ma) that could be identified in the study area. Consequently N directed declinations that were found in the Northern Alpine Foreland Basin (sites 10/11, 16-22, Tab.1) in Helvetic nappes close to the Alpine front in eastern Bavaria (sites 38/39, Tab.1) in the para-autochthonous cover of the Zentralgneises of the Tauern window (site 97, Tab.1) and in numerous sites from the Lepontine dome (Heller, 1980; Rosenberg and Heller, 1997) are interpreted to indicate clockwise rotation of 30°. This rotation documents the transition of orogeny from internal parts into the external parts incorporating the foreland basins. Without any exception, sites (10/11, 16-22, Tab.1) from the Northern Alpine Foreland Basin are indicating that folding was postdating clockwise rotation. The rotation was carried out on the basal Alpine thrust plain.

7.2.1. Reasons for clockwise rotation

A reason for this rotation might be differential Oligocene slab retreat along the strike of the still existing lower European crust (Kissling, 2007) (Fig.28). Slab break off at 45Ma did only affect the oceanic lithosphere but not the European mantle lithosphere (Blanckenburg and Davies, 1995). In the Western and Swiss Alps slab retreat rates are thought to be constant along strike of the slab, causing NW to W movements of the upper plate but no rotation. Concerning the Eastern Alps differential rates of retreat are interpreted to result from differential amount of mantle lithosphere that is retreating northward, being more to the W at the transition to the Swiss Alps and less at the rotation pole, close to the Bohemian spur (Wessely, 1987).
It is speculated that the Eastern and Southern Alps are follow the retreating slab, consequently rotating clockwise. At about 20Ma rotation is stopped, possibly due to rebound of the lower plate causing increased friction at the plate boundary and uplift of the upper plate related to convective removal of the mantle lithosphere (Houseman et al., 1981; Fügenschuh et al., 1997) (Fig.28).

Concerning the Swiss and Eastern Alps, Kuhlemann and Kempf (2002) additionally defined a peak in sediment discharge towards the foreland basins between 25 to 20Ma, possibly caused by the rebound of the lower plate and the consequent surface uplift of the upper plate.

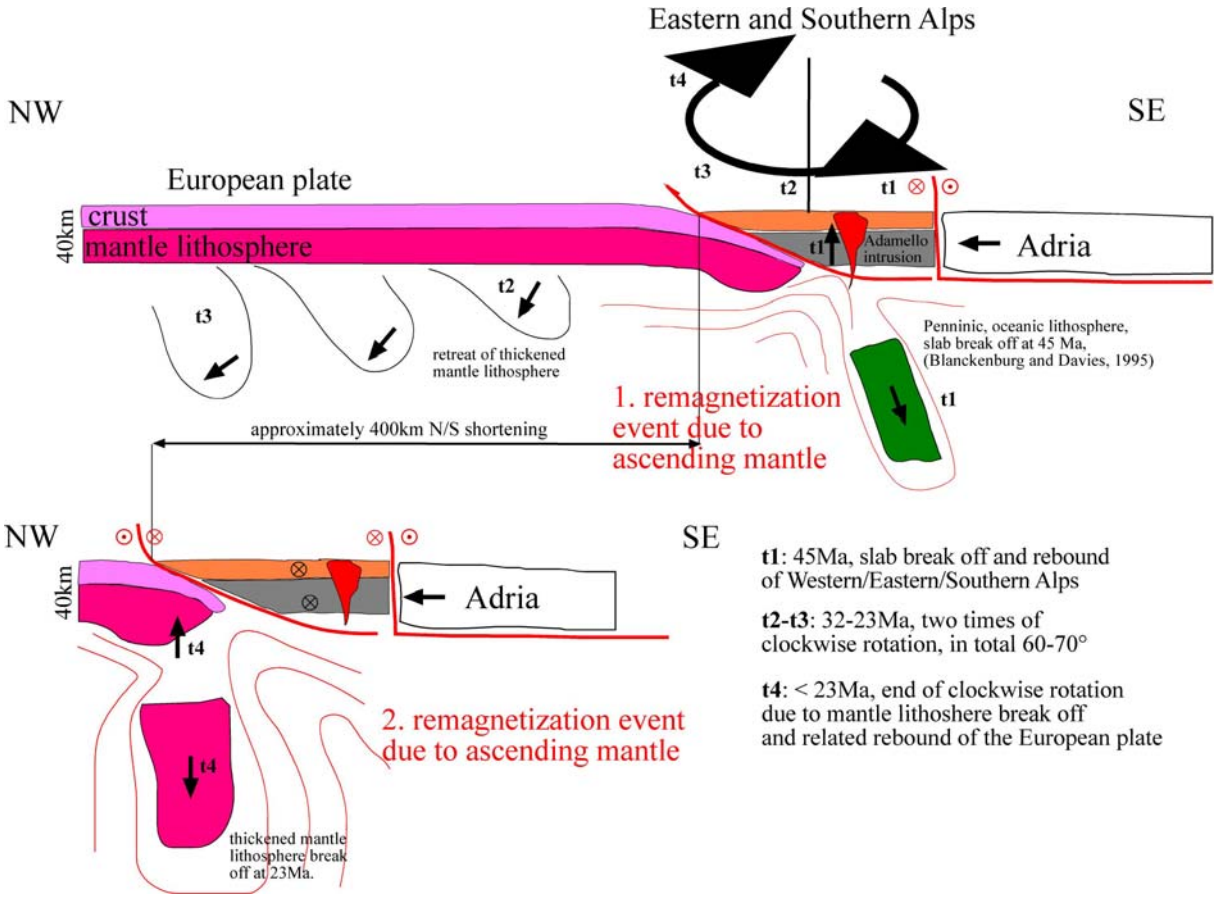

Fig. 28. N/S oriented cross section. Clockwise rotation of Eastern and Southern Alps might be caused by retreat of the European mantle lithosphere and NW directed movement of Adria. 400 km of N/S shortening (x) are calculated as follows: x= tan 60°*250km. E/W extent of the Eastern Alps (250km) are derived after subtracting 300km of lateral extrusion related extension (Frisch et al., 2000) from current dimensions. The elimination of crustal units is still a matter of debate and possibly was partly achieved by the lateral extrusion of the Austro-Alpine nappe pile.

7.3. Counter-clockwise rotation

7.3.1. The reference frame

Usually vertical axis rotations are defined by deviations from the apparent polar wander path e.g. calculated for the last 200Ma by Besse and Courtillot (2002). The European APWP is well defined. Declinations reported in the magnetostratigraphic studies of Kempf et al. (1998) in Upper Oligocene to Middle Miocene sediments of the Swiss Subalpine Molasse are indicating 5-10° of clockwise rotation relative to geographic N. Results by Abdul Aziz et al. (in press) derived from primary magnetizations of Upper Miocene autochthonous Molasse sediments in eastern Bavaria north of Munich strongly support a Miocene European reference direction with N directed declination values (D/I= 365 / 56; α_{95}= 3,9°; k= 16,5 for normal polarity; D/I= 183 / -44; α_{95}= 10,8°; k= 7,6 for reverse polarity). This study adds results from four sites north of the frontal Alpine thrusts. These data from the tilted Molasse are again characterized by N directed declinations indicating no vertical axis rotation (D/I= 3 / 56; α_{95}= 6,0°; k= 232,1).

Marton et al. (2006b) reported paleomagnetic data from the Miocene cover of the Bohemian massif. These sites were partly indicating counterclockwise rotation. Consequently, presuming a N/S directed European reference declination the Bohemian massif must have rotated in a counterclockwise sense during/after the Miocene separated from “stable“ Europe by a major fault. To the west and southwest no geological structures, caused by rotation related shortening could be observed in the North Alpine foreland basin. Possibly the “Pfahl” fault, striking NW/SE at the SE rim of the Bohemian massif, is limiting the rotating part.

Therefore, it is speculated that during a time of decrease of the dipole part of the Earth magnetic field, a relative increase of non dipole parts may have shifted the pole position causing declinations for stable Europe that were possibly NW directed and not N directed. Singer et al. (2007 submitted) described similar deviations from the N/S dipole alignment in volcanites from the W-Eifel/Germany during the excursion of the earth magnetic field in the Brunhes chron. It is speculated (Marton, 2006b) that the reference declination for stable Europe during the Miocene was possibly NW directed, and deviations from that NW direction have to be explained by vertical axis rotations. Consequently the data from the Bohemian massif (Marton, 2006b) would not indicate any rotation.

On the other hand, accepting a NW directed reference declination, all primary, Miocene declinations that are N/S directed would indicate a clockwise rotation. This would be the case e.g. for the data from the autochthonous Molasse north of Munich by Abdul Aziz (in press). The only way to rotate the autochthonous Molasse would be derived by a rotation of the European plate. As the Bohemian massif would be stable (according to this interpretation) a Miocene **orogenic belt** should have evolved surrounding the Bohemian massif, at the boundary to the rotating European plate. There are absolutely no geological arguments supporting that kinematic scenario.

Consequently, especially based on the data from the autochthonous Molasse by Abdul Aziz (in press), the following interpretations, favouring the model of a strong Miocene dipole with N-directed declination for stable Europe, are proposed.

7.3.2. Late Miocene to Early Pliocene counter-clockwise rotation

Concerning Miocene (re)magnetizations, all structural units sampled south of the Alpine frontal thrust i.e. the Subalpine Molasse, EA, SA, SAFB are characterized by NW directed declinations, supporting a model of a large scale, counterclockwise vertical axis rotation relative to stable Europe. In the following, amounts of vertical axis rotations are always related to the geographic N as reference direction.

Counter-clockwise rotated declinations in overprint magnetizations in the western Northern Calcareous Alps were observed only locally in previous studies (Channell et al., 1992). Primary paleomagnetic data from Karpatian/Badenian sedimentary rocks were derived from the eastern part of the Alpine foreland basin (Scholger and Stingl, 2002) indicating 20° of counterclockwise rotation in post Badenian times (<13Ma). Data from intra-Alpine Middle Miocene sedimentary basins (Márton et al., 2000) indicate two stages of counter-clockwise rotations. 30° of counter-clockwise rotation is related to the lateral escape in Ottnangian to Karpatian. Another 30° counter-clockwise rotation is explained by “en block” rotation of the Eastern Alps in post Sarmatian times (<12Ma). 20° of post Karpatian (<16Ma) counterclockwise rotation affected sediments in the most southeastern part of the Eastern Alps, namely the Klagenfurt and Lavantal basins (Márton et al., 2000).

Paleomagnetic data from the Adriatic microplate from Slovenia/Mura zala (Marton et al., 2002a) and northern Croatia (Marton et al., 2000b) indicate 30° of counterclockwise rotation in post Messinian (<5Ma) times.

From the internal massifs of the Western Alps (Thomas et al., 1999; Collombet et al., 2002) and the Sesia-Lanzo zone (Lanza, 1977, 1978) remagnetizations of Late Eocene to Early Oligocene with NW directed declinations were reported. The external massifs are not rotated with respect to the Oligocene/Miocene N-directed declinations of stable Europe (Crouzet et al., 1996; Aubourg and Chabert-Pelline, 1999).

In the frame of this study sampling along N/S striking profiles crossed several prominent, approximately E/W striking Alpine fault systems (e.g. Inntal fault, SEMP line, DAV fault, Periadriatic line, Val Sugana Fault, Belluno fault, Bassano fault).

Secondary and primary magnetizations, younger than 23Ma, systematically show NW directed declinations. These declination values scatter in a range of 5°, independently from the structural position (Fig. 29). Therefore the individual structural units did not rotate relative to each other. In the southernmost part of the study area, in the Bassano area NW-directed declination values are found in primary and postfolding magnetizations from Serravallian to Messinian sediments (14-5Ma). The youngest, counterclockwise rotated declinations were derived from folded Messinian Montello conglomerates of the northern Venetian plain. Consequently a vertical axis rotation postdates folding of the Messinian sediments and is younger than 5Ma.

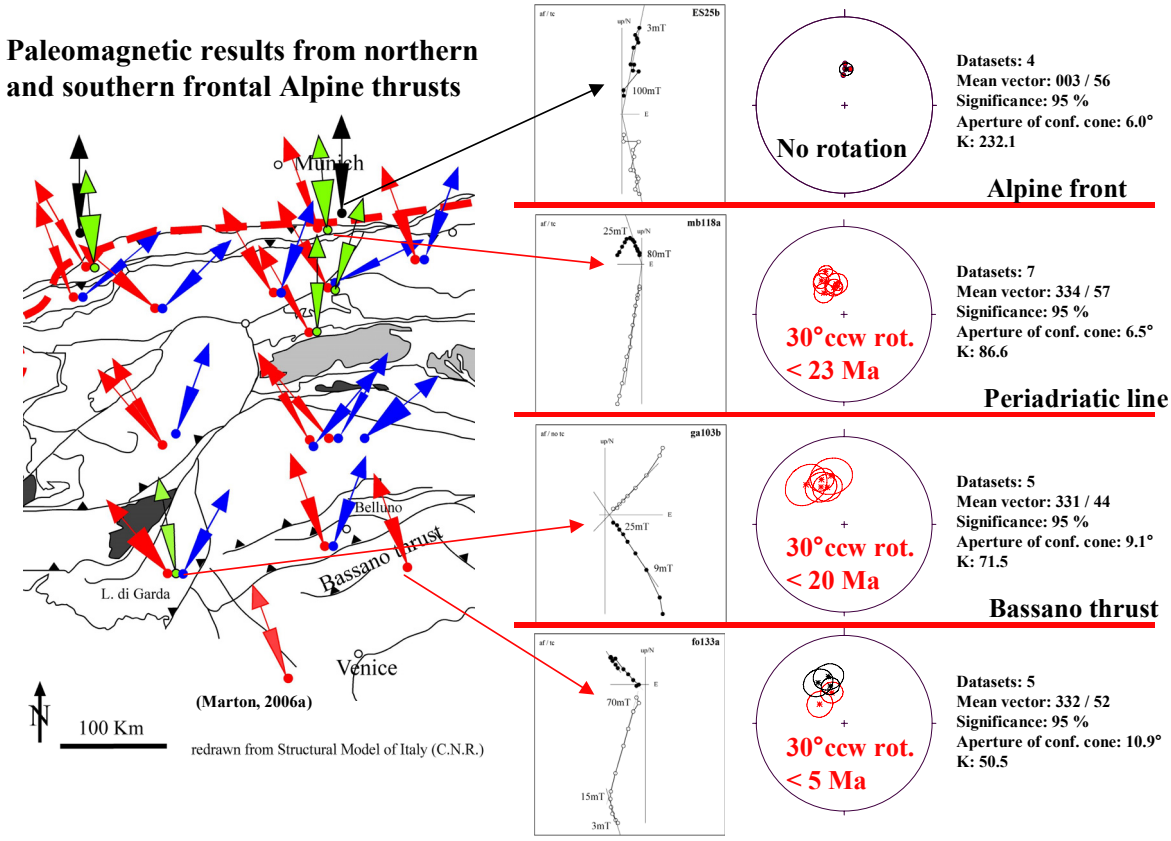

Fig. 29. Paleomagnetic results from the study area. The amount of counterclockwise rotation does not change although the rotating units are separated by prominent Alpine thrusts and strike slip faults (marked by strong red lines). No rotations of tectonic units relative to each other are indicated. Red confidence cones mark secondary magnetizations, black confidence cones mark primary magnetizations.

Obviously, the Northern Alpine foreland basin, the Northern Calcareous Alps, Central Alps, Southern Alps and their foreland, stable Adria and part of the Swiss and Western Alps faced uniform, synchronous 30° of counterclockwise rotation in post Messinian times, i.e. younger than 5Ma.

7.3.3. Contradicting/ supporting data from Structural Geology

The rotated unit roughly corresponds to the intra-Alpine part of the Adriatic plate and the units, which were accreted to it during Alpine orogeny up to the Middle Miocene. Therefore, the northern margin of the rotated block should be the surface trace of the basal thrust of the Alpine orogen, and rotation should have taken place on top of the thrust plane (Fig.30). As the youngest only slightly deformed sediments (UFM) at the Alpine front are Tortonian in age, thrusting was still, decreasingly active in Tortonian (Ganns and Schmid-Thomé, 1953).

Counterclockwise vertical axis rotation even must be younger because the observed remanences were acquired after folding.

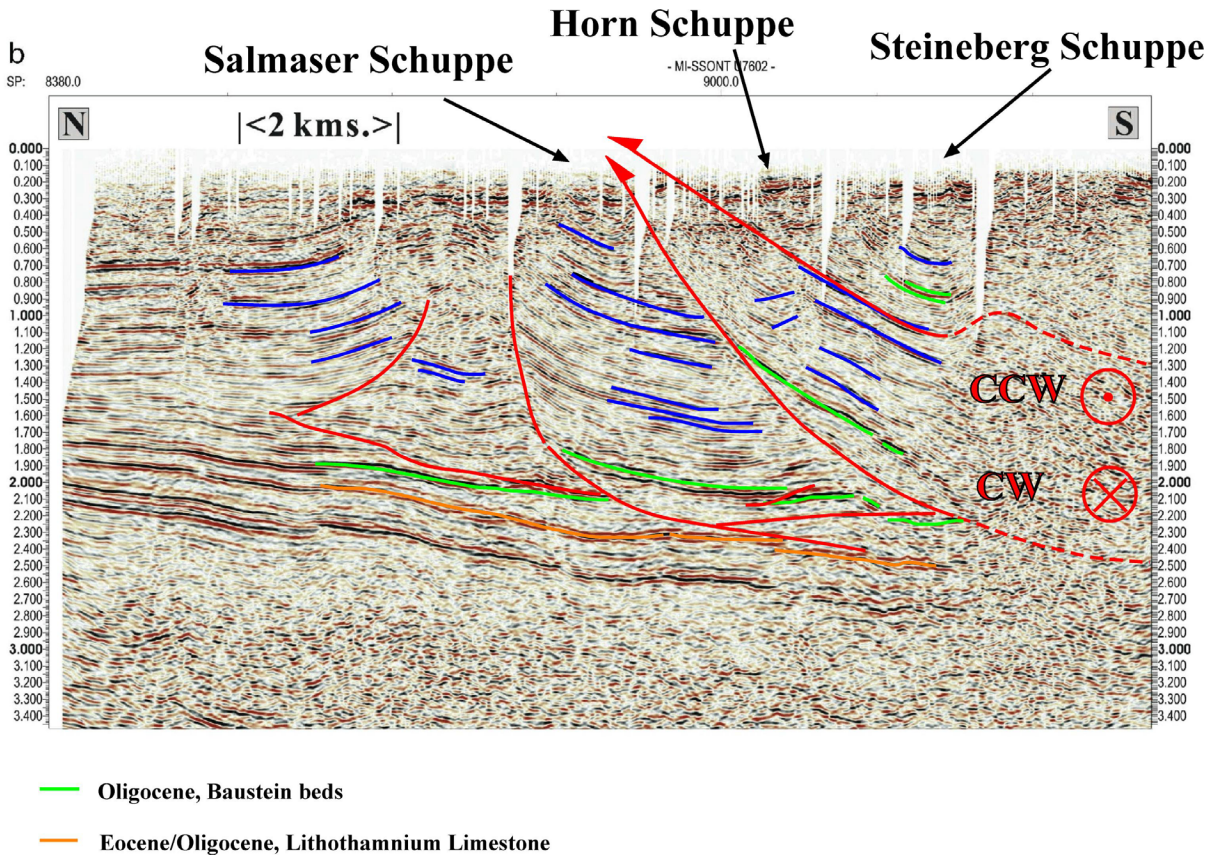

Fig. 30. N/S oriented cross section at the transition from Autochthonous to Allochthonous Molasse. The counterclockwise rotation is compensated at the Alpine basal thrust and at sinistral, transpressive faults that are disintegrating the slices of Subalpine Molasse. Modified from Berge and Veal (2005). Post-folding and Pre-rotational remagnetizations south of Salmaser Schuppe do not show inclination shallowing (e.g. sites 4-9, Tab.1). Only site 3 (Tab.1) from locality Sulzberg at Salmaser Schuppe is characterized by shallow inclinations (D/I= 33/29). Presuming a simple ramp-flat system at the contact between rotated to unrotated Molasse units, the site at locality Sulzberg (site 3, Tab.1) may represent a position at the ramp interpreted from shallow inclinations due to tilting. All other results from Horn- and Steineberg Schuppe (e.g. sites 4-9, Tab.1) with steep inclinations (around 60°) are derived from a position at the lower flat.

Using GPS data Anderson and Jackson (1987), Noquet and Calais (2003) and Weber et al. (2005) could locate the current rotation pole for Adria in the area of Torino. Although calculated rotation rates must have been much higher in Late Miocene to Pliocene times than observed from recent GPS-measurements, the rotation pole derived from GPS- measurements is also used for kinematic reconstructions in Late Miocene to Pliocene times.

For minimizing kinematic consequences a fixed rotation pole at the meridian of Torino near Bregenz/Lake Konstanz is assumed. A restoration of the youngest, 30° counterclockwise rotation transfers the Alpine nappe stack southward with increasing distances according to the lateral distance from the rotation Pole.

At meridian Kempten 40km east of the rotation pole 20km of N/S shortening have to be restored, at meridian Schliersee, 150km east of the rotation pole about 90km. At the supposed eastern rim of the rotating mega unit, 580km towards E at the meridian of Lake Neusiedl SSE of Vienna, 330km of N/S shortening have to be restored. In the western part of the NAFB, data from structural geology contradict these shortening values as geological data indicate only some tens of kilometers of relative shortening at the frontal Alpine thrusts (e.g. Ganns and Schmid-Thome, 1953). Also the style of deformation at the frontal Alpine thrust does not indicate large scale thrusting (pers. comment H. Ortner). However, this restoration might open an enormous area that would connect the Pannonian Basin to the Northern Alpine foreland basin and that would be closed with the beginning of the counterclockwise rotation at about 5Ma (Fig.31). Consequently below the Austroalpine nappe stack remnants of Molasse sediments have to be supposed. Grassl et al. (2004) identified a so called “Mélange zone” between the overthrusting Penninic units and the crystalline basement of the European distal continental margin below in deep reflection seismic images at an WNW/ESE striking profile, crossing the Austroalpine crystallin units W of Penninic window group of Rechnitz. It was interpreted that the “Melange zone” may consist of remnants of the parautochthonous Mesozoic cover of the European continental margin and remnants of Penninic units but it was also speculated, that Molasse sediments possibly contribute to this zone.

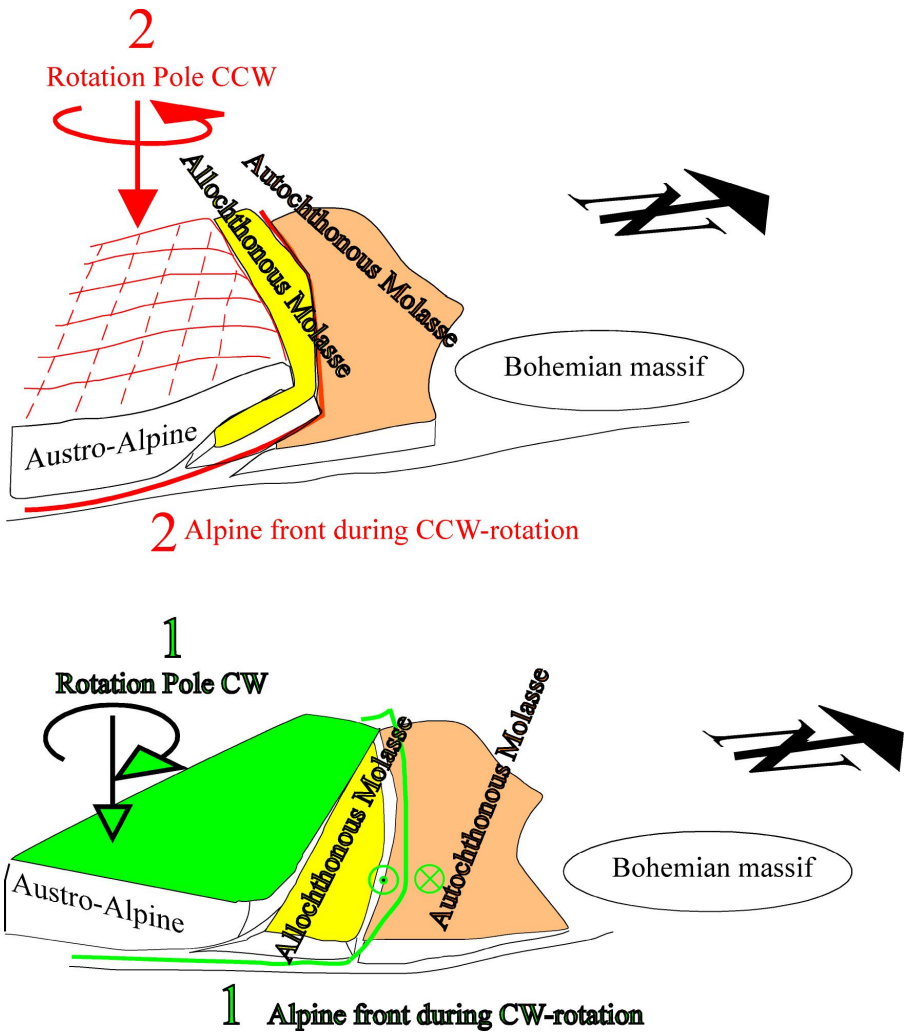

Fig. 31. Due to the lateral extrusion friction is reduced at basal Alpine thrust. After clockwise rotation repeated (counterclockwise) rotation is enabled by changing the rotation pole from the Bohemian massif (**1**) to the area of the meridian Torino / Lake Konstanz (**2**).

At the boundary to the Swiss/Western Alps no fault system was active during Late Miocene to Pliocene times that was able to accommodate 30° of counterclockwise rotation of the Eastern Alps relative to the Swiss/Western Alps. Consequently the NW directed declinations that can be observed in the Swiss/Western Alps (Thomas et al., 1999; Collombet et al., 2002; Rosenberg and Heller, 1997) are interpreted to result from a joined counterclockwise rotation of parts of Swiss/Western Alps together with Eastern and Southern Alps. Concerning the Swiss/Western Alps the basal thrust/rotation plane is thought to be at the transition from upper to lower crust incorporating the Lepontine nappes into the rotating units. To the N the counterclockwise rotation is limited by the Aar massif, which is showing together with the northerly adjacent nappes of the allochthonous Molasse 5° to 10° clockwise rotation relative to the N direction of stable Europe (Heller, 1980; Kempf et al., 1998).

Zwingmann and Mancktelow (2004) were dating brittle tectonics at the Simplon fault to 6-3Ma. Possibly, the Simplon fault separates these two opposite rotating units during Late Miocene to Pliocene times.

Another problem arises with the eastern limitation of the rotating unit, especially with the geodynamic evolution of the Vienna Basin. Based on sediment thickness the main activity of the strike slip faults, related to the pull apart basin was dated to Burdigalian/ Tortonian times (17-8Ma) (Hinsch et al., 2005). Traditionally the Vienna basin is kinematically linked towards southwest to sinistral strike slip faults in the Mur-Mürz valley (e.g. Ratschbacher, 1991) and towards northeast to strike slip faults (e.g. Schrattenberg-Bulhary fault) running into the Western Carpathian arc, showing absolutely no displacements on map scale by younger crosscutting faults. If 30° of counterclockwise rotation younger than 5Ma was restored, the Vienna Basin that was obviously incorporated into the rotating mega-unit, should be oriented approximately ENE/WSW before 5Ma. Also Western and Northern Carpathians should join this rotation postdating 5Ma (see Marton, 2007), because no displacements between the Vienna Basin and the Western Carpathians can be observed. Marton and Fodor (2003c) were interpreting 25° of counterclockwise rotation younger than 5Ma for the Transdanubian Range that is located in the south of the North Pannonian unit north of Mid-Hungarian line. Marton et al. (2006) reported paleomagnetic data from the Miocene cover of the Bohemian massif.

These sites were partly indicating counterclockwise rotations as well. If a stable N/S oriented dipole was expected for Miocene times the EA, the SA, stable Adria (Apulia), the North Pannonian unit and the Bohemian massif, should have jointly rotated counterclockwise, postdating 5Ma. However, based on geological arguments there is no doubt that relative shortening of several hundred kilometers between the units mentioned above and "stable Europe" north of the Bohemian massif did not occur. Contrarily, paleomagnetic data definitely support this kinematic model as outlined in the following.

7.3.4. Constraints by means of paleomagnetism

A mean remanence direction was calculated from results from 3 paleomagnetic studies (Nairn, 1960; Angenheister, 1956; Sherwood, 1990) at locality Vogelsberg at φ= 50,5°N on sites of Early to Late Miocene magmatic rocks (5-23Ma). The resulting overall D/I= (3 / 62; α_{95}= 7,2°; k= 293,4) is indicating 6° difference from the inclination values that are currently observed at φ=50,5°N (i.e. I= 67,7°) implying 700 km N/S directed displacement.

Obviously this N/S directed displacement postdates the age of the youngest rock that showed inclinations of 62°, i.e. younger than 5 Ma.
Similar 7° of difference between the calculated inclination values and the values that could be expected based on the geographic position were derived from Suevites (14-18Ma) at Nördlinger Ries impact structure (Petersen et al., 1965).

Based on paleomagnetic data (locality Follina, sites 137-140, Tab.1) the Cenozoic counterclockwise rotation, observed in the study area, is dated to post 5Ma (Fig. 32). No thrust is known in the Alpine to W/N-Carpathian region that could accommodate thrust distances related to the counterclockwise rotation at 5Ma by internal shortening i.e. nappe stacking. Therefore, most probably kinematics propagated at the basal Alpine thrust plane. Consequently the rotating units are interpreted as a coherent block and inclination values are compared with actual values of inclinations that can be easily calculated from the geographic latitude φ of the sampling locality using the equation: tan I = 2* tan φ.

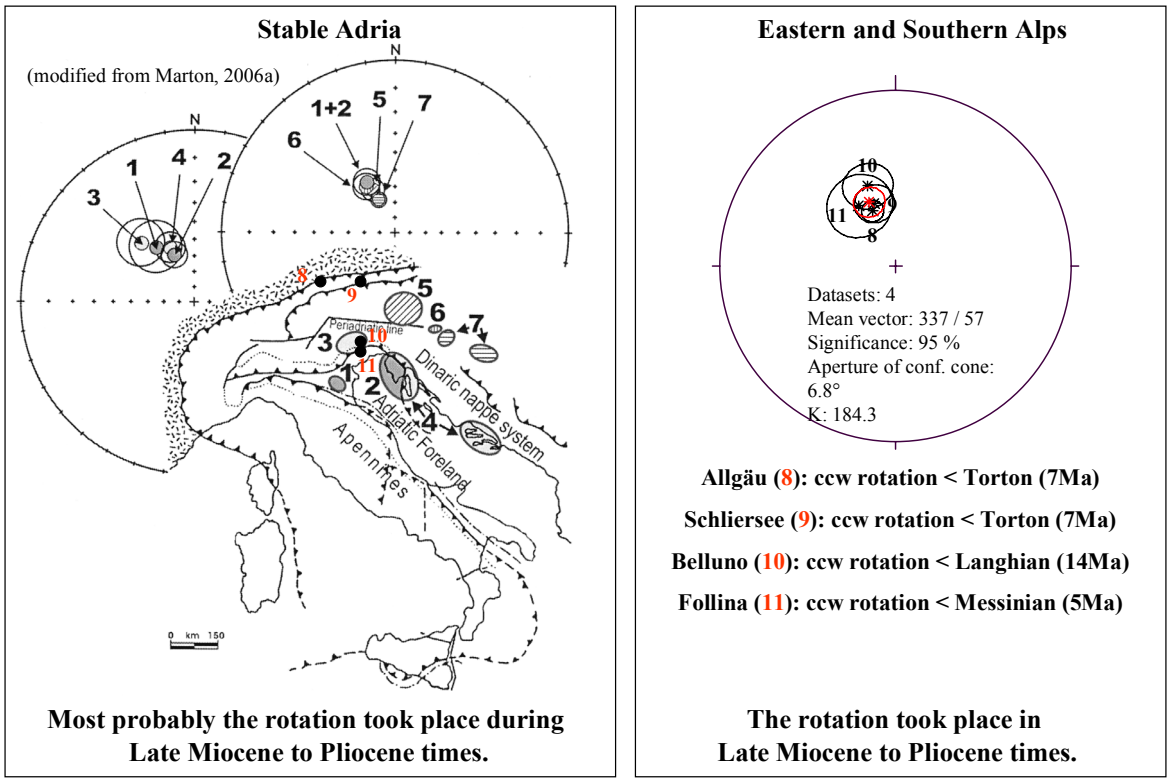

Fig. 32. Paleomagnetic results from the study area (red numbers, Tab.1). For comparison: paleomagnetic results from stable Adria by Marton (2006a) (black numbers). Stable Adria and Eastern/Southern Alps indicate a joined counterclockwise rotation relative to geographic N in post Messinian times, i.e. younger than 5Ma. Red confidence cone in right figure marks primary magnetizations from Schliersee area (Tab.1).

Concerning the current study the inclination that is expected for φ = 47,6°N (i.e. the sampling localities in the western NAFB (Allgäu/ Schliersee area) is I = 65,5°. Characteristic components derived from a sampled fold structure at the northern limb of the southernmost Subalpine Molasse slice (i.e. Steineberg synform) indicated a significant, negative fold test (McElhinny 1964) with best concentration parameter at 0% unfolding, Cr = 1,636 (sites 7-9, Tab.1, i.e. sites EA 1, EA5, EA4). Consequently internal deformation of the fold structure, i.e. tilting of the fold limbs relative to each other, did not occur after post-folding remagnetization. Tilting of the overall Steineberg fold structure that is located southernmost among the slices of Subalpine Molasse is not very probable. Kinematics were carried out on the basal thrust and the currently active frontal Alpine thrust and not in between the slices of the Subalpine Molasse (Fig.30). Therefore the inclination values indicate the paleogeographic latitude of the sampling localities in post-folding to pre-rotational times. Insitu remanences of 7 sites (sites 4-9, 23; Tab.1) from the western NAFB south of the frontal Alpine thrust showed a mean D/I= 334 / 57; α_{95}= 6,5°; k= 86,6 implying a difference concerning the inclination values of 8° compared with actual values.
Subtracting 6°-7° of overall inclination difference that is caused by the translation of stable Europe, 1°-2° (i.e. 110-220km) inclination difference related to N/S shortening and accompanying counterclockwise rotation remains.

In the western NAFB shortening at the frontal Alpine thrusts is limited by data from structural geology to some tens of kilometers and was finished in Tortonian i.e. latest at 7Ma, according to progressive unconformities (Ganns and Schmid-Thomé, 1953). Shortening related to rotation, i.e.<5Ma was possibly accommodated at the basal thrust plane.

The eastern NAFB (Korneuburger Basin, Vienna Basin, Carpathian foredeep) was studied by Scholger (1998), Scholger and Stingl (2004). Karpatian to Badenian (17-13Ma) sediments yielded a mean D/I= 338 / 54; α_{95}= 4,3; k= 449,3. The inclination that can be observed currently at the sampling locality (φ= 48,5°N) I= 66,1° is implying 12° of overall inclination difference and 5°-6° of inclination difference related to relative shortening caused by the counterclockwise rotation. This value for the eastern NAFB is 4° larger compared to the western NAFB and would indicate 440km of rotation related N/S shortening.

Paleomagnetic results (Marton and Fodor, 2003c) from 4 sites in Pannonian (11,5-7,1Ma) sediments at the Transdanubian Range were showing a mean remanence direction of D/I= 336 / 56; α_{95}= 8,6°; k= 114,2. The inclination that can be observed currently at the sampling locality (i.e. 47- 47,5° northern latitude) I= 65,0° - 65,4° is implying 9° of overall inclination difference. After subtracting 6°-7° caused by northward translation of stable Europe, 2°-3° of inclination difference remains, indicating a maximum value of 330km of N/S shortening related to counterclockwise rotation.

Consequently, as the eastern NAFB (Vienna Basin, Korneuburg Basin, Carpathian foredeep) and southerly adjacent small Pannonian Basin and the Transdanubian Range form a coherent block (part of ALCAPA unit), about 110km N/S directed shortening in the eastern NAFB (Vienna Basin, Korneuburg Basin, Carpathian foredeep) has to be related to pre-rotational thrusting and folding in post Karpatian/Badenian to pre-Pannonian times. The successive counterclockwise rotation was carried out on the basal Alpine thrust plane incorporating the folded sequences.

To the W the Rhine-Rhone lineament most probably does not limit the rotating Alpine nappe stack and the northward moving stable European plate as inclination values from Early Pliocene lavas from Massif Central (Besse and Courtillot, 2002) are similarly shallow.
To conclude, data from structural geology and paleomagnetic data strongly contradict each other. It is beyond the scope of this study to solve this problem. However, two possibilities remain, either geological structures related to the counterclockwise rotation (e.g. positive flower structures) at the frontal Alpine thrust at the contact to not rotated units are completely eroded, or fundamental basics about the nature of the dipole model of the earth magnetic field are not valid, at least in Miocene times. The author of this study prefers the first possibility due to enormous physical consequences of the second one, concerning the paradigm of the GAD (geocentric axial dipole) model of the earth magnetic field.

7.3.5. Reasons for counter-clockwise rotation

The driving force of the counter-clockwise rotations in the Alps might be the rotation of the autochthonous parts of the Adriatic plate, which is a matter of debate in the Cenozoic due to a lack of paleomagnetic data from young sediments, except from the northern part of the Adriatic plate, where paleomagnetic data from Late Eocene to Lower Miocene sedimentary rocks indicate counter-clockwise rotations of about 30° (Thio, 1988; Vandenberg, 1979; Bormioli and Lanza, 1994; Márton et al., 2003c; Márton, 2006; Márton 2007). Counter-clockwise rotation of the Adriatic plate was also proposed on the base of structural data (Vialon et al., 1989; Schmid and Kissling, 2000) and presently ongoing counterclockwise rotation was detected by GPS measurements (Nouquet and Calais, 2003).

Oligocene clockwise rotation around the rotation pole of the Bohemian spur was probably caused by oblique collision and slab retreat of the lower lithosphere of the lower European plate. The Late Miocene/Pliocene counterclockwise rotation has a rotation pole, located 500km west, at the meridian Lake Konstanz/Torino (Anderson and Jackson 1987; Noquet and Calais, 2003; Weber et al., 2005). Possibly, changing of the rotation pole and unblocking of the Austroalpine nappe stack, which was fixed on the Bohemian spur was triggered by the initiation of the lateral extrusion (Ratschbacher et al., 1991) at about 20Ma (Fig. 31). It is supposed that extrusion of Austroalpine nappes to SE might decrease the friction resistance at the basal thrust plane, which is the contact to the Bohemian spur.
The counterclockwise rotation itself is related to the opening (5-3Ma) of the Tyrrhenian Sea/ Vavilov basin (Mattei et al., 2004) in the Central Mediterranean (Fig. 33, 34).

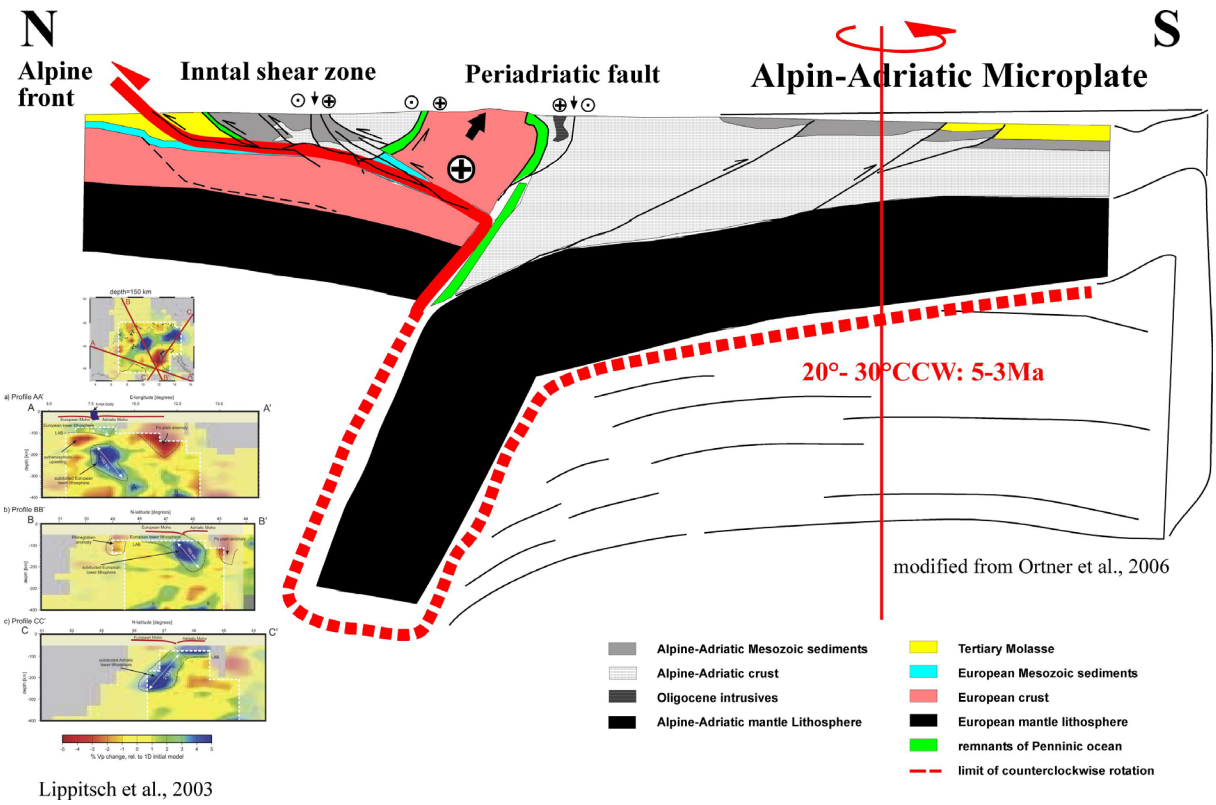

Fig. 33. N/S oriented cross section. The counterclockwise rotation of Eastern and Southern Alps is caused by a counterclockwise rotation of the Adriatic microplate. The Adriatic slab below the Dinarides is rotated into the Eastern/Southern Alps as also indicated by data from Lippitsch et al. (2003).

These geodynamics were not only an effect of retreating subduction of the Adriatic slab below the Apennines (e.g. Bois, 1993; Gueguen et al., 1998), but (also) of a counter-clockwise rotation of the Adriatic plate, probably due to E-directed mantle convection that moved the downgoing Adriatic slab (Doglioni et al., 2002; Facenna et al., 2004) (Fig. 34).

Opening of the Mediterranean basins:
-E-directed mantle flow
-subduction retreat

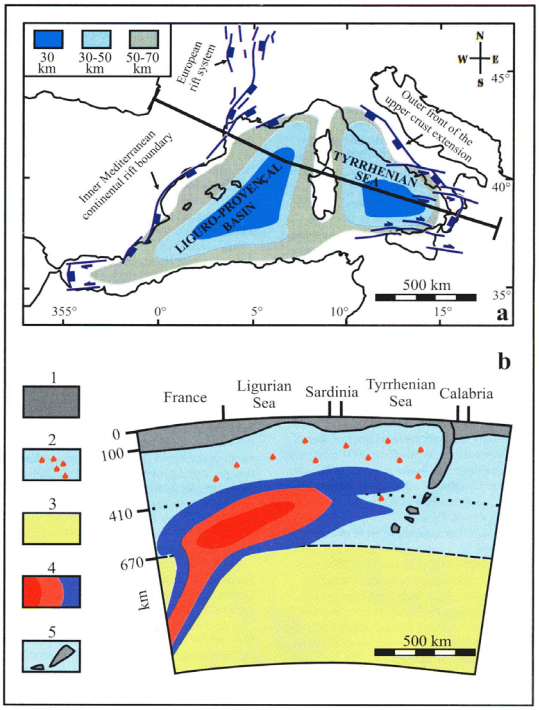

Bell et al., 2004

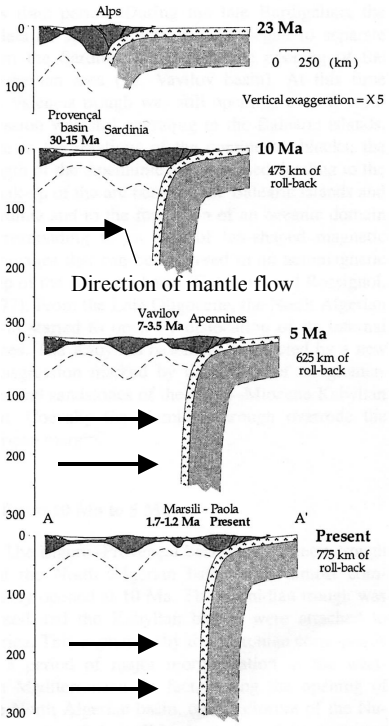

Gueguen et al., 1998

Upper plate:

Rotation due to slab retreat compression in Adriatic foredeep, in back arc basins no rotation, detachment faults

Lower plate:

Rotation due to differing rates of E-directed mantle flow;

Fig. 34. Opening of the Balearic ocean is causing Corsica-Sardinia rotation. Below the Apennines E –directed mantle flow is possibly responsible for the retreat of the Adriatic slab. This retreat is causing the opening of the Tyrrhenian Sea and the counterclockwise rotation of the Adriatic microplate.

At 3Ma crustal thinning in the Vavilov basin stopped and was transferred to the Marsilia basin (Mattei et al., 2004) most probably causing a dramatic decrease in rotation velocity. Recent GPS- measurements document only very small rotation rates. Consequently using these data, reconstructions of the kinematics at 5 to 3Ma cannot be successful. Calculations are resulting in shortening values that are far too small.

7.4. Mesozoic rotations

The Mesozoic kinematics that could be identified during this paleomagnetic study are mainly connected with the Late Cretaceous to Eocene closure of the Piemontais/Valais ocean.
Paleomagnetic data from Penninic nappes from previous studies (Pueyo et al., 2002; Hauck, 1998) are showing N-directed declinations from primary magnetizations, independently from the area where these data are derived along strike of the Penninic-Austro Alpine nappe contact. Data from Pueyo et al. (2002) were derived from a sampling campaign at the Mariazell meridian in the eastern Northern Calcareous Alps. Hauck (1998) reported results from Penninic nappes from the Schliersee area in the western Rhenodanubian Flysch zone. Restoring the younger Oligocene/Miocene rotational history enables to quantify the older, Eocene/Cretaceous portions of finite value of vertical axis rotations.

30° of Miocene counterclockwise rotation is restored first and rotated to geographic N. Consequently the Oligocene mean declination at 40° moves to 70°. The paleomagnetic data from the Penninic units are restored similarly. Consequently the N-directed remanence direction moves clockwise to 30°. In a second step the Oligocene mean declination is restored to geographic N by rotating 70° in a counterclockwise sense.

Restoring the paleomagnetic data from the Penninic units in the same way results in a pre-Oligocene orientation of the Penninic remanence directions of about 320°. This declination indicates 40° of counterclockwise rotation in pre-Oligocene times relative to the Late Cretaceous/Eocene European reference directions that are N/S aligned (Besse and Courtillot, 2002). Most probably this rotation is linked to the closure of the Penninic Ocean in post Mid-Eocene times (Frisch, 1979, Froitzheim et al., 1994; Froitzheim et al., 1997).

Prefolding magnetizations from Early Jurassic to Early Cretaceous sediments (this study, Tab.1 sites 42-45; sites 81-86), primary magnetizations from Early Cretaceous lithologies (this study, Tab.1 sites 46, 63) and Late Cretaceous sediments (this study, Tab.1 sites 57,60) from the western part of the Northern Calcareous Alps, and primary magnetizations from Late Cretaceous to Lower Eocene sediments of the Southern Alps (this study, Tab.1 sites 121,122,128, 132-134; Agnini et al., 2006) are characterized by NW directed declinations, indicating an additional post Early Eocene counterclockwise rotation compared with the data derived from Penninic units that show N-directed declinations.

According to data available from literature, this additional rotation is not known in the Bajuvaric units of the central and eastern Northern Calcareous Alps located E of the Inn valley (e.g. Pueyo et al., 2007; Pueyo et al., 2002). But this additional rotation was identified during this study in the Lechtal nappe and Inntal nappe and in the Southern Alps.

Primary magnetizations from Late Cretaceous sediments of "Neue Welt Gosau (Haubold et al., 1999) from the Tirolic parts of the eastern Northern Calcareous Alps south of SEMP (Salzach-Ennstal-Mariazell-Puchberg) line yielded also counterclockwise rotated declinations (Haubold et al., 1999). Similar results were derived by Agnoli et al. (1989) from Late Cretaceous sediments of the Central Austroalpine units at localities Kainach and Krappfeld located east of the Tauern window.

The well Vordersee 1 (Geutebrück et al., 1984), placed in the Osterhorn Tirolic unit/ Tieftirolikum (Frisch and Gawlick, 2003) southeast of the city of Salzburg was penetrating the Tirolic unit and reached Paleogene sediments on top of the underlying Bajuvaric unit. Therefore the thrusting of the Tirolic unit above the Bajuvaric unit has a Paleogene age. The boundary between Bajuvaric and Tirolic units most probably corresponds to the Brixlegg thrust (Ortner et al., 2006).

Based on the paleomagnetic data it is speculated that W of Inn valley also the Lechtal nappe, although part of the Bajuvaric unit, was incorporated into the hanging wall of the Brixlegg thrust (Ortner et al., 2006) as Lechtal nappe and Tirolic units show identical remanence directions. Along this thrust possibly Lechtal nappe, Inntal nappe, Tirolic units, Central and Southern Alps were rotating 30° counterclockwise relative to the Bajuvaric units E of Inn valley in post Early Eocene times. The Penninic Ocean would have been closed during a repeated period of counterclockwise rotation, jointly affecting Penninic and all Austroalpine nappes.

About Jurassic vertical axis rotations related to the opening of the Piemontais Ocean only a few interpretations are possible due to scarce primary magnetizations. In the frame of this study not a single Jurassic primary magnetization could be detected from sites located in the Northern Calcareous Alps. After restoring the Miocene to Eocene vertical axis rotations that affected parts of the Northern Calcareous Alps and the Southern Alps identically, primary Cretaceous to Jurassic magnetizations derived from the Southern Alps (this study Tab. 1 sites

121-124; 132-136) are showing approximately N-directed declinations. The African APWP nearly does not indicating any vertical axis rotation younger than Early Cretaceous (Besse and Courtillot, 2002). Counterclockwise rotation was active in Late Liassic (Toarcian) to Early Cretaceous (Berriasian) (Besse and Courtillot, 2002). Obviously during opening of the Central Atlantic and the counterclockwise rotation of Africa the Southern Alps did not undergo that rotation and were separated from southerly-ajacent stable Adria by a shear zone possibly acting in a sinistral manner (Thöny et al., 2005). It is assumed that northerly-ajacent Eastern Alps joined this inactivity concerning vertical axis rotations.

Marton (2006) was identifying a 20° counterclockwise rotation of stable (autochthonous) Adria in Late Miocene to Pliocene times relative to Africa. After restoring this component, declinations of Jurassic primary magnetizations still indicate 30° of counterclockwise rotation (Muttoni et al., 2001), which is related to the opening of the Central Atlantic Ocean.

Concluding, from the Jurassic and the opening of the Central Atlantic Ocean onwards Adria/Africa and the EA/SA were affected by differential rotational movements. In the Oligocene the EA/SA prolonged this individual geodynamic evolution with the clockwise rotations between 32-29Ma and between 25-23Ma, which cannot be found in stable Adria. Concerning the counterclockwise rotation at 5-3Ma, EA/SA and stable Adria joined, including parts of the Swiss and Western Alps.

8. Conclusion

During this study the method of paleomagnetism was identifying a surprisingly high number of individual vertical axis rotations affecting large-scale tectonic units during Jurassic to Pliocene geodynamics in the study area of the northwestern Tethyan realm. If interpretations based on these paleomagnetic data paid out to be correct, some parts of Alpine geodynamic evolution might be worth for reinterpretations, if they did not, some fundamental doubts about the reliability of the paleomagnetic method at all should be allowed.
The paleomagnetic data presented, constrain several phases of vertical axis rotations in Cenozoic (Fig.35) to Mesozoic times that are listed chronologically from recent to past.

1) A 30° counterclockwise rotation between Late Miocene to Pliocene (<5Ma) affected the Northern Alpine Foreland Basin, the Eastern Alps, the Southern Alps, the Southern Alpine Foreland Basin and the internal parts of the Western Alps, stable Adria and the W/N Carpathians. The rotation was carried out on the basal Alpine thrust and was driven by a counterclockwise rotation of the Adria during opening of the Tyrrhenian Sea.

2) A 30° clockwise rotation at 25-23Ma affected the Northern Alpine Foreland Basin, the Eastern Alps, the Southern Alps, the Southern Alpine Foreland Basin and the internal parts of the Western Alps. The rotation was carried out on the basal Alpine thrust and incorporated the Lepontine nappes/ Tauern imbricates. Folding of the Northern Alpine Foreland Basin started after clockwise rotation of 30°. The rotation was driven by the slab retreat of the lower European continental crust.

3) A 30-40° clockwise rotation of the EA/SA between earliest to Late Rupelian (32-29Ma) affected parts of the Helvetic nappes, the Penninic units, the Northern Calcareous Alps, the Central Alps and the Southern Alps. The basal thrust plain was located above the crystalline core complexes (Lepontine nappes/ Tauern) and acted in an out of sequence manner. The Rotation was driven by slab retreat of the lower European continental crust.

4) A 30° counterclockwise rotation of Penninic nappes and EA/SA is related to final closure of the Penninic Ocean and continent/continent collision in post Middle Eocene to Early Oligocene times.

5) A 30° counterclockwise rotation was active in Paleogene times before final closure and continent/continent collision of the Penninic Ocean that started in post Middle Eocene. The rotation is linked to the thrusting of Tirolic above Bajuvaric units.

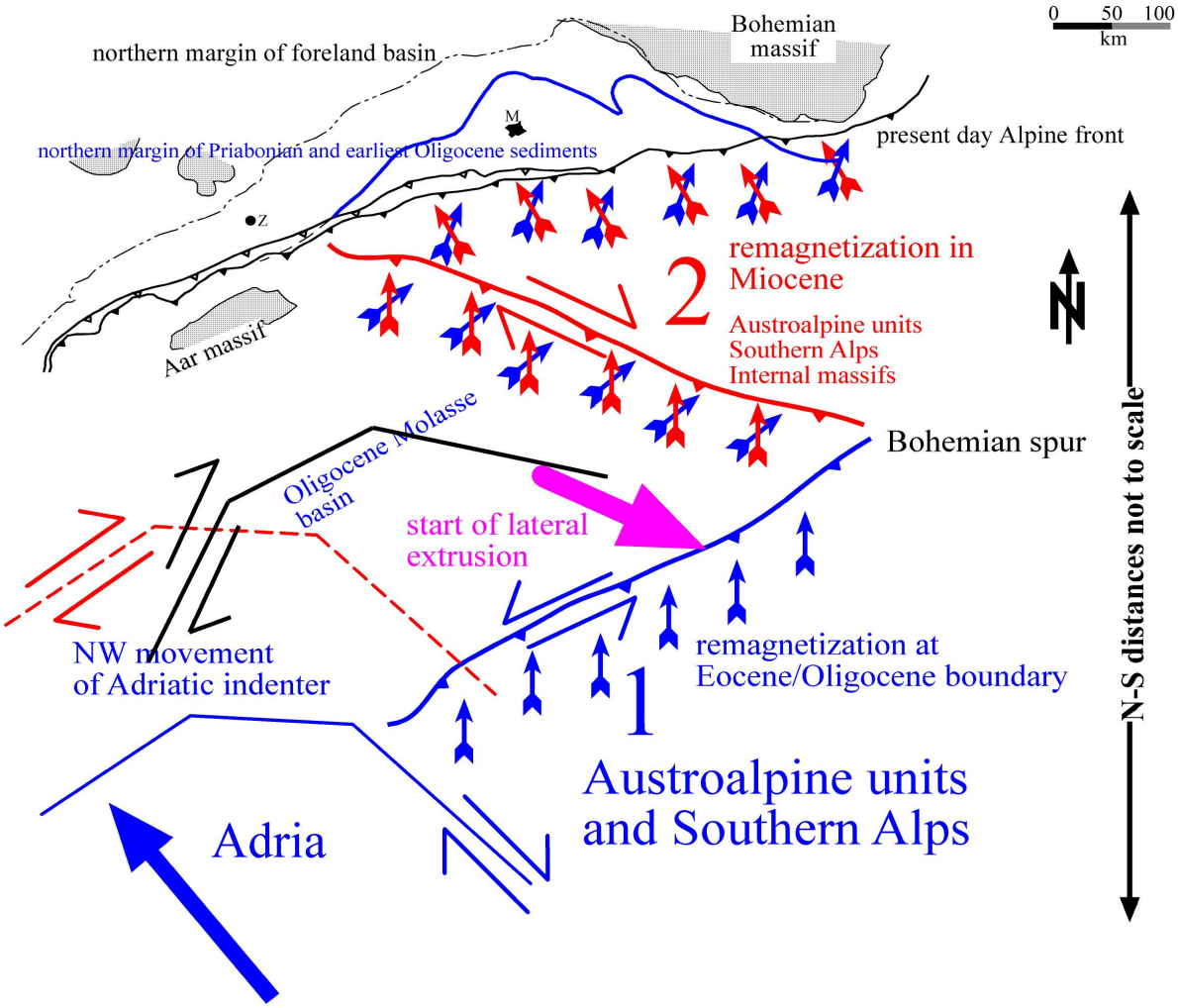

Fig. 35. Summary of Oligocene to Miocene Geodynamics derived from paleomagnetic data.
Blue, red and black colors represent the paleogeographic position of Adria and Eastern/ Southern Alps with the northern frontal Alpine thrust in times prior to clockwise rotation (blue), prior to counterclockwise rotation (red) and in present times (black). Pink arrow indicates time and orientation of the onset of lateral extrusion. Numbers 1,2 mark prominent remagnetization and rotation events. **1**: Two clockwise rotations (60°-70° in total) in Oligocene times. **2**: 30° of counterclockwise rotation in Late Miocene to Pliocene times.

Rotations mentioned above took place during Alpine nappe stacking. In all cases, the allochthonous units of the Alpine nappe stack rotated during translation on the basal thrust. Movement of the nappes was therefore by no means dip-slip. Balancing cross section is usually based on dip slip restorations, not including shortening caused by vertical axis rotations. Consequently the shortening distances might be calculated far to less. Future models of nappe stacking in the Eastern Alps should account for the rotational component of thrusting, which would result in changing thrust distances along the strike of nappe boundaries.

Concerning Mesozoic paleogeography the most important result of this study is related to the paleogeographic position of the Southern Alps on the Neo-Tethys continental rim. Paleomagnetic data do not indicate any differences in Jurassic to Pliocene geodynamics between Eastern and Southern Alps. Consequently the dextral shear zone that might have separated the Austroalpine realm from the "African promontory" has to be placed to the south of the Southern Alps and the northeasterly adjacent Northern Calcareous Alps. The Southern Alps were definitely placed on the northern shore of Neo-Tethys Ocean. Today the prominent fault that was separating the Austroalpine units from the African promontory is probably hidden below the Po plain.

9. Appendix

9.1. References

Abdul Aziz, H., Böhme, M., Rocholl, A., Zwing, A., Prieto, J., Wijbrans, J.R., Heissig K., Bachtadse, V., (in press). Integrated stratigraphy and $^{40}Ar/^{39}Ar$ chronology of the Early to Middle Upper Freshwater Molasse in eastern Bavaria (Germany). Int. J. Earth Sci. (Geol. Rundsch.), DOI 10.1007/s00531-006-0166-7.

Agnini, C., Muttoni, G., Kent, D. V., Rio, D., 2006. Eocene biostratigraphy and magnetic stratigraphy from Possagno, Italy: The calcareous nannofossil response to climate variability. EPSL, 241, 815-830.

Agnoli, F., Reisinger, J., Mauritsch, H. J., 1989. Paläomagnetische Ergebnisse aus zwei ostalpinen Gosau-Vorkommen (Oberkreide). N. Jb. Geol. Paläont. Mh., H.5, 265-281.

Allerton, S., 1998. Geometry and kinematics of vertical-axis rotations in fold and thrust belts. Tectonophysics, 199, 15-30.

Anderson, H., Jackson, J., 1987. Active tectonics of the Adriatic region. Geophys. J. R. astr. Soc., 91, 937-983.

Angenheister, G., 1956. Über die Magnetisierung der Basalte des Vogelsberges. Nachrichten der Akademie der Wissenschaften in Göttingen Math. Nat., 1956, 187-204.

Aubourg, C., Chabert-Pelline, C., 1999. Neogene remagnetization of normal polarity in the Late Jurassic black shales from the Subalpine chains (French Alps): Evidence for late anticlockwise rotations. Tectonophysics, 308, 473-486.

Auer, M. and Eisbacher, G. H., 2003. Deep structure and kinematics of the Northern Calcareous Alps (TRANSALP profile). Int. J. Earth Sci., 92: 210-227.

Badertscher, N. P., Burkhard, M. 2000. Brittle-ductile deformation in the Glarus thrust Lochseiten (LK) calc-mylonite. Terra nova, 12, 281-288.

Bell, K., Castorina, F., Lavecchia, G., Rosatelli, G., Stoppa, F., 2004. Is There a Mantle Plume Below Italy?, Eos Trans. AGU, 85(50), 541, 10.1029/2004EO500002.

Berge, T. B., Veal, S. L. 2005. Structure of the Alpine foreland. Tectonics, 24, TC5011, doi:10.1029/2003TC001588.

Bernoulli, D., Caron, C., Homewood, P., KaÈlin, O., van Stuijvenberg, J., 1979. Evolution of continental margin in the Alps. Schweiz. Min. Petr. Mitt 59, 165-170.

Bertotti, G., Picotti, V., Bernoulli, D., Castellarin, A., 1993. From rifting to drifting: tectonic evolution of the South-Alpine upper crust from the Triassic to the Early Cretaceous. Sedimentary Geology 86, 53-76.

Bosellini, A., 1973. Modello geodinamico e paleotettonico delle Alpi Meridionali durante il Giurassico-Cretacico. Sue possibili applicazioni agli Appennini. Accordi B. (Ed.), Moderne vedute sulla geologia dell'Appennino. Acc. Naz. Lincei, Quadezno N 183, pp. 163-205.

Besse, J., Courtillot, V., 2002. Apparent and true polar wander and the geometry of the geomagnetic field over the last 200 Myr. J. Geophys. Res. 107(B11), 6-1 - 6-31.

Bingham, C. 1964. Distributions on a sphere and the projective plane. PhD. Thesis. Yale University. 93 pp; New Haven.

Blanckenburg, F. V., Villa, I. M., Baur, H., Morteani, G., Steiger, R.H., 1989. Time calibration of a PT-path from the Western Tauern Window, Eastern Alps: the problem of closure temperatures: Contributions to Mineralogy and Petrology, 101, 1-11.

Blanckenburg, F., Davies, J., 1995. Slab breakoff: A model for syncollisional magmatism and tectonics in the Alps. Tectonics, 14, 120-131.

Bigi, G., Cosentino, D., Parotto, M., Sartori, R., Scandone, P., 1990. C.N.R.—Structural Model of Italy. Scale 1:500.000. Sheets I–II, Selca Publisher, Firenze.

Bois, C., 1993. Initiation and evolution of the Oligo-Miocene rift basins of southwestern Europe: contribution of deep seismic reflection profiling. Tectonophysics 226, 227-252.

Bormioli, D., Lanza, R., 1995. Rotazioni antiorarie nelle rocce terziarie delle Alpi Occidentali e dell'Apennino Settentrionale. In: Polino, R., Sacchi, R. (Eds.), Rapporti Alpi-Appenninio, Scr. e Doc. XIV. , Roma , pp. 277-289.

Burgschwaiger, E., Mauritsch, H. J., Bierbaumer, M., Scholger, R., 1996. Miocene overprint in the Paleozoic of Graz, Eastern Alps, Austria. Geologica Carpathica 47, 5-12.

Butler, R. F., 1992. Paleomagnetism: Magnetic Domains to Geologic Terranes. Blackwell, Boston. 319 pp.

Casati, P., Tomai, M., 1969. Il Giurassico ed il Cretacico del versante settentrionale del Vallone Bellunese e del gruppo del M. Brandol.- Riv. Ital. Paleontol. Stratigr., 75, 205-340, Milano.

Castellarin, A., Cantelli, L., 2000. Neo-Alpine evolution of the Southern Eastern Alps. J. Geodyn. 30, 251– 274.

Castellarin, A., Nicolich, R., Fantoni, R., Cantelli, L., Sella, M., Selli, L., 2006. Structure of the lithosphere beneath the Eastern Alps (southern sector of the TRANSALP transect). Tectonophysics 414, 259–282.

Channell, J. E. T., Grandesso, P., 1987. A revised correlation of Mesozoic polarity chrons and calpionellid zones.- EPSL, 85, 222-240, Amsterdam.

Channell, J. E. T., Brandner, R., Spieler, A., Smathers, N. P., 1990. Mesozoic paleogeography of the Northern Calcareous Alps-Evidence from paleomagnetism and facies analysis. Geology, 18, 828-831.

Channell, J. E. T., Brandner, R., Spieler, A., Stoner, J. S., 1992. Paleomagnetism and paleogeography of the Northern Calcareous Alps (Austria). Tectonics, 11, 792-810.

Channell, J. E. T., Doglioni, C., 1994. Early Triassic paleomagnetic data from the Dolomites (Italy). Tectonics, 13, 157-166.

Collinson, D. W., 1983. Methods in rock magnetism. Techniques and instrumentation. Chapman and Hall, London, 503pp.

Collombet, M., Thomas, J. C., Chauvin, A., Tricart, P., Bouillin, J. P., Gratier, J. P., 2002. Counterclockwise rotation of the western Alps since the Oligocene, New insights from paleomagnetic data. Tectonics 21, 14-1 - 14-15.

Coward, M., Dietrich, D., 1995. Alpine tectonics Ð An overview. In: Alpine tectonics, vol.45. Geological Society Special Publication, London, pp. 21±29.

Crouzet, C., Ménard, G., Rochette, P., 1996. Post-Middle Miocene rotations recorded in the Bourg d'Oisans area (Western Alps, France) by paleomagnetism. Tectonophysics 263, 137-148.

Dal Piaz, G. V., Del Moro, A., Martin, S., Venturelli, S., 1988. Post-Collisional Magmatism in the Ortler-Cevedale Massiv, Northern Italy. Jahrb. Geol. Bundesanst. 131, 533-551.

Dal Piaz, G., 1995. Plate tectonics and Mountain Building: the Alps. Historical Review and personal comments.Plate tectonics: the First twenty-®ve years. In: Proceedings of the Eighth Summer School, Siena, 171±251.

Dal Piaz, G.V., 1999. The Austroalpine–Piedmont nappe stack and the puzzle of Alpine Tethys. Mem. Sci. Geol., Padova 51 (1), 155– 176.

Di Napoli Alliata, E., Proto Decima, F., Pellegrini, C. B., 1970. Studio geologico, stratigraphico e micropaleontologico dei dintorni di Belluno.- Mem. Geol. Soc. It., 9, 1-28, Roma.

Doglioni, C., 1987. Tectonics of the Dolomites (Southern Alps Northern Italy). J. Struct. Geol 9, 181±193.

Doglioni, C., Agostini, S., Crespi, M., Innocenti, F., Manetti, P., Riguzzi, F., Savascin, Y., 2002. On the extension in western Anatolia and the Aegean sea. India-Asia convergence in NW Himalaya. In: Rosenbaum, G. and Lister, G. S., Reconstruction of the evolution of the Alpine-Himalayan Orogen. Journal of the Virtual Explorer 8, 169-183.

Dunlop, D. J., Özdemir, Ö., 1997. Rock Magnetism: Fundamentals and Frontiers. Cambridge Univ. Press, Cambridge. 573 pp.

Eisbacher, G. H., Linzer, G. H., Meier, L., 1990. A Depth extrapolated Structural Transect Across the Northern Calcareous Alps of Western Tirol. Ecl. Geol. Helv., 83/3: 711 - 725.

Eisbacher, G. H., Brandner, R., 1995. Role of high angle faults during heteroaxial contraction, Inntal thrust sheet, Northern Calcareous Alps, Western Austria. Geol. Paläont. Mitt. Innsbruck, 20, 389-406.

Eisbacher, G. H., Brandner, R., 1996. Superposed fold-thrust structures and high-angle faults, Northwestern Calcareous Alps, Austria; Eclogae geol. Helv., 89, 553-571.

England, P. C., Houseman, G., 1989. Extension during continental convergence, with application to the Tibetan plateau. J. Geophys. Res., 94, 17561-17579.

Faupl, P., Tollmann, A., 1979. Die Roßfeldschichten, Ein Beispiel für Sedimentation im Bereich einer tektonisch aktiven Tiefseerinne aus der kalkalpinen Unterkreide. Geol. Rdsch. 68 (1), 93-120.

Facenna, C., Piromallo, C., Crespo-Blanc, A., Jolivet, L., Rossetti, F., 2004. Lateral slab deformation and the origin of the western Mediterranean arcs. Tectonics, 23, TC1012, doi: 10.1029/2002TC001488.

Felber, P., Wyssling, G., 1979. Zur Stratigraphie und Tektonik des Südhelvetikums im Bregenzerwald (Vorarlberg). Ecl. Geol. Helv., 72: 673-714.

Fisher, R., 1953. Dispersion on a sphere. Proc. R. Soc. London, Ser. A 217, 295-305.

Freudenberger, W., Schwerd, K., 1996. Erläuterungen zur geologischen Karte von Bayern 1:500 000.- 329 p., 67 Abb., 21 Tab., 8 Taf., München

Frisch, W., 1981. Plate motions in the Alpine region and their correlation to the opening of the Atlantic ocean. Geol. Rundsch. 70: 402-411.

Frisch, W., Gawlick, H. J., 2003. The nappe structure of the central Northern Calcareous Alps and its disintegration during Miocene tectonic extrusion- a contribution to understanding the orogenic evolution of the Eastern Alps. Int. J. Earth Sci. (Geol. Rundsch.), 92, 712-727.

Froitzheim, N., Schmid, S. M., Conti, P., 1994. Repeated change from crustal shortening to orogen-parallel extension in the Austroalpine units of Graubünden. Eclogae geol. Helv. 87, 559-612.

Froitzheim, N., Schmid, S. M., Frey, M., 1996. Mesozoic paleogeography and the timing of eclogite-facies metamorphism in the Alps, A working hypothesis.- Eclogae Geologicae Helvetiae 89/1, 81-110.

Froitzheim, N., Conti, P., van Daalen, M., 1997. Late cretaceous, synorogenic, low-angle normal faulting along the Schlinig fault (Switzerland, Italy, Austria) and its significance for the tectonics of the Eastern Alps. Tectonophysics, 280, 267-293.

Fuchs, W., 1976. Gedanken zur Tektogenese der nördlichen Molasse zwischen Rhone und March. Jahrb. Geol. Bundesanst. 119, 207-249.

Fügenschuh, B., Seward, D., Mancktelow, N., 1997. Exhumation in a convergent orogen: the Tauern window. Terra nova, 9, 213-217.

Ganss, O., Schmidt - Thomé, P., 1953. Die gefaltete Molasse am Alpenrand zwischen Bodensee und Salzach.- Zeitschrift der Deutschen Geologischen Gesellschaft, 105, 402-495, Hannover.

Gattacceca, J., Speranza, F., 2002. Paleomagnetism of Jurassic to Miocene sediments from the Apenninic carbonate platform (southern Apennines, Italy): evidence for a 60° counterclockwise Miocene rotation. EPSL 201, 19-34.

Gawlick, H. J., Frisch, W., Hoxha, L., Dumitrica, P., Krystyn, L., Lein, R., Missoni, S., Schlagintweit, F., 2007. Mirdita Zone ophiolites and associated sediments in Albania reveal Neotethys Ocean origin. Int. J. Earth Sci. (Geol. Rundsch.). DOI 10.1007/s00531_007-0193-z

Geyer, O. F., 1993. Die Südalpen zwischen Gardasee und Friaul.- Sammlung geologischer Führer, 86, 576 p., 175 Abb., 4 Tab., Stuttgart (Bornträger).

Grandesso, P., Stefano, C., 1990. Volcanic contributions to sedimentation in Upper Burdigalian - Lower Langhian sediments of the Venetian Molassic basin.- Riv. It. Paleont. Strat., 96, 337-350, Milano.

Graßl, H., Neubauer, F., Millahn, K., Weber, F., 2003. Seismic image of the deep crust at the eastern margin of the Alps (Austria): indications for crustal extension in a convergent orogen. Tectonophysics, 380, 105-122.

Grottenthaler, W., 1966. Erläuterungen zum Blatt Nr. 8036 Otterfing und Blatt Nr.8136 Holzkirchen. Geologische Karte von Bayern 1:25000, München.

Gruber, A., 1997. Stratigraphische und strukturelle Analyse im Raum Eiberg (Nördliche Kalkalpen, Unterinntal, Tirol) unter besonderer Berücksichtigung der Entwicklung in der Oberkreide und im Tertiär. GPM Innsbruck, 22, 159-197.

Gueguen, E., Doglioni, C., Fernandez, M., 1998. On the post-25 Ma geodynamic evolution of the western Mediterranean. Tectonophysics, 298, 259-269.

Hagn, H., 1982. Neue Beobachtungen in der Unterkreide der Nördlichen Kalkalpen (Thierseer Mulde etc.). Mitt. Bayer. Staatslg. Paläont. Hist. Geol., 22, 117-135.

Hargraves, R. B., Fischer A. G., 1959. Remanent Magnetism in Jurassic Red Limestones and Radiolarites from the Alps. Geophys. J., 2, 34-41.

Haubold, H., Scholger, R., Frisch, W., Summesberger, H., Mauritsch H.J., 1999. Reconstruction of the Geodynamic Evolution of the Northern Calcareous Alps by Means of Paleomagnetism. Phys. Chem. Earth. (A), 24, 697-703.

Hauck, J., 1998. Paläomagnetische Untersuchungen an ausgewählten Profilen der Kreide in der Rhenodanubischen Flysch-Zone. Unpubl. PhD - Thesis, München.

Heller, F., 1980. Paleomagnetic Evidence for the Late Alpine Rotation of the Lepontine Area. Ecl. Geol. Helv., 73, 607-618.

Hinsch, R., Decker, K., Peresson, H., 2005. 3-D seismic interpretation and structural modelling in the Vienna Basin: implications for Miocene to recent kinematics. Austr. J. Earth Sci., 97, 38-50.

Hong Kie, T., 1988. Magnetotectonics in the Piemont Tertiary basin. Phys. Earth Planet Int., 52, 308-319.

Horrelt, R., 1987. Teil I: Paläontologische und mikrofazielle Untersuchungen des Jura und der Kreide im Bereich der Alpe Ra Stua (Südtiroler Dolomiten, Italien); Teil II Geologische Kartierung der weiteren Umgebung der Alpe Ra Stua.- Unveröff. Dipl.-Arb. Univ. Erlangen, 108 p., 26 Abb., 3 Tab., 13 Taf., Erlangen

Hunziker, J. C., Frey, M., Clauer, N., Dallmeyer, R.D., Friedrichsen, H., Flehming, W., Hochstrasser, K., Roggwiller, P., Schwandner, H., 1986. The evolution of illite to muscovite; mineralogical and isotopic data from the Glarus Alps, Switzerland. Contr. Miner. Petrol., 92, 157-180.

Jaksch, K., 1996. Aptychen aus den Thitonprofilen von Achenkirch und Schwendt (Tirol) mit Einbeziehung von Vergleichsexemplaren von den Ionischen Inseln.- Jahrb. Geol. Bundesanst., 139, 453 - 466, 2 Abb., 2 Taf., Wien.

Janák, M., Froitzheim, N., Lupták, B., Vrabec, M., Ravna, E. J. K., 2004. First evidence for ultrahigh-pressure metamorphism of eclogites in Pohorje, Slovenia: Tracing deep continental subduction in the Eastern Alps.- Tectonics, 23, TC5014, Washington, D.C..

Jung, W., Schleich, H., Kästle, B., 1978. Eine neue stratigraphisch gesicherte Fundstelle für Angiospermen - Früchte und Samen in der oberen Gosau Tirols.- Mitt. Bayer. Staatslg. Paläont. Hist. Geol., 18, 131-142.

Kappler, P., Zeeh, S., 2000. Relationship between fluid flow and faulting in the Alpine realm (Austria, Germany, Italy). Sedimentary Geology, 131, 147-162.

Kempf, O., Schlunegger, F., Strunck, P., Matter, A., 1998. Paleomagnetic evidence for Late Miocene rotation of the Swiss Alps: Results from the north Alpine foreland basin. Terra Nova, 10: 6-10.

Kempf, O., Matter, A., Burbank, D. W., Mange, M., 1999a. Depositional and structural evolution of a foreland basin margin in a magnetostratigraphic framework, the eastern Swiss Molasse Basin. Int. J. Earth Sci. (Geol. Rundsch.), 88, 253-275.

Kempf, O., Matter, A., 1999b. Magnetostratigraphy and depositional history of the Upper Freshwater Molasse (OSM) of Eastern Switzerland. Eclogae Geologicae Helvetiae, 92: 97-103.

Kempf, O., Pross, J., 2005. The lower marine to lower freshwater Molasse transition in the northern Alpine foreland basin (Oligocene; central Switzerland-south Germany): age and geodynamic implications. Int. J. Earth Sci. (Geol. Rundsch.), 94, 160-171.

Kipfer, R., Heller, F., 1988. Paleomagnetism of Permian red beds in the contact aureole of the Tertiary Adamello intrusions (northern Italy). Phys. Earth Planet Int., 52, 365-375.

Kirschvink, J. L, 1980. The least squares line and plane and the analysis of paleomagnetic data. Geophys. J. R. Astron. Soc., 62, 699-718.

Kissling, E., 2007. Towards a plate tectonic model of Alpine orogeny. 8th workshop on Alpine geological studies. Davos, Abstracts. p32.

Kligfield, R., Lowrie, W., Hirt, A. M., Siddans, A. W. B., 1983. Effect of progressive deformation on remanent magnetization of Permian redbeds from the Alpes Maritimes (France). Tectonophysics, 97, 59– 85.

Krois, P., Stingl., V., Purtscheller, F., 1990. Metamorphosed weathering horizon from the Oetztal-Stubai crystalline complex (Eastern Alps, Austria). Geology, 18, 1095-1098.

Kruiver, P. P., Dekkers, M. J., Heslop, D., 2001. Quantification of magnetic coercivity components by the analysis of acquisition curves of isothermal remanent magnetisation. EPSL 189, 269-276.

Kuhlemann, J., Kempf, O., 2002. Post-Eocene evolution of the North Alpine Foreland Basin and its response to Alpine tectonics. Sedimentary Geology 152, 45-78.

Lammerer, B., 1986. Das Autochthon im westlichen Tauernfenster. Jahrb. Geol. Bundesanst. 129, 51-67.

Lammerer, B., Weger, M., 1998. Footwall uplift in an orogenic wedge, the Tauern Window in the Eastern Alps of Europe. Tectonophysics, 285, 213-230.

Lanza, R., 1977. Paleomagnetic data from the andesitic and lamprophyric dikes of the Sesia-Lanzo zone (Western Alps). Schweiz. Mineral. Petrograph. Mitt., 57, 281-290.

Lanza, R., 1978. Paleomagnetic data on the andesitic cover of the Sesia-Lanzo (Western Alps). Geol. Rundsch., 68, 83-92.

Laubscher, H. P., 1988. Decollement in the Alpine System: An Overview.- Geologische Rundschau, 77/1, 1 - 9, Stuttgart.

Linzer, H. G., Ratschbacher, L., Frisch, W., 1995. Transpressional collision structures in the upper crust, the fold thrust belt of the Northern Calcareous Alps. Tectonophysics, 242, 41-61.

Lippitsch, R., Kissling, E., Ansorge, J., 2003. Upper mantle structure beneath the Alpine orogen from high-resolution teleseismic tomography. J.Geophys. Res., 108(B8), 2376, doi: 10.1029/2002JB002016.

Lowrie, W., 1990. Identification of ferromagnetic minerals by coercivity and unblocking temperatures properties. Geophys. Res. Lett., 17, 159-162.

Luciani, V., 1989. Stratigrafia sequenziale del Terziario nella catena del Monte Baldo.- Memorie di Scienze Geologiche, 41, 263 - 351, 43 Abb., 1 Tab., 5 Taf., Padova.

Maher, B. A., Thompson, R., (Eds.), 1999. Quaternary Climates, Environments, and Magnetism. Cambridge University Press, Cambridge, UK.

Mair, V., Purtscheller, F., 1995. A study on a dyke swarm related to the Königsspitze (Gran Zebru) pluton, Ortler-Campo-crystalline (Venosta Valley, W South Tyrol), Implications on magma evolution and alteration processes. GPM Innsbruck, 20, 67-86.

Marton, E., Veljovic, D., 1983. Paleomagnetism of the Istria peninsula, Yugoslavia. Tectonophysics 91, 73-87.

Márton, E., Nardi, G., 1994. Cretaceous paleomagnetic data from Murge (Apulia, Southern Italy), tectonic implications. Geophys. J. Int., 119, 842-856.

Márton, E., Kuhlemann, J., Frisch, W., Dunkl, I., 2000. Miocene rotations in the Eastern Alps —palaeomagnetic results from intramontane basin sediments. Tectonophysics, 323, 163-182.

Marton, E., Fodor, L., Jelen, B., Marton, P., Rifelj, H., Kevric, R., 2002a. Miocene to Quaternary deformation in NE Slovenia, complex paleomagnetic and structural study.-Journal of Geodynamics 34, 627-651.

Marton, E., Pavelic, D., Tomljenovic, B., Avanic, R., Pamic, J., Marton., P., 2002b. In the wake of a counterclockwise rotating Adriatic microplate, Neogen paleomagnetic results from northern Croatia.-Int. J. Earth Sciences 91, 514-523.

Márton, E., Scholger, R., Mauritsch, H. J., Tokarski, A. K., Thöny, W., Krejci, O., 2003a. Counterclockwise rotated Miocene Molasse at the southern margin of stable Europe indicated by paleomagnetic data. In: Csontos, L. (Eds.), 6th Workshop of Alpine Geological Studies, Sopron, Abstracts. Ann. Univ. Sci. Budapest., Sect. Geol., 35, 96-97.

Márton, E., Drobne, K., Cosovic, V., Moro, A., 2003b. Paleomagnetic evidence for Tertiary counterclockwise rotation of Adria. Tectonophysics, 377, 143– 156.

Márton, E., Fodor, L., 2003c. Tertiary paleomagnetic results and structural analysis from the Transdanubian Range (Hungary): rotational disintegration of the Alcapa unit. Tectonophysics, 363, 201-224.

Marton, E., 2006a. Paleomagnetic evidence for Tertiary counterclockwise rotation of Adria with respect to Africa. In: N. Pinter et al. (Eds.), The Adria Microplate: GPS Geodesy, Tectonics and Hazards. Springer, pp 71-80.

Marton, E., Krejci, O., Tokarski, A., K., Bubik, M., 2006b. Do we have a satisfactory Late Cretaceous –Tertiary stable European reference framework? In: 10th "Castle Meeting" new trends in Geomagnetism, Paleo, Rock and Environmental Magnetism, Abstracts. Travaux Geophysiques XXVIII (2006), p76.

Márton, E., 2007. Carpatho-Pannonian region: Paleomagnetic indicators for important tectonic movements during the last 20Ma. 8th workshop on Alpine geological studies. Davos, Abstracts, pp 42-43.

Massari, F., Grandesso, P., Stefani, C., Zanferrari, A., 1986. The Oligo-Miocene Molasse of the Veneto - Friuli region, Southern Alps.- Giornale die Geologia, 48, 235-255, Bologna.

Massari, F., Mellere, D., Doglioni, C., 1993. Cyclicity in non-marine foreland-basin sedimentary fill: the Messinian conglomerate-bearing succession of the Venetian Alps (Italy).- In: Marzo, M., Puigdefabregas, C. (Eds..): Alluvial Sedimentation, Spec. Publ. Int. Ass. Sediment. Nr. 17, 501-520, Oxford (Blackwell).

Mattei, M., D`Agostino, N., Facenna, C., Piromallo, C., Rosetti, F., 2004. Some remarks on the geodynamics of the Italian region. Per. Mineral., 73, 7-27.

Mauritsch, H. J., Becke, M., 1987. Paleomagnetic investigationsin the eastern Alps and the Southern Border Zone. In: Flügel, H. W., Faupl, P. (Eds.), Geodynamics of the Eastern Alps. Deuticke, Vienna, pp. 283-308.

McElhinny, M. W., 1964. Statistical significance of the fold test in paleomagnetism. Geophys. J. R. Astron. Soc. 8, 338 – 340.

McElhinny, M. W., McFadden, P. L., 2000. Paleomagnetism: Continents and Oceans. Academic press, International Geophysics Series 73, 386 pp.

Muheim, F., 1934. Die subalpine Molasse im östlichen Vorarlberg. Ecl. Geol. Helv., 27: 181-296.

Muttoni, G., Lanci, L., Argnani, A., Hirt, A. M., Cibin, U., Abrahamsen, N., Lowrie, W., 2001. Paleomagnetic evidence for a Neogene two-phase counterclockwise tectonic rotation in the northern Apennines (Italy). EPSL 192, 159-174.

Neubauer, F., 1994. Kontinentkollision in den Ostalpen. Geowissenschaften 12, 136-140.

Nairn, A. E. M., 1960. Paleomagnetic results from Europe. J. Geology, 68, 285-306.

Nairn, A. E. M., 1962. Paleomagnetic investigations of Tertiary and Quaternary igneous rocks. 1.Preliminary collections in the Eifel, Siebengebirge and Westerwald. Notizbl. Hess. L.-Amt Bodenforschung., 90, 412-424, Wiesbaden.

Najman, Y. M. R., Enkin, R.J., Johnson, M.R.W., Robertson, A. H. F., Baker, J., 1994. Palaeomagnetic dating of the earliest continental Himalayan foredeep sediments: implications for Himalayan evolution. Earth Planet. Sci. Lett. 128, 713– 718.

Noquet, J. M., Calais, E., 2003. Crustal velocity field of western Europe from permanent GPS array solutions. Geophys. J. Int. 154, 72-88.

O'Reilly, W., 1984. Rock and Mineral Magnetism. Blackie, Glasgow. 220 pp.

Ortner, H., 2001. Growing folds and sedimentation of the Gosau Group, Muttekopf, Northern Calcareous Alps, Austria. Int. J. Earth Sci. (Geol. Rundsch.) 90, 727-739.

Ortner, H., Stingl, V., 2001. Facies and basin development of the Oligocene in the Lower Inn Valley, Tyrol/Bavaria. In: Piller, W., Rasser, M. (Eds.), Paleogene in Austria. Schriftenreihe der Erdwissenschaftlichen Kommissionen 14, 153-196.

Ortner, H., Reiter, F., Acs, P., 2002. Easy handling of tectonic data, the programs TectonicVB for Mac and TectonicsFP for Windows. Computers and Geosciences 28, 1193-1200.

Ortner, H., 2003. Cementation and Tectonics in the Inneralpine Molasse of the Lower Inn Valley. GPM Innsbruck, 26, 71-89.

Ortner, H., Reiter, F., Brandner, R., 2006. Kinematics of the Inntal shear zone–sub-Tauern ramp fault system and the interpretation of the TRANSALP seismic section, Eastern Alps, Austria. Tectonophysics, 414, 241-258.

Piper, J. D. A., 1987. Palaeomagnetism and the Continental Crust. Open Univ. Press, Milton Keynes. 434 pp.

Pfiffner, O. A., 1977. Tektonische Untersuchungen im Infrahelvetikum der Ostschweiz. Translated title: Tectonic studies of the Infrahelvetic Complex, eastern Switzerland. Techn Hochsch. Geol. Inst. Mitt., 217, 164.

Pfiffner, O. A., Erard, P. F., Stäuble, M., 1997. Two cross sections through the Swiss Molasse basin (line E4-E6, W1, W7-W10). In: Pfiffner, O. A., Lehner, P., Heitzmann, P., Mueller, S. and Steck, A. (Editors), Results of NRP20. Birkhäuser, Basel ,pp. 64-72.

Pflaumann, U., Stephan, W., 1968. Erläuterungen zum Blatt Nr. 8237 Miesbach. Geologische Karte von Bayern 1:25000, München.

Peacock, D. C. P., Anderson, M. W., Morris, A., Randall, D. E., 1998. Evidence for the importance of "small" faults on block rotation. Tectonophysics 299, 1-13.

Pohl, J., Soffel, H., 1977. Paleomagnetic and rock magnetic investigation of Tertiary volcanics in Northern Bavaria. J. Geophys., 42, 459-474.

Pueyo, E. L., Mauritsch, H. J., Gawlick, H. J., Scholger, R., Frisch, W., 2002. Block, thrust and escape-related rotations in the Central Northern Calcareous Alps. In: Institut Für Geologie Und Paläontologie, Univ. Salzburg (Editors), Kurzfassungen, PANGEO Austria. , Salzburg, p.138.

Pueyo, E. L., Schneider, M., Mauritsch, H. J., Scholger, R., Lein, R., 2002. A paleomagnetic cross section through the Eastern Northern Calcareous Alps: preliminary data in the Mariazell meridian. In: Institut Für Geologie Und Paläontologie, Univ. Salzburg (Editors), Kurzfassungen, PANGEO Austria. , Salzburg, p.138-139.

Pueyo, E. L., Mauritsch, H. J., Gawlick, H. J., Scholger, R., Frisch, W., 2007. New evidence for block and thrust sheet rotations in the central northern Calcareous Alps deduced from two pervasive remagnetization events. Tectonics, 26, TC5011, doi:10.1029/2006TC001965.

Ratschbacher, L., Frisch, W., Linzer, G., Merle, O., 1991. Lateral extrusion in the Eastern Alps, Part 2, Structural analysis. Tectonics, 10, 257-271.

Risch, H., 1985. Gosau.- In: Wolff, H. (Eds..), Erläuterungen zum Blatt Bayrischzell, Geologische Karte von Bayern 1:25 000. München, 94-99.

Rosenberg, C. L., 2004. Shear zones and magma ascent: A model based on a review of the Tertiary magmatism in the Alps. Tectonics, 23, TC3002, doi:10.1029/2003TC001526.

Rosenberg, C. L., Heller, F., 1997. Tilting of the Bergell pluton and Lepontine area, combined evidence from paleomagnetic, structural and petrological data. Ecl. Geol. Helv. 90, 345-356.

Roure, F., Heitzmann, P., Polino, R., 1990a. Deep structure of the Alps. Vol. Spec. Soc. Geol. It. 1, 1±367.

Sanders, D., 1998. Tectonically controlled Late Cretaceous terrestrial to neritic deposition (Northern Calcareous Alps, Tyrol, Austria). Facies 39, 139-178.

Selverstone, J., Axen, G., Bartley, J., 1995. Kinematic tests of dynamic models for footwall unroofing during extension in the Eastern Alps. Basel, 2nd workshop on Alpine Geological studies, Abstracts, p. 56-58.

Schätz, M., Tait, J., Bachtadse, V., Heinisch, H., Soffel, H., 2002. Palaeozoic geography of the Alpine realm, new palaeomagnetic data from the Northern Greywacke Zone, Eastern Alps. Int. J. Earth Sci. (Geol. Rundsch.), 91, 979-992.

Schmid, S. M., Kissling, E., 2000. The arc of the western Alps in the light of geophysical data on deep crustal structure. Tectonics 19, 62-85.

Schnepp, E., Rolf, C., Sruck, J., 2001. Paläo- und gesteinsmagnetische Untersuchungen an Kernen der Forschungsbohrung Vogelsberg 1996. – In: Hoppe, A., Schulz, R., (Eds.) Die Forschungsbohrung Vogelsberg 1996- Einblicke in einen miozänen Vulkankomplex.- Geol. Abh. Hess, 107, 151-169, Wiesbaden (Hessisches Landesamt für Umwelt und Geologie).

Scholger, R., 1998. Magnetostratigraphic and paleomagnetic analysis from the Early Miocene (Karpatian) deposits Teiritzberg and Obergänserndorf (Korneuburg Basin, Lower Austria). Beitr. Paläont., 23, 25-26, Wien.

Scholger, R., Stingl, K., 2002. Paleomagnetic reconstruction of geodynamic events in the Eastern Alpine Miocene. In: Institut Für Geologie Und Paläontologie, Univ. Salzburg (Eds.), Kurzfassungen, PANGEO Austria. , Salzburg , 159-160.

Scholger, R., Stingl, K., 2004. New paleomagnetic results from the Middle Miocene (Karpatian and Badenian) in Northern Austria. Geologica Carpathica, 55, 199-206.

Scholz, H., 1993. Der Grenzbereich zwischen Falten- und Vorlandmolasse im Gebiet zwischen Rhein- und Illergletscher im Westallgäu (Exkursion G am 16. April 1993). Jber. Mitt. oberrhein. geol. Ver., N.F., 75: 155-176.

Scholz, H., 1999. Die "klassische" Molasse-Gliederung vom Südrand des Molassebeckens in Südwestbayern - bewährt oder problematisch? N. Jb. Geol. Paläont., Abh., 214: 391-413.

Scholz, H., 2000. Die tertiären Grobschüttungen am Südrande des Molassebeckens im Allgäu (Südwestbayern) - eine Synopsis. N. Jb. Geol. Paläont., Abh., 218: 61-84.

Schwerd, K., Ebel, R., Jerz, H., 1983. Erläuterungen zum Blatt Nr. 8427 Immenstadt i. Allgäu. Geologische Karte von Bayern 1:25000, München.

Sherwood, G., 1990. A paleomagnetic and rock magnetic study of tertiary volcanics from the Vogelsberg (Germany). Phys. Earth Planet. Interiors, 62, 32-45.

Shipunov, S., 1997. Synfolding magnetization: detection, testing and geological applications. Geophys. J. Int. 130, 405-410.

Singer, B. S., Singer, B., Hoffman K., Schnepp, E., Guillou, H., (submitted). Multiple Brunhes Chron Excursions Recorded in the West Eifel/Germany Volcanics: Support for Long-Held mantle Control Over the Non-Axial Dipole Field. Phys. Earth Planet Int.

Speranza, F., Villa, I. M., Sagnotti, L., Florindo F., Cosentino D., Cipollari P., Mattei, M., 2002. Age of the Corsica-Sardinia rotation and Liguro-Provencal basin spreading: new paleomagnetic and Ar/Ar evidence.- Tectonophysics 347, 231-251.

Stephan, W., Hesse, R., 1966. Erläuterungen zum Blatt Nr. 8236 Tegernsee. Geologische Karte von Bayern 1:25000, München.

Steininger, F. F., Wessely, G., Rögl, F., Wagner, L., 1991. Tertiary Sedimentary History and Tectonic Evolution of the Eastern Alpine Foredeep. Gior. Geol. 48, 285-295.

Stingl, V., Krois, P., 1990. Sedimentological investigations of metamorphic clastics, the basal clastic rocks of the Brenner Mesozoic (Stubai Alps, Austria/Italy). Terra Nova 2, 273-281.

Stock, H. W., 1994. Stratigraphie, Sedimentologie und Paläogeographie in den nordöstlichen Dolomiten (Italien).- Jahrb. Geol. Bundesanst., 137, 383 - 406, Wien.

Stuewe, K., 2007. Geodynamics of the Lithosphere. Springer, Berlin Heidelberg New York, 493pp.

Suk, D., Van Der Voo, R., Peacor, D. R., 1993. Origin of magnetite responsible for remagnetization of Early Paleozoic limestones of New York state. J. Geophys. Res. 98, B1, 419-434.

Tarling, D. H., 1983. Palaeomagnetism: Principles and Applications in Geology, Geophysics and Archaeology. Chapman & Hall, London. 379 pp.

Tarling, F., Hrouda, D. H., 1993. The Magnetic Anisotropy of Rocks. Chapman and Hall, London, 217pp.

Tauxe, L., 1998. Paleomagnetic Principles and Practice. Kluwer Academic Publishing, Dordrecht.

Thio, H. K., 1988. Magnetotectonics in the Piemont Tertiary Basin. Phys. Earth Planet. Int. 52, 308-319.

Thiele, O., 1976. Der Nordrand des Tauernfensters zwischen Mayrhofen und Innerschmirn (Tirol).- Geologische Rundschau 65, 410-421.

Thomas, J. C., Claudel, M. E., Collombet, M., Tricart, P., Chauvin, A., Dumont, T., 1999. First paleomagnetic data from the sedimentary cover of the French Penninic Alps, evidence for Tertiary counterclockwise rotations in the Western Alps. EPSL 171, 561-574.

Thöni, M., Jagoutz, E., 1993. Isotopic constraints for eo-Alpine high-P metamorphism in the Austroalpine nappes of the Eastern Alps, Its bearing on Alpine orogenesis. Schweiz. mineralog. petrogr. Mitt. 73, 177-189.

Thöny, W., Ortner, H., Scholger, R., 2005. Do the Southern Alps belong to the African/ Adriatic promontory during the Neogene? Preliminary paleomagnetic data from the Southern Alps. In: Tomljenovic B., Balen D. and Vlahovic I. (Eds.) 7th Workshop of Alpine Geological Studies. Abstracts Book, 95-96.

Thöny, W., Ortner, H., Scholger, R., 2006. Paleomagnetic evidence for large en-bloc rotations in the Eastern Alps during Neogene orogeny. Tectonophysics 414, 169-189.

Torsvik, T. H., Briden, J. C., Smethurst, M. A., 1996. SuperIAPD.
www. geodynamics. no/iapd/.

Tollmann, A., 1976b. Der Bau der Nördlichen Kalkalpen. Monographie der Nördlichen Kalkalpen, Teil III. Deuticke, Wien. 449 pp.

Urbanek, Ch., Frank, W., Decker, K., 2001. Dating transpressional deformation along the Salzachtal fault (Austria), new implications for the exhumation history of the Tauern window. GPM Innsbruck, Abstracts 5th Workshop for Alpine Geological Studies 25, 227-229.

Vandenberg, J., 1979. Preliminary results of a paleomagnetic research on Eocene to Miocene rocks of the Piemont basin (NW Apennines, Italy). Geol. Ultraiectina 20, 147-153.

Vandenberg, J., 1983. Reappraisal of paleomagnetic data from Gargano (south Italy). Tectonophysics 98, 29-41.

Van der Voo, R., 1993. Paleomagnetism of the Atlantic, Tethys and Iapetus Oceans. Cambridge Univ. Press, Cambridge. 405 pp.

Vialon, P., Rochette, P., Menard, G., 1989. Indentation and Rotation in the Western Alpine Arc. In: Coward, M. P., Dietrich, D. and Park, R. G. (Editors), Alpine Tectonics. Spec. Publ. Geol. Soc. London 45, 329-338.

Vollmayr, Th., 1958. Erläuterungen zum Blatt Nr. 8426 Oberstaufen. Geologische Karte von Bayern 1:25000, München.

Vollmayr, T., Ziegler, J., 1976. Erläuterungen zum Blatt Nr. 8425 Weiler i. Allgäu. Geologische Karte von Bayern 1:25000, München.

Vollmayer, T., Jäger, S., 1995. Interpretation seismischer Daten und Modell zur Vorbereitung und Auswertung der Bohrung Hindelang 1 (Allgäuer Alpen). Geol. Bav. 100, 153-165.

Wagner, L., Kuckelkorn, K., Hiltmann, W., 1986. Neue Ergebnisse zur alpinen Gebirgsbildung Oberösterreichs aus der Bohrung Oberhofen 1 - Stratigraphie, Fazies, Maturität und Tektonik. Erdöl, Erdgas, Kohle 102/1, 12-19.

Waldhör, M., 1999. The small-circle reconstruction in paleomagnetism and its application to paleomagnetic data from the Pamirs. In: Frisch, W., Kuhlemann, J. (Eds.). Tübinger Geowissenschaftliche Arbeiten, A 45. 99 pp.

Waldhör, M., Appel, E., 2006. Small Circle Methods IN Paleomagnetism. In: 10th "Castle Meeting" new trends in Geomagnetism, Paleo, Rock and Environmental Magnetism, Abstracts. Travaux Geophysiques XXVIII (2006), p122.

Weber, J., Vrabec, M., Stopar, B., Pavlovcic Preseren, P., Dixon, T., 2005. Active Tectonics at the NE Corner of the Adria-Europe Collision Zone (Slovenia and NorthernCroatia): GPS Constraints on Adria Motion and Deformation at the Alps-Dinarides-Pannonian Basin Junction. In: Tomljenovic B., Balen D. and Vlahovic I. (Eds.) 7th Workshop of Alpine Geological Studies. Abstracts, 103-104.

Wessely, G., 1987. Mesozoic and Tertiary evolution of the Alpine-Carpathian foreland in eastern Austria. Tectonophysics 137, 45- 49.

Winkler, W., 1988. Mid to Early Cretaceous Flysch and Melange Formations. Jahrb. Geol. Bundesanst., 131, 341-390.

Winterer, E.L., Bosellini, A., 1981. Subsidence and sedimentation in Jurassic passive continental margin SouthernAlps, Italy. Am. Ass. Petr. Geol 65, 394-421.

Wyssling, G., 1986. Der frühkretazische helvetische Schelf in Vorarlberg und im Allgäu - Stratigraphie, Sedimentologie und Paläogeographie. Jahrb. Geol. Bundesanst, 129, 161-265.

Zacher, W., 1973. Das Helvetikum zwischen Rhein und Iller (Allgaeu - Vorarlberg). Tektonische, palaeographische und sedimentologische Untersuchungen. Geotektonische Forschungen, 44: I-II: 74 pp.

Zeeh, St., Walter, U., Kuhlemann, J., Herlec, U., Keppens, E., Bechstedt, Th., 1997. Carbonate cements as tool for fluid flow reconstruction, a study in parts of the Eastern Alps (Austria, Germany, Slovenia). In: Montanez, I. P., Gregg, S. M. and Shelton, K. L. (Editors), Basin-wide diagenetic patterns, Integrated petrologic, geochemical and hydrological considerations. SEPM Special Publication No. 57, 167-181.

Zijderveld, J. D. A., 1967. Demagnetization of rocks, Analysis of results. In: Collinson, D. W., Creer, K. M. and Runcorn, S. K. (Editors), Methods in Paleomagnetism. Elsevier, Amsterdam, pp. 254-286.

Zwingmann, H., Mancktelow, N., 2004. Timing of Alpine fault gouges. EPSL, 223, 415-425.

9.2. Figure Captions

Fig. 1. Geological sketch of the Western, Eastern and Southern Alps (Schmid et al., 2004) with structural units sampled during this study. Red frames indicate sampling areas. Numbering of the frames refers to Tab.1. Frames 8a and 8b mark the sampling areas of Lake Garda and Belluno/Follina, respectively.

Fig. 2. **A**: Geological sketch of the Eastern and Southern Alps with structural units sampled during this study. S(ite) numbers refer to Tab.1. **B**: Geological sketch of the Western, Eastern and Southern Alps with paleomagnetic results from previous studies. Locality numbers refer to Tab.2.

Fig. 3. Rock magnetic properties, demagnetization behavior and statistical parameters from site 2 (ES2), (Tab.1).
A= IRM component analysis according to Kruiver et al. (2001); **B**= Typical IRM acquisition curves; **C**= Thermal demagnetization of three component IRM (Lowrie, 1990); **D**= Zijderveld demagnetograms of representative samples in stratigraphic (tc, **D1**) and geographic (no tc, **D2**) coordinates, in the Zijderveld diagrams, full/hollow circles: projection of the NRM in the horizontal/vertical plane. Stereogeographic projection of the characteristic remanence magnetization direction, bedding corrected (tc), in situ (no tc) coordinates; **E**= AMS results, after bedding correction/ in situ coordinates.

Fig. 4. Rock magnetic properties, demagnetization behavior and statistical parameters from site 10 (EA2, **A1-F1**) and site 11 (WA3, **A2-F2**), (Tab.1).
A= IRM component analysis according to Kruiver et al. (2001); **B**= Typical IRM acquisition curves; **C**= Thermal demagnetization of three component IRM (Lowrie, 1990); **D**= Zijderveld demagnetograms of representative samples in stratigraphic (tc) and geographic (no tc) coordinates, in the Zijderveld diagrams, full/hollow circles: projection of the NRM in the horizontal/vertical plane. Stereogeographic projection of the characteristic remanence magnetization direction, bedding corrected (tc), in situ (no tc) coordinates; **E**= AMS results, after bedding correction/ in situ coordinates; **F**= fold test according to McElhinny (1964).

Fig. 5. Rock magnetic properties, demagnetization behavior and statistical parameters from site 16 (M10, **A1-E1**) and site 14 (MB11, **A2-E2**), (Tab.1).
A= IRM component analysis according to Kruiver et al. (2001); **B**= Typical IRM acquisition curves; **C**= Thermal demagnetization of three component IRM (Lowrie, 1990); **D**= Zijderveld demagnetograms of representative samples in stratigraphic (tc) and geographic (no tc) coordinates, in the Zijderveld diagrams, full/hollow circles: projection of the NRM in the horizontal/vertical plane. Stereogeographic projection of the characteristic remanence magnetization direction, bedding corrected (tc), in situ (no tc) coordinates; **E**= AMS results, after bedding correction/ in situ coordinates.

Fig. 6. Rock magnetic properties, demagnetization behavior and statistical parameters from site 22 (RB3, **A1-F1**) and site 17 (SG6, **A2-F2**), (Tab.1).
A= IRM component analysis according to Kruiver et al. (2001); **B**= Typical IRM acquisition curves; **C**= Thermal demagnetization of three component IRM (Lowrie, 1990); **D**= Zijderveld demagnetograms of representative samples in stratigraphic (tc) and geographic (no tc) coordinates, in the Zijderveld diagrams, full/hollow circles: projection of the NRM in the horizontal/vertical plane. Stereogeographic projection of the characteristic remanence magnetization direction, bedding corrected (tc), in situ (no tc) coordinates; **E**= AMS results, after bedding correction/ in situ coordinates; **F**= fold test according to McElhinny (1964).

Fig. 7. Results from Allgäu area. Sites were sampled in Autochthonous to Allochthonous Molasse units and Helvetic nappes. Site abbreviations refer to Tab.1. Colors of red, green and blue indicate counterclockwise, moderate clockwise and strong clockwise rotation, respectively. (Tectonic map of Voralrberg, 1: 200.000, Oberhauser and Rataj, 1998).

Fig. 8. Lithostratigraphy of Helvetic units (Freudenberger and Schwerd, 1996). Declination orientations and α95 cones indicate results. Colors of red, green and blue indicate counterclockwise, moderate clockwise and strong clockwise rotation, respectively. Sites 34-37, at locality Sünserspitze belong to South-Helvetic units, characterized by Ultra-Helvetic facies.

Fig. 9. Results from Muttekopf area indicating two times of remagnetization and two times of successive vertical axis rotations in post-folding times (personal comment H.Ortner).

Fig. 10. Rock magnetic properties, demagnetization behavior and statistical parameters from site 50 (UAN2/3/4, **A-C, D1, F1, D3, F3, G3**) and site 51 (OA2, **A-C, D2, F2**), (Tab.1).
A= IRM component analysis according to Kruiver et al. (2001); **B**= Typical IRM acquisition curves; **C**= Thermal demagnetization of three component IRM (Lowrie, 1990); **D**= Zijderveld demagnetograms of representative samples in stratigraphic (tc) and geographic (no tc) coordinates, in the Zijderveld diagrams, full/hollow circles: projection of the NRM in the horizontal/vertical plane. Stereogeographic projection of the characteristic remanence magnetization direction, bedding corrected (tc), in situ (no tc) coordinates; **F**= fold test according to McElhinny (1964), **G**= Susceptibility versus temperature curves.

Fig. 11. Rock magnetic properties, demagnetization behavior and statistical parameters from site 53 (BH), (Tab.1).
A= IRM component analysis according to Kruiver et al. (2001); **B**= Typical IRM acquisition curves; **C**= Thermal demagnetization of three component IRM (Lowrie, 1990); **D**= Zijderveld demagnetograms of representative samples in stratigraphic (tc) and geographic (no tc) coordinates, in the Zijderveld diagrams, full/hollow circles: projection of the NRM in the horizontal/vertical plane. Stereogeographic projection of the characteristic remanence magnetization direction, bedding corrected (tc), in situ (no tc) coordinates; **E**= AMS results, after bedding correction/ in situ coordinates; **F**= fold test according to McElhinny (1964); **G**= Susceptibility versus temperature curves.

Fig. 12. Stratigraphic summary section of Late Cretaceous to Oligocene rocks in the Unterinntal area and associated cross plots of age of rock and declination/inclination of secondary/primary magnetizations. Note that declinations do not change systematically with age of rock. Shaded squares illustrate mean direction of inclinations and declinations of clockwise and counter-clockwise rotated remagnetizations in the Unterinntal area in Cenozoic times. Numbers at arrows refer to Tab. 1. The black square marks the only primary magnetization that could be derived in the Lower Inn valley area (sites 50, 51; Tab.1).

Fig. 13. **A:** Geologic sketch of the Ampelsbach area (Ortner, personal communication). Geology redrawn from Sausgruber (1994). Declinations of magnetizations are indicated by arrows. Inset a) local fold axes related to fault activity calculated from bedding planes, Inset b) orientation of paleomagnetic vectors insitu and after first and second correction, Inset c) orientations of paleomagnetic vectors after first correction with cones of confidence arranged along a small circle. This is interpreted to be the result of remagnetizing during folding. Site abbreviations AB3-AB9 (=Sites 70-76) and GU1-GU7 (=Sites 64-69) refer to Table 1. **B:** N/S oriented cross section illustrating tilting of remagnetization vectors during folding. **C**: Fold test according to McElhinny (1964).

Fig. 14. Geologic sketch of the Schwendt area. Declinations of magnetization are indicated by arrows (Ortner, personal communication). Sites were sampled in Late Triassic to Early Cretaceous rocks. Inset **a**) circles: poles to bedding planes of Jurassic rocks, black squares: mean orientation of bedding in paleomagnetic sampling sites, numbers correspond to numbers in arrows. Inset **b**) a positive foldtest indicates prefolding magnetization (sites 82/83, Ks4/5, Tab.1). Inset **c**) positive Fold test according to McElhinny (1964).

Fig. 15. Stratigraphic section of Late Triassic to Early Cretaceous rocks in the Unken syncline area and associated cross plots of age of rock and declination/inclination of secondary magnetizations. For comparison: African and European "APWP (apparent polar wander path)" are marked by dark- and light gray curves, respectively (Ortner, personal communication). Numbers (S87-S91) refer to Tab.1.

Fig. 16. Rock magnetic properties, demagnetization behavior and statistical parameters from site 92 (HG), (Tab.1).
C= Thermal demagnetization of three component IRM (Lowrie, 1990); **D**= Zijderveld demagnetograms of representative samples in stratigraphic (tc) and geographic (no tc) coordinates, in the Zijderveld diagrams, full/hollow circles: projection of the NRM in the horizontal/vertical plane. Stereogeographic projection of the characteristic remanence magnetization direction, bedding corrected (tc), in situ (no tc) coordinates; **E**= AMS results, after bedding correction/ in situ coordinates; **G**= Susceptibility versus temperature curves.

Fig. 17. Rock magnetic properties, demagnetization behavior and statistical parameters from site 94 (SBH), (Tab.1).

A= IRM component analysis according to Kruiver et al. (2001); **B**= Typical IRM acquisition curves; **D**= Zijderveld demagnetograms of representative samples in stratigraphic (tc) and geographic (no tc) coordinates, in the Zijderveld diagrams, full/hollow circles: projection of the NRM in the horizontal/vertical plane. Stereogeographic projection of the characteristic remanence magnetization direction, bedding corrected (tc), in situ (no tc) coordinates; **E**= AMS results, after bedding correction/ in situ coordinates.

Fig. 18. Rock magnetic properties, demagnetization behavior and statistical parameters from site 96 (KJ), (Tab.1).

D= Zijderveld demagnetograms of representative samples in stratigraphic (tc) and geographic (no tc) coordinates, in the Zijderveld diagrams, full/hollow circles: projection of the NRM in the horizontal/vertical plane. **D1**= counterclockwise rotated magnetization component, **D2=** clockwise rotated magnetization component. Stereogeographic projection of the characteristic remanence magnetization direction, bedding corrected (tc), in situ (no tc) coordinates; **G**= Susceptibility versus temperature curves.

Fig. 19. Rock magnetic properties, demagnetization behavior and statistical parameters from site 97 (HST), (Tab.1).

B= Typical IRM acquisition curves; **C**= Thermal demagnetization of three component IRM (Lowrie, 1990); **D**= Zijderveld demagnetograms of representative samples in stratigraphic (tc) and geographic (no tc) coordinates, in the Zijderveld diagrams, full/hollow circles: projection of the NRM in the horizontal/vertical plane. **D1**= counterclockwise rotated magnetization component, **D2=** clockwise rotated magnetization component. Stereogeographic projection of the characteristic remanence magnetization direction, bedding corrected (tc), in situ (no tc) coordinates; **G**= Susceptibility versus temperature curves.

Fig. 20. Geological sketch of the Southern Alps with structural units sampled during this study. S(ite) numbers refer to Tab.1.

Fig. 21. Rock magnetic properties, demagnetization behavior and statistical parameters from site 100 (FT, **C1, D1, G1**) and site 101 (FTNG, **B2, D2**), (Tab.1).

B= Typical IRM acquisition curves; **C**= Thermal demagnetization of three component IRM (Lowrie, 1990); **D**= Zijderveld demagnetograms of representative samples in stratigraphic (tc) and geographic (no tc) coordinates, in the Zijderveld diagrams, full/hollow circles: projection of the NRM in the horizontal/vertical plane. Stereogeographic projection of the characteristic remanence magnetization direction, bedding corrected (tc), in situ (no tc) coordinates; **G**= Susceptibility versus temperature curves.

Fig. 22a. Rock magnetic properties, demagnetization behavior and statistical parameters from sites 111 (RA2, **C, D, E**) and site 110 (RA3, **C**, **D**), (Tab.1).

Fig. 22b. Rock magnetic properties, demagnetization behavior and statistical parameters from sites 109 (RA4, **C, D, E**) and site 108 (RA5, **C**, **D, E**), (Tab.1). **C**= Thermal demagnetization of three component IRM (Lowrie, 1990); **D**= Zijderveld demagnetograms of representative samples in stratigraphic (tc) and geographic (no tc) coordinates, in the Zijderveld diagrams, full/hollow circles: projection of the NRM in the horizontal/vertical plane; **E**= AMS results, after bedding correction/ in situ coordinates.

Fig. 22c. Lithostratigraphy and summary of paleomagnetic results at locality Alpe di Ra Stua (Sites 104-111, Tab.1). For comparison: Magnetic polarity time scale with polarity zones indicated by black (normal polarity) and white (reverse polarity) fields.

Fig. 23. Geological sketch of the study area comprising the western part of the Eastern Alps and the northern part of the Southern Alps (Thöny et al., 2006). Arrows indicate trend of declinations, and cones depict α_{95}. Characteristic zijderveld demagnetograms that are indicating 2 component magnetization systems are pasted. Numbers at arrows refer to Tab. 1. In the Northern Calcareous Alps and the Southern Alps two magnetic components occur during demagnetization in single samples. Small scale vertical axis rotations can be excluded therefore.

Fig. 24. Rock magnetic properties, demagnetization behavior and statistical parameters from site 115 (GA11, **A1-D1**), site 116 (GA9, **A2-D2**) and site 114 (GA10, **D3**), (Tab.1).
A= IRM component analysis according to Kruiver et al. (2001); **B**= Typical IRM acquisition curves; **C**= Thermal demagnetization of three component IRM (Lowrie, 1990); **D**= Zijderveld demagnetograms of representative samples in stratigraphic (tc) and geographic (no tc) coordinates, in the Zijderveld diagrams, full/hollow circles: projection of the NRM in the horizontal/vertical plane. Stereogeographic projection of the characteristic remanence magnetization direction, bedding corrected (tc), in situ (no tc) coordinates.

Fig. 25. Rock magnetic properties, demagnetization behavior and statistical parameters from site 137 (FO13, **A1-D1**) and site 138 (FO12, **A2-D2**), (Tab.1).
A= IRM component analysis according to Kruiver et al. (2001); **B**= Typical IRM acquisition curves; **C**= Thermal demagnetization of three component IRM (Lowrie, 1990); **D**= Zijderveld demagnetograms of representative samples in stratigraphic (tc) and geographic (no tc) coordinates, in the Zijderveld diagrams, full/hollow circles: projection of the NRM in the horizontal/vertical plane. Stereogeographic projection of the characteristic remanence magnetization direction, bedding corrected (tc), in situ (no tc) coordinates.

Fig. 26. Paleomagnetic results from the study area. Declination orientations and α95 cones indicate results. Colors of red, green and blue indicate counterclockwise, moderate clockwise and strong clockwise rotation, respectively.

Fig. 27. Paleomagnetic results from the study area. Primary magnetizations from the Northern Alpine Foreland basin, the Northern Calcareous Alps and the Southern Alpine Foreland basin are indicating contemporaneous, identical vertical axis rotations.

Fig. 28. N/S oriented cross section. Clockwise rotation of Eastern and Southern Alps might be caused by retreat of the European mantle lithosphere and NW directed movement of Adria. 400 km of N/S shortening (x) are calculated as follows: x= tan 60°*250km. E/W extent of the Eastern Alps (250km) are derived after subtracting 300km of lateral extrusion related extension (Frisch et al., 2000) from current dimensions. The elimination of crustal units is still a matter of debate and possibly was partly achieved by the lateral extrusion of the Austro-Alpine nappe pile.

Fig. 29. Paleomagnetic results from the study area. The amount of counterclockwise rotation does not change although the rotating units are separated by prominent Alpine thrusts and strike slip faults (marked by strong red lines). No rotations of tectonic units relative to each other are indicated. Red confidence cones mark secondary magnetizations, black confidence cones mark primary magnetizations.

Fig. 30. N/S oriented cross section at the transition from Autochthonous to Allochthonous Molasse. The counterclockwise rotation is compensated at the Alpine basal thrust and at sinistral, transpressive faults that are disintegrating the slices of Subalpine Molasse. Modified from Berge and Veal (2005). Post-folding and Pre-rotational remagnetizations south of Salmaser Schuppe do not show inclination shallowing (e.g. sites 4-9, Tab.1). Only site 3 (Tab.1) from locality Sulzberg at Salmaser Schuppe is characterized by shallow inclinations (D/I= 33/29). Presuming a simple ramp-flat system at the contact between rotated to unrotated Molasse units, the site at locality Sulzberg (site 3, Tab.1) may represent a position at the ramp interpreted from shallow inclinations due to tilting. All other results from Horn- and Steineberg Schuppe (e.g. sites 4-9, Tab.1) with steep inclinations (around 60°) are derived from a position at the lower flat.

Fig. 31. Due to the lateral extrusion friction is reduced at basal Alpine thrust. After clockwise rotation repeated (counterclockwise) rotation is enabled by changing the rotation pole from the Bohemian massif (**1**) to the area of the meridian Torino / Lake Konstanz (**2**).

Fig. 32. Paleomagnetic results from the study area (red numbers, Tab.1). For comparison: paleomagnetic results from stable Adria by Marton (2006a) (black numbers). Stable Adria and Eastern/Southern Alps indicate a joined counterclockwise rotation relative to geographic N in post Messinian times, i.e. younger than 5Ma. Red confidence cone in right figure marks primary magnetizations from Schliersee area (Tab.1).

Fig. 33. N/S oriented cross section. The counterclockwise rotation of Eastern and Southern Alps is caused by a counterclockwise rotation of the Adriatic microplate. The Adriatic slab below the Dinarides is rotated into the Eastern/Southern Alps as also indicated by data from Lippitsch et al. (2003).

Fig. 34. Opening of the Balearic ocean is causing Corsica-Sardinia rotation. Below the Apennines E –directed mantle flow is possibly responsible for the retreat of the Adriatic slab. This retreat is causing the opening of the Tyrrhenian Sea and the counterclockwise rotation of the Adriatic microplate.

Fig. 35. Summary of Oligocene to Miocene Geodynamics derived from paleomagnetic data. Blue, red and black colors represent the paleogeographic position of Adria and Eastern/ Southern Alps with the northern frontal Alpine thrust in times prior to clockwise rotation (blue), prior to counterclockwise rotation (red) and in present times (black). Pink arrow indicates time and orientation of the onset of lateral extrusion. Numbers 1,2 mark prominent remagnetization and rotation events. **1**: Two clockwise rotations (60°-70° in total) in Oligocene times. **2**: 30° of counterclockwise rotation in Late Miocene to Pliocene times.

9.3. Table Captions

Tab. 1. Basic geographical and geological data of the paleomagnetic sampling localities. Site no. refer to numbers in Fig.2. Dec/Inc insitu= declination/inclination before any correction, Dec/Inc (abc)= declination/inclination after bedding correction, α_{95}= radius of cone of 95% confidence about the mean direction (Fisher, 1953), K= precision parameter, N= number of samples used to calculate the mean, Lith. age= Lithology age, Dip= dip direction/dip, P=L*F degree of anisotropy (Tarling and Hrouda, 1993), Remarks= lithostratigraphic classification, AMS= anisotropy of magnetic susceptibility, L/F= mean lineation/foliation, K=L/F Flinn-diagramm ratio (Flinn, 1962; Soffel, 1991), K1/K3 α_{95} bac= orientation of maximum and minimum axis of susceptibility ellipsoid before any correction, K1/K3 α_{95} abc= orientation of maximum and minimum axis of susceptibility ellipsoid after bedding correction, N K1/K3= number of samples used to calculate the mean orientation of K1/K3, IsT= thermal demagnetization of 3-component IRM, LF/MF/HF-cmp/T= low/medium/high field component of 3 component IRM and T_{ub} during thermal demagnetization (Lowrie, 1990), T_{ub}= unblocking temperature during thermal demagnetization, H_{cr}= coercivity of remanence.

Tab. 2. Selected Tertiary and Cretaceous results from Western and Eastern Alps, the Apennines and stable Adria. Locality no. refers to numbers in Figure 2B; Age of ChRM= Age of the characteristic remanent magnetization according to quoted literature; Dec/ Inc of ChRM= declination/inclination of the characteristic remanent magnetization according to quoted literature; K= precision parameter; α_{95}= radius of cone of 95% confidence about the mean direction (Fisher, 1953).

1. North Alpine Foreland Basin

Site Nr.	Locality	Dec (insitu)	Inc (insitu)	alpha95	K	Dec (abc)	Inc (abc)	alpha95	K	N	Lith. Age	Dip	site abbrev.	Latitude	Longitude	Lithology	Remarks	AMS	L/F	K=L/F	P=L*F	K1/a95 bac K1/a95 abc	K3/a95 bac K3/a95 abc	N K1/K3	IRM	B1/2 (mT)	IsT	LF-cmp/ T	MF-cmp/T	HF-cmp/T	Tub	Hcr
Allgäu/Autochtonous Molasse																																
1	Enschenstein	**358**	**62**	6,9	49,7	346	35	6,9	49,6	10	Burdigalian	331/28	ES 2	47,555	9,908	silt/sandston	UMM	yes	1,010 / 1,013	99,70%	2,30%	60 / 09; 11,6° 56 / 08	101 / 79; 9,6° 354 / 68	7	Magn/Goeth	50,1/ 1258,9	yes	< 600°C	400-500°C			3-30mT 30-100mT
		47	60	7,2	114,9	**14**	**45**	7,2	114,8	5																						
2	Enschenstein	**10**	**56**	13,1	35,2	357	36	13,1	35,3	5	L. Aquitan	332/24	ES 1	47,555	9,908	silt/sandston	LFM/Kojen	no							Mgn/He/Goe	39,8/281,8	yes	< 600°C	> 600°C	>600°C		3-15mT
Allgäu/Salmaser Schuppe																																
3	Sulzberg	19	7	12	32,2	**33**	**29**	11,9	32,5	6	L. Aquitan	143/45	SP	47,573	9,922	marls	LFM/Kojen	yes	1,016 / 1,011	100,50%	2,70%	50 / 06; 7,8°	288 / 80; 10,3°	5	He/Mgn/Goet	1995,3 35,5/ 158,5	yes	< 600°C	> 600°C	100°C/>600°C	620-680°C	
Allgäu/Hornschuppe																						56 / 06	153 / 53			1995,3						
4	Littenbach	**326**	**52**	6,8	67,8	167	68	6,8	67,9	8	Chattian	154/59	LB 2	47,517	9,973	silt/sandston	LFM	yes	1,010 / 1,009	100,10%	1,90%	238 / 08; 7,6°	333 / 14; 14,0°	6	Mgn/He/Goe	39,8/ 316,2	yes	< 600°C	> 600°C	>600°C	200-450°C	3-15mT
5	Littenbach	**332**	**55**	12	41,4	179	79	12	41,5	5	Chattian	159/46	LB 3	47,517	9,973	silt/sandston	LFM	no							Magn/Goeth	1584,9 44,7/ 501,2	yes	< 600°C	600°C		200-400°C	3-15mT
6	Krumbach	**347**	**63**	4,3	92,9	100	83	4,6	83,2	13	Rupel/Chatt	156/32	KB	47,483	9,936	silt/sandston	LMM/Baust	no							Magn	39,8	yes	< 600°C	300-600°C			3-15mT
Allgäu/Steinbergmulde																																
7	Eibele Alm	**339**	**63**	8,4	30,3	160	83	8,4	30,7	11	E.-L.Chattian	159/34	EA 1	47,507	10,064	silt/sandston	LFM/Top Stg	no							Magn/Goeth	35,5/ 1000	yes	500-600°C	500-600°C			3-15mT
8	Eibele Alm	**317**	**62**	9,3	68,3	285	-73	9,3	68,5	5	E. Chattian	171/31 (ov.)	EA 5	47,507	10,064	silt/sandston	LFM/Weiß	no							Magn/Goeth	39,8/ 631	yes	500-600°C	500-600°C			3-30mT
9	Eibele Alm	**345**	**60**	10,1	31	152	64	10,1	31	8	Rupel/Chatt	159/56	EA 4	47,507	10,064	silt/sandston	LMM/ Baust	no							Magn/Goeth	39,8/ 1000	yes	500-600°C	500-600°C			3-21mT
10	Eibele Alm	167	-11	13,5	25,7	**175**	**-60**	13,5	25,7	6	Rupelian	159/50	EA 2	47,507	10,063	marls	LMM/ Tonm	yes	1,013 / 1,052	96,30%	6,50%	64 / 08; 8,0° 73 / 09	328 / 36; 8,2° 272 / 81	6	Magn/Sulfide	39,8/ 141,3	no					25-80mT
11	Wilhelmine A	311	-32	10,7	40	**181**	**-47**	10,7	39,9	6	Rupelian	153/84 (ov.)	WA 3	47,482	10,155	marls	LMM/Tonm	yes	1,013 / 1,045	96.9%	5,80%	69 / 13; 7,6°	336 / 10; 7,0°	7	Magnetite	56,2	yes	300-500°C	500-600°C			30-80mT
		6	**71**	7,6	148,8	344	-22	7,5	150,2	4												50 / 06	199 / 84									3-20mT

Site Nr.	Locality	Dec (insitu)	Inc (insitu)	alpha95	K	Dec (abc)	Inc (abc)	alpha95	K	N	Lith. Age	Dip	site abbrev.	Latitude	Longitude	Lithology	Remarks	AMS	L/F	K=L/F	P=L*F	K1/a95 bac K1/a95 abc	K3/a95 bac K3/a95 abc	N K1/K3	IRM	B1/2 (mT)	IsT	LF-cmp/ T	MF-cmp/T	HF-cmp/T	Tub	Hcr
Schliersee/Mangfall																																
12		**1**	**51**	5,8	62,9	3	-40	5,8	62,9	11	Serravallian	192/88 (ov.)	K 14	47,818	11,873	marls	UFM	yes	1,014 / 1,009	100,50%	2,30%	91 / 09; 3.3°	330 / 72; 17,9°	6	Magn/Goeth	50,1/ 1258,9	yes	< 600°C	600°C			5-50mT
13		**1**	**56**	9,7	39,7	5	-35	9,7	39,6	7	Serravallian	192/88 (ov.)	K 15	47,818	11,873	marls	UFM	yes	1,009 / 1,016	99,30%	2,50%	274 / 03; 10,1°	08 / 57; 5,2°	5	Magn/Goeth	50,1/ 1258,9	yes	< 600°C	600°C			5-40mT
Schliersee/Miesbach																																
14		354	32	6,3	115,1	**328**	**66**	6,3	114,9	6	L. Chattian	(194/39)	MB 11	47,802	11,821	silt/sandston	Cyrenensch	yes	1,006 / 1,006	100%	1,20%	356 / 49; 5,5°	146 / 37; 4,2°	16	Magn/Goeth	39,8/ 1258,9	yes	< 600°C	600°C			20-60mT
		2	**71**	3,5	370,7	205	69	3,5	371,9	6												288 / 79	158 / 07									3-18mT
15		358	22	6,9	94,4	**344**	**58**	6,9	94,8	6	L. Chattian	(194/39)	MB 12	47,802	11,821	marls	Cyrenensch	yes	1,014 / 1,019	99,5	3,30%	267 / 20, 15,2°	19 / 39; 32,0°	5	Magn/Goeth	35,5/ 501,2	yes	500-600°C	500°C			20-70mT
		7	**44**	9,1	102,9	335	82	9,1	102,5	4												259 / 06	34 / 77									20-70mT
16		160	80	6,9	65,5	**11**	**40**	6,9	65,5	8	E.-L.Chattian	(6/59)	M 10	47,786	11,789	silt/sandston	Sattelflözgr	yes	1,015 / 1,034	98,20%	4,90%	99 / 00; 9,0°	189 / 49; 8,6°	7	Magn/Goeth	50,1/ 562,3	yes	< 600°C	500°C			20-60mT
		7	**68**	8,6	80,1	10	16		2	5												98 / 04	359 / 72									3-15mT
Schliersee/Hausham																																
17		1	1	4,4	160	**182**	**-42**	4,4	160,5	8	E. Chattian	(176/41)	SG 6	47,762	11,767	silt/sandston	Flözgruppe	no							Magn/Goeth	44,7/ 501,2	yes	< 600°C	500-600°C			25-60mT
18		178	-8	7,2	60,9	**182**	**-53**	7,2	61	8	L. Rupelian	(171/45)	SG 7	47,763	11,765	silt/sandston	LMM/Baust	yes	1,016 / 1,015	100,10%	3,10%	79 / 01; 7,9°	350 / 28; 7,8°	8	Magnetite	44,7	yes	500°C	500°C			20-50mT
																						81 / 02	350 / 73									
19		175	-13	15,9	10,2	**176**	**-56**	15,9	10,2	10	Rupelian	(173/43)	SG 8	47,763	11,766	marls	LMM/ Tonm	yes	1,011 / 1,020	99,10%	3,10%	82 / 00; 8,2°	352 / 48; 5,4°	6	Magn/Goeth	39,8/ 631,0	yes	< 600°C	500-600°C			20-50mT
																						84 / 01	196 / 89									
20		188	16	2,6	884,2	**190**	**-29**	2,6	891,6	5	Rupelian	(175/46)	SG 9	47,764	11,766	marls	LMM/ Tonm	yes	1,009 / 1,021	98,80%	3,00%	85 / 05; 7,6°	360 / 42; 6,8°	6	Magnetite	44,7	yes	< 600°C	500°C			20-60mT
																						90 / 03	65 / 85									
21		343	5	17,5	12,9	**173**	**-52**	17,5	12,9	7	E. Chattian	(167/47,inv)	RB 4	47,759	11,902	silt/sandston	Flözgruppe	no							Magn/Goeth	50,1/ 1258,9	yes	< 600°C	600°C			20-50mT
22		344	23	10,3	35,5	**175**	**-70**	10,3	35,5	7	E. Chattian	(167/47,inv)	RB 3	47,759	11,902	silt/sandston	Flözgruppe	yes	1,011 / 1,033	97,90%	4,40%	257 / 07; 8,0°	354 / 42; 7,5°	10	Magnetite	44,7	yes	< 600°C	500°C			15-50mT
																						83 / 06	264 / 83									
23		**336**	**45**	5,5	146,9	133	-76	5,6	146,6	6	Rupelian	(150/31,inv)	GR 1	47,756	11,9	marls	LMM/ Tonm	yes	1,011 / 1,020	99,10%	3,10%	77 / 01; 7,0°	350 / 65; 5,2°	6	Magn/Goeth	44,7/ 794,3	yes	500°C	500°C			20-50mT

2. Helvetic units

Site Nr.	Locality	Dec (insitu)	Inc (insitu)	alpha95	K	Dec (abc)	Inc (abc)	alpha95	K	N	Lith. Age	Dip	site abbrev.	Latitude	Longitude	Lithology	Remarks	AMS	L/F	K=L/F	P=L*F	K1/a95 bac K1/a95 abc	K3/a95 bac K3/a95 abc	N K1/K3	IRM	B1/2 (mT)	IsT	LF-cmp/ T	MF-cmp/T	HF-cmp/T	Tub	Hcr
Allgäu/ Starzlachklamm																																
24		**339**	**57**	5,2	164,7	252	71	5,2	164,5	6	L. Maastricht	(191/38)	SZK 2	47,53	10,309	marls	Dreiangelserie	yes	1,002 / 1,007	99,50%	0,90%	n. signif.	44 / 71; 10,9	5	Magn/Hemat	35,5/ 251,2	yes	< 600°C	500°C			3-20mT
25		**344**	**63**	7,6	46,9	150	41	7,6	46,8	9	Campan/Maa	(155/75)	SZK 3	47,534	10,317	carbonates	Wangschicht	no							Magn/Hemat	44,7/ 316,2	yes	< 600°C	500°C			3-30mT
26		**342**	**60**	11,2	47,7	150	45	11,2	47,8	5	Campan/Maa	(155/75)	SZK 4	47,534	10,317	marls	Wangschicht	no							Magn/Goeth	39,8/ 1000	yes	< 600°C	300-500°C			3-30mT
Site Nr.	**Locality**	**Dec (insitu)**	**Inc (insitu)**	**alpha95**	**K**	**Dec (abc)**	**Inc (abc)**	**alpha95**	**K**	**N**	**Lith. Age**	**Dip**	**site abbrev.**	**Latitude**	**Longitude**	**Lithology**	**Remarks**	**AMS**	**L/F**	**K=L/F**	**P=L*F**	**K1/a95 bac K1/a95 abc**	**K3/a95 bac K3/a95 abc**	**N K1/K3**	**IRM**	**B1/2 (mT)**	**IsT**	**LF-cmp/ T**	**MF-cmp/T**	**HF-cmp/T**	**Tub**	**Hcr**
Bregenzer Wald/ Schwarzenberg																																
27		**30**	**70**	6,6	134,9	18	15	6,6	135,1	5	Coniac-L.Cam	(12/56)	SB 3	47,4	9,851	marls	Amdener Mergel	yes	1,019 / 1,040	98,00%	6,00%	277 / 02; 8,6°	189 / 31; 8,2°	6	Magn/Goeth	39,8/ 501,2	yes	< 600°C	600°C			3-30mT
		340	**66**	4,1	186,5	359	13	4,1	184,9	8																						3-30mT
28		**157**	**-39**	4	284,5	163	20	4	287,7	6	Barreme-Apt	(7/65)	SB 1	47,4	9,851	carbonates	Schrattenkalk	no							Magn/ Sulf	28,2/ 79,4	yes	500°C	200-400°C 500°C			30-80mT
29		154	35	6,4	89,6	**246**	**-49**	6,4	89,6	7	Barreme	(13/75)	SB 5	47,4	9,851	marls	Drusbergsch.	no							Magn/ Sulf	28,2/ 79,4	yes	500°C	200-400°C 500°C			35-70mT
30		**347**	**61**	GCF 89%	Cirap 69°	177	0	GCF 89%	Cirap 69°	8	L. Berriasian	(7/63)	SB 4	47,4	9,851	carbonates	Örfla Sch.	no							Magn/Goeth	44,7/ 631,0	yes	500°C	500°C			3-20mT
Bregenzer Wald/ Kanisfluh																																
31	Schnepfegg	317	-45	5,1	174,8	**206**	**-63**	5,1	174,8	6	Barreme	(343/62)	SG 1	47,357	9,948	marls	Drusbergsch.	no							Ti-Mgn/Sulf Goethite	31,6/ 79,4 794,3	yes	200-400°C	200-400°C			40-80mT
32	Ortbg-Vorsäß	281	-53	15,2	26,4	**232**	**-59**	15,2	26,4	5	Tithon/Berria	(337/32)	OV 3	47,351	9,958	marls	Zementsteinsch	yes	1,014 / 1,069	94,80%	8,40%	292 / 17; 15,7° 115 / 06	163 / 59; 28,1° 267 / 87	7	Magnetite	44,7	yes	500°C	500°C			50-110mT
33	Au	**230**	**-53**	3,8	410,2	158	57	3,8	407,1	5	Oxford/Tithon	(196/59)	GA 1	47,325	9,983	carbonates	Quintener kalk	no							Mgn/He/Goe	39,8/ 251,2 1000	yes	500°C	500°C	600°C		35-80mT
Bregenzer Wald/ Sünserspitze																																
34		160	2	12,1	10,2	**159**	**-39**	12,1	10,2	16	E. Eocene	(166/41)	SS 5	47,302	9,834	marls	Schelpenserie	no							Magn/He/Go	39,8/ 281,8 1000	yes	500°C	200-400°C			20-50mT
35		335	26	8,7	60,4	**312**	**59**	8,7	60,5	6	Maastricht	(181/40)	SS 6	47,302	9,834	marls	Leimernsch.	yes	1,007 / 1,048	96,10%	5,50%	110 / 18; 4,1° 117 / 2	356 / 52; 1,5° 235 / 86	16	Magn/He/Go	39,8/ 251,2 1258,9	yes	< 600°C	600°C	600°C		10-25mT
36		**227**	**-47**	14,5	22,3	307	-35	14,5	22,3	6	Maastricht	(350/72)	SS 3	47,302	9,834	marls	Leimernsch.	yes	1,017 / 1,014	100,30%	3,10%	262 / 08; 3,7°	170 / 14; 4,4°	14	Magn/Sulf/He	31,6/ 89,1 199,5	yes	< 600°C	300-400°C			40-70mT
37		**248**	**-65**	7,1	61,7	295	-52	7,1	61,9	8	Apt	(158/30)	SS 1	47,302	9,834	carbonates	Mittagspitzsch.	no							Magn/Goeth	39,8/ 1258,9	yes	500°C	300-400°C			20-70mT
Site Nr.	**Locality**	**Dec (insitu)**	**Inc (insitu)**	**alpha95**	**K**	**Dec (abc)**	**Inc (abc)**	**alpha95**	**K**	**N**	**Lith. Age**	**Dip**	**site abbrev.**	**Latitude**	**Longitude**	**Lithology**	**Remarks**	**AMS**	**L/F**	**K=L/F**	**P=L*F**	**K1/a95 bac K1/a95 abc**	**K3/a95 bac K3/a95 abc**	**N K1/K3**	**IRM**	**B1/2 (mT)**	**IsT**	**LF-cmp/ T**	**MF-cmp/T**	**HF-cmp/T**	**Tub**	**Hcr**
Schliersee/Ostin																																
38		355	8	7,6	54,3	**356**	**49**	7,6	54,5	8	L. Ceno-Con	(171/41)	O5	47,741	11,771	carbonates	Seewerkalk	no							Magn/Goeth	22,4/ 501,2	yes	< 600°C				20-50mT
39		359	30	4,1	161,5	**348**	**62**	4	163,2	9	Barreme-Apt	(190/34)	O1	47,741	11,771	carbonates	Schrattenkalk	no							Mgn/He/Goet	44,7/ 251,2 2511,9	yes	< 600°C	>600°C	100°C/>600°C		20-100mT

3. Western Northern Calcareous Alps (western part)

Site Nr.	Locality	Dec (insitu)	Inc (insitu)	alpha95	K	Dec (abc)	Inc (abc)	alpha95	K	N	Lith. Age	Dip	site abbrev.	Latitude	Longitude	Lithology	Remarks	AMS	L/F	K=L/F	P=L*F	K1/a95 bac K1/a95 abc	K3/a95 bac K3/a95 abc	N K1/K3	IRM	B1/2 (mT)	IsT	LF-cmp/ T	MF-cmp/T	HF-cmp/T	Tub	Hcr
Muttekopf / Imst																																
40		**307**	**49**	10,9	31,5	116	69	34,5	4	7	Santonian	mean	MG	47,251	10,592	marls	Gosau	yes	1,014 / 1,023	99,10%	3,70%	n.signif.	n.signif.		Magnetite		no				200-500°C	3-30mT
		209	**-47**	15	27,1	200	32		2,2	5	Santonian	343 / 77	MG 3																			
		52	**49**	9,6	26,5	89	26	13,4	13,9	10		137 / 48	MG 4/7																			
		44	**49**	8,1	23,1	108	36	neg.FT	2,7	15		mean	MG 3/4/7						1,014 / 1,023	99,10%	3,70%	n.signif.	n.signif.									
Site Nr.	**Locality**	**Dec (insitu)**	**Inc (insitu)**	**alpha95**	**K**	**Dec (abc)**	**Inc (abc)**	**alpha95**	**K**	**N**	**Lith. Age**	**Dip**	**site abbrev.**	**Latitude**	**Longitude**	**Lithology**	**Remarks**	**AMS**	**L/F**	**K=L/F**	**P=L*F**	**K1/a95 bac K1/a95 abc**	**K3/a95 bac K3/a95 abc**	**N K1/K3**	**IRM**	**B1/2 (mT)**	**IsT**	**LF-cmp/ T**	**MF-cmp/T**	**HF-cmp/T**	**Tub**	**Hcr**
Lähnbach																																
41		58	79	4,7	265,1	**1**	**48**	4,7	264,6	5	Tithonian	346/41	LB 1	47,406	10,953	carbonates	J.Ammergau F	no							Magn/Sulf		yes	< 600°C	200°C		100-330°C	3-15mT
42		281	56	9,1	54,9	**317**	**53**	9,1	55	6	Malm	24/25	LB 2	47,406	10,953	carbonates	L.Ammergau F	no							Magn/Goeth		yes	< 600°C	600°C		300-580°C	
43		276	64	6,7	82,6	**283**	**54**	6,7	82,6	7	Malm	63/11	LB 3	47,406	10,953	carbonates	L.Ammergau F	yes	1,003 / 1,014	98,90%	1,70%	16 / 03; 9,9° 196 / 05	144 / 85; 7,8° 86 / 77	5	Magn/Hem		yes	< 600°C	650°C	650°C	300-590°C	
44		334	58	6,7	101,4	**319**	**45**	6,7	100,7	6	Oxfordian	256/52	LB 4	47,406	10,953	radiolarite	Ruhpolding F	yes	1,013 / 1,012	100,10%	2,50%	311 / 10; 10,3° 136 / 19	219 / 04; 3,1° 29 / 36	4	Magn/Goeth		yes	500°C	500°C		300-590°C	
45		341	67	5,9	88,9	**328**	**52**	6	86,4	8	E. Liassic	312/16	LB 5	47,406	10,953	carbonates	L.Allgäu Fm.	no							Magn/Goeth		yes	< 600°C	600°C	200°C	200-400°C 200-400°C	10-70mT
		46	**62**	7,5	81,3	15	60	8,5	62,9	6																						
	Lähnbach/mea	307	64	19	24,3	**313**	**52**	14,5	41,2	4 sites	E.Liass-Malm	mean	LB2-LB5	47,406	10,953																	
Site Nr.	**Locality**	**Dec (insitu)**	**Inc (insitu)**	**alpha95**	**K**	**Dec (abc)**	**Inc (abc)**	**alpha95**	**K**	**N**	**Lith. Age**	**Dip**	**site abbrev.**	**Latitude**	**Longitude**	**Lithology**	**Remarks**	**AMS**	**L/F**	**K=L/F**	**P=L*F**	**K1/a95 bac K1/a95 abc**	**K3/a95 bac K3/a95 abc**	**N K1/K3**	**IRM**	**B1/2 (mT)**	**IsT**	**LF-cmp/ T**	**MF-cmp/T**	**HF-cmp/T**	**Tub**	**Hcr**
Kotbach																																
46		**26**	**56**	14,1	30,3	173	32	14,1	30,2	5	Albian/100Ma	186/89	KB 2/3	47,394	11,016	magm. dyke	Ehrwaldit	yes	1,012 / 1,005	100,70%	1,70%	61 / 37; 12,5° 139 / 27	350 / 24; 33,6° 218 / 63	4	Magnetite		yes	< 600°C			200-550°C	
		350	-39	17,6	28,4	**168**	**-48**	17,6	28,3	4																						20-50mT
47		41	-38	11,8	33,3	**47**	**48**	11,8	33,3	6	Tithonian	11/84	KB 4	47,394	11,016	carbonates	Ammergau F.	no							Mgn/He		yes	< 600°C	>600°C	>600°C	300-530°C	
48		20	-28	4	278,3	**28**	**50**	4	279	6	Oxfordian	181/82	KB 1	47,394	11,016	radiolarite	Ruhpolding F	no							Mgn/He	20/ 316,2	no				300-550°C	

4. Western Northern Calcareous Alps (eastern part)

Site Nr.	Locality	Dec (insitu)	Inc (insitu)	alpha95	K	Dec (abc)	Inc (abc)	alpha95	K	N	Lith. Age	Dip	site abbrev.	Latitude	Longitude	Lithology	Remarks	AMS	L/F	K=L/F	P=L*F	K1/a95 bac K1/a95 abc	K3/a95 bac K3/a95 abc	N K1/K3	IRM	B1/2 (mT)	lsT	LF-cmp/ T	MF-cmp/T	HF-cmp/T	Tub	Hcr
	Lower Inn Valley																															
49	Oberangerbg	**321**	**43**	13,2	21,8	150	3	14	19,5	7	Chattian	mean	OA	47,458	11,904	sandstone	Ob.angerbg.Fm	yes	1,034 / 1,041	99,30%	7,60%	260 / 06; 8,5°	168 / 21; 7,4°	4	Mgn/He		yes	< 600°C	>600°C	>600°C	300-450°C	6-12mT
50	Unterangerbg	**316**	**49**	11,8	23	255	26	11,8	23,1	8	L. Rupelian	210/68	UAN 3/4	47,499	12,058	siltstone	Ut.angerbg.Fm	yes/ UAN4	1,007 / 1,052	95,70%	5,90%	200 / 72; 20,7°	26 / 19; 4,2°	6	Magn/Sulf	39,8	yes	< 600°C	300-400°C		200-400°C	
		196	30	14,6	12	**195**	**-36**	14,6	12	10		210/68	UAN 2/3/4					yes/ UAN2	1,009 / 1,054	95,70%	6,30%	n. signif.	23 / 28; 3,2° 253 / 82	6							200-400°C	15-50mT
51	Unterangerbg	249	-46	18,6	13,9	**199**	**-45**	18,6	14	6	L. Rupelian	315/45	OA 2	47,499	12,058	siltstone	Ut.angerbg.Fm	yes	1,004 / 1,037	96,80%	4,10%	n. signif.	131 / 58; 4,1° 324 / 77	5	Magn/Sulf		no					15-30mT
52	Häring	**307**	**54**	9,5	18,3	308	15	9,7	17,7	14	Rupelian	310 / 40	ZM	47,501	12,124	marls	Paisslbg Fm	yes	1,019 / 1,024	99,50%	4,30%	285 / 43; 11,3°	102 / 47; 17,3°	5	Magn/Sulf		no					3-15mT
53	Bruckhäusl	**244**	**-42**	4,1	80,4	271	-81	4,4	72,3	16	E. Rupelian	236/40	BH	47,495	12,101	carbonates	Werlbg. Mb	no							Magnetite	39,8	yes	< 600°C			300-500°C	20-70mT
54	Gfallermühle	**333**	**37**	15,2	20,3	152	57	28,9	6,3	6	Priabonian	mean	GF1 / 2	47,634	12,166	carbonates	Oberaudorf F	no							Magnetite		no				150-400°C	3-40mT
		14	**61**	15,2	26,2	145	59	33,9	6	5		mean	GF1 / 2																			
		101	29		3,6	**20**	**39**	19,4	16,5	5		mean	GF1 / 2																			
		1	**54**	SCF 76%	CircAp 102°	125	69	SCF 75%	CircAp 104°	15		mean	GF1 / 2																			
55	Sebi	**332**	**59**	8,7	41,2	223	56	11,7	23,2	8	Eocene	mean	SB1/2/3	47,648	12,236	marls	Gosau	no							Magnetite		no					3-30mT
		32	**53**	10,7	24	59	82	29,3	4	9		mean																				3-30mT
56	Sebi	**27**	**53**	15,6	19,3	287	85	16,9	16,6	6	Maastricht.	220 / 39	SBM	47,649	12,235	carbonates	Gosau	no							Magnetite		no				200-450°C	
57	Mühlbergerb.	278	64	10,3	56,3	**323**	**37**	10,3	56,3	5	Camp/Maast	355/42	MBB 1	47,68	12,42	marls	Gosau	yes	1,023 / 1,118	91,50%	14,30%	277 / 18; 14,4° 286 / 05	174 / 32; 14,1° 173 / 74	5	Magn/Hemat		no				550-625°C	
58	Hechtsee	**17**	**56**	14,6	28,2	170	78	14,7	28,1	5	Campanian	190 / 45	IHG	47,612	12,171	siltstone	Gosau	yes	1,024 / 1,039	98,50%	6,40%	261 / 11; 6,5°	3 / 50; 13,1°	5	Magn/Sulf		no					5-20mT
59	Schwoich	**326**	**51**	10,2	17,4	323	30	12,7	11,6	13	L. Campanian	320 / 20	SZM/NS	47,542	12,164	marls	Gosau	yes	1,017 / 1,028	98,90%	4,50%	64 / 03; 5,1°	161 / 68; 5,8°	6	Magn/Sulf		no				200-500°C	
60	Mühlbach	**334**	**48**	9,9	24,5	273	67	11,3	19,2	10	L. Santonian	175 / 36	NF	47,501	11,915	marls	Gosau	yes	1,015 / 1,027	98,80%	4,20%	96 / 12; 5,0°	343 / 63; 5,5°	23	Magnetite		no				200-500°C	
		12	15	8,9	27	**19**	**49**	8,9	27	11												101 / 03	205 / 79									
		337	20	11,3	43,2	**328**	**52**	7	62,8	8																						
61	Mösl	**339**	**57**	9,7	33,6	291	77	8,5	43,4	8	E.Santonian	190 / 40	IMG	47,503	11,897	marls	Gosau														200-450°C	
		18	9	9,1	72,3	**20**	**48**	9,1	72,1	5																					500-580°C	
62	Niederndorf	**56**	**53**	6,9	77,6	25	42	6,9	77,7	7	Cenomanian	331/30	ND	47,653	12,208	carbonates	Branderfl F.	no							Mag/Hemat		no				600-680°C	
63	Kurz	34	11	6,1	122,4	**133**	**-57**	6,1	122,4	6	Aptian/Albian	202/48	KZ	47,616	12,155	carbonates	Tannheim F.	yes	1,009 / 1,008	100,10%	1,70%	282 / 01; 14,6°	n.signif.	5	Magnetite		no				300-550°C	

Site Nr.	Locality	Dec (insitu)	Inc (insitu)	alpha95	K	Dec (abc)	Inc (abc)	alpha95	K	N	Lith. Age	Dip	site abbrev.	Latitude	Longitude	Lithology	Remarks	AMS	L/F	K=L/F	P=L*F	K1/a95 bac K1/a95 abc	K3/a95 bac K3/a95 abc	N K1/K3	IRM	B1/2 (mT)	lsT	LF-cmp/ T	MF-cmp/T	HF-cmp/T	Tub	Hcr
	Guffert																															
64		**59**	**59**	11,6	44,8	117	35	11,6	44,5	5	Malm	155/52	GU 7	47,581	11,764	carbonates	U.Ammergau F	no							Magnetite		no					5-20mT
65		**21**	**24**	5,8	135	107	71	5,8	135,2	6	Malm	181/70	GU 6	47,581	11,764	carbonates	L.Ammergau F	no							Magn/He/Go		no				200-645°C	
66		**2**	**25**	13,1	35	52	53	13,1	34,9	5	Oxfordian	140/59	GU 4	47,581	11,764	radiolarite	Ruhpolding F	no							Magnetite		no					10-60mT
67		**30**	**40**	7	119,5	103	41	7	119	5	Dogger	157/70	GU 3	47,581	11,764	carbonates	Klauskalk Fm.	no							Magn/He/Go	31,6/ 251,2 1000	no				200-550°C	
68		**359**	**32**	12,9	22,8	111	75	12,9	22,7	7	Liassic	165/66	GU 2	47,581	11,764	carbonates	Adnet Fm.	no							Magn/Goeth	35,5/ 631 1000	no				200-500°C	
69		236	8	11,6	23,9	**69**	**40**	11,5	24	8	L.Triassic	200/62	GU 1	47,581	11,764	carbonates	Kössen Fm	no							Magnetite		no					5-50mT
	Guffert/mean	**18**	**38**	22	13,1	98	57	22,7	12,3	5 sites	Liassic-Malm	mean	GU 7/6/4/3/2	47,581	11,764																	

Site Nr.	Locality	Dec (insitu)	Inc (insitu)	alpha95	K	Dec (abc)	Inc (abc)	alpha95	K	N	Lith. Age	Dip	site abbrev.	Latitude	Longitude	Lithology	Remarks	AMS	L/F	K=L/F	P=L*F	K1/a95 bac K1/a95 abc	K3/a95 bac K3/a95 abc	N K1/K3	IRM	B1/2 (mT)	lsT	LF-cmp/ T	MF-cmp/T	HF-cmp/T	Tub	Hcr
	Ampelsbach																															
70		**72**	**55**	15,4	25,8	218	29	15,4	25,8	5	Neocom	178/65	AB 7	47,571	11,766	carbonates	Schrambach F	yes	1,028 / 1,104	93,10%	13,50%	289 / 03; 12,0°	17 / 25; 11,8°	5	Magnetite		no				200-450°C	
71		**73**	**67**	12	26,4	205	28	12	26,4	7	Malm	178/65	AB 8	47,571	11,766	carbonates	U.Ammergau	no							Magnetite		no				200-450°C	
72		**129 / 102**	**67 / 63**	10,3	55,7	206	15	10,3	55,7	5	Malm	141/49	AB 9	47,571	11,766	carbonates	L.Ammergau	no							Magnetite		no					10-40mT
73		**330 / 24**	**73 / 53**	9	56,3	208	55	9	56,3	6	Oxfordian	141/49	AB 6	47,571	11,766	radiolarite	Chiemgau Fm	no							Magnetite		no				200-525°C	
74		**126 / 87**	**72 / 66**	15	20,8	206	22	15	20,8	6	L. Toarcian	141/49	AB 5	47,571	11,766	carbonates	M. Allgäu Fm	yes	1,008 / 1,006	100,20%	1,40%	88 / 15; 5,4°	206 / 60; 12,5°	4	Magnetite		no				300-550°C	
75		**51**	**72**	12,6	29,3	198	34	12,6	29,3	6	Liassic	178/65	AB 4	47,571	11,766	carbonates	Scheibelbg F	no							Magnetite		no				200-525°C	5-30mT
76		**17 / 43**	**65 / 41**	6,9	125,5	235	49	6,9	125,5	5	Liassic	141/49	AB 3	47,571	11,766	carbonates	L.Allgäu Fm	no							Magnetite		no				100-300°C	
	Abmeaninsitu	**67**	**74**	14,3	18,9					7 sites	Liassic-Neoc	mean	AB	47,571	11,766																	
	ABmean 1.Cr	**61**	**62**	13	22,4	210	33	13,1	22,2	7 sites	Liassic-Neoc	mean	AB																			
	Thiersee	**39**	**54**	SCF55%	CircAp 66°	194	50	SCF76%	CircAp 106°	12 sites	Liassic-Neoc	mean	AB/GU																			

5. Central Northern Calcareous Alps

Site Nr.	Locality	Dec (insitu)	Inc (insitu)	alpha95	K	Dec (abc)	Inc (abc)	alpha95	K	N	Lith. Age	Dip	site abbrev.	Latitude	Longitude	Lithology	Remarks	AMS	L/F	K=L/F	P=L*F	K1/a95 bac K1/a95 abc	K3/a95 bac K3/a95 abc	N K1/K3	IRM	B1/2 (mT)	lsT	LF-cmp/ T	MF-cmp/T	HF-cmp/T	Tub	Hcr
Strobl a. Wolfgangsee																																
77	Weißenbach	325	59	5	147,8	27	47	5	147,8	7	E. Santonian	73/43	WB	47,699	13,491	carbonates	Grabenbach F	no							Magnetite		no				400-525°C	
78	Wirling	332	46	8,7	60,6	23	39	8,7	60,8	6	E. Santonian	81/51	WG	47,725	13,563	carbonates	Grabenbach F	no							Magnetite		no					30-90mT
79	Gall	**61**	**62**	14,7	17,8	207	-31	14,7	17,8	7	Coniacian	38/33 (ov.)	GA 1	47,712	13,512	carbonates	Schmalnau Fm	no							Magnetite		no					3-30mT
80	Gall	**50**	**55**	9,5	50,5	53	42	9,5	50,4	6	Coniacian	65/13	GA 2	47,712	13,512	carbonates	Schmalnau Fm	no							Magnetite		no					5-30mT
Site Nr.	**Locality**	**Dec (insitu)**	**Inc (insitu)**	**alpha95**	**K**	**Dec (abc)**	**Inc (abc)**	**alpha95**	**K**	**N**	**Lith. Age**	**Dip**	**site abbrev.**	**Latitude**	**Longitude**	**Lithology**	**Remarks**	**AMS**	**L/F**	**K=L/F**	**P=L*F**	**K1/a95 bac K1/a95 abc**	**K3/a95 bac K3/a95 abc**	**N K1/K3**	**IRM**	**B1/2 (mT)**	**lsT**	**LF-cmp/ T**	**MF-cmp/T**	**HF-cmp/T**	**Tub**	**Hcr**
	Kohlstatt																															
81		333	69	4,3	320,1	**340**	**48**	4,3	319,9	5	Neocom	348/21	KS 6	47,632	12,403	carbonates	Schrambach F	yes	1,026 / 1,018	100,80%	4,40%	n. signif.	n. signif.		Magn/Hemat		no				200-450°C	
82		316	43	7,2	113,3	**330**	**46**	7,2	113,3	7	Malm	82/19	KS 5	47,632	12,403	carbonates	Ammergau Fm	no							Magn/Hemat		no				200-500°C	
83		247	56	6,8	80,9	**327**	**38**	6,8	80,9	7	Malm	354/56	KS 4	47,632	12,403	carbonates	Ammergau Fm	no							Magnetite		no				400-525°C	
84		212	79	5,4	127,7	**358**	**58**	5,3	128,5	7	Dogger	7/42	KS 3	47,632	12,403	carbonates	Klauskalk	no							Magn/Hemat		no				550-660°C	
85		332	62	6,1	122,3	**350**	**46**	6,1	122,3	6	Liassic	5/18	KS 2	47,632	12,403	carbonates	Scheibelbg. Fm	no							Mgn/He/Goet		no				300-500°C	
86		265	62	3,5	358,5	**349**	**57**	3,5	358,1	6	Rhaetian	30/42	KS 1	47,632	12,403	carbonates	Eiberg Mb.	no							Magnetite		no				200-475°C	
	Kohlstatt/mear	293	68	19,2	13,1	**341**	**49**	9,1	54,8	6 sites	Rhaet-Neoc	mean	KS	47,632	12,403																	
Site Nr.	**Locality**	**Dec (insitu)**	**Inc (insitu)**	**alpha95**	**K**	**Dec (abc)**	**Inc (abc)**	**alpha95**	**K**	**N**	**Lith. Age**	**Dip**	**site abbrev.**	**Latitude**	**Longitude**	**Lithology**	**Remarks**	**AMS**	**L/F**	**K=L/F**	**P=L*F**	**K1/a95 bac K1/a95 abc**	**K3/a95 bac K3/a95 abc**	**N K1/K3**	**IRM**	**B1/2 (mT)**	**lsT**	**LF-cmp/ T**	**MF-cmp/T**	**HF-cmp/T**	**Tub**	**Hcr**
	Unken																															
87		**20**	**57**	6,3	78,4	38	49	6,3	79	8	Tithonian	87/16	UK 5	47,637	12,609	carbonates	Ammergau F	no							Magnetite		no				200-360°C	
88		**21**	**40**	5,7	82,2	6	17	5,7	83	9	Oxfordian	324/35	UK 4	47,637	12,609	radiolarite	Ruhpolding F	no							Magn/ Hemat		no				300-550°C	
89		**30**	**53**	8,6	62,1	37	31	9	56,9	6	Sin.-Plien.	54/ 29	UK 3	47,637	12,609	carbonates	Scheibelbg. F	no							Magnetite		no				200-400°C	
90		**10**	**58**	6,5	74,5	22	44	6,5	74,5	8	Hettangian	52/17	UK 2	47,637	12,609	carbonates	Hierlatz K.	no							Magnetite		no				200-400°C	
91		**2**	**61**	3,1	281,4	25	40	3,1	281,2	9	Rhaetian	55/27	UK 1	47,637	12,609	carbonates	Eiberg Mb.	no							Magnetite		no				200-500°C	
	Unken/mean	**18**	**54**	9,7	62,8	25	37	16	23,9	5 sites	Rhaet-Tithon	mean	UK 5- UK 1	47,637	12,609																	

6. Central Alps (Eastern Alps)

Site Nr.	Locality	Dec (insitu)	Inc (insitu)	alpha95	K	Dec (abc)	Inc (abc)	alpha95	K	N	Lith. Age	Dip	site abbrev.	Latitude	Longitude	Lithology	Remarks	AMS	L/F	K=L/F	P=L*F	K1/a95 bac K1/a95 abc	K3/a95 bac K3/a95 abc	N K1/K3	IRM	B1/2 (mT)	IsT	LF-cmp/ T	MF-cmp/T	HF-cmp/T	Tub	Hcr
92	Hintergrat	**335**	**56**	3,2	67					30	E.Oligocene		HG	46,502	10,577	basaltic dyke	32Ma	yes	1,010 / 1,024	98,60%	3,40%	341 / 26; 9,1°	249 / 04; 5,6°	10	Maghemite		yes	400-600°C	400-600°C		200-500°C	
93	Gran Cebru	**316**	**60**	9,9	24,6					10	E.Oligocene		AZ/IZ	46,486	10,589	basaltic dyke	32Ma	yes	1,008 / 1,032	97,70%	4,00%	162 / 24; 26,0°	251 / 10; 10,3°	7	Maghemite		yes	< 600°C			200-560°C	
94	Schaubach H.	**19**	**64**	9,6	49,7					6	Permo-Skyth		SBH	46,488	10,605	conglomer.	Alp. Verruc	yes	1,105 / 1,052	105,00%	16,20%	315 /39; 5,0°	108 / 47; 5,9°	6	Magnetite		no					5-50mT
95	Serles	**319**	**14**	7,7	75,9	318	39	7,8	74,5	6	Permoskyth.	144 / 25	BS	47,124	11,361	sandstone	Alp. Verruc	yes	1,133 / 1,177	96,30%	33,60%	134 / 10; 3,2°	28 / 58; 7,7°	9	Magn/Magh	15,8/ 125,9	yes	500-600°C	500-600°C	500-600°C	200-500°C	
96	Kropfraderj.	**319** **49**	**54** **48**	13,6 SCF 89%	32,8 SpAp 116°					5 7	Paleozoic		KJ	47,433	12,097	diabas	Greywacke								Magnetite		yes				200-575°C 200-575°C	
97	Hochstegen	**327** **4**	**63** **61**	8,2 6,6	88,4 135,2					5 5	Malmian		HST	47,157	11,844	marble	Hochstegen F	no							Ti-Magnetite		no				200-360°C 200-360°C	

7. Southern Alps

Site Nr.	Locality	Dec (insitu)	Inc (insitu)	alpha95	K	Dec (abc)	Inc (abc)	alpha95	K	N	Lith. Age	Dip	site abbrev.	Latitude	Longitude	Lithology	Remarks	AMS	L/F	K=L/F	P=L*F	K1/a95 bac K1/a95 abc	K3/a95 bac K3/a95 abc	N K1/K3	IRM	B1/2 (mT)	IsT	LF-cmp/ T	MF-cmp/T	HF-cmp/T	Tub	Hcr
	Nonsberg syncline																															
98	Revo	350	60	13,9	31,2	**340**	**57**	13,9	31,2	5	E-M.Eocene	280/07	RV 1	46,391	11,066	carbonates	Pte. Pia Fm.	no							Magn/Goeth	39,8/ 1584,9	no				3-40mT	
99	Revo	**6**	**56**	2,1	375,3	355	33	2,1	374,1	14	L.Cretaceous	334/25	RV 3	46,389	11,066	carbonates	Scaglia rossa	yes	1,009 / 1,102	91,60%	11,20%	235 / 03; 2,8°	126 / 83; 1,2°	12	Magn/Hemat	35,5/ 316,2	no				200-500°C	
	Dolomites/magm.dykes																															
100	Fischleintal	**231**	**-44**	14	14,5					9	E.Rupelian		FT	46,655	12,367	magm. dyke	34Ma	yes	1,008 / 1,008	100%	1,60%	n. signif.	n. signif.		Magnetite	20	yes	500°C			400-560°C	
101	FT Nebengest	**199**	**-45**	8,1	90,5	211	-43	8,1	90,1	5	Ladin	104/13	FTNG	46,655	12,367	carbonates	Schlerndolm	no							Ti-Mgn/Sulf/Go		yes	0-200°C	0-200°C	0-200°C	200-400°C	20-100mT
102	Braida freida	**156** **151** 149	**-55** **-56** -25	5,9 6,3 11,3	78,1 54 29,6	190 184 **158**	-66 -69 **-42**	5,9 6,3 11,3	78,2 54 29,3	9 11 7	L. Cretaceous	113/21	BF	46,551	11,898	magm. dyke	68Ma	yes	1,004 / 1,005	99,90%	0,90%	n. signif.	339 / 73; 18,8° 59 / 75	6	Magnetite	50,1	yes	< 600°C			150-400°C 400-575°C 400-575°C	20-50mT 20-50mT
103	BF Nebengest	**155**	**-44**	6,6	83,8	176	-57	6,6	83,6	7	L. Ladinian	113/21	BFNG	46,551	11,898	volcanoclstic	Wengen Fm	yes	1,005 / 1,015	99,00%	2,00%	n. signif.	285 / 63; 17,5°	5	Mag/Sulf/ He	141,3/ 251,2	yes	< 600°C 200-300°C	300-400°C	300-400°C 600°C	200-590°C	10-100mT
	Dolomites/Alpe Ra Stua																															
104		**28**	**67**	3,8	256,3	341	27	3,8	258	7	Albian-Turon	317/53	RA 9	46,629	12,101	carbonates	Ruoibes Fm	yes	1,007 / 1,055	95,40%	6,20%	332 / 61; 7,4°	136 / 28; 5,5°	3	Magn/ Hemat Goethite	50,1/ 199,5 794,3	yes	< 600°C	>620°C	>620°C	400-590°C	
105		358	63	10,5	33,7	357	56	10,6	33,6	7	Albian	351/07	RA 8	46,629	12,101	sandstone	Rastua Flysch	yes	1,016 / 1,011	100,50%	2,70%	322 / 12; 3,5°	231 / 05; 4,7°	9	Magn/He	39,8/ 316,2	yes	< 600°C	620°C		400-590°C	
106		360	47	7,4	67,5	358	38	7,4	67,5	6	Aptian/Albian	348/09	RA 7	46,629	12,101	carbonates	cherty red carb	yes	1,027 / 1,038	98,90%	6,60%	345 / 07; 4,4°	224 / 78; 12,9°	10	Magn/Goeth	50,1/ 1258,9	yes	< 600°C	< 600°C		300-590°C	
107		**160**	**-30**	11	49,5	155	-24	11	49,2	6	Haut/Barrem	283/10	RA 6	46,629	12,101	marls	Puez Fm.	yes	1,031 / 1,082	95,30%	11,60%	336 / 05; 4,4°	136 / 85; 4,8°	9	Magn/Goeth	31,6/ 631,0	yes	< 600°C	< 600°C		400-590°C	
108		**142**	**-37**	12,1	31,7	136	-24	11,3	36,3	6	Haut/Barrem	280/16	RA 5	46,629	12,101	carbonates	silty red carb	yes	1,016 / 1,105	91,90%	12,30%	335 / 06; 4,6°	79 / 68; 13,6°	9	Magn/Goeth	39,8/ 631,0	yes	< 600°C	< 600°C		500-590°C	
109		**134** **28**	**-44** **45**	17,1 12,8	13,4 23	134 9	-35 46	17,6 12,9	12,8 23	7 7	Haut/Barrem	314/13	RA 4	46,629	12,101	carbonates	silty red carb	yes	1,018 / 1,057	96,30%	7,60%	335 / 19; 7,8°	119 / 67; 6,5°	9	Magn/Sulf	44,7/ 125,9	yes	550°C	200-400°C		400-590°C 100-360°C	
110		**140** **28**	**-49** **45**	9,7 8,4	17,9 44,5	134 15	-42 48	9,9 8,4	17,3 44,5	14 8	Berria/Valang	277/12	RA 3	46,629	12,101	carbonates	Maiolica Fm.	no							Magn/Hemat	31,6/ 316,2	yes	550°C			530-590°C	10-50mT 3-10mT
111		**129**	**-33**	3,3	330,9	127	-21	3,3	329,3	7	Dogger/Malm	289/12	RA 2	46,629	12,101	carbonates	Rosso Ammo	yes	1,004 / 1,003	100,10%	0,70%	n. signif.	n. signif.		Magn/Goeth	39,8/ 501,2	yes	550°C			530-590°C	
	A.Rast/mean	**141** **26**	**-39** **55**	11,8 17,3	43,2 51,5	137 360	-30 41	12,4 28,5	39,3 19,8	5 sites 3sites	Malm/Barre Berrias/Turon	mean mean	RA6-RA2 RA9/4/3	46,629	12,101																	
	Paleozoic basement																															
112	Ultental	**287**	**11**	6	165,6					5	L.E. Permian		UT	46,561	11,098	basaltic dyke	275 Ma	yes	1,011 / 1,017	99,40%	2,80%	322 / 20; 12,5°	189 / 63; 28,1°	4	Magnetite		yes	< 600°C	< 600°C		200-600°C	
113	UT Nebengest	**333**	**58**	10,1	58,5					5	Permian		UTNG	46,561	11,098	granite									Ti-Magn		no				200-360°C	

8. South Alpine Foreland Basin and Mesozoic basement units

Site Nr.	Locality	Dec (insitu)	Inc (insitu)	alpha95	K	Dec (abc)	Inc (abc)	alpha95	K	N	Lith. Age	Dip	site abbrev.	Latitude	Longitude	Lithology	Remarks	AMS	L/F	K=L/F	P=L*F	K1/a95 bac K1/a95 abc	K3/a95 bac K3/a95 abc	N K1/K3	IRM	B1/2 (mT)	IsT	LF-cmp/ T	MF-cmp/T	HF-cmp/T	Tub	Hcr
	Gardasee																															
114		**136**	**-37**	19,1	10,9	136	-16	19,1	10,9	7	Aquitan	317/21	GA 10	45,873	10,854	sandstone	U. Mt. Brione	yes	1,024 / 1,011	101,30%	3,50%	210 / 19; 11,5°	n. signif.	8	Magn/Goeth	39,8/ 631,0	yes	< 600°C	< 600°C			3-30mT
115		17	61	7,3	40,4	**355**	**51**	7,2	40,6	11	Chattian	309/18	GA 11	45,874	10,855	sandstone	L. Mt. Brione	yes	1,006 / 1,006	100%	1,20%	245 / 06; 18,9°	n. signif.	8	Magn/Goeth	39,8/ 631,0	yes	< 600°C	< 600°C			3-30mT
116		64 4	59 55	4,9 5,4	128,1 154,7	**29** **349**	**60** **40**	4,9 5,4	128,1 154,8	8 6	L. E. Rupelian	313/20	GA 9	45,889	10,867	carbonates	Linfano Fm.	no							Ti-Magn/He Goethite	39,8/ 199,5 2511,9	yes	300-400°C		100°C/>600°C		3-50mT 3-50mT
117		48	53	13	22,6	**3**	**63**	13	22,6	7	E. L. Eocene	277/28	GA 8	45,876	10,885	carbonates	Nago Fm.	no							Mgn/Goeth	44,7/ 1778,3	no					3-50mT
118		221	-41	5,1	104,1	**192**	**-32**	5,1	104,5	9	L. M. Eocene	311/28	GA 7	45,871	10,876	tuffite	Nago	yes	1,012 / 1,030	98,30%	4,20%	66 / 01; 14,6°	151 / 58; 11,2°	7	Magnetite	20	no					20-100mT
119		180	-44	3,8	120,4	**175**	**-30**	3,8	119,9	13	L. M. Eocene	335/15	GA 12	45,784	10,901	tuff	Mt. Baldo	yes	1,009 / 1,020	98,90%	2,90%	115 / 01; 3,6°	208 / 75; 3,4°	15	Magn/Goeth	39,8/ 631,0	no					10-100mT
120		226	-61	7,6	79,6	**177**	**-48**	7,6	79,6	6	E. M. Eocene	311/35	GA 6	45,868	10,876	carbonates	Torbole Fm.	no							Magn/Goeth	31,6/ 1995,3	no					20-50mT
121		348 18	71 66	6,5 2,8	41,1 156,2	**323** **337**	**40** **43**	6,5 2,8	41,1 156,7	13 18	Campan	304/35	GA 5	45,868	10,876	carbonates	Scaglia rossa	no							Ti-Magn/He Goethite	38,9/ 316,2 1000	no				150-250°C 450-600°C	
122		190 17	-76 67	9 3,2	30 136,1	**140** **334**	**-51** **47**	9 3,2	30 135,7	10 16	Campan	299/32	GA 4	45,871	10,887	carbonates	Scaglia rossa	yes	1,011 / 1,015	99,60%	2,60%	n. signif.	159 / 78; 10,5° 280 / 66	20	Ti-Magne/He Goethite	28,2/ 316,2 1995,3	no				200-300°C 525-595°C	
123		139	61	8,9	34,4	**123**	**-31**	8,9	34,5	9	Malm	284/33	GA 2	45,876	10,903	carbonates	Maiolica Fm.	no							Magn/Goeth	31,6/ 501,2	no					20-60mT
124		21	84	13,4	25,8	**319**	**63**	13,4	25,8	6	Lias	307/25	GA 1	45,871	10,891	carbonates	Ronzo Fm.	no							Magn/Goeth	35,5/ 1000	no					3-30mT
Site Nr.	**Locality**	**Dec (insitu)**	**Inc (insitu)**	**alpha95**	**K**	**Dec (abc)**	**Inc (abc)**	**alpha95**	**K**	**N**	**Lith. Age**	**Dip**	**site abbrev.**	**Latitude**	**Longitude**	**Lithology**	**Remarks**	**AMS**	**L/F**	**K=L/F**	**P=L*F**	**K1/a95 bac K1/a95 abc**	**K3/a95 bac K3/a95 abc**	**N K1/K3**	**IRM**	**B1/2 (mT)**	**IsT**	**LF-cmp/ T**	**MF-cmp/T**	**HF-cmp/T**	**Tub**	**Hcr**
	Belluno																															
125		**345**	**42**	17,7	19,7	354	45	17,7	19,6	5	Langhian	94/10	BE 14	46,106	12,028	marls	Monfumo Fm.	yes	1,012 / 1,016	99,60%	2,80%	79 / 03; 3,5°	263 / 86; 4,1°	11	Magn/Goeth	39,8/ 631,0	yes	< 600°C	< 600°C			6-20mT
126		**7**	**50**	12,3	30,8	3	29	12,3	30,7	6	E.Burdigalian	353/21	BE 11	46,152	12,0164	marls	Bolago Fm.	yes	1,008 / 1,037	97,20%	4,50%	252 / 07; 5,6°	128 / 77; 2,8°	12	Magn/Goeth	39,8/ 631,0	yes	< 600°C	< 600°C			6-20mT
127		**335**	**51**	13,2	21,9	336	26	13,2	21,9	7	E. Rupelian	336/25	BE 15	46,112	12,11	sandstone	Curzoi Sdst.	yes	1,010 / 1,004	100,60%	1,40%	146 / 56; 6,1°	330 / 33; 5,5°	13	Magn/Goeth	44,7/ 794,3	yes	< 600°C	< 600°C			3-20mT
128		**4** **333** 324	**34** **42** 5	7,6 11,1 11	46,3 69 49,8	69 163 **318**	65 84 **48**	7,7 11,1 11	46,2 69,5 49,5	9 4 5	E. Eocene	154/54	BE 7	46,155	12,125	sandstone	Belluno Flysc	yes	1,007 / 1,006	100,10%	1,30%	72 / 01; 2,2° 250 / 06	344 / 79; 6,4° 152 / 47	18	Magn/Hemat	35,5/ 251,2	no					3-30mT 3-60mT 10-80mT
129		**216**	**-32**	13,8	20,2	210	-17	13,8	20,2	7	E. Eocene	352/19	BE 18	46,042	12,141	carbonates	Scaglia ciner	yes	1,009 / 1,024	98,50%	3,30%	269 / 06; 5,3°	154 / 74; 7,3°	14	Magn/He/Go	35,5/ 231,8 1995,3	no				300-500°C	
130		**354**	**55**	9,9	46,7	353	41	9,9	46,8	6	L.Maastricht	350/14	BE 17	46,04	12,141	carbonates	Scaglia rossa	yes	1,009 / 1,031	97,90%	4,00%	289 / 05; 9,5°	173 / 79; 5,5°	14	Magn/Hemat	35,5/ 281,8	no					3-20mT
131		**328**	**48**	14	30,9	205	64	14	30,8	5	Maastricht	170/61	BE 6	46,157	12,089	carbonates	Scaglia rossa	yes	1,011 / 1,033	97,90%	4,40%	242 / 24; 4,9°	348 / 31; 3,6°	13	Magn/He/Go	56,2/ 251,2 1258,9	no				200-500°C	
132		328	-40	9	46,2	**338**	**61**	9	46,2	7	Campan	317/77	BE 5	46,158	12,088	carbonates	Scaglia rossa	yes	1,008 / 1,079	93,40%	8,80%	228 / 50; 3,9° 277 / 09	318 / 00; 2,0° 145 / 76	14	Magn/Goeth	63,1/ 501,2	no				500-575°C	
133		351 333	-5 -35	6,3 7,2	115,7 52,8	**35** **335**	**61** **50**	6,2 7,1	116,1 53	6 9	Campan	143/86	BE 4	46,158	12,088	carbonates	Scaglia rossa	yes	1,013 / 1,057	95,80%	7,10%	239 / 30; 5,1° 204 / 08	144 / 09; 3,9° 332 / 77	12	Magn/He/Go	28,2/ 251,2 1412,5	no				300-500°C 500-575°C	
134		331	-40	8,7	59,7	**331**	**44**	8,8	59,5	6	Coniac/Santon	145/84	BE 3	46,158	12,088	carbonates	Scaglia rossa	no							Magn/He/Go	31,6/ 316,2 501,2	no				300-550°C	
135		114	41	14,1	23,4	**120**	**-29**	14,1	23,5	6	Malm-E.Creat	150/79	BE 2	46,159	12,084	carbonates	Maiolica Fm.	no							Magn/Sulf/G	28,2/ 79,4 794,3	no				400-550°C	20-80mT
136		138	44	16,3	17,8	**140**	**-35**	16,3	17,8	6	Malm	150/80	BE 1	46,159	12,084	carbonates	Rosso Ammo	no							Magn/Goeth	31,6/ 2238,7	no				300-500°C	
Site Nr.	**Locality**	**Dec (insitu)**	**Inc (insitu)**	**alpha95**	**K**	**Dec (abc)**	**Inc (abc)**	**alpha95**	**K**	**N**	**Lith. Age**	**Dip**	**site abbrev.**	**Latitude**	**Longitude**	**Lithology**	**Remarks**	**AMS**	**L/F**	**K=L/F**	**P=L*F**	**K1/a95 bac K1/a95 abc**	**K3/a95 bac K3/a95 abc**	**N K1/K3**	**IRM**	**B1/2 (mT)**	**IsT**	**LF-cmp/ T**	**MF-cmp/T**	**HF-cmp/T**	**Tub**	**Hcr**
	Follina																															
137		346 **338**	24 **59**	7,7 10,4	40,7 34,9	19 154	77 65	7,7 10,4	40,8 35	10 7	Messinian	156/56	FO 13	45,938	12,192	sandstone	Montello cgl.	no							Magn/Sulf	35,5/ 141,3	yes	< 600°C	< 600°C	300-400°C		15-60mT 3-15mT
138		149	18	13,2	18,6	**147**	**-44**	13,4	18,1	8	Tortonian	157/62	FO 12	45,941	12,189	sndst/congl	M. Piai congl	no							Magnetite	39,8	yes	< 600°C	< 600°C			20-60mT
139		**308** 158	**61** 10	12 7,9	31,9 95,4	179 **159**	51 **-52**	12 7,9	31,9 95,2	6 5	Tortonian	157/62	FO 11	45,941	12,189	sndst/congl	M. Piai congl	no							Magnetite/Sulf	25,1/ 79,4	yes	< 600°C	< 600°C 200-300°C			3-12mT 20-40mT
140		160	32	13,2	16,2	**161**	**-43**	13,2	16,2	9	Serravallian	154/75	FO 10	45,944	12,185	marls	Tarzo Fm.	no							Magn/Goeth	39,8/ 794,3	yes	< 600°C	< 600°C			15-40mT

Locality Nr.	Locality	Age of ChRM	N	Dec of ChRM	Inc of ChRM	K	alpha95	reference
	Stable Adria							
23	Gargano	Turon-Senon	21sites	328	38	21	4	Vandenberg (1983)
22	Murge	Cenom.-Senon	12sites	327	40	42	7	Marton and Nardi (1994)
12	Voltri, Liguria	L. Eoc.-E. Oligo.	33 samples	333,2	50,3		5,8	Vandenberg (1979)
11	Ramero-Garb.	L. Oligo.-E.Mioc.	10 sites	318	38	62,3	5,5	Hong Kie (1988)
10	Turin mountains	mid E.Miocene	51 samples	340,8	46,7		9	Bormioli and Lanza (1994)
16	Istria	E.-L. Cretac.	3localities	318	44	56	17	Marton and Veljovic (1983)
16	Istria	Senon	3sites/19sampl.	341	56	150,5	10,1	Marton and Veljovic (1983)
16	Istria	Eocene	8sites	340	49	30	10	Marton et al., (2003)
	Pannonian Basin							
19	Mura zala	Karptian-Pontian	8 sites	326	62	50,5	7,9	Marton et al., (2002a)
18	north. Croatia	Pontian	22 samples	333	66	160	10	Marton et al., (2002b)
	Western Alps							
3	Brianconnais	Oligocene	9 sites	142,3	-57	44	8	Thomas et al., (1999)
2	Ubaye	Oligocene	12 sites	121	-52	17	11	Collombet et al., (2002)
4	Sesia lanzo	L.Oligocene	5 sites	157,2	-39,3		9,7	Lanza (1977)
5	Aar massif	Oligocene	21 samples	6,7	70,1		8,1	Heller (1980)
			6 samples	15,3	74,2		8,1	Heller (1980)
7	Bergell	Oligocene	22 samples	331	59	24,1	6,4	Rosenberg and Heller (1997)
6	Lepont. Dom	Oligocene	9 sites	360	63	58,2	6,8	Rosenberg and Heller (1997)
1	Corsica, Sardin.	Karpat/Baden	24 samples	340,6	39,3	58,6	3,9	Speranza etal., (2002)
	Apennines							
17	north. Apennines	Torton/Messinian	19 sites	154,6	-51,8	23	7,1	Muttoni et al., (2001)
		E.Oligo.-M.Mioc.	18 site	312,5	42,2	34	6	Muttoni et al., (2001)
	south. Apennines	L.-M. Miocene	2 sites	119	-56	964	8,1	Gattacceca and Speranza (2002)
	Eastern Alps							
8	Lower Austria	Karpat/Baden	5 sites	339,2	53,9	86,1	9,4	Scholger and Stingl (2004)
9	Vienna basin	middle Miocene	4 sites	336,6	57,3	139,1	9	Scholger and Stingl (2004)
20	Klagenfurt basin	L.Sarmatian	6 samples	336	62	44	10	Marton et al.,(2000)
21	Lavanttal basin	Pannonian	11 samples	332	61	35	8	Marton et al., (2000)
	Miocene	Ottn.- Karpat	6 sites	293	59	31,6	12,1	Marton et al., (2000)
	Intramontane basins	L.Karp.- Pann.	7 sites	328	59	98,3	6,1	Marton et al., (2000)
28	Graz Paleozoic	Miocene	28 samples	47,6	61,4	25,6	5,5	Burgschwaiger et al., (1996)

Tab.2